56/2/2024
ISSN 1338-3523
ISSN 0369-2086

Mineralia Slovaca

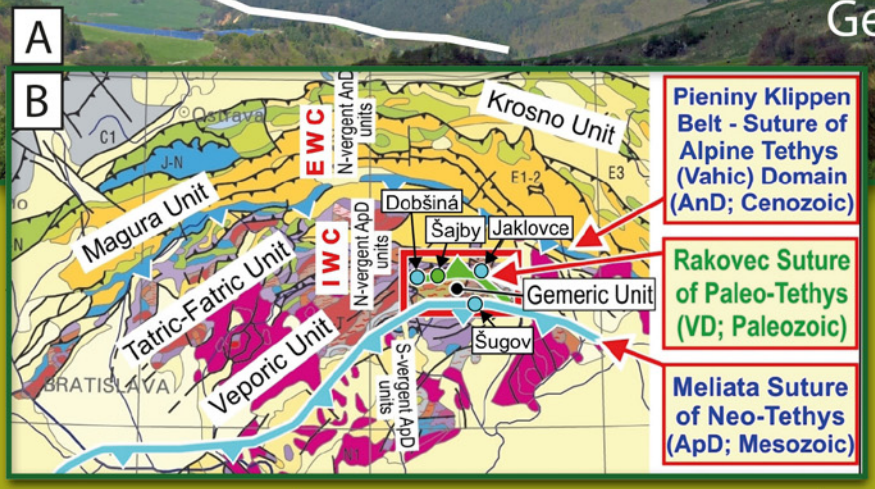

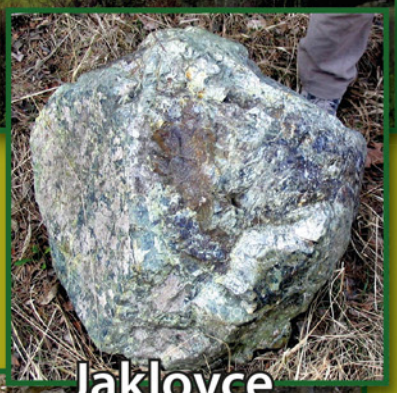

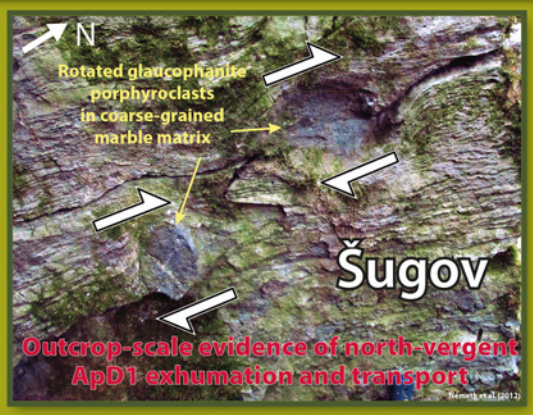

Štátny geologický ústav Dionýza Štúra Bratislava

Mineralia Slovaca

Časopis pre regionálnu a environmentálnu geológiu
a aktivity Slovenskej geologickej spoločnosti a geologických asociácií

Mineralia Slovaca (Web ISSN 1338-3523, ISSN 0369-2086), EV 3534/09, vychádza dvakrát ročne. Vydavateľ a tlač: Štátny geologický ústav Dionýza Štúra, Mlynská dolina 1, 817 04 Bratislava, IČO 31 753 604. Dátum vydania čísla 56/2/2024: december 2024. Predplatné v roku 2024 vrátane DPH, poštovného a balného pre jednotlivcov 22,00 €, pre členov SGS a geologických asociácií 20,90 €, pre organizácie v SR 31,90 €, pre organizácie v ČR 55,00 €. Cena jednotlivého čísla pri osobnom nákupe v predajniach ŠGÚDŠ v Bratislave a v Košiciach je 6,05 € vrátane DPH. Časopis možno objednať v redakcii a v knižnici regionálneho centra v Košiciach. Adresa redakcie: Štátny geologický ústav D. Štúra – RC Košice (Mineralia Slovaca), Jesenského 8, 040 01 Košice. Telefón: 055/625 00 43; fax: 055/625 00 44, e-mail: mineralia.slovaca@geology.sk, e-mail knižnica: secretary.ke@geology.sk

Mineralia Slovaca (Web ISSN 1338-3523, ISSN 0369-2086) is published twice a year by the State Geological Institute of Dionýz Štúr Bratislava, Slovak Republic. The date of issuing of the number 56/2/2024: December 2024.
Subscription for the whole 2024 calendar year (two numbers of the journal): 66.00 € (Europe), 77.00 € (besides Europe), including VAT, postage and packing cost. Claims for nonreceipt of any issue will be filled gratis.
Order of the Editorial Office: Štátny geologický ústav D. Štúra – RC Košice (Library), Jesenského 8, SK-040 01 Košice, Slovak Republic. Phone: +421/55/625 00 43; fax: +421/55/625 00 44, e-mail: mineralia.slovaca@geology.sk, library: secretary.ke@geology.sk

www.geology.sk/mineralia

PÔVODNÉ ČLÁNKY – ORIGINAL PAPERS

COVER: Manifestations of syn-subduction exhumation in two orogenic cycles – Variscan and Paleo-Alpine – in the region of Western Carpathians: A – First-order sequence of lithotectonic units – Tatricum, Veporicum and Gemericum with Meliaticum (the Bôrka nappe). View from the Folkmarský kopec Hill northward; **B** – Position of three suture zones in the Western Carpathians:

The Variscan Rakovec suture zone is a product of south-vergent collisional closure (VD1c) of elongated Paleo-Tethyan basin with the crust of oceanic type (VD0c; green colour line in the North-Gemeric zone). It contains in obducted position on the Šajby mountain ridge (as indicated in part B) the syn-subduction exhumed (VD1se) metagabbro porphyroclasts (pictures right up).

The Paleo-Alpine Meliata suture zone is a product of ApD1c collision closure of elongated Neo-Tethyan Meliata basin with oceanic crust. It is marked by light-blue colour in the South-Gemeric zone. In the area of **Šugov valley** (cf. B) this suture zone is characteristic with Paleo-Alpine syn-subduction north-vergent exhumed (ApD1se) glaucophanite sigma and delta porphyroclasts (diameter up to 20 cm) in the environment of crystalline limestones (detail picture is in the lowermost position). In the pre-metamorphic state the basalt pyroclastic interbeds in limestones represented the protolith

of glaucophanite porphyroclasts. During the Paleo-Alpine obduction-collision tectogenesis (ApD1oc) a part of exhumation mélange was displaced by the kinematics of superficial nappe over the imbricated Paleozoic sequences of Gemericum to the North-Gemeric zone. Relics of this displaced mélange are preserved in the Dobšiná and Jaklovce areas as the nappe outliers. In the **Dobšiná** area (detail pictures are left up) the glaucophanite porphyroclasts to megaporphyroclasts (with also further syn-subduction exhumed high pressure metamorphites) occur in the serpentinite matrix. The glaucophanite megaporphyroclast in the picture left (of these two pictures) has a diameter over 3 meters. In the **Jaklovce** area (below the quarry left in picture **A**; cf. position of Šugov, Dobšiná and Jaklovce localities in map **B**), the Paleo-Alpine syn-subduction exhumed (ApD1se) and transported as a nappe, the marble, chert and serpentinite porphyroclasts to megaporphyroclasts occur, having diameter locally over 1 meter (detail pictures occur right down).

The Neo-Alpine suture zone after Alpine Tethys (Váhic zone, Klippen Belt, marked dark-blue) is the youngest and occurs in position north of previous two sutures. The southern AnD1s subduction polarity in this zone is interpreted as well as the north-vergency collision thrusting (AnD1c).

The arc bended course of the Western Carpathians and their lithotectonic units of higher order is interpreted as a product of Neo-Alpine subhorizontal shear offsets along AnD3 shear zones trending generally NW–SE (dextral shears) and NE–SW (sinistral shears). Present outcropping of various levels of the Western Carpathian lithosphere at present erosion cut is besides the ApD1 nappe setting of Internal Western Carpathians (IWC in part B) and AnD1 thrusts in External Western Carpathians (EWC) also a product of uplift / subsidence kinematics during the AnD4 phase. Further details of the topics of this cover composition are presented in article by Z. Németh on pages 103–145 in this journal. Generalized geological map in part B represents a segment of IGME 5000 (*The 1 : 5 Million International Geological Map of Europe and Adjacent Areas*; Asch, 2005), being presently used as a background map at defining of European lithotectonic units. Author of all photographs: Z. Németh.

OBÁLKA: Prejavy synsubdukčnej exhumácie v prípade dvoch orogenetických cyklov – variského a paleoalpínskeho – v regióne Západných Karpát: A – zostava litotektonických jednotiek prvého rádu – tatrika, veporika a gemerika – s nasunutým príkrovom Bôrky patriacim k meliatiku; pohľad z Folkmarského kopca smerom na sever; **B** – pozícia troch sutúrnych zón v Západných Karpatoch:

Variská rakovecká sutúra – produkt juhovergentného kolízneho uzavretia (VD1c) pretiahnutého paleotetýdneho bazénu s kôrou oceánskeho typu (VD0c), vyznačená zelenou farbou v severogemerickej zóne, nesie v obdukovanej pozícii na horskom hrebeni Šájb (pozri pozíciu v časti B) synsubdukčne exhumované (VD1se) porfyroklasty metagabier (v detailnom zobrazení vpravo hore).

Paleoalpínska meliatska sutúra – produkt ApD1c kolízneho uzavretia pretiahnutého neotetýdneho meliatskeho bazénu s oceánskou kôrou, vyznačená svetlomodrou farbou v juhogemerickej zóne v oblasti **Šugovskej doliny** (cf. B), sa vyznačuje paleoalpínsky synsubdukčne severovergentne exhumovanými (ApD1se) sigma a delta porfyroklastami glaukofanitu s veľkosťou v priemere 20 cm v prostredí kryštalických vápencov (detail poskytuje obrázok v najspodnejšej časti kompozície). V stave pred metamorfózou protolit glaukofanitu tvorili preplástky bazaltových pyroklastík vo vápencoch. Počas paleoalpínskej obdukčno-kolíznej tektogenézy (ApD1oc) bola časť exhumačnej melanže presunutá kinematikou superficiálneho príkrovu ponad komprimované paleozoické sekvencie gemerika do severogemerickej zóny. Relikty tejto presunutej melanže sú tam zachované v podobe príkrovových trosiek v oblasti Dobšinej a Jakloviec. V oblasti **Dobšinej** (detailné obrázky vľavo hore) sú v prostredí serpentinitu dominantne exhumované a spolu príkrovovo prenesené porfyroklasty až megaporfyroklasty glaukofanitu (popri ďalších synsubdukčne exhumovaných vysokotlakových metamorfitoch). Megaporfyroklast glaukofanitu na obrázku vľavo z tejto dvojice obrázkov má priemer vyše troch metrov. V oblasti **Jakloviec** (pod kameňolomom vľavo na obrázku **A**; cf. pozíciu Šugova, Dobšinej a Jakloviec na schematickej mape **B**) sa vyskytujú paleoalpínsky synsubdukčne exhumované (ApD1se) a príkrovovo prenesené porfyroklasty až megaporfyroklasty mramoru, rohovca a serpentinitu (detailné obrázky vpravo dole), ktorých rozmery tiež lokálne presahujú jeden meter.

Neoalpínska sutúrna zóna po alpínskej Tetýde (váhickej zóny, bradlového pásma), vyznačená tmavomodrou čiarou, je najmladšia a nachádza sa v pozícii severne od predchádzajúcich dvoch. Polarita subdukcie AnD1s v tejto zóne je interpretovaná na juh, kolízne násuny (AnD1c) sú generálne na sever.

Oblúkovitý priebeh zóny Západných Karpát a západokarpatských litotektonických jednotiek vyšších rádov je interpretovaný ako produkt neoalpínskych subhorizontálnych strižných posunov na strižných zónach AnD3 smeru generálne SZ – JV (pravostranný strih) a SV – JZ (ľavostranný strih). Odkrytosť jednotlivých úrovní litosféry Západných Karpát v súčasnom erozívnom zreze je popri ApD1 príkrovovej stavbe Vnútorných Západných Karpát (IWC v časti B) a AnD1 násunoch vo Vonkajších Západných Karpatoch (EWC) aj produktom výzdvihovo-poklesovej kinematiky v štádiu AnD4. Problematikou sa zaoberá článok Z. Németha na str. 103 – 145 v tomto čísle časopisu. Generalizovaná geologická mapa na kompozícii v časti B je segmentom mapy IGME 5000 (*The 1 : 5 Million International Geological Map of Europe and Adjacent Areas*; Asch, 2005), ktorá sa v súčasnosti používa ako základná mapa pri definovaní litotektonických jednotiek Európy. Autor všetkých fotografií: Z. Németh.

Mineralia Slovaca, Web ISSN 1338-3523, ISSN 0369-2086, https://doi.org/10.56623/ms.2024.56.2.1
56, 2 (2024), 103 – 142, © Authors 2024. CC BY 4.0

Geodynamics of polyorogenic zones: Case study from the Western Carpathians

ZOLTÁN NÉMETH

State Geological Institute of Dionýz Štúr, Mlynská dolina 1,
SK-817 04 Bratislava, Slovak Republic; zoltan.nemeth@geology.sk

Abstract: Within the Alpine-Carpathian-Himalayan belt, the remnants of polyorogenic evolution are usually documented with a series of parallel suture zones of subequatorial course. In several cases some suture zones are interpreted as remnants of back-arc basins. In the Western Carpathians, the products of three principal Phanerozoic orogenic (Wilson) cycles were exemplarily documented – Variscan (Paleozoic), Paleo-Alpine (Mesozoic) and Neo-Alpine (Cenozoic) ones. The processes and products of the post-Cadomian Cenerian orogenesis are not treated in this article due to their ongoing research in the Western Carpathians, which is not yet completed. Based on presented geological and tectonic observations, as a driving force for polyorogenesis and multiple continental breakup a long time mantle convection (during a whole Phanerozoic eon) is interpreted, acting along a global subequatorial-course mantle bulge (ECMB) and parallel subequatorial-course mantle convection currents (ECMCCs). The submeridian zones with different kinematics are driven by submeridian-course mantle convection currents (MCMCCs), producing submeridian trending global rifts, but also subduction zones. Both systems of mantle convection currents – subequatorial (ECMB, ECMCCs), submeridian (MCMCCS) and their eventual interconnections, all briefly descriptively named as hot lines, are interpreted as principal drivers of global geodynamics. They are acting simultaneously with columnar mantle plumes (mantle diapirs). According to cited studies of different authors the heat for mantle convection currents and plumes is supplied by the thermonuclear fusion in innermost zones of the Earth. Combining the interpretation of global importance of mantle convection currents and their effect on processes within the lithosphere with the principles of plate tectonics, gives a basis for establishing a hypothesis of New Global Tectonics 2.0. For the simple and understandable description of a succession of orogenic cycles and their phases within polyorogenic evolution, including overprinting relations within tectonic and deformation phenomena, the methodology of XD labelling is applied in this contribution.

Key words: polyorogenic processes, extended orogenic cycle, subequatorial-course mantle bulge (ECMB), subequatorial-course mantle convection current (ECMCC), submeridian-course mantle convection current (MCMCC), hot line, XD and MX labelling, Western Carpathians

Graphical abstract

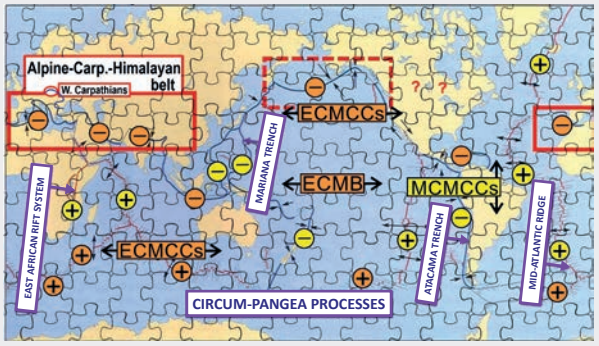

Highlights

- The Western Carpathians segment of Alpine-Carpathian-Himalayan belt is characteristic with polyorogenesis – geodynamics of the sequence of multiple orogenic cycles.
- Synthesis of research results, documenting evolution of the Western Carpathians, indicates a role of linear subequatorial-course mantle convection current (ECMMC) as a driver of Phanerozoic geodynamics of all three orogenic cycles – Variscan, Paleo-Alpine and Neo-Alpine.

1 Introduction

This contribution aims to introduce several new terms, not used (or used only marginally) in geological practice. The term **polyorogenesis** means action of a sequence of several orogenic cycles in a distinct zone, e.g. Alpine-Carpathian-Himalayan zone and producing a sequence of divergences with multiple parallel continental breakups, as well as convergences producing suture zones and orogenic belts. The continent-continent type collision at polyorogenic processes in zones of Intra-Pangea-type of subequatorial direction differs them from the Cordilleran-type mountain building at standard subduction / accretion prism forming processes in submeridian course zones of the Circum-Pacific-type. For the easy use and understandability of this sequence of orogenic cycles and their phases – they are described by the simple symbols of **XD labelling** methodology (Németh, 2021), being described further in the text.

Article provides a comprehensive review focused on polyorogenic evolution in the Western Carpathians, as a representative segment of generally subequatorial trending Alpine-Carpathian-Himalayan belt (Figs. 1 and 2). This contribution is based on detail knowledge on kinematics and products of three orogenic cycles in the Western Carpathians: Variscan (abbreviation **V**; Paleozoic), Paleo-Alpine (**Ap**; Mesozoic; western extension of Cimmerian cycle) and Neo-Alpine (**An;** Cenozoic; eastern extension of Penninic cycle). The processes and products of the post-Cadomian Cenerian orogenesis are not treated in this article due to their ongoing research in the Western Carpathians, which is not yet completed.

The present configuration of three suture zones (alternative term: geosutures) in the Western Carpathians (Fig. 1B) and polarity of subduction exclude an interpretation of backarc-type evolution of described three elongated basins: The Variscan equatorial trending geosuture (named Rakovec geosuture; Németh, 2002), located along the axis of the Western Carpathian polyorogenic belt, was produced by convergence having subduction polarity to north (l.c.). Younger Paleo-Alpine geosuture (Meliata geosuture, incl. Bôrka nappe; Mello et al.,1998; Putiš et al., 2019c; Potočný et al., 2023, 2025; Molčan Matejová et al., 2025), was located parallel, but south of Variscan geosuture, being produced by convergence with southern subduction polarity – slab dipping to south. Such geometry of these two orogenic cycles excludes the Paleo-Alpine basin position as a backarc developed during older Variscan process.

The youngest geosuture, present in the W. Carpathians – the Neo-Alpine Pieniny Klippen Belt Penninic-Váhic-Magura geosuture (cf. Plašienka et al., 2020 and references therein), is located parallel to both previous geosutures, but north of them. Related subduction slab was in this case

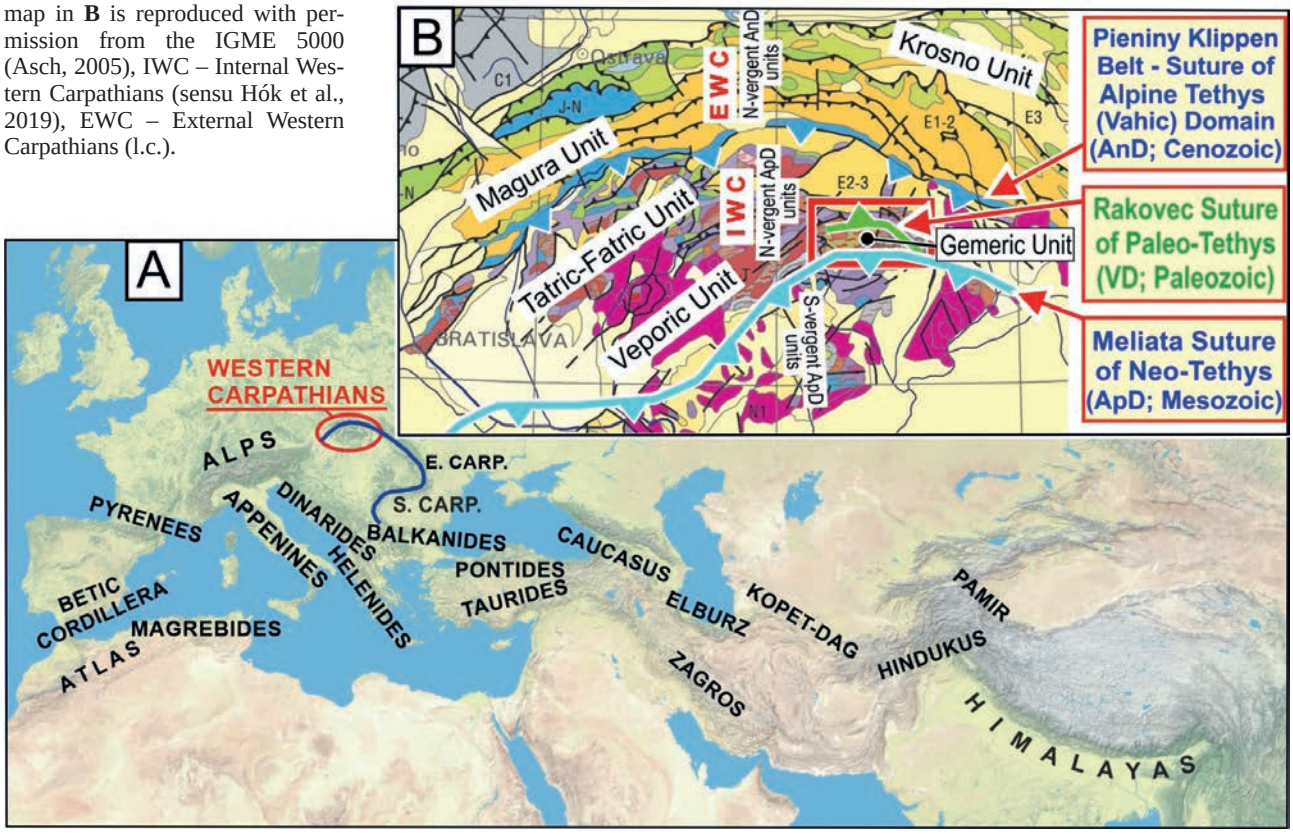

Fig. 1. A – Position of Western Carpathians (northernmost located red oval in part **A** within the polyorogenic Alpine-Carpathian-Himalayan belt. The Carpathian belt of triple oroclinal bend (syneclisis) is indicated by blue line drawn from Western Carpathian red oval towards SE – depicting the segment of Eastern Carpathians – and next to W, S and shortly to SE – depicting the segment of Southern Carpathians. The location and names of mountain ranges, located SW and SE of Western Carpathians were taken from van Hinsbergen et al. (2014) and Marko et al. (2020). The entire area shown in A is located north of the equator. **B** – Nearly symmetric course and northward convex oroclinal bending of Western Carpathians show very distinctly the course of three suture zones – Paleozoic Variscan (Rakovec geosuture of Paleo-Tethys sensu Németh, 2002; VD; light green), Mesozoic Paleo-Alpine (suture zone after Meliata ocean of Neo-Tethys; sensu Mello et al., 1998; ApD; light-blue) and Cenozoic Neo-Alpine suture zone (Pieniny Klippen Belt – Alpine Tethys / Vahic suture – presently summed up by Plašienka et al., 2020; AnD; dark blue). Despite clear zonality of these suture zones, the Western Carpathians contain also scattered remains of earlier Lower Paleozoic Rheic ocean Cenerian evolution (e.g. Putiš et al., 1997, 2024). Presented segment of geological map in **B** is reproduced with permission from the IGME 5000 (Asch, 2005), IWC – Internal Western Carpathians (sensu Hók et al., 2019), EWC – External Western Carpathians (l.c.).

dipping to south, which again excludes the possibility that elongated Neo-Alpine basin represented a back-arc basin during subduction of the crust of Paleo-Alpine basin. Position of suture zones, including the dips of subduction slabs are visualized in Fig. 1B.

It is important to note that the definition of Tethys Ocean varies among different authors. The Western Carpathian geologists, owing to distinct zonality of Variscan and Alpine successive events, use designation applied in this contribution: The Paleozoic Variscan elongated oceanic basin, having well developed suture zone in the W. Carpathians, is named the **Paleo-Tethys** (Grecula, 1982; Putiš et al., 2009, 2024; Plašienka et al., 1997a; Németh, 2002; Németh et al., 2016). The elongated Paleo-Tethyan Rakovec basic was closed by subduction-collision process in Upper Carboniferous (Németh, 2002; Dallmeyer et al., 2005), the Mesozoic one – **Neo-Tethys,** represented by Meliata Ocean, was closed by Lower Cretaceous collision (Plašienka et al., 1997b; Mello et al., 1998; Lexa et al., 2007). The youngest – third elongated oceanic basin in this succession consists of two zones – the southern – Piemont-Váhic Ocean as elongation of South Pennine Ocean subducted and closed at 80 Ma and northern zone – the Magura Ocean as elongation of North Pennine one subducted and closed between 35–20 Ma (cf. Plašienka et al., 2020). These two zones were primarily separated by so-called Oravic continental ribbon (Czorsztyn Ridge; l.c.). This gradual two-stadial partial subduction is interpreted as **Neo-Alpine evolution** in the W. Carpathians and the course of its suture zone is very spectacularly evidenced by the Pieniny Klippen Belt.

1.1 The XD labelling as a tool for simple and efficient classification of orogenic phases within orogenic cycles

To express understandable and readily depictable, the relations and time succession within individual orogenic

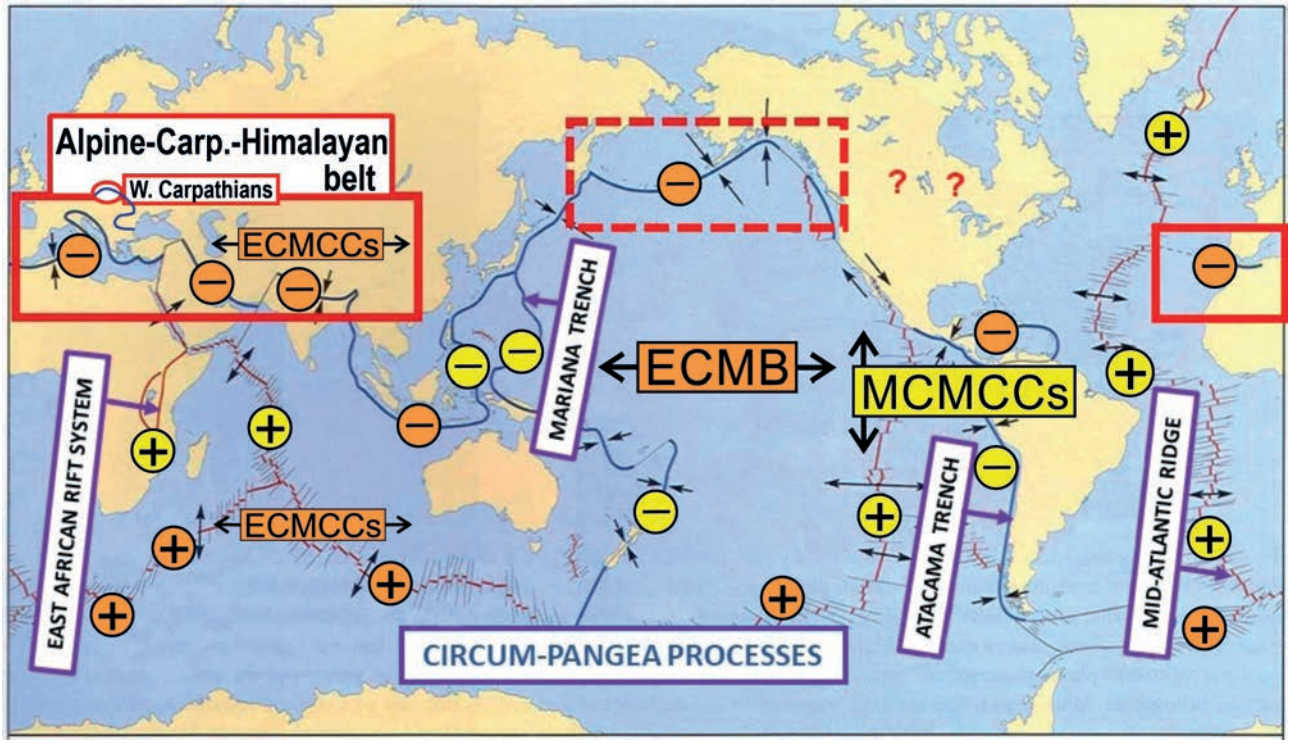

Fig. 2. Spatial orientation of subequatorial trending Intra-Pangea polyorogenic zone (red full or dashed line rectangles). The continuation of this zone within North American continent is not clear, its shift to Caribbean area is interpreted due to dextral displacement starting in San Andreas fault (located in western side of North American continent; cf. Wallace – ed., 1990). The designation of Circum-Pangea-type processes, chosen correspondingly with the situation during the existence of compact Pangea supercontinent in Permian, covers dominantly the processes of submeridian-course divergence (e.g. East African Rift System representing the embryonal stage of riftogenesis within continental crust or the Mid-Atlantic Ridge in mature stage of riftogenesis within oceanic crust), as well as convergence of submeridian course (e.g. subduction along Mariana and Atacama trenches as type localities). On the publicly available basemap the rift zones are marked with red curved lines and subduction zones with blue lines. The plus signs in circles indicate the upwelling mantle currents producing rift zones and minus signs in circles indicate downwelling mantle currents producing subduction zones. Both types of signs related to ECMB and ECMCCs are highlighted by orange circles. In the case of submeridian-course mantle convection currents (MCMCCs) the signs are placed to yellow circles.

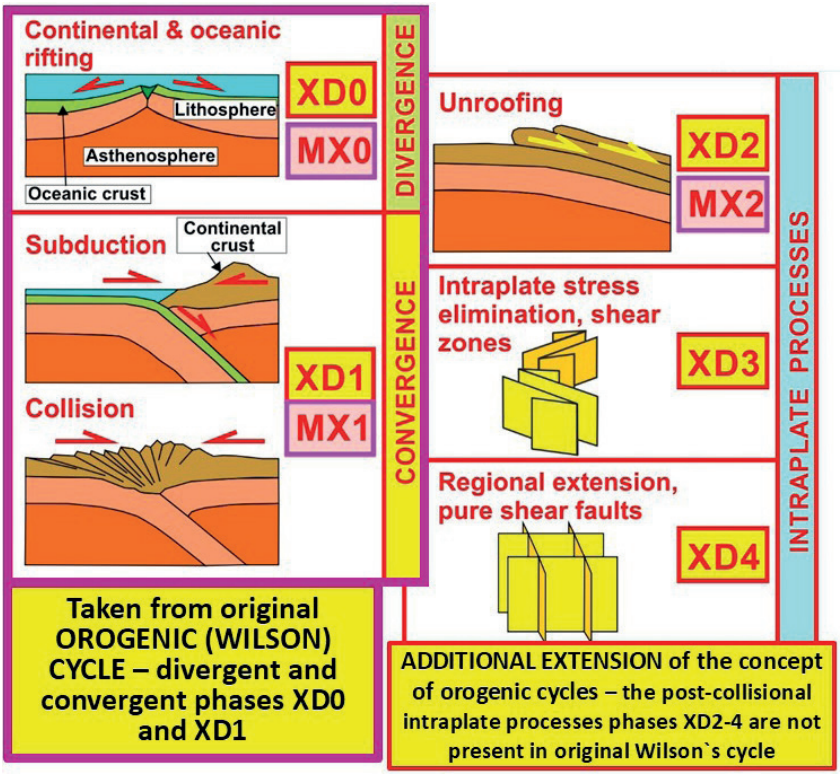

Fig. 3. The schematic visualization of a sequence of orogenic phases (XD0-4) and metamorphic overprints (MX0-2) within an orogenic cycle (Németh, 2021; reproduced with permission) highlights adding new orogenic phases (XD2-4) to primarily defined orogenic (Wilson) cycle (XD0-1), owing to extensive research in the Western Carpathians, focussed on tectonic and structural manifestations of individual phases and overprinting relations.

phases of orogenic cycles, the "XD labelling" methodology was suggested by Németh (2021; Fig. 3). Despite this methodology may be partly reminiscent of the concept of Hans Stille (1924), who postulated the idea of globally synchronous orogenic phases, the XD labelling is not targetted to global synchronization. Its aim is preferably descriptive – to mark simply and readily the orogenic cycles and their phases when discussing the geodynamic evoluton and orogenesis in the territory of interest.

At XD labelling, the name of particular orogenic cycle is expressed by the X variable – e.g. in the case of orogenic cycles in European territory: Sv – Svecofennian, Go – Gothian, Sn – Sveconorwegian, Ti – Timanide, Cd – Cadomian, Cl – Caledonian, **V – Variscan,** Ur – Uralian, **A – Alpine** (in W. Carpathians: **Ap – Paleo-Alpine – western extension of Cimmerian cycle** and **An – Neo-Alpine – eastern extension of Penninic subduction / collision events**) and He – Hellenic orogeny. Also further orogenic cycles with specific X labels (even word-wide) can be involved into this classification. A specific orogenic phase in the frame of orogenic cycle is expressed by adding relevant number after D: **XD0** – divergent process of riftogenesis – this orogenic phase is subdivided to three subphases: XD0a – stretching subphase, XD0b – thinning subphase (both relate to evolution within continental crust) and XD0c – ocean spreading subphase. The **XD1** phase designates the convergent processes of subduction (XD1s), obduction (XD1o) and closure of elongated oceanic space by collision (XD1c). In original plate tectonic (Wilson) cycle the collision represents the final phase of the cycle. Extended research in the Western Carpathians revealed the significance of post-collision evolution (revealed for both Variscan and Paleo-Alpine orogenic cycles (Németh, 2021), being classified by three additional phases within a cycle, covering the **post-collisional thermal / deformation processes, metamorphic core complex active evolution and related unroofing – XD2 phase;** intraplate stress consolidation – **XD3 phase** (strike slips, transpression, transtension, rotation of blocks, etc.) and regional extension – **XD4 phase** (pure shear-type regional faults – preferably of N-S and E-W trends, as well as the continental grabens developments and Basin & Range-type tectonics. Possible is even more detail classification applying the subphases. Metamorphic overprints related to specific phases of orogenic cycle are labelled by similar way: MX0 – metamorphism related to mid-oceanic ridges, MX1 – subduction metamorphism (MX1s) and collision metamorphism (MX1c), MX2 – post-collision evolution of metamorphic core complexes and related metamorphism.

1.2 Interconnection of earlier geodynamic findings in the Western Carpathians with new designation of orogenic cycles and phases

In the Western Carpathians it is clearly decipherable that within orogenic cycles of **the subequatorial Intra-Pangea-type the regional extension leading to continental breakup acts dominantly in phases XD2 and XD4, being followed by $X^{+1}D0$ rifting of a new orogenic cycle.** Concerning the extensional phase XD4, the extended regional faults (lineaments) with pure shear kinematics, trending generally E-W (subequatorial trend) or N-S (submeridian trend) were important for continental breakups. These faults represent a common sign of Intra-Pangea as well as Circum-Pangea processes and on a global scale, they represent the embryonic phase of future rifts,

being a consequence of mantle convection currents. In regional, or even local scales, the **XD4 pure shear faults can also be a product of XD3 shearing – they represent merging of synthetic as well as antithetic mega-shears of the same course within NW-SE and NE-SW trending XD3 shear zones** (cf. Németh et al., 2017; Németh in Gaál et al., 2017).

Regarding the topic of this contribution, we focus dominantly on **VD0 / ApD0 / AnD0 as well as on VD2 / ApD2 phases of Variscan and Alpine evolution**. The **VD2 / ApD2 phases** actively generated metamorphic core complexes **MV2** / **MAp2** and extensional unroofing tectonics, in both cases leading to new continental (Pangea) breakups and origin of generally E-W trending basins with oceanic-type crust. For complexity, also other orogenic phases acting in evolution of the Western Carpathians will be briefly described in the XDs time succession. By this way this contribution provides reader a complete information about evolution of the Western Carpathian segment of Alpine-Carpathian-Himalayan orogenic belt, which can be useful e.g. when comparing this evolution with the evolution of other segments of polyorogenic belts in Europe or in the world.

1.3 Peculiarities of Intra-Pangea polyorogenic evolution in zones of subequatorial direction

We differ the **Intra-Pangea orogenic processes** in zones of subequatorial direction, encompassing dominantly the Alpine-Carpathian-Himalayan zone (being along the western margin of North American continent possibly shifted to Caribbean area), from the submeridian processes that acted not only in Pangea, but also in the rest of the world, being named as the **Circum-Pangea-type processes** (earlier designation was Circum-Pacific-type processes; Németh et al., 2016; Németh, 2018). In this division, the situation along the NNW-SSE trending San Andreas Fault System is much more complicated – simultaneously with regional dextral shearing this fault system represents also northern continuation of submeridian rifting zone separating the Pacific plate from Cocos and Nazca lithospheric plates (cf. Wallace – ed., 1990; Fig. 2),

At the **Circum-Pangea-type processes / zones** the rift zones and trenches have generally N-S – submeridian trend and their tectogenesis corresponds to present convergent processes along western coast of South America – e.g. the Atacama trench zone as well as east of Japanese islands – the Mariana trench zone, both as exemplary cases (Fig. 2). As an example of submeridian-course divergent zones there can serve the spreading of the Mid-Atlantic ridge, or presently developing East African Rift System. The continent-continent-type collisions are significantly less common at the submeridian Circum-Pangea zones than in the case of subequatorial Intra-Pangea-type polyorogenic zoness (cf. Fig. 2). There is necessary to emphasize that the Intra-Pangea orogenic processes in zones of subequatorial direction occur presently in evolutionary stage of finishing Neo-Alpine phases AnD1 / AnD2 and the Alpine-Carpathian-Himalayan belt is undergoing mainly the Neo-Alpine shearing (AnD3) and extensional faulting (AnD4), which is interconnecting the Intra-Pangea and Circum-Pangea processes. In the Mediterranean area the Hellenic orogenic cycle occurs now in the subduction phase HeD1s.

In the case of pre-Pangea supercontinents of Rodinia (Mesoproterozoic and Neoproterozoic in age) and Nuna (Paleoproterozoic and Mesoproterozoic in age) we suppose the corresponding kinematics of divergent processes, continental breakups, as well as convergent processes, as in younger, here described, Pangea-type processes – having similar kinematic evolution, spatial orientation and sequence of events, though acting in slightly warmer conditions.

1.4 Earth rotation and its role in positioning of principal mantle convection currents

As reviewed in monograph by Frisch et al. (2022), Alfred Wegener, professor at the University of Graz (Austria) in the 1920s, unsuccessfully attempted to add credibility to his theory of continental drift explaining its driving forces by the rotation of the Earth. Parallel with Alfred Wegener at the same university worked professor Robert Schwinner, developing far-reaching theory of convective heat transport, producing the currents in the Earth's interior. If both professors would have communicated, they could unify the drift theory with accepted theory of its driving force, thus markedly accelerating the birth of the theory of plate tectonics (l.c.).

The concept presented in our further text and its conclusion are built exclusively on the theory of mantle convection heat currents, emphasizing that on a global-scale the Earth's rotation organizes them preferably to mantle currents of subequatorial-course (ECMB and ECMCCs), as well as submeridian-course (MCMCCs), contributing to location of rift zones / subduction zones in the lithosphere. All author's interpretains are based on geological and tectonic observations, so he only reports primary reasons of mantle convection currents citing works of other authors (in chapter 5).

The variability of the Earth-rotation vector relative to the body of the planet or in inertial space is caused by the gravitational torque exerted by the Moon, Sun and planets, displacements of matter in different parts of the planet and other excitation mechanisms (IERS, 2023). Concerning geodynamics, the oscillations can be interpreted in terms of mantle elasticity, Earth flattening, structure and properties

of the core-mantle boundary, rheology of the core, and the understanding of the coupling between the various layers of our planet (l.c.). The role of Earth rotation in plate tectonics was considered by numerous earlier authors:

The existence of a global westward rotation of the lithosphere independently from the location of the hot spots sources was suggested by Ricard et al. (1991). These authors emphasized that this rotation is a real one and is not an artifact of the choice of the reference frame in which plate motions are defined. As a consequence of the westward rotation of the lithosphere an anchoring effect in the case of subduction slabs at submeridian trending subduction zones acts in the mantle which is migrating east. This mechanism could explain the observed steeper dips of the west dipping subduction slabs which contrast the mantle flow. This concept was further developed by Doglioni et al. (1991, 1999, 2006).

Hide et al. (1993) review earlier models of the topography of core-mantle boundary as well as the hypothesis that the astronomically determined irregular fluctuations in the Earth's rotation vector is due to the fluctuating torque on the lower surface of the Earth's mantle produced by magnetohydrodynamic flow in the underlying liquid metallic core as well as **equatorial bulge**.

Wilson (1995) emphasized that only few local observations and satellite remote sensing observations measurements of Earth rotation changes offer genuinely global measures. The Earth's long term rotation stability was explained by Richards et al. (1997) by the slow rate of change in the large-scale pattern of plate tectonic motions during Cenozoic and late Mesozoic time, as well as relatively **slow changes in the global pattern of subduction zones**. The subducted lithosphere represents a **major component of the mantle density heterogeneity generated by convection**. This effect of three-dimensional mantle density heterogeneity on Earth rotation was confirmed by Liu et al. (2016): The difference of the observed Earth polar motion and length of day, taking into account the model only considering ocean tides, **must have added also the contributions of the lateral density heterogeneity of the mantle**. Study of the effect of mantle density heterogeneity on torque-free Earth rotation may provide useful constraints to construct the Reference Earth Model.

Sun and Xu (2012) improved prediction accuracy of Earth's rotation parameters (ERP), based on improved weighted least squares (WLS) and autoregressive (AR) model. **Earthquakes may lead to mass redistribution in the Earth interior and by this way to influence the Earth**'**s rotation** due to the change of Earth inertia moment (Xu & Sun, 2012). Authors (l.c.) adopted the elastic dislocation to compute the co-seismic polar motion and variation in length of day (LOD) caused by the 2011 Sumatra earthquake. They **indicate the tendency of earthquakes make the Earth rounder and to pull the mass toward the centre of the Earth**.

The rotation rate of Earth determines **its uniaxial compression along the axis of rotation**. The **Earth's ellipticity variations, caused naturally by the rotation rate variations**, are manifested in **vertical components of various surface elements**, which can be determined by precise GPS measurements (Levin et al., 2017). Analysis of the observations made by the International Earth Rotation and Reference System Service (IERS) **revealed regularities in the natural variations of the Earth's angular rotation rate**. The work by Levin et al (l.c.) performs comparison of geodetic ellipsoid dynamics theoretical estimates obtained from studies of **the pulsation model of the Earth's shape due to variations of its rotation rate**. By this way this study has added a new dimension for understanding of **the variations in the Earth rotation caused by mass redistribution**.

Relation of geodynamics to the Earth rotation was extensively researched by a number of Polish institutions in the 2010s (Bogusz et al., 2015). The tectonic plate motions models and the map of the continuous velocity field were developed applying information from over 300 permanent reference stations of the EUREF Permanent Network (EPN) as well as Polish Active Geodetic Network (ASG-EUPOS) and interpolating velocities using the Kriging method with the nugget effect. The robustness of geodetically-defined kinematic model, describing recent geodynamics, was tested using numerical finite element modelling of stress and strain distribution in Central Europe (Bogusz et al., 2011). Simplified mechanical model of the lithosphere was developed using geological and geophysical data including tectonically defined discontinuities. The results of model predictions were evaluated by comparison with measured present-day stress and strain.

2 Brief description of regional geological setting of the Western Carpathians

The Western Carpathians represent arcued elongated orogenic segment of the Alpine-Carpathian-Himalayan belt (Fig. 1A, B). They are characteristic with dominant northern vergency of Alpine ApD1c tectonic imbrication and nappe stacking, despite having incorporated also southern vergency tectonic structures of earlier Variscan evolution VD01.

Despite the triple division of the Western Carpathians to Outer, Central and Inner W. Carpathians was dominantly used in the past (e.g. Mahel', 1986), we prefer simpler division to Outer (External – EWC) and Inner (Internal – IWC) W. Carpathians (cf. Hók et al., 2019), better distinguishing units with dominant Neo-Alpine (Cenozoic) vs. dominant Paleo-Alpine / Variscan (Mesozoic /

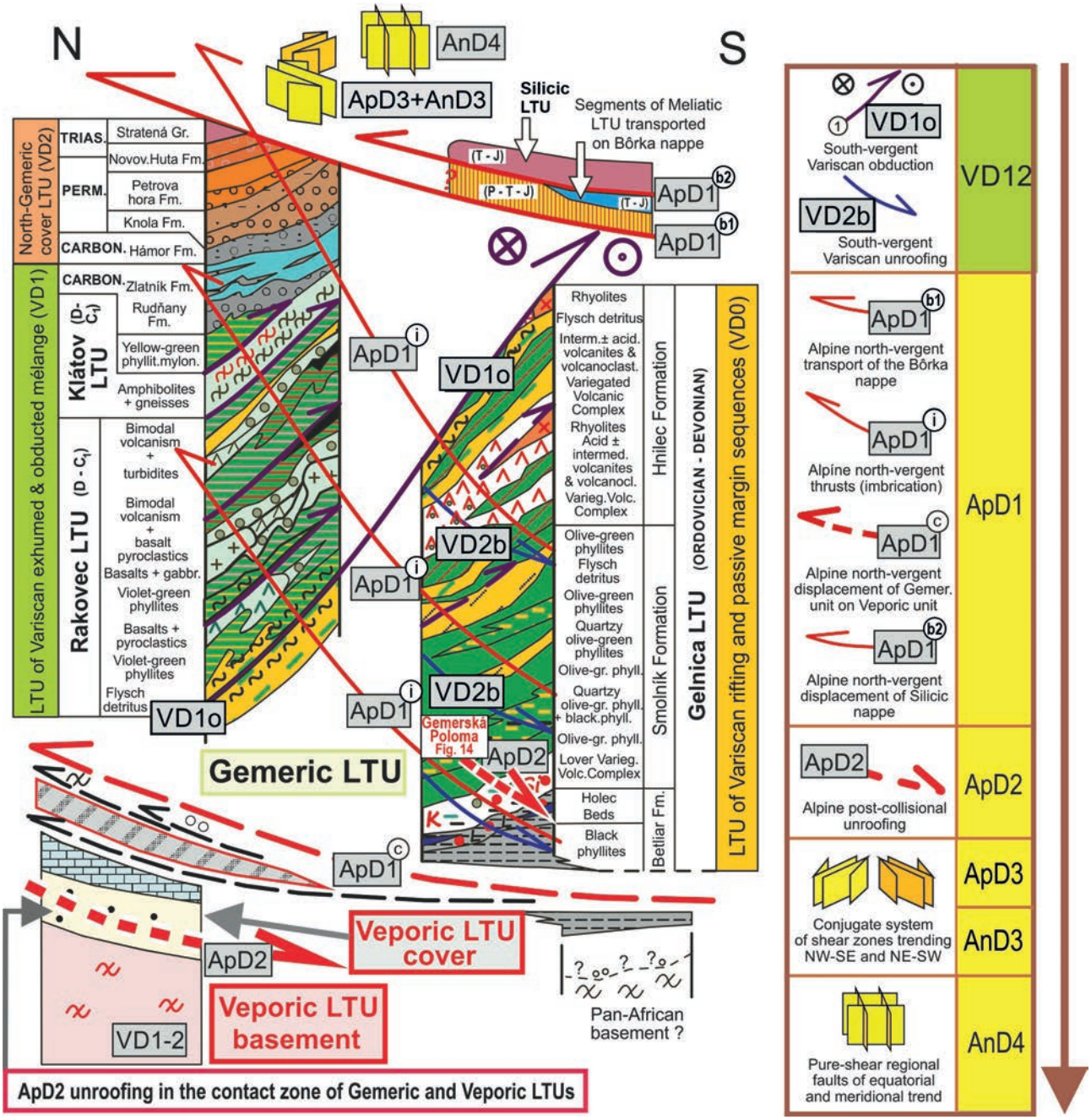

Fig. 4. Detail lithotectonic column of the innermost zone of Internal Western Carpathians (IWC), depicting succession of orogenic phases in Variscan (VD) and Paleo-Alpine (ApD) orogenic cycles, as well as their overprint by Neo-Alpine shearing (AnD3) and faulting (AnD4). Orientation of this lithotectonic column is N–S, localized it is in the middle the red rectangle in Fig. 1B. This lithotectonic column expresses the relations of supreme order lithotectonic units of Internal W. Carpathians: Gemeric, Veporic, Meliatic (incl. the Bôrka nappe) and Silicic units (cf. Németh, 2005b; Németh et al., 2012; reproduced with permission). Methodology of XD labelling of lithotectonic units (LTUs) and lithotectonic limits (LTLs) allows to express clearly the succession of tectonic structures and overprints. Red arrow lines express the Early Cretaceous north-vergent thrusts of Meliatic Bôrka nappe on Gemeric lithotectonic unit (LTU; ApD1b1), north-vergent imbrication (ApD1i), then thrust of Gemeric + Bôrka nappe pile on Veporic one (ApD1c). The whole lithotectonic sequence is then overthrust by the Silicic nappe (ApD1b2). Apparent paradox of Lower Cretaceous evolution of IWC is that simultaneous with this prominent ApD1 compressional / collisional phase taking place in the innermost (i.e. southernmost) zones of IWC, an extension was prevailing in the outermost (northernmost) zones of the Western Carpathians, forming here several longitudinal elevated and subsided domains (cf. Plašienka, 2018). The same paradox is characteristic for the Late Cretaceous evolution of IWC – the southernmost zones underwent ApD2 extension and unroofing (designated by red thick dashed arrow line), but in the northernmost zones of Western Carpathians this period is characterized with contraction and its differentiated topography was inverted and previous facial zones became constituents of regional tectonic units (cf. l.c.).

Paleozoic) evolution. Superficially, the dividing line between External and Internal W. Carpathians is represented by the Klippen Belt, geometrically parallelized with the Penninic evolution in the Eastern Alps and Briançonnais domain (Tomek, 1993) in the Western Alps. The Klippen Belt marks simultaneously boundary between Neo-Alpine nappes in External W. Carpathians and Pre-Paleogene Paleo-Alpine nappes of Internal W. Carpathians.

2.1 Internal Western Carpathian belt

In Paleo-Alpine nappe pile the following main lithotectonic units, having northern general vergency of thrusting and nappe displacement, will be described from the bottom upwards: *Tatric*, *Veporic* and *Gemeric units* (all three represent so-called basement nappes), *Meliatic (Bôrka nappe)*, *Turnaic (Tornaic in Hungary)* and *Silicic units* (representing the superficial nappes; cf. Figs. 1B and 4). Moreover, from the space between Tatric and Veporic units the *Fatric Unit (Krížna nappe) wa*s derived and from the space between *Veporic* and *Gemeric units* it was the *Hronic Unit (Choč nappe)*. The geodynamic evolution of these sequences is described in more details in relevant chapters in further text.

The Tatric Unit (*Tatricum*; probable equivalent of Lower Austroalpine Unit of the Eastern Alps) – crops out in the W. Carpathian core mountains and consists of Variscan medium to high-grade metamorphic rocks (schistose gneisses with sporadic HP metamorphics and granitoids). The primary cover of Tatricum starts with Upper Paleozic / Lower Triassic clastics, being followed by Middle Triassic carbonates. The sedimentary area became differentiated during the Jurassic period, encompassing radiolarian limestones, radiolarites, crinoid and sandy limestones. The Lower Cretaceous pelagic, cherty limestones sedimentation ended with flysch formation. The Tatricum represents the lowermost unit of Internal Carpathians. In present north-vergent tectonic setting the Tatric tectonic underlier is represented by *Váhicum* as equivalent of southern *Penninicum*, and tectonic overlier by flat-lying nappe of *Fatricum*, containing sedimentary sequences corresponding with that of Tatric cover.

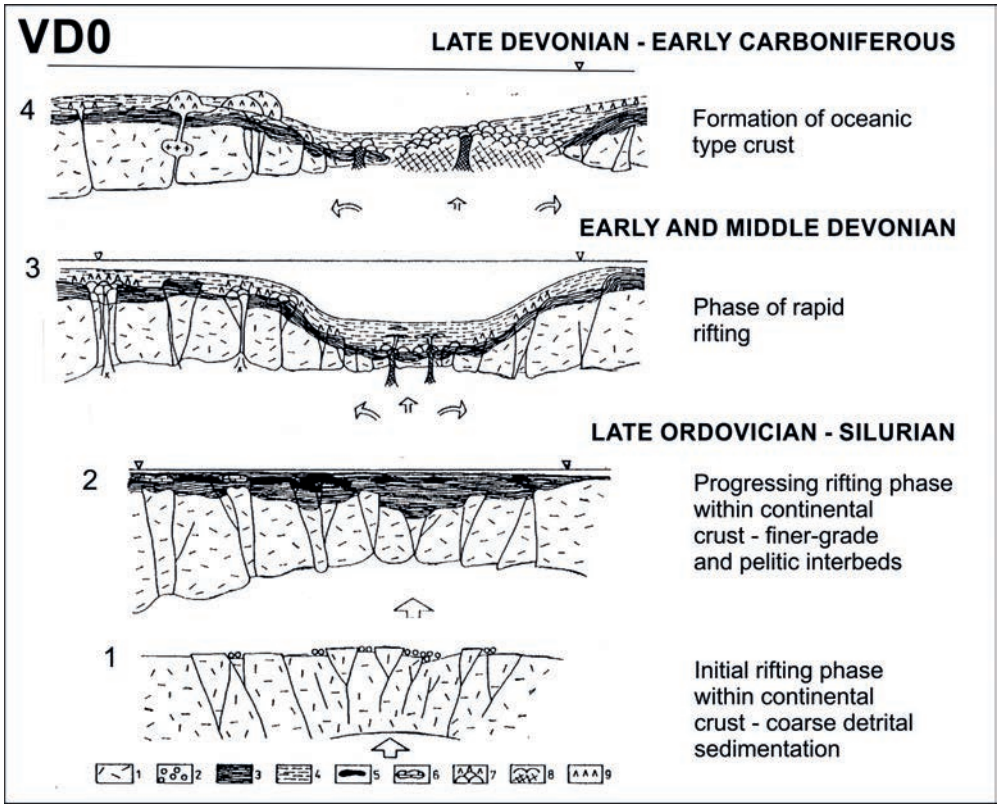

Fig. 5. The Early Paleozoic Variscan continental breakup and origin of Paleo-Gemeric riftogenous basin VD0 in the territory of future Western Carpathians (slightly modified after Grecula, 1982 – Plate 3.1 ibid., Grecula in Grecula et al., 1995 – Fig. 1.8 ibid; reproduced with permission). The source of convectional heat (EC-MCC; hot line) is indicated by arrows beneath the rift zone. Development phase **1** (VD0a) is not preserved in present Gemeric Unit due to ApD1c north-vergent amputation of coarse-grained detrital Gemeric sequences from their Pan-African homeland (cf. in Fig. 4 – middle column down), applying the soft horizon preferably of black phyllites (lithology 3 in this Fig.) in the Paleo-Alpine nappe detachment ApD1c. This rheologically soft horizon of black phyllites is presently affiliated with the Gemeric **Betliar Formation** (former Late Ordovician-Silurian sedimentation in anoxic environment; in this figure shown in evolution phase **2**), **3** – development of **Smolník Fm.** with bimodal volcanism of first rapid rifting phase VD0b; all sequences belong to **Gelnica Group** (**LTU**; cf. Fig. 4), **4** – opening of ocean and development of mid-oceanic ridge VD0c, which sequences are included into the **Hnilec Fm.** of **Rakovec Group (LTU)** and – in higher temperature metamorphosed facies – to the **Klátov Group (nappe; gneiss-amphibolite complex; LTU)**. Lithology in the legend beneath sketches: 1 – rocks of continental crust, 2 – coarse-clastic sediments, 3 – formation of black phyllites – dominantly organic matter / graphite bearing pelites and psammites, 4 – formation of greenish (dominantly chlorite bearing) pelites and flysch sequences, 5 – lydite, 6 – carbonate, 7 – basalt-keratophyre bimodal volcanic complex, 8 – magmatic series of the mid-oceanic ridge, 9 – rhyolite domes.

The Veporic Unit (Veporicum), similarly like Tatric Unit, comprises of Variscan crystalline basement and Upper Paleozoic / Mesozoic cover. The Alpine evolution zone between Veporic and Gemeric units is interpreted to be the homeland of *Hronic Unit (Hronicum)* with conspicuous development of Carboniferous-Permian volcanosedimentary formations.

The *Gemeric Unit (Gemericum)* represents the uppermost Paleo-Alpine basement nappe, having well preserved Lower Paleozoic volcano-sedimentary sequences of Variscan riftogenous phase (VD0; Fig. 5), as well as – in Northern-Gemeric rim – well preserved suture zone with a wide range of rock sequences, including also HP and UHP blocks exhumed from Variscan subduction zone and VD1oc thrust southward on Variscan passive margin sequences (Radvanec & Németh, 2018; Figs. 6, 7 and 8). The Gemeric Upper Paleozoic / Mesozoic cover sequences are bearing superficial nappes of *Meliatic Unit (Meliaticum; Bôrka nappe), Turnaic and Silicic units* (cf. Fig. 4, upper part).

2.2 External Western Carpathian (Flysch) belt

This belt is a product of Upper Cretaceous-Cenozoic Neo-Alpine evolution. External Carpathian Flysch belt consists of Cenozoic rootless nappes thrust over the North-European platform. The flysch-like Mesozoic and Paleogene formations predominate. The *Magura group of nappes (Unit)* consists mainly of Paleogene flysch formations with prevailing sandstones. These are as a whole, thrust northward over the north located *Krosno Unit of Flysch Belt, built of prevailing variegated claystones.*

The Klippen Belt (Oravic Unit; cf. Hók et al., 2019, p. 39 ibid.) represents in pre-Neo-Alpine deformation phase the hypothetical continental ribbon named as Czorsztyn ridge, separated from the European Platform on the north by oceanic domain of the Northern Penninicum (Magura Ocean) and from the Internal Western Carpathians by the oceanic domain of the Southern Penninicum of the Váhicum (Plašienka, 2012; Plašienka & Soták, 2015). The most widespread here are the Czorsztyn and Kysuca (Kysuca–Pieniny) sedimentary successions starting with Lower Jurassic rocks.

The more detail characteristics of individual Western Carpathian lithotectonic units are available in further text, describing them in the frame of their polyorogenic evolution.

3 Methodology of research

Research consisted of three decades of author's field geological mapping and study of relations of rock sequences with individual phases of orogenic cycles in the Western Carpathians, and in some special cases also besides this territory. This research was accompanied with structural analysis, revealing the overprinting relations and displacement kinematics of individual rock sequences and lithotectonic units (Németh et al., 1997, 2001, 2004; Németh, 2005a, 2018, 2021; Németh et al., 2012b, 2016, 2023 and references for structural and tectonic investigations in these publications). Ductile deformation was studied also by techniques of structural petrology (microtectonics; Németh, 2002). The deformation gradient within regional ductile shear zones was calculated by paleopiezometry, applied on monocrystalline calcite marbles and quartzites (Németh, 2005b; Németh et al., 2012a). Present study benefits also from published regional geological, tectonic and petrological results of hundreds other researchers from the Western Carpathians, Alpine-Carpathian-Himalayan belt and further parts of the world (cf. following works and references herein: Plašienka, 2018, 2021; Plašienka et al., 1997a, b, 1999, 2020); Putiš, 1992, 1994; Putiš et al., 2008, 2009a, b, 2019a, b, c, 2024; Radvanec et al., 2007, 2009, 2017; Radvanec & Németh, 2018; Kováč, 2000; Kováč & Plašienka, 2002; Kováč et al., 2002; Lexa & Konečný, 1998; Konečný et al., 2002; and many others).

For simple and efficient description of a succession of orogenic cycles and their phases, including overprinting relations within tectonic structures, the methodology of XD labelling was developed, intending to make the research of lithotectonic units (LTUs) and lithotectonic limits (LTLs) much more effective (Németh, 2021). The geological units (tectonic, sedimentary, magmatic, etc.), treated in this contribution, are presented in lithotectonic meaning (i.e. having attributed geodynamic aspects). Despite the terms *Unit* / *units* are in some cases preserved, in all cases they represent lithotectonic units (LTUs).

4 Geodynamic evolution of the Western Carpathians with emphasis on extensional tectonics leading to continental breakups, formation of elongation basins with oceanic-type crust along their axis and their closure during convergence – wider geodynamic considerations

The advantage of the Western Carpathians, as an appropriate study territory within the polyorogenic Alpine-Carpathian-Himalayan belt (Fig. 1A), is their distinct zonality and nearly symmetric northward convex oroclinal bending (Fig. 1B). Owing this zonality, the products of individual orogenic phases of three orogenic cycles (Variscan – VD, Paleo-Alpine – ApD and Neo-Alpine – AnD), as well as their tectonic and metamorphic overprints are decipherable directly in the field and can be easily studied by structural, microtectonic, petrologic and geochronologic methodologies. As indicated above, Alpine evolution in the Western Carpathians manifests a special case of two "intermingling" orogenic cycles –

Paleo-Alpine (Triassic-Cretaceous; ApD) and Neo-Alpine (Jurassic-Recent; AnD), which orogenic phases are time shifted.

Further information, describing the zonality of the W. Carpathians and their geodynamic evolution, are provided in summarizing contributions by Plašienka et al. (1997a, b) as well as Hók et al. (2019), but mainly in monographic issues edited by Grecula et al. (1997), Rakús (1998), Vozár and co-eds. (2010), Kováč (2000) and Janočko and Elečko (eds., 2003). Presently there was issued an extended paper about an Early Alpine tectonic evolution (**ApD**) of the Western Carpathian by Plašienka (2018). In the frame of Alpine-Carpathian-Dinaridic belt the orogenic evolution of W. Carpathians is treated by Schmid et al. (2008, 2020), van Hinsbergen et al. (2020) and a number of Polish authors, referred in chapter about AnD processes.

The Variscan and Paleo-Alpine continental breakups can be best characterized in the innermost zones of Internal W. Carpathians. The principal basement unit in this zone (red rectangle in Fig. 1B) is the *Gemeric Unit* (ApD), representing the ApD1c nappe overlier on north-located ApD *Veporic Unit*. The *Gemeric unit* is bearing superficial nappe outliers of *Meliatic Unit* (*Bôrka nappe*; ApD1b1; cf. Fig. 4) and *Turnaic* (*Tornaic* in Hungary) *Unit*. This basement and superficial nappes sequence was as a whole thrust over north-located *Veporic Unit* (ApD1c; cf. Fig. 4 – lower left side). Moreover – over both – the *Gemeric* and *Veporic units* the *Silicic Unit* was displaced at the end of ApD1 phase (cf. Fig. 4 – upper middle side). Two generations of continental breakups (Variscan and Paleo-Alpine) as well as their later convergent – collisional phases are in described region well proved with two continuous–course suture zones (Fig. 1B), but also by obduction and nappe displacement of two generations of exhumed ultramafic rocks and further ophiolite suite fragments (Fig. 6). The third generation Neo-Alpine continental breakup, registered in the W. Carpathians, is characterized by the course of *Pieniny Klippen Belt* as suture after the Alpine Tethys (Váhic) ocean, representing the boundary between Internal and External W. Carpathians.

4.1 Geodynamics of Variscan orogenic cycle revealed in the innermost zones of W. Carpathians

VD0 divergent – continental breakup phase

The Variscan continental breakup and riftogenesis in the Western Carpathian zone was well described owing to extended (the 1970s–2010s) geological-geophysical and geochemical research of *Gemeric Unit* (Grecula, 1982; Grecula et al., 1995 – Figs. 1.5 and 1.8 ibid.; Grecula & Kobulský – eds., 2011). This breakup (Fig. 5) was

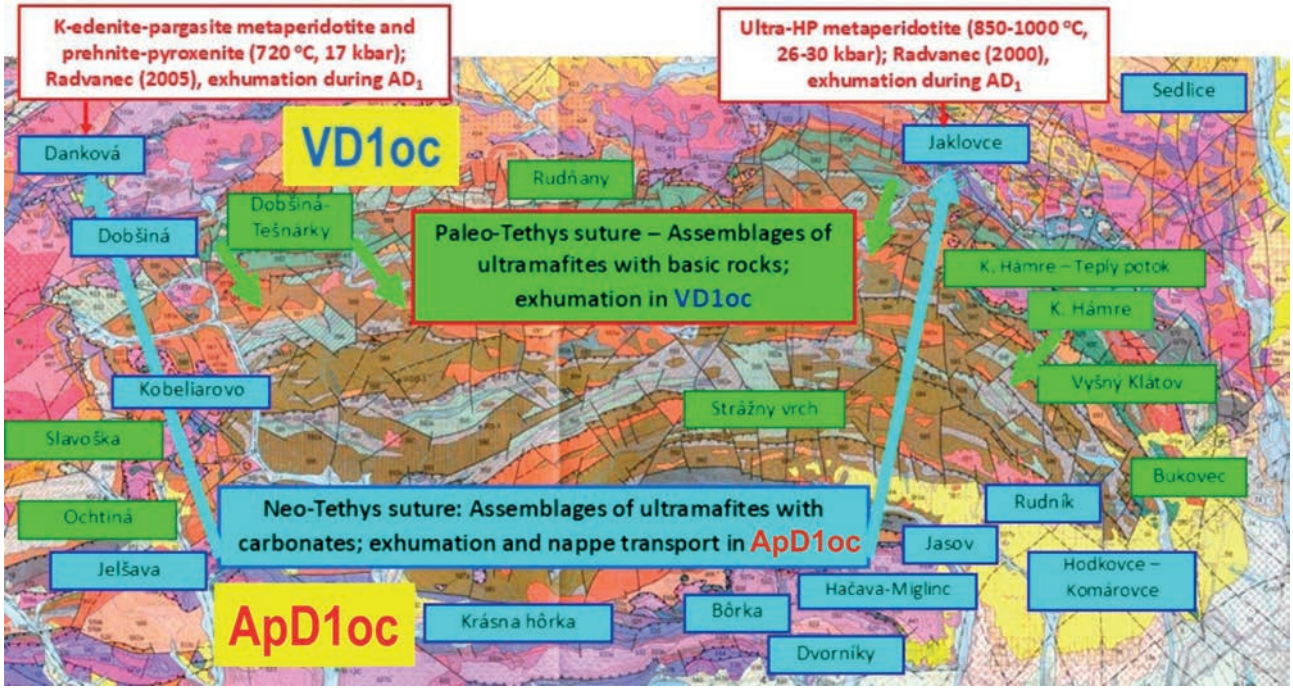

Fig. 6. Two generations of exhumed, obducted and locally distantly displaced ultramafic rocks in Gemeric region: Green colour – south-vergent VD1oc exhumation and obduction of Variscan Paleo-Tethys Rakovec basin ultramafics and other fragments of ophiolite suite, related to collisional closure of this basin. Blue colour – north-vergent ApD1co exhumation and collisional obduction of Paleo-Alpine Neo-Tethys Meliata basin ultramafics with ophiolites fragments. Compilation of data from Hovorka (ed., 1985) and Radvanec (2000, 2005). Basemap: segment of the map by Grecula in Mello and Ivanička (eds., 2008; reproduced with permission).

registered by Early Paleozoic riftogeneous **(VD0)** and later passive margin **(VD1a)** lithology of the **Gelnica LTU** (central part of the Fig. 4; originally defined as a lithostratigraphic group; Bajaník et al., 1983; Grecula et al., 2009), as well as the pre-subduction lithology of the **Rakovec** and **Klátov LTUs** (cf. left side column of Fig. 4), representing Variscan oceanic-type crust (Fig. 4 shows later – their VD1o obducted position on Gelnica LTU). Because Gemeric Unit (Gemericum) as LTU was individualized in Paleo-Alpine ApD1c phase, from the viewpoint of one generation earlier Variscan origin and evolution of Gelnica, Rakovec and Klátov LTUs, for the sake of correctness in naming – they belong to Variscan **Paleo-Gemeric Unit** (or **Paleo-Gemericum**).

The Paleo-Tethys passive margin sequences from the side of Gondwana – **Gelnica LTU** – were deposited on Pan-African basement. This situation is shown in Fig. 5, though the Pan-African coarse-detrital sediments are not present on recent surface due to their amputation during Early Alpine north-vergent **ApD1c** basement nappe displacement (Fig. 4 – this **ApD1c** amputation is shown below the column of Gelnica LTU). Progressing Variscan rifting on continental crust (cf. Figs. 4 and 5) was accompanied with changes in volcanosedimentary activity within three distinguished formations (Grecula, 1982): The lowermost Upper Ordovician-Silurian **Betliar Formation** (built of prevailing black phyllites and lydites in so-called Holec Beds; Fig. 4 – lower part of middle columg), next

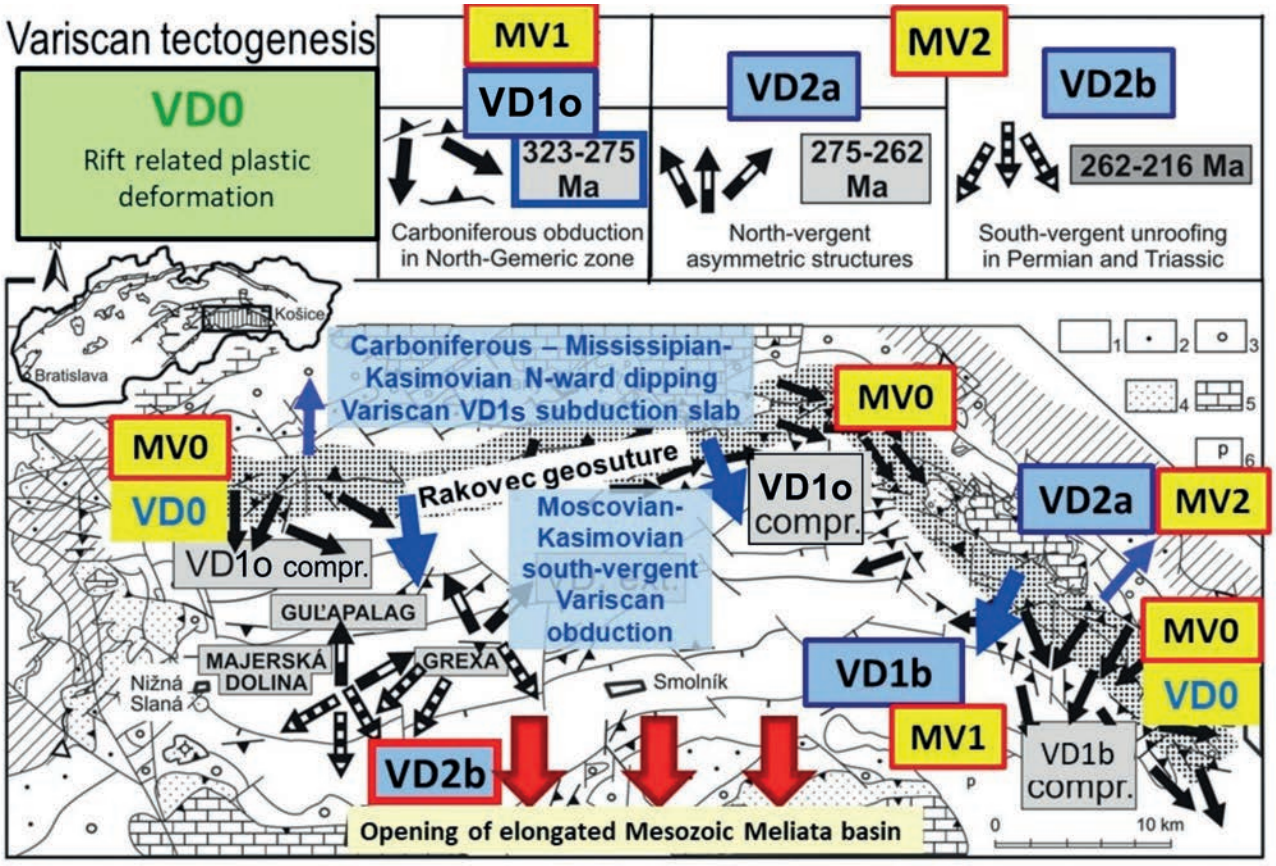

Fig. 7. Summary of field structural and microtectonic evidences of Variscan evolution in the Gemeric region of Internal Western Carpathians. Arrows indicate situation after Variscan VD1c collision with obducted sequences situated along Rakovec geosuture (suture zone) and before Paleo-Alpine ApD0 continental breakup and opening of new elongated Mesozoic Paleo-Alpine Meliata basin (Neo-Tethys; thick red arrows in the lower part of the figure indicating south vergent VD2b unroofing – indicated also in the summary Variscan geodynamic review in upper bar in Fig. 7). Red thick arrows targeted to south in lower part of Fig. 7 indicated start of the Paleo-Alpine Neo-Tethys continental breakup. The Variscan VD1c collision was preceded by VD1o Late Carboniferous south-vergent obduction partially of Rakovec, but mainly Zlatník and Klátov LTUs (terranes) on Gelnica LTU (cf. in Fig. 4). In localities of Guľapalag, Majerská dolina and Grexa, depicted in lower right side of the Fig. 7, the switch of Late Variscan unroofing from north-vergent (VD2a) to south-vergent (VD2b) was discovered by microtectonic studies (Németh in Radvanec et al., 2007). The sequence of Variscan kinematics and metamorphic overprints during Variscan obduction and later post-collisional unroofing is shown in bar in upper side of this figure. Explanation of lithology (rectangles in the right side middle): 1 – Lower Paleozoic sequences of Gemeric Unit, 2 – Carboniferous rocks of Gemeric Unit and its contact zone with Veporic Unit, 3 – Permian rocks of Gemeric Unit, 4 – Upper Paleozoic and Mesozoic rocks of Meliatic Unit, 5 – Mesozoic rocks of Silicic Unit, 6 – Paleogene cover.

Fig. 8. Variscan VD1o exhumation and obduction of HP-UHP rocks (Radvanec & Németh, 2018; reproduced with permission), being finished by Variscan collision VD1c with origin of Rakovec suture zone. **a** – Position of described segment of Rakovec geosuture (red rectangle) within Gemeric Unit and the W. Carpathians, **b** – Projection of Variscan planar and linear mesoscopic structures into the lower hemisphere of the tectonograms (Schmidt projection). **c** – Detail map with the occurrences of exhumed Cpx/SrEp metagabbro blocks (l.c.; item No. **1**) in the zone of Ostrá – Babiná – Šajby localities. Geological map by Grecula et al. (2009) was slightly modified and supplemented with new structural data. Lithology (cf. with Fig. 4): **Early Paleozoic of the Gemeric Unit** (Ordovician to Devonian) – **Hnilec Fm: 1** – **Cpx/SrEp metagabbro**; 2 – coarse-grained basalt (dolerite); 3 – basalt locally with thin intercalations of ultrabasic rocks, basalt metapyroclastics, green and violet phyllites; 4 – basalt metapyroclastics, locally with intercalations of green and violet phyllites, greenish and pinkish silicites and carbonates; 5 – basalt metapyroclastics, locally with fine-grained amphibolites, intercalations of keratophyre metapyroclastics and phyllites. **Smolník Fm.:** 6 – dark-green, green and yellow-green chl.-ser. phyllites with intercalations of violet hematite phyllites and basic, locally keratophyre metapyroclastics; 7 – crystalline to porphyroblastic violet-green chl.-ser. phyllites; 8 – crystalline to eyed green chl.-ms. phyllites, locally violet with intercalations of silicites, basalt and keratophyre rocks locally recrystallized in amphibolite facies; 9 – metamorphosed variegated volcanic complex. **Betliar Fm.:** 10 – black and grey gr.-ser. phyllites (alternation of light and dark lamina and bodies) with intercalations of metapsammites; 11 – alternation of coarse-laminated recrystallized to eyed grey to black gr.-bt. metapelites and metapsammites. **d** – The exhumed metagabbro mylonite in the Šajby locality situated in VD1 Rakovec suture zone manifests a pervasive Variscan ductile mylonitic foliation. As manifested also by tectonograms (**b**), the combination of WSW-ENE and ESE-WNW trending lineations and secondary foliation planes generally dipping to NWN-N, locally also to NNE, indicates the transpression kinematics in this phase of exhumation. The outcrop is penetrated by Alpine cleavage directed to NNW. **e-f** – hand-samples of exhumed metagabbro mylonite, showing recrystallization fabric from the magmatic phase and overprints by succession of tectonometamorphic events **MV1a** and **MV2** (more details are available in Radvanec & Németh, 2018).

the overlying Lower Devonian **Smolník Fm.** of Lower Variegated Volcanic Complex, green phyllites and flysch psammitic-pelitic sediments, as well as the uppermost Middle-Upper Devonian **Hnilec Fm.**, built dominantly of acid volcanic products. More distantly developed sequence of **Rakovec LTU** (Grecula & Kobulský – eds., 2011) have characteristic dominance of basic volcanic products in the Hnilec Fm. These facial changes place the Rakovec LTU to zone to evolving oceanic-type crust. In recent polyorogenic setting and erosional cut the Rakovec LTU consists of lithology of Variscan passive margin situated more distantly than marginal sequences of Gelnica LTU. On Rakovec LTU there were south-vergently obducted the sequences with remnants of Variscan oceanic crust (parts of Zlatník Group sensu Ivan, 1996; Ivan & Méres, 2012), but also blocks of ultra-high-pressure rocks – Cpx/SrEp metagabbro – being exhumed from the lower crust (cf. Radvanec, 1999; Radvanec & Németh, 2018; cf. Figs. 7 and 8). The magmatic activity along the Variscan VD0 mid-oceanic ridge is documented by the sequences of **Klátov LTU** (dominantly mafic and ultramafic rocks; cf. Figs. 5 and 6), together with Rakovec LTU marking **Variscan Upper Paleozoic continental breakup of Pangea** and mature stage of Variscan Paleo-Tethys oceanic-type crust (the metaophiolite suite of the Klátov gneiss-amphibolite complex, Cpx metagabbro, plagiogranite, as well as ultramafic rocks) and its multiple metamorphic overprint (MV0, MV1, MV2; Radvanec et al., 2017). The Klátov gneiss-amphibolite complex was earlier defined as Klátov Group (Spišiak et al., 1985), as well as the Klátov nappe consisting of the oceanic-type crust lithology (Hovorka et al., 1984; Hovorka, ed., 1985).

The polyorogenic evolution of the W. Carpathians and opposite dips of Variscan VD1s vs. Paleo-Alpine ApD1s subduction slabs and related exhumation vergencies – Variscan (south-vergent), but Paleo-Alpine (north-vergent) caused exhumation of two generations of ultramafic rocks – Variscan vs. Paleo-Alpine in age (Fig. 6). Besides exhumed Variscan VD1oc ultramafics (green rectangles in Fig. 6; generally south-vergent transport) also the presence of the younger – ApD1oc generation of ultramafic rocks was revealed, being exhumed from the Neo-Alpine Meliata zone (with generally north-vergent transport; blue rectangles;) and displaced over the territory of Gemeric Unit from the South-Gemeric Zone to the North-Gemeric Zone (Dobšiná and Jaklovce areas), and even more to the north of it to Danková and Sedlice areas on neighbouring Veporic Unit (the red rectangles in Fig. 7 contain an information by Radvanec, 2000, 2005).

VD1 convergent phase – origin of Rakovec suture zone

The Rakovec suture zone after Variscan elongated basin of Paleo-Tethys (Németh, 2002) is a product of Variscan convergence and south-vergent VD1c collision (earlier subduction slab with northern polarity; Fig. 8). Nowadays a large amount of data is available about Variscan ophiolite suite (Radvanec et al., 2017), as well as subduction and exhumation / obduction kinematics (Fig. 8; Németh, 2002 – Fig. 1 ibid.; Németh et al., 2012; Németh in Radvanec et al., 2007 – Fig. 28 ibid.; Radvanec & Németh, 2018). The exhumed sequences of Klátov, Zlatník and partly Rakovec LTUs were obducted south-vergent on former passive margin sequences of transitional Rakovec and Gelnica LTUs (cf. Figs. 4, 6 and 8; Németh, 2005a).

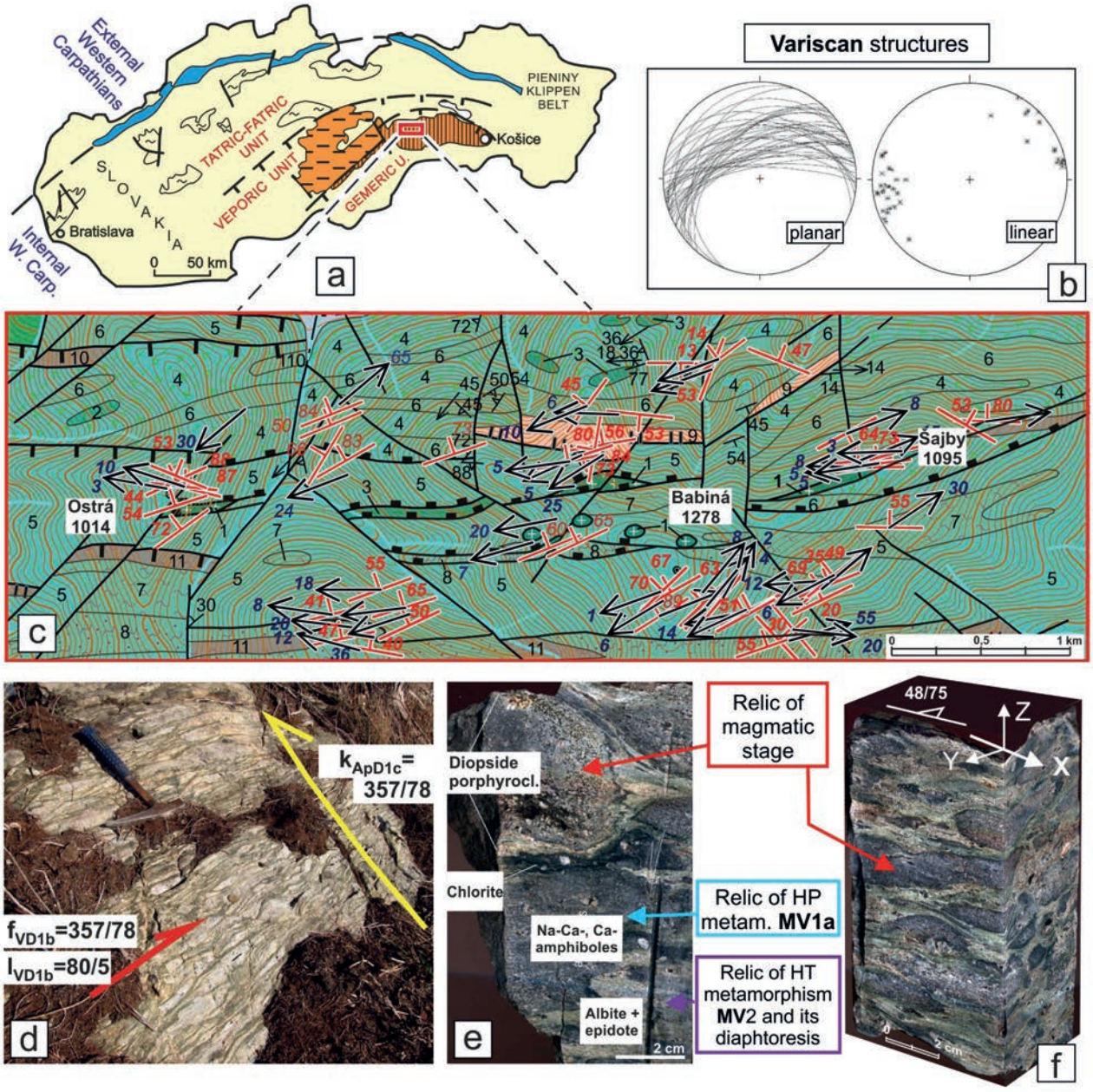

VD2 Variscan metamorphic core complex formation and related unroofing, initiating new continental breakup = new orogenic cycle

After the VD1c collisional closure of Variscan Rakovec Paleo-Tethyan basin, the rock sequences during the **Late Variscan post-collisional evolution VD2** were heated (Fig. 9) by the same linear subequatorial-course mantle convection current (ECMCC) as that causing the Variscan VD0 riftogenesis (cf. Fig. 10). This interpretation is based not only on assumption that there was no reason for the termination of heat production in ECMCC when the VD0 spreading zone was closed by collision. **The main proof of this concept of continual action of ECMCC is represented by numerous petrological evidences of VD2 amphibolite facies Permian overprints of already exhumed and obducted VD1o HP-UHP rock sequences and even the VD1c collided orogenic belt**. Important argument is also Permian, or even Triassic A-type magmatism / volcanism in zones parallel to orogenic belt (and besides of any remnant of former subduction slab), i.e. parallel with the ECMCC. Heating of rock sequences in formed orogenic belt over this still existing hot line caused also magmatic corrosion of the root of orogenic belt, heat induced uplift along the axis of orogenic belt,

metallogenesis (forming of ore veins in orogen parallel brittle fractures in the uppermost crust levels due to fluid influx), as well as unroofing to both sides of orogenic belt. The Permian metamorphism up to amphibolite facies and anatexis is commonly reported from the Gelnica Unit (earlier representing the Lower Paleozoic passive margin sequences; cf. Radvanec, 2007, 2009), as well as from the lithologies of exhumed Variscan ophiolite suite, incl. metagabbro, in Permian being already obducted and positioned on lithology of Gelnica Unit (Radvanec et al., 2017; Radvanec & Németh, 2018).

Our geodynamic considerations about Permian post-collisional evolution VD2 are based on generally accepted interpretation of Pangea, in Permian forming uniform supercontinent without active subduction processes. **This important moment in Earth's history – joining the whole continental crust into one – Pangea supercontinent – still encompasses one principal fact, may-be neglected in present geodynamic interpretations: The mantle convection in ring of subequatorial-course mantle bulge (ECMB) and related subequatorial-course mantle convection currents (ECMCCs), related to Earth's rotation had no reason to change their thermal-kinematic parameters at least during the Neo-Proterozoic-Phanerozoic time span.** So, all divergent / convergent processes in subequatorial trending polyorogenic zones are related to them. **This is the reason of their thermal contribution to Variscan (an earlier) orogenic processes in divergent phases (XD0), but also contributing with heat after subduction of the mid-oceanic ridge, and especially at the time after the collision (cf. Fig. 10). Using other expression – lithospheric plates were drifing on the Earth (some of them carrying continents), but the ECMB and ECMCCs remained in their same subequatorial circular position.** The polyorogenic processes driven with ECMB and related ECMCCs differ

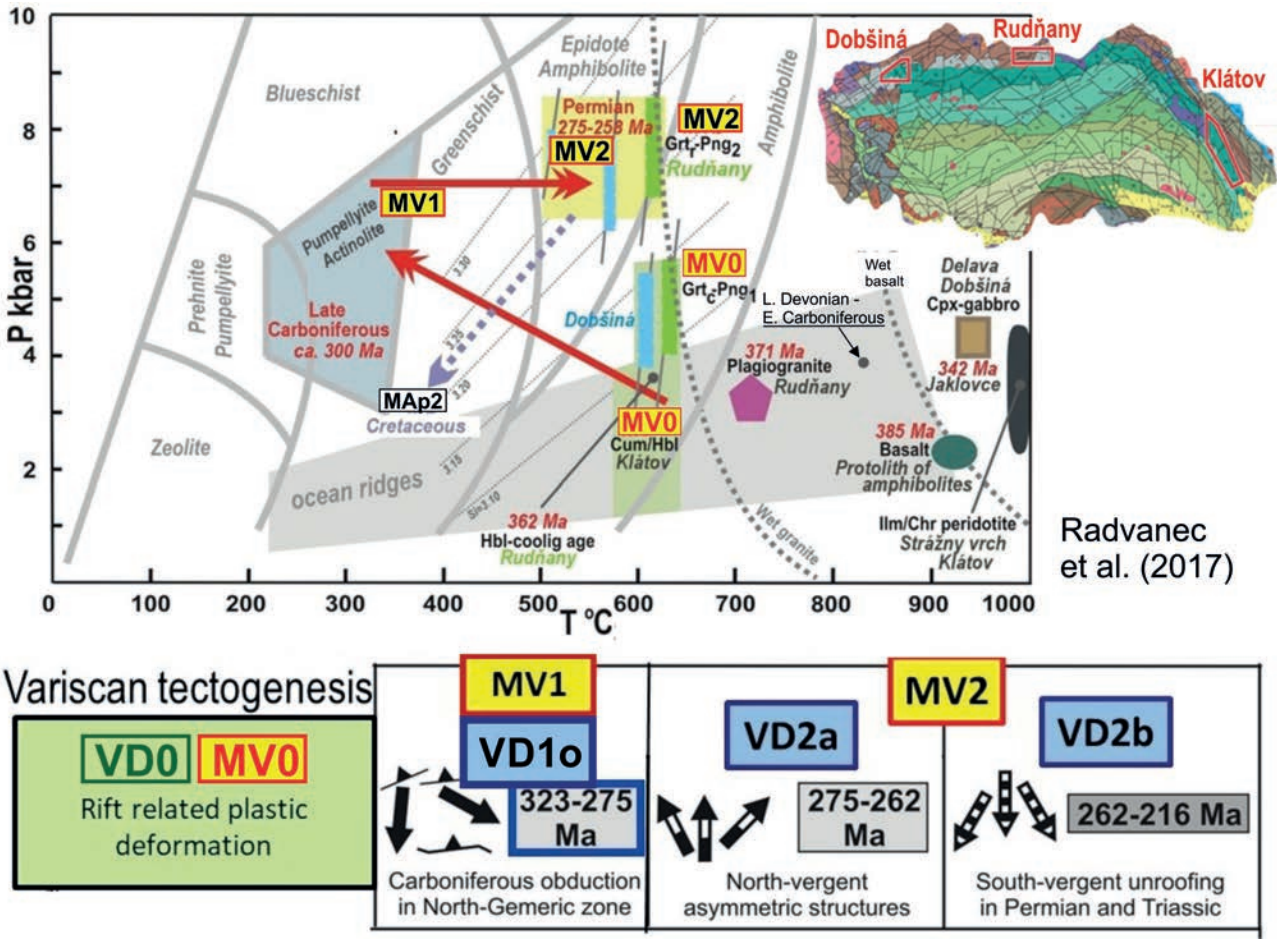

Fig. 9. Petrological proofs of the increase of MV2 temperature in Permian, postdating the MV1 Late Carboniferous metamorphic recrystallizatin at the beginning of Variscan exhumation of ophiolite suite sequences in Gemeric Unit (Radvanec et al., 2017; slightly modified, reproduced with permission). The map in right up side up of the figure shows localities of ophiolite suite along Rakovec suture zone in Gemeric Unit, where such metamorphic overprints of rocks were revealed. Bar in the lower part of the figure shows relations of individual metamorphic overprints (MVX) to orogenic phases (VDX).

from perpendicular meridian trending rifting and subduction processes driven by linear submeridian-course mantle convection currents (MCMCCs), being genetically more closely related to "classical" columnar mantle plumes with genesis interpreted by Dewey and Burke (1974) on example of N-S located series of rift-rift-rift (r-r-r) junctions in continental crust.

Magmatic evidences of VD1s and VD2 processes in the Western Carpathians

Until the moment of submerging of axis of the diverging zone (mid-oceanic ridge) under active margin of northern continent, the Upper Devonian-Lower Carboniferous I-type subduction-related granites in north-located Paleo-Tatric and Paleo-Veporic units were abundant. The additional convectional mantle heat caused switch of magmatism from I to I/S, or exclusively to S type magmatism. These later S-type granitoids differ from the I-type Veporic granitoids by increased contents of K, Rb, B, Y, U, Be, Sn, W, (F) and reduced contents of Sr, Ca and Ba and high Rb/Sr ratio. They can be distinguished also by high-iron biotite and mixed A-S-type zircon population. Most their attributes, including tourmalinization, are reminiscent of the granitoids known in the Permian post-collisional Paleo-Gemeric Unit (cf. Hraško et al., 1997). Due to the Permian orogen parallel convectional heat input the rocks underwent the thermal overprint leading to anatexis and origin of specialized S-type Gemeric granites. They belong to alkaline type with high SiO_2 content (73–78 wt. %) and distinctly peraluminous character – Shand's index A/CNK = 1.2–1.6, having low concentration of Sr, Ba, Zr and V (Tauson et al., 1977; Petrík & Kohút, 1997; Broska & Uher, 2001). High initial ratio is I_{Sr} = 0.711 9–0.714 4 (Kovách et al., 1979, 1986). The negative value $e_{Nd}(I)$ = –4.6 and increased values $d^{18}O_{(SMOV)}$ = 10 ‰ and $d^{34}S_{(CDT)}$ = 4.48 ‰ indicate that granites originated by remelting of continental crust sources (Cambel et al., 1989; Kohút et al., 1999, 2001; Kohút & Recio, 2002).

According to Kohút (2012), the granite apophyses in innermost territory of Internal W. Carpathians are derived from a huge underlying post-orogenic granite body 50 km long and 15 km wide, revealed by geophysics. This granite was generated by melting of crustal rocks of reworked Pan-African basement remnants which experienced earlier seafloor (VD0) weathering and were permeated by volcanic (boron) emanations, as well as finally modified by ore bearing fluids (l.c.). The emplacement of volatile-enriched magmas into upper crustal conditions was followed by deeper rooted porphyric magma portion, undergoing second boiling and re-melting to form the porphyric granite or granite-porphyry during its ascent (Broska & Kubiš, 2018). Variscan orogenic prograde metamorphism (MV2) was produced by high geothermal gradient, reaching 40–60 °C, being accompanied with the main post-collisional extensional tectonic events in orogenic belt (Radvanec et al., 2007). The Upper Permian–Lower Triassic (260–240 Ma), or even Middle and rarely Upper Triassic (225–205 Ma) monazite-uraninite isochrones in granites of southern zones of Internal Western Carpathians (IWC) orogenic belt (Radvanec et al., 2007, 2009) were not revealed in the northern zone of this orogenic belt. This fact confirms northward shift of lithosphere over the subequatorially directed linear source of convectional heat (hot line; ECMCC). The new Paleo-Alpine orogenic cycle – **ApD0 continental breakup** starts in Triassic and is exclusively localized in the southern zone of IWC. The northern zone of IWC reflects these processes by disjunctive tectonics.

According interpretation presented in our contribution, the northward shift of lithosphere over the axis of convectional heat (hot line) was documented also by geochronological data, demonstrating older ages of Variscan geodynamic processes in the northern zones of Internal W. Carpathians (IWC; Tatric Unit, Veporic Unit) – including the tectogenesis of the Rheic Ocean – then in southern zones of IWC (Gemeric Unit). The classical work by Finger et al. (2002) provides following general scheme of Variscan tectonometamorphic events: Collision in **IWC northern zones** within 370–360 Ma (probable related to closure of parallel Rheic Ocean) caused crustal thickening and orogenic (regional) metamorphism. Then at 360–340 Ma the decompression crustal melting acted, producing mainly S-types granites and at 340–310 Ma the post-collisional I-type plutons were generated. This scheme is supported also by geochronological results of other authors – Kohút et al. (2009), Radvanec et al. (2009) and Vozárová et al. (2020, 2021). The process of origin of post-collisional (Rheic collision) I-type plutons can be explained with contribution of heat produced by still acting Paleo-Tethys subduction (its subduction slab was dipping just beneath that collisional zone). In the **IWC southern zones** (Gemeric Unit) the collision terminated later – inbetween Kasimovian and Gzhelian of Pennsylvanian (uppermost Carboniferous; 303 Ma).

The Mid-Permian ages of S and A-type plutons were uniformly proved by numerous researches (Finger et al., 2002; Villasenor et al., 2021; Vozárová et al., 2012, 2016). In the Infratric Inovec nappe in Považský Inovec Mts the 267–262 Ma rhyolite intercalations occur in Permian siliciclastics, as well as rhyodacite dyke in micaschists (Putiš et al., 2016). The rhyodacite dyke suggests the within plate acid volcanism, typical for the Pangea breakdown and rift-related volcanism (l.c.).

As documented by results of several generations of Western Carpathian geologists, from the uppermost

Carboniferous (Gzhelian) throughout Permian and Triassic on both sides of Paleo-Gemeric collisional belt the VD2 extension started to produce orogen parallel sedimentary basins (Fig. 10; VD2 and ApD0 phases). For the sake of more precise expression the north-vergent unroofing we mark as **VD2a** and the south-vergent one as **VD2b** (Fig. 7). The north-vergent unroofing VD2a ended in Triassic, and dominant for the further evolution of the W. Carpathians

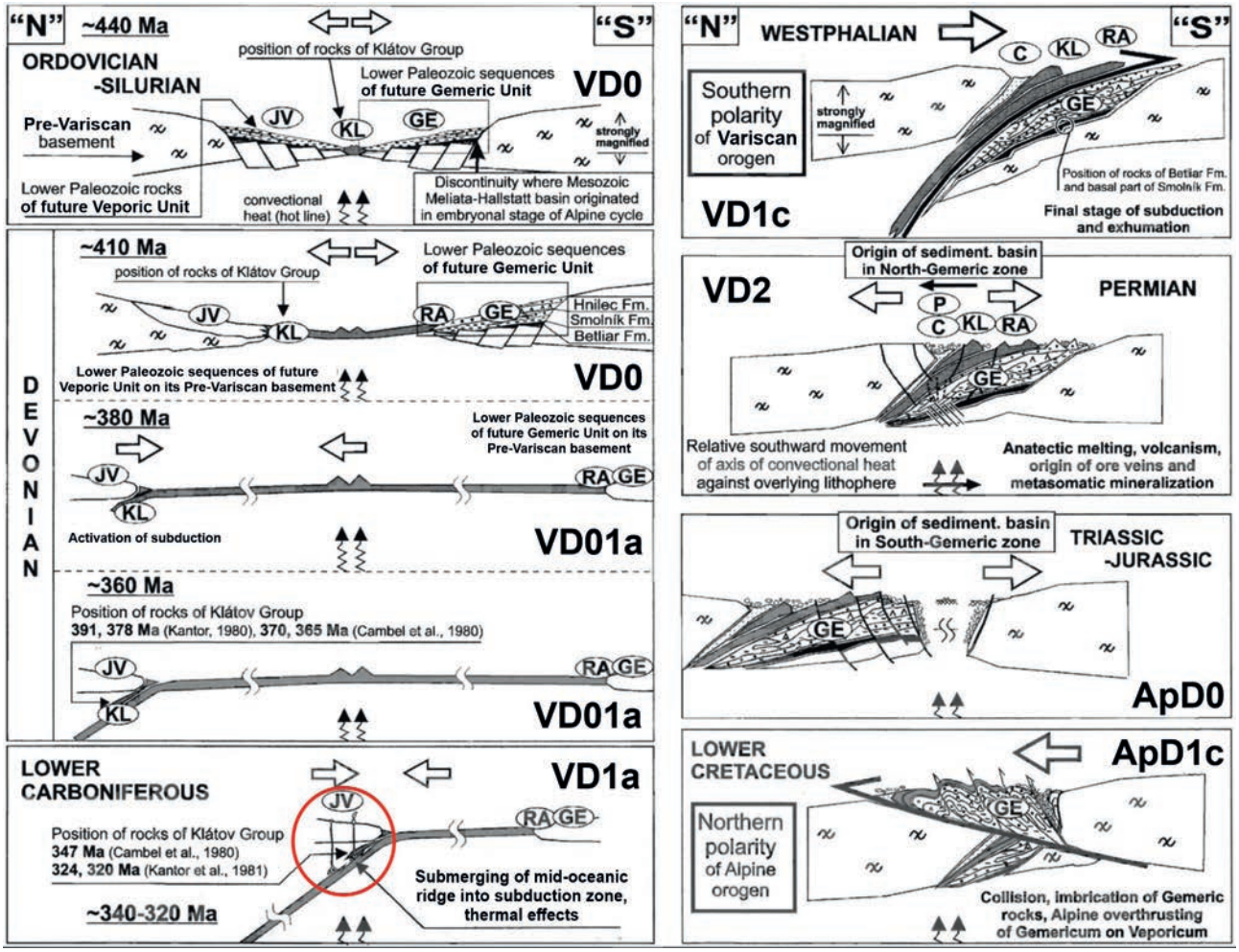

Fig. 10. Pilot concept of the role of hot lines (ECMB and ECMCCs) in polyorogenic evolution (Németh, 2005; slightly updated; reproduced with permission). Differing from traditional plate tectonic interpretations – in this model both – the Variscan spreading zone (VD0 mid-oceanic ridge), as well as the source of convectional heat (hot line) after progress of subduction (subducting ca half of the basin width = segment between the trench and the rift – will appear over the hot line (marked by red circle in the left down side of figure for lower Carboniferous evolution). The convection heat in position beneath the continental arc contributes to processes of magmatism / volcanism, including the mineral deposits formation. After subducting of the whole oceanic-type crust this convection heat contributes to metamorphic and granitization processes in collisional (orogenic) VD1c belt (including the unroofing to one or both sides of orogenic belt and opening of orogen parallel brittle fractures for fluid ingress and origin of vein mineralization; for details see Fig. 11). **Shift of lithosphere over this linear heat source (hot line; black horizontal thin arrows in VD2 part of the figure) causes the shift of lithosphere and developing of a new divergence zone away from the axial zone of former orogenic belt** (in this particular case it is the start of a new – post-Variscan Paleo-Alpine orogenic cycle; ApD0). Visualization in the left shows Variscan divergent and convergent evolution finishing with Variscan collision in Upper Carboniferous (Kasimovian; VD1c; upper right segment of the figure). Northward shift of lithosphere over this hot line caused new divergence and Paleo-Alpine ApD0 opening of Triassic-Jurassic basin of Neo-Tethys (Meliata) Basin. Lower Cretaceous ApD1c closure of this basin (right down segment of the figure) produced in the Western Carpathians a new metamorphic core complex (MAp2). Explanation of abbreviations (for further details see also lithotectonic column in Fig. 4): **JV** – South Veporic Unit, representing north Ordovician / Silurian passive margin of Paleo-Tethys and in Devonian / Carboniferous the active margin of Laurasian lithospheric plate; Gemeric Unit: **GE** – Gelnica lithotectonic unit (LTU) of Variscan passive margin, **RA** – Rakovec LTU represents generating Variscan oceanic-type crust, **KL** – *Klátov LTU – lithology of Variscan mid-oceanic rift zone;* **C** – Carboniferous syntectonic sequences, **P** – post-collisional cover sequences of Uppermost Carboniferous (Stephanian) and dominating Permian age (cf. positions of these lithologies in Fig. 4).

became the south-vergent extension and unroofing VD2b, leading in Jurassic to opening of elongated Neo-Tethys Meliata oceanic basin. (If not stated explicitly – in this article the designation VD2 indicates the south-vergent unroofing, which is principal in further evolution).

Revealing that north of the axis of orogenic belt the unroofing evolution stopped in Triassic, but south of the belt it continued to Jurassic (Fig. 11), leading to opening of Meliata Neo-Tethys basin, we interpret the northern shift of orogenic belt with respect to hot line (ECMCC heat). The translation / drift of lithospheric plates is common phenomenon (interpreted already from the Wegener's and Holmes' time; the 1920s). The opposite alternative – change of position of mantle bulge of subequatorial course to south in relation to fixed lithosphere – was not proved yet by geo-sciences and it has no meaning concerning the Phanerozoic Earth's geodynamics. Other reason of the opening the elongated Meliata Neo-Tethys basin does not exist, because the pre-collisional (pre-VD1c) dip of Paleo-Tethys subduction slab was to the north – just to the opposite side with respect to originated Meliata basin, i.e. an interpretation of eventual back-arc position of the Meliata basin with respect to Variscan one can be excluded.

The shift of lithosphere over hot lines resulting to continental breakups we interpret as the peculiarity of polyorogenic processes in zones of subequatorial direction (Figs. 10 and 11).

VD3 Variscan intraplate stress consolidation

Disjunctive structures of this Variscan phase are not unambiguously defined because of younger overprints by tectonic processes of two subsequent orogenic cycles. Their existence is very probable and they could represent weakened zones for preferred establishing of younger (ApD and AnD) disjunctive structures.

VD4 Variscan phase of regional extension

Equatorial and meridian trending faults of VD4 phase acted simultaneously with originating dominant extensional orogen parallel basins north and south of Variscan orogenic belt. The Permo-Triassic pure shear type transcrustal discontinuities can be manifested also

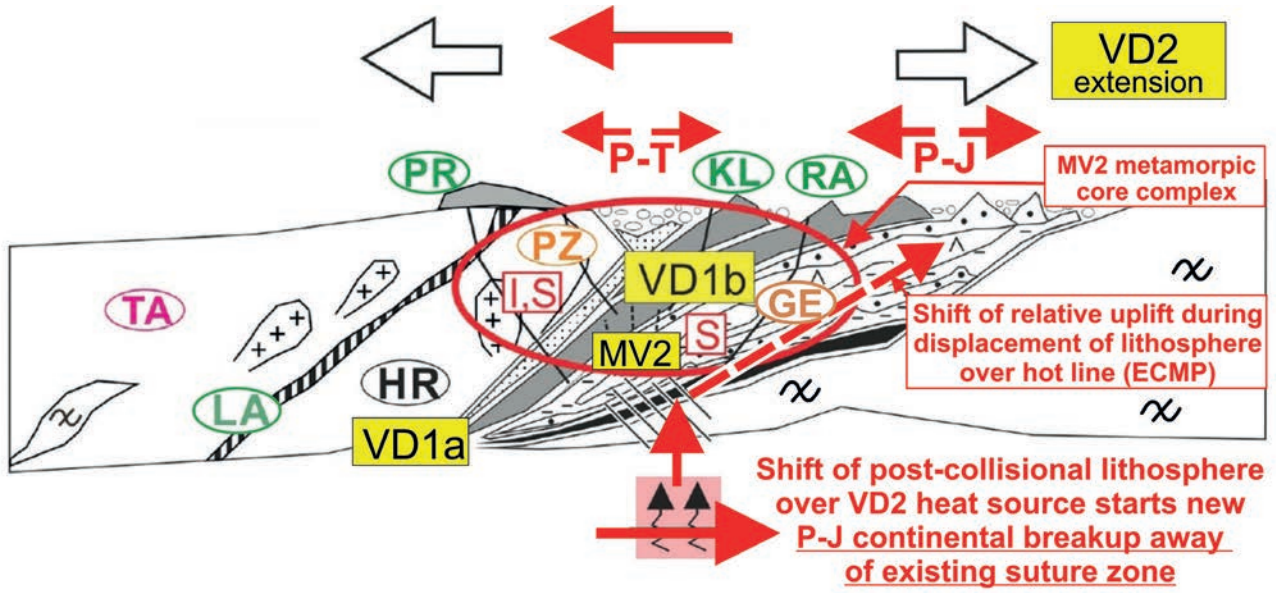

Fig. 11. Variscan post-collisional evolution in inner zone of Internal Western Carpathians leading to **Paleo-Alpine continental break-up and opening of elongated Neo-Tethys Meliata basin** (detail of general VD2 scheme in Fig. 10). In presented interpretation all geodynamic processes in polyorogenic zones are caused by a convection heat of linear course (ECMCC), parallel with the zone of equatorial-course mantle bulge (ECMB). This heat causes the orogen parallel uplift of VD1 collided zone and VD2 unroofing on both sides of bulging belt, resulting in origin of elongated basins on both sides of orogenic belt. In the case of Paleo-Gemeric bulging the evolution in north located basin stopped in Triassic, but the south located basin developed continually to Jurassic. This we interpret as a consequence of the northward shift of post-collisional lithosphere in Permian-Jurassic, being accompanied in Jurassic with ApD0 spreading with production of Neo-Tethys oceanic-type crust. Explanation of used symbols for lithotectonic units (LTUs) is from the left side: TA – Paleo-Tatricum, mainly crystalline basement, LA – Layered amphibolite complex, HR + PZ – Hron and Pezinok LTUs – both represent continental crust north of Rakovec suture zone (which is shown in this figure by dark grey colour slices), PR + KL + RA – Pernek, Klátov and Rakovec LTUs – ocean-type and transitional crust of Variscan Paleo-Tethys Rakovec zone, GE – Gelnica LTU – Paleozoic sequences of Variscan passive margin south of Rakovec zone. Convectional heat caused the MV2 metamorphic overprint of collided rock sequences in suture zone and generating metamorphic core complex. Northward shift of lithosphere over the hot line (ECMCC) caused the change of geochemical character of generating granites – from I-type to specialized anatectic S-type (marked by letters I and S in rectangles). For further details see Németh et al. (2016) and Putiš (1994); cf. Figs. 4, 7, 9 and 10.

by numerous A-type non-orogenic magmatic and volcanic bodies, known in the Western Carpathians and located in orogen-parallel position.

4.2 Geodynamics of Paleo-Alpine (Mesozoic) orogenic cycle in the W. Carpathians

The Paleo-Alpine (ApD) Mesozoic orogenic cycle in the Western Carpathians has attracted attention of geologists already from the time of pioneering works of Dionýz Štúr (1827–1893). Divergent and convergent orogenic phases ApD0 and ApD1 of Paleo-Alpine evolution, as well as post-collisional evolution ApD2 are presently comprehensively documented regarding their causes, kinematics and products. Similar as at Variscan orogenesis, a novel point of our interpretation is a principal role of Paleo-Alpine post-collisional ApD2 evolution for Upper Cretaceous Penninic (Váhic, Magura) continental breakup and a convection heat contribution of the same hot line (ECMCC) as in the Variscan evolution and Paleo-Alpine divergent processes. Moreover, similarly as at Variscan orogenic phase **VD1se** (index "**se**" means subduction exhumation, resp. exhumation during subduction), describing the exhumation peculiarities of rotated rigid blocks (megaporphyroclasts) during subduction VDs, also in Paleo-Alpine we have found relics of **ApD1se** – the syn-subduction exhumation megaporphyroclasts ("exhumation balls") – moving in ductile environment of subduction slab upwards against "the flow" of subducting rocks. The findings in the Western Carpathians can be applicable also in other segments of polyorogenic Alpine-Carpathian-Himalayan belt, and evidently also in other relevant places in the world (cf. Fig. 13G).

For general information about the Paleo-Alpine orogenesis in the Western Carpathians we recommend to reader the summarizing monographs by Grecula, Hovorka and Putiš (eds., 1997), Rakús (ed., 1998), Vozár (and co-eds., 2010) as well as review paper by Hók et al. (2020). The schematic visualization of the sequence of Paleo-Alpine events, following after the Variscan ones and preceding the Váhic-Penninic Neo-Alpine ones is in Németh et al. (2016; Fig. 1 ibid.).

ApD0 divergent phase

As documented in previous text, the asymmetric – dominantly south-vergent VD2b unroofing (VD2 in further text for simplifying the designation) led to opening of Neo-Tethys Meliata basin with formation of oceanic-type crust in Jurassic. During this basin evolution, after thin Lower Triassic detrital sequence and dominant Middle / Upper Triassic carbonatic sequence of marginal *Silicic* and *Turnaic (Tornaic)* units, the sequences of Meliatic Unit represented the basin axial zone and started to be intercalated by basic volcaniclastic material and later there originated the spreading zone with basaltic volcanism. The Paleo-Alpine AD1s subduction and MAp1s HP metamorphic recrystallization changed the basic volcanic / volcaniclastic rocks to glaucophanites. The asymmetric structures demonstrate their north-vergent exhumation (Figs. 12 and 13F) and ApD1o obduction on Gemeric Unit. The remnants of the obduction ApD1o Bôrka nappe outliers, bearing also ApD1se "exhumation balls" occur in the Dobšiná area (Fig. 13C + E) as well as in the Jaklovce area (Fig. 13B + D). The Bôrka nappe consists mainly of high-pressure recrystallized limestones, basic and ultramafic rocks. Within the Internal W. Carpathians, the pre-metamorphic lithology of ApD0 *Silicic*, *Turnaic (Tornaic)* and *Meliatic units* is presently on display dominantly in ApD1o nappe outliers positioned on older units (cf. upper side of Fig. 4). Concerning the ApD0 as well as ApD1 geodynamic evolution, the research of numerous authors was focused mainly on *Meliaticum / Bôrka nappe* sequences, providing the principal information about tectogenesis of Paleo-Alpine orogenic cycle (Kozur & Mock, 1995; Mock et al., 1998; Mello et al., 1998; Németh, 2005b; Ivan et al., 2009; Putiš et al., 2011; Németh et al., 2012).

ApD1 convergent phase – origin of Meliata suture zone

Besides geophysics and volcanic manifestations, the southern dip = southern polarity of the Neo-Tethys Meliata subduction slab was proved also by dominant north-vergent ApD1oc obduction and collision kinematics, building present north-vergent basement / cover nappes setting of the whole Internal Western Carpathians. Minor part of the collision fan was thrust to south, building e.g. the Bükk Mts in the present Hungary.

The Paleo-Alpine ApD1 north-vergent kinematics in the innermost zones of Internal W. Carpathians (Fig. 12; cf. Figs. 4, 6 and 10), encompassing *Gemeric Unit*, southern zone of *Veporic Unit* as well as superficial *Bôrka nappe* (exhumed HP sequences from the Meliata subduction slab), was proved parallel with other authors (extensively referenced above in this subchapter 4.2) also by regional structural as well as microtectonic research applying oriented rock samples (Németh, 2002; Fig. 1 ibid.). Proofs of allochthonous position of the *Meliatic Bôrka nappe* on sequences of the North-Gemeric zone in Jaklovce area (cf. Fig. 12 right side) by Németh (2005b) and Németh et al. (2012a) have excluded the existence of so-called Northern branch of the Meliata Ocean (sensu Kozur & Mock, 1995). Extremely high differential stresses in the frontal part of the Bôrka nappe in the Jaklovce area, revealed by paleopiezometry (Németh et al., 2012a), indicate fast exhumation and north-vergent nappe displacement by the superficial nappe kinematics, which has preserved the state of strong dynamic recrystallization – extreme grain-size reduction in marbles inside the subduction zone, occurring now "fro-

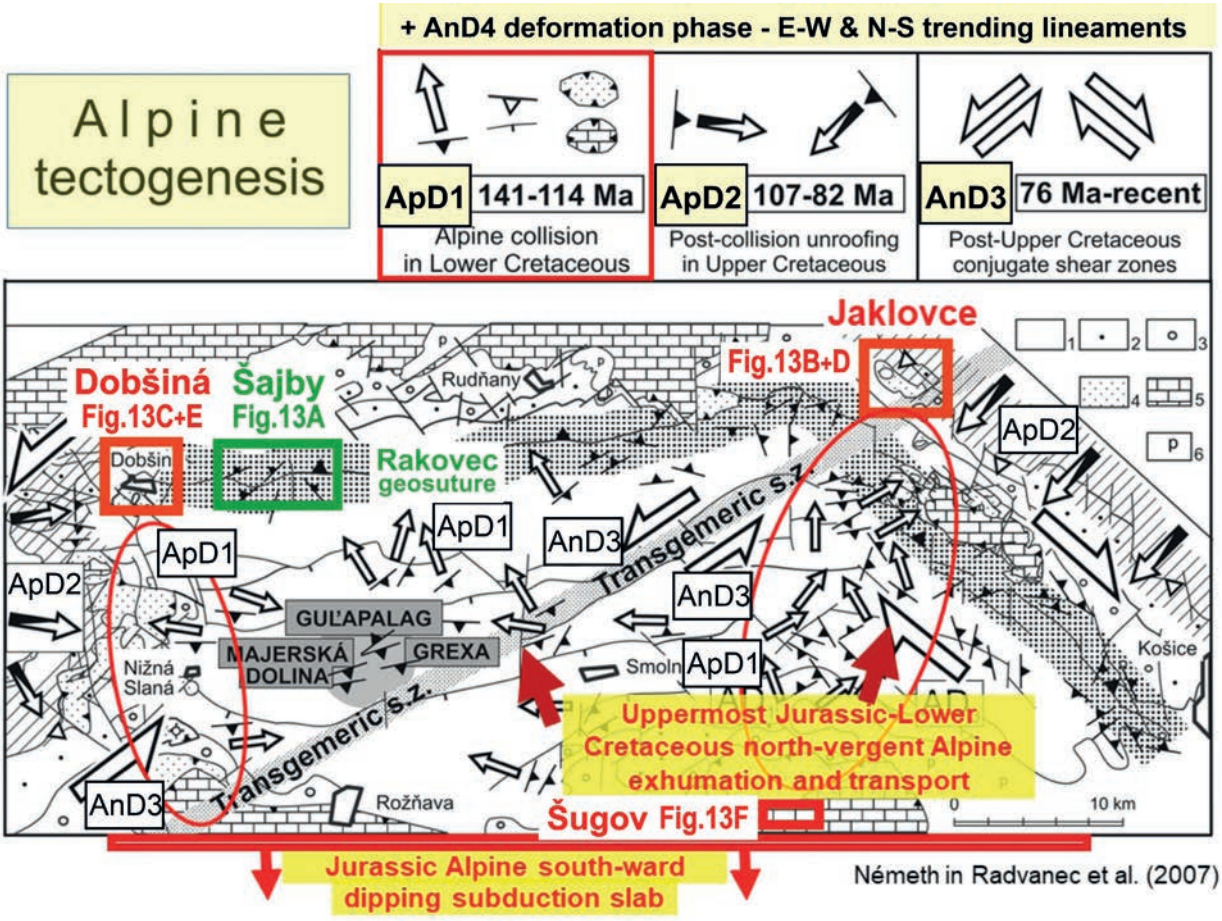

Fig. 12. Review of kinematics of Paleo-Alpine events in inner zone of Internal W. Carpathians: ApD1 – Early Cretaceous north-vergent obduction and collision thrusting – red ellipses mark transport of the Bôrka nappe Neo-Tethys Meliatic HP ophiolite suite sequences from the closing Meliatic basin over the Gemeric Unit to areas of Dobšiná and Jaklovce municipalities in the North-Gemeric zone. Similarly as in Variscan subduction-obduction process VD1so there was revealed a special type of syn-subduction exhumation (VD1se; ApD1se), being manifested by "ball-shaped" individualized megaporphyroclasts of rigid rocks in exhumed rock suite (cf. Fig. 13A–F; position of characteristic localities bearing such exhumation products – in Rakovec geosuture – Šajby – VD1se; as well as Šugov, Dobšiná and Jaklovce – ApD1se – is visualized in schematic map of Fig. 12). Further explanation of this special kind o exhumation is in explanation to Fig. 13 and the text. ApD2 – Late Cretaceous south-vergent post-collisional unroofing of Gemeric Unit from Veporic one. Present apparently opposite unroofing trend to SW in the eastern segment of the Neo-Alpine oroclinal bend (in present geological setting) and to E and SE in western segment of this bend was caused by younger bending due to conjugate system of Neo-Alpine AnD3 shear zones (dextral ones trending NW–SE and sinistral ones trending NE–SW; cf. Fig. 15C). This complicated tectonic setting of Internal W. Carpathians is further segmented by the Neo-Alpine AnD4 E–W and N–S trending pure-shear type regional faults / lineaments (not shown in this figure due to sake of simplification).

zen" in frontal parts of the nappe. This completely differs with the situation in the rear parts of this nappe, where input of convectional heat from the hot line to the rock volume, including that present in subduction slab, caused static recrystallization and growth of new large calcite grains at the expense of older small dynamically recrystallized calcite grains. The process of static recrystallization is a reason of lowered differential stresses revealed by paleopiezometry (l.c.).

The suture zone after Neo-Tethys Meliata basin is located at the southern margin of Gemeric Unit in so-called Rožňava discontinuity zone. In this zone, the extended ultramafic body large of several square kilometers and moderately inclined to south is present and was documented also by boreholes and N–S trending magnetotelluric profile in the eastern part of *Gemeric Unit* (Pavliszyn, 1980, in Grecula et al., 1995). These ultramafic rocks were partly displaced northward over *Gemeric Unit*, forming ApD1o nappe outliers at Dobšiná and Jaklovce localities in the North-Gemeric zone or even besides *Gemeric Unit* in Danková and Sedlice localities (cf. Fig. 6, blue rectangles). The northern vergency of displacement is demonstrated by numerous asymmetric structures at outcrop scale as well as in microscale.

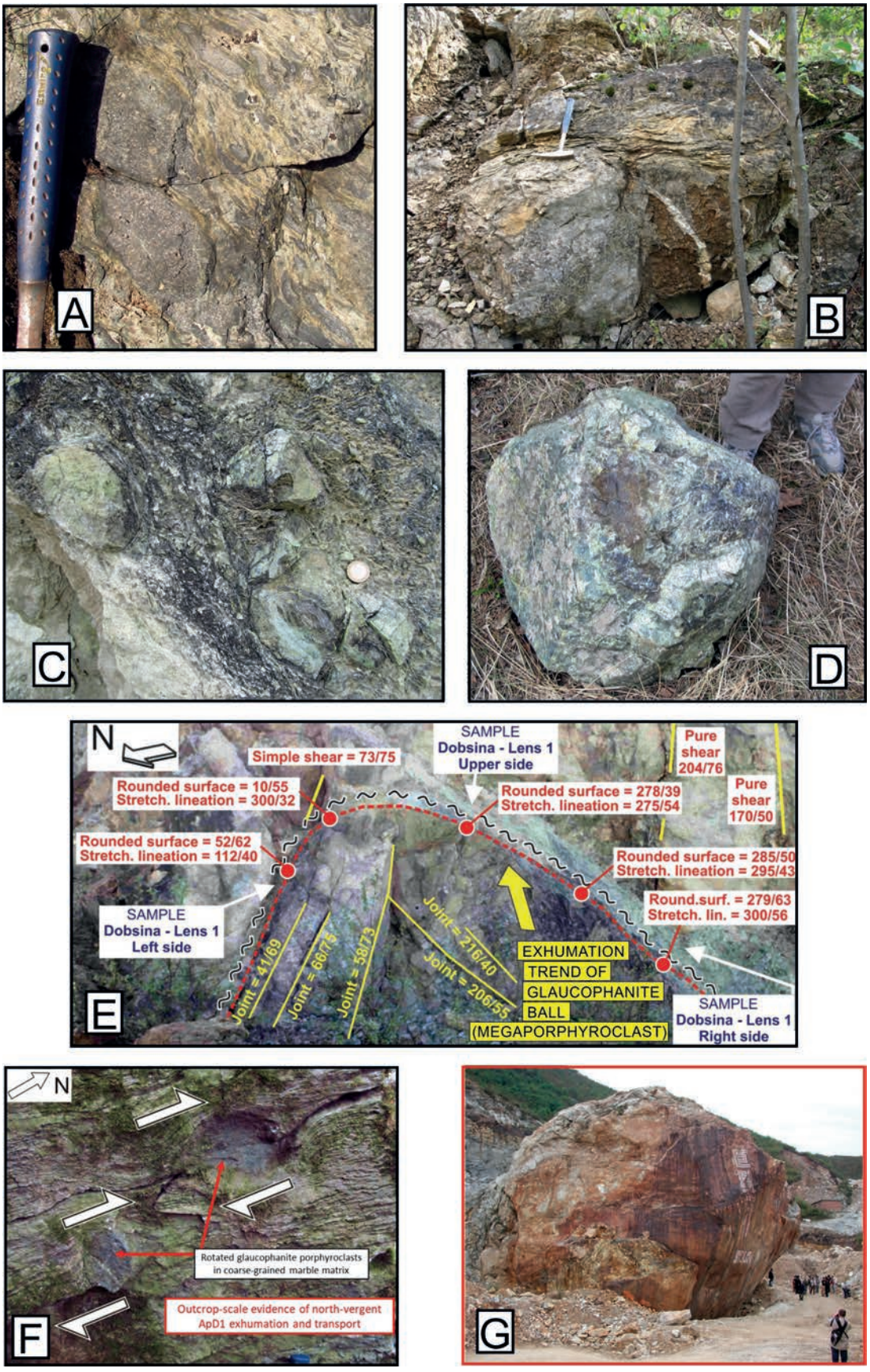
A
B
C
D
N
Simple shear = 73/75
SAMPLE
Dobsina - Lens 1
Upper side
Pure
shear
204/76
Pure
shear
170/50
Rounded surface = 10/55
Stretch. lineation = 300/32
Rounded surface = 278/39
Stretch. lineation = 275/54
Rounded surface = 52/62
Stretch. lineation = 112/40
Rounded surface = 285/50
Stretch. lineation = 295/43
Round.surf. = 279/63
Stretch. lin. = 300/56
SAMPLE
Dobsina - Lens 1
Left side
Joint = 41/69
Joint = 66/75
Joint = 58/73
Joint = 216/40
Joint = 206/55
EXHUMATION
TREND OF
GLAUCOPHANITE
BALL
(MEGAPORPHYROCLAST)
SAMPLE
Dobsina - Lens 1
Right side
E
N
Rotated glaucophanite porphyroclasts
in coarse-grained marble matrix
Outcrop-scale evidence of north-vergent
ApD1 exhumation and transport
F
G

Fig. 13. Exhumed megaporphyroclasts – products of syn-subduction exhumation. **A** – Variscan VD1se exhumation revealed in the Rakovec suture zone in the Šajby mountain range – the exhumed metagabbro megaporphyroclasts reach dimensions up to 25 cm. **B + D** – The ApD1se marble, chert and peridotite megaporphyroclasts in the Jaklovce locality of Meliatic Bôrka nappe outliers reach meter dimensions; for more information read article by Németh et al. (2012). **C + E** – The ApD1se megaporphyroclasts of Meliatic Bôrka nappe outlier at Dobšiná town (abandoned chrysotile asbestos quarry) represent mainly rounded glaucophanites in serpentinite matrix. Individual glaucophanite porphyroclasts reach here the diameter up to 3 m (Fig. 13E). **F** – Evidences of north-vergent exhumation directly in Paleo-Alpine suture zone in the Šugov valley: Glaucophanite sigma and delta porphyroclasts in pre-metamorphic (pre-MAp1s) state represented the ApD0c basic pyroclastic interbeds in limestones – products of the volcano-sedimentary evolution at the margin of widened Meliata Ocean. During ApD1s subduction the pyroclastic material as well as limestones were recrystallized to glaucophanites and calcitic marbles and during syn-subduction exhumation glaucophanite bed was disintegrated and underwent in ductile environment of calcitic marbles the reverse transport towards the surface in form of individual porphyroclasts of dimensions up to 20 cm. **G** – Presently probably the largest exhumed gigaporphyroclast in the world – jadeite in serpentinite matrix in Xiuyan Jade Mine, Anshan, Liaoning, China. For comparison of its enormous dimensions see standing persons on the right side of exhumed gigaporhyroclast. Authors of pictures: A–F – Zoltán Németh, G – Martin Radvanec.

ApD2 metamorphic overprint in South-Veporic zone and related unroofing tectonics leading to Neo-Alpine continental breakup north of Paleo-Alpine orogenic belt

The Paleo-Alpine Lower Cretaceous ApD1 collision produced dominant north-vergent setting of the Internal Western Carpathians. The strongest post-collisional thermal overprint MAp2 of post-ApD1c thickened continental crust was revealed in the South-Veporic zone, being overthrust by Gemeric basement nappe as well as superficial nappes dominantly of the *Silicic* and *Meliatic units* (the *Bôrka nappe*; cf. Fig. 4). This MAp2 thermal overprint of thickened crust we interpret (similarly as in the case of earlier Variscan MV2 thermal overprint during VD2 phase) as the consequence of mantle convection (hot-line) heat contribution (Németh et al., 2016). Thermobarometric data document in South-Veporic zone increasing PT conditions from ca 500 °C and 7–8 kbar to ca 620 °C, 9–10 kbar, reflecting a coherent metamorphic field gradient from greenschists to middle amphibolite facies (Janák et al., 2001a, b). The $^{40}Ar/^{39}Ar$ data obtained by high spatial resolution in situ ultraviolet (UV) laser ablation of white micas constrain the timing of cooling and exhumation to Late Cretaceous (77 a 73 Ma). Anatectic melt at 650 °C and 9 kbar bound to local unroofing ApD2 normal fault was revealed also by Radvanec (1994). The geochronological data of the Upper Cretaceous Rochovce granite crystallization in the western segment of unroofing zone of Gemeric Unit from Veporic Unit provide 82 ± 1 Ma U-Pb age of zircon population (Hraško et al., 1999). Mineralization related to Rochovce granite provided Re-Os ages of 81.4 ± 0.3 Ma and 81.6 ± 0.3 Ma (Kohút et al., 2013). The Rochovce granite is bearing the northernmost occurring Cretaceous calc-alkaline magmatism mineralization in the Alpine-Balkan-Carpathian-Dinaride metallogenic belt (l.c.). The ApD2 unroofing normal faults locally crosscut the ore bodies of U-Mo deposit Košice I – Kurišková, situated in the eastern Gemeric segment of the Gemeric-Veporic unroofing zone, and by this way they form the pathways for remobilization of the U mineralization to hanging wall of the main ore body (cf. Kohút et al., 2013; Szabó et al., 2014).

The MAp2 thermal overprint in South-Veporic zone and ApD2 unroofing kinematics were revealed as the key factors in Upper Cretaceous MAp2 talc genesis from the former Paleozoic limestones protolith, being in Permian replaced to magnesite (Figs. 14 and 15).

Similarly as in the case of Variscan VD2 evolution, where unroofing from the uplifting orogenic belt was double sided, but principal in following evolution there became the south-vergent unroofing – i.e. to the opposite side of orogenic belt to that side, where the VD1c thrusting took place, also within the Paleo-Alpine evolution, leading to opening of younger generation Váhic – Alpine Tethys and Magura elongated orogen parallel oceanic basins, the same principle took place, though in opposite spatial orientation: The ApD1 processes and collision were located south of VD orogenic belt, with dip of ApD1s subduction zone to south and acting north-vergent ApDoc obduction and collision – but the final Neo-Alpine AnD0 opening of elongated oceanic space was located north of uprising ApD1 orogenic belt. This principle, documented in both (VD and ApD) subsequent orogenic cycles, clearly manifests that the dip of subduction slab is a criterion for the same lithosphere shift direction over the still lasting convection heat of subequatorial-course mantle convection current. At VD1s subduction, the slab was dipping north and later collided VD1c orogenic belt was displaced also to north over the ECMCC, at ApD1 subduction the slab was dipping south and collided ApD1 orogenic belt was displaced also to south over the ECMCC. At the beginning of the plate tectonic concept postulation this phenomenon was defined as the subduction slab pull. Despite – in our concept **the subduction is not a reason of geodynamics, but it is a consequence due to the convection heat mantle flow processes. The importance of a concept of sub-**

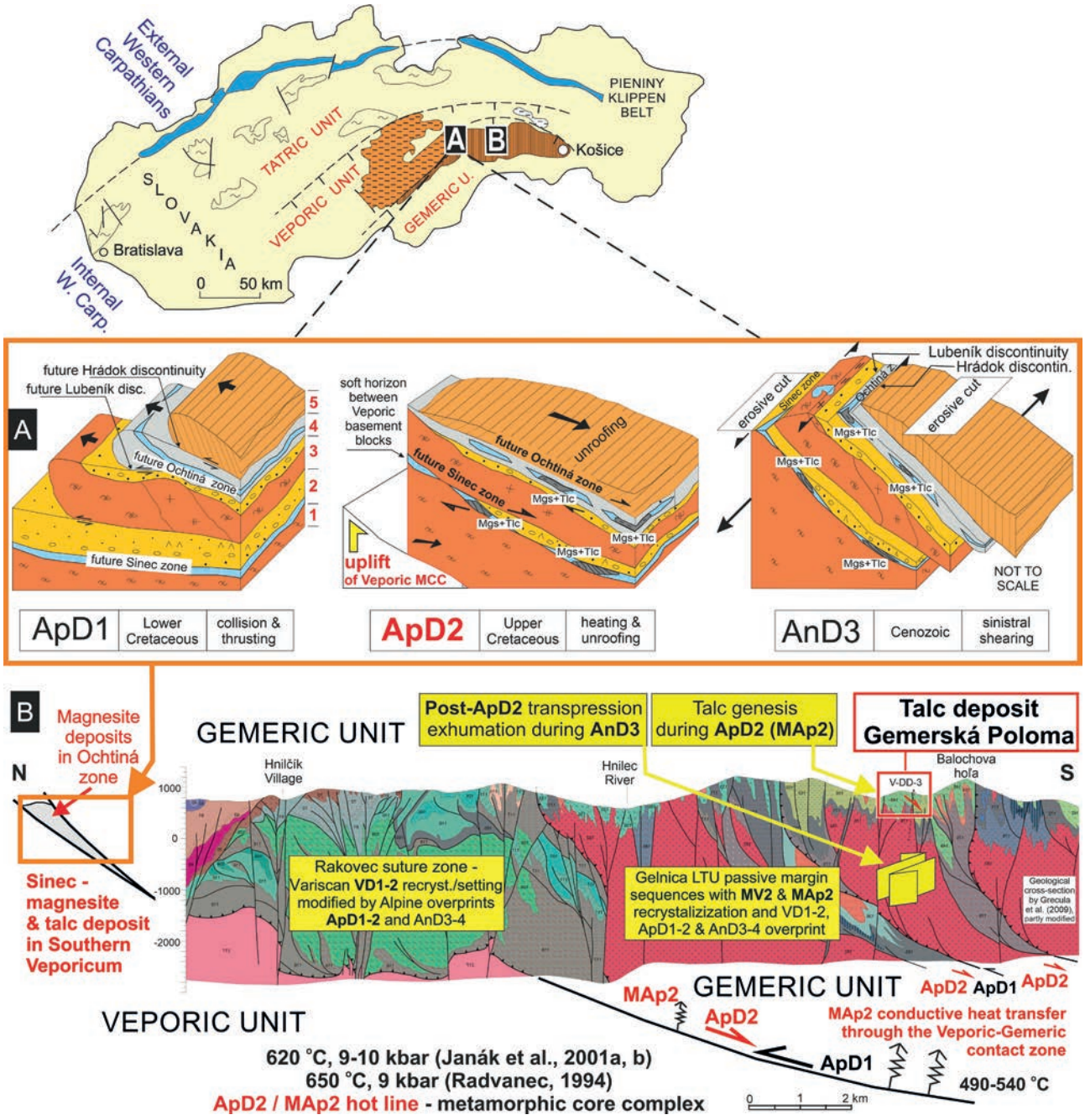

Fig. 14. The south-vergent Upper Cretaceous Paleo-Alpine ApD2 unroofing kinematics is manifested also by talc genesis in the Internal Western Carpathians as a product of MAp2 metamorphism and ingress of fluids to appropriate magnesite protolith: **A** – Situation in the western contact zone of Veporic and Gemeric units (Németh in Radvanec, Németh & Bajtoš – eds., 2010; reproduced with permission): **A** – ApD1 – Imbrication and north-vergent overthrust of the Gemeric basement nappe on Veporic basement and cover sequences during the Lower Cretaceous ApD1 phase caused "sandwiching" of magnesite bodies and accompanying lithologies inbetween crystalline blocks. ApD2 – Talc genesis is a consequence of increased thermic gradient (heat from hot line), ingress of relevant fluids, upwelling the crystalline core of Veporic Unit and post-collisional unroofing of Gemeric sequences from it. AnD3 – Present zonality in occurrence of two magnesite-talc belts along contact zone of Veporic and Gemeric units was produced by Cenozoic AnD3 sinistral shearing. **B** – Similar evolution of talc deposit as in **A** was revealed also in higher level of Alpine setting of Gemeric Unit at the presence of Lower Paleozoic magnesite host rocks, tectonothermal overprint and ingress of fluids. Cross-section of B presents in the left (northern) side the place of evolution of Ochtiná and Sinec zones (shown in A), as well as overthrust of Gemeric Unit on Veporic Unit. Within Gemeric Unit the profile shows Variscan Rakovec suture zone with Alpine overprint, as well as variegated lithology of Gelnica Unit representing former Variscan passive margin (cf. Fig. 5). The MAp2 PT conditions are stated in lower parts of B. Used geological section in B by Grecula et al. (2009) was slightly modified and horizontally overturned.

duction slab pull is further lowered by revealing the mega- and gigaporphyroclasts exhuming just opposite the flow of subducting matter. It means that principal at geodynamics is not a subduction slab pull, but mantle convection currents – in this case forcing also compressional processes in subduction channel and exhuming rigid and heavy blocks from lower crust or even mantle lithosphere by rotation movement in soft ductile environment of subducting rocks in subduction channel (cf. Fig. 13).

In the time of the most vigorous Upper Jurassic convergence within the Neo-Tethys during the Paleo-Alpine cycle, reflected in ApD1s subduction in the Paleo-Alpine southern zone of IWC, the northern zone of IWC registered the synchronous AnD0 divergence – riftogenesis of Penninic – Váhic basin. It seems that this sequence of events, being proved in the Western Carpathians by many ways (cf. Plašienka, 2003), is not fully reflected in paleogeographic maps of the Alpine areas based on van Hinsbergen et al. (2020) reconstruction (cf. Fig. 43 and 44 ibid.).

ApD3 Paleo-Alpine intraplate stress consolidation and AnD4 regional extension

The interpretation of Paleo-Alpine ApD34 evolution in the Western Carpathians faces to difficulties in unambiguous identification due to younger Neo-Alpine overprint of post-AnD12 structures. Due to divergence in AnD0 Váhic and Magura basins, being timely coeval with ApD12 evolution of Meliata basin, **the ApD34 and AnD34 intraplate stress consolidation shearing and faulting represent the same processes**.

Concerning the scale of the whole Carpathian belt (Western, Eastern and Southern Carpathians), the age of Alpine oroclinal bending deserves discussion. Published reconstructions (e.g. van Hinsbergen et al., 2020) show N-S trending Meliata ocean, in Hettangian (200 Ma), dividing the Greater Adria and Dacia continents. Principal in reconstructions of the wider Mediterranean area (l.c.) is the Moesian block, having within the Europe fixed reference frame the same position from Ladinian (240 Ma) up to present. At this architecture also the Neo-Alpine riftogenous zone (AnD1), subduction zone (AnD1s) and related volcanic arc zone should have the same bent course. Kinematics of these processes can be interpreted with difficulties. **Author of this paper prefers an interpretation of general linearity also at Neo-Alpine AnD12 processes (similar like during VD12 and ApD12 processes) and oroclinal bending (syneclisis) of the whole Carpathian zone is interpreted by him as a product of AnD3 evolution with contribution of Hellenic HeD convergent evolution.**

Kinematics of oroclinal AnD3 bending (syneclisis) in inner zones of Internal Carpathians is well documented in the case of contact zone of Gemeric and Veporic units (left side of Fig. 15C). The AnD3 shearing explains well also the apparently antagonistic ApD2 unroofing kinematics in the western and eastern parts of contact zone of these units (Fig. 15C).

4.3 The Neo-Alpine (Cenozoic) orogenic cycle in the Western Carpathians

The subdivision of the Alpine orogenic cycle in the Western Carpathians into two orogenic sub-cycles – Paleo-Alpine (ApD) and Neo-Alpine (AnD) was caused by the time shift of divergent and convergent phases in the Alpine elongated basins with oceanic crust developed south and north of the axis of Internal Western Carpathians, represented by elevated zone of crystalline basement. Moreover – the Paleo-Alpine evolution represents the western extension of Cimmerian evolution and Neo-Alpine evolution represents eastern extension of the Penninic evolution. The late Mesozoic-Cenozoic Neo-Alpine processes of divergence (AnD0) and convergence (AnD1) of External W. Carpathians took place along the northern rim of Internal W. Carpathians, occurring that time already in the post-collisional ApD2 evolutionary phase, following after Paleo-Alpine convergent processes ApD1, which took place along southern rim of Internal W. Carpathians.

The principal tectonic unit dividing Internal and External W. Carpathians – the *Pieniny Klippen Belt* (PKB; *Oravicum*; cf. Fig. 1B) is characteristic with intensive AnD1 and AnD3 deformation. The units being described in subchapters about Variscan and Paleo-Alpine evolution occur south of this belt.

The zones of *Oravic (Pieniny Klippen Belt)* and *Magura units* represent eastern continuation of the Southern and Northern Penninic zones of Eastern Alps. The *Oravic units* of the *Pieniny Klippen Belt* (Fig. 1B) were primarily geodynamically defined by Sikora (1971, 1974; *Zlatná Unit*) and Maheľ (1981; *Váhicum*). The present knowledge about tectonic setting and lithology of *Oravic* and *Magura units* was summarized by Plašienka (2018) and Plašienka et al. (2020 and references therein). We emphasize also principal contributions of Polish authors, namely Birkenmajer (1986, 1988), Birkenmajer and Oszczypko (1989), Cieszkowski et al. (2009), Barski et al. (2012), Gawęda et al. (2021), Golonka (2011), Golonka et al. (2003, 2018), Jurewicz (2005), Krobicki et al. (2003), Ludwiniak et al. (2019) as well as Czech authors: Picha et al. (2006) and Skupien and Vašíček (2008).

The post-collisional evolution (AnD234) in Neo-Alpine orogenic zone has influenced geology and tectonics in wide areas north and south of it, encompassing also Internal Western Carpathians. Despite, reconstruction of the origin of whole Western / Eastern / Southern Carpathian sigmoidal oroclinal bend (syneclisis; cf. Fig.

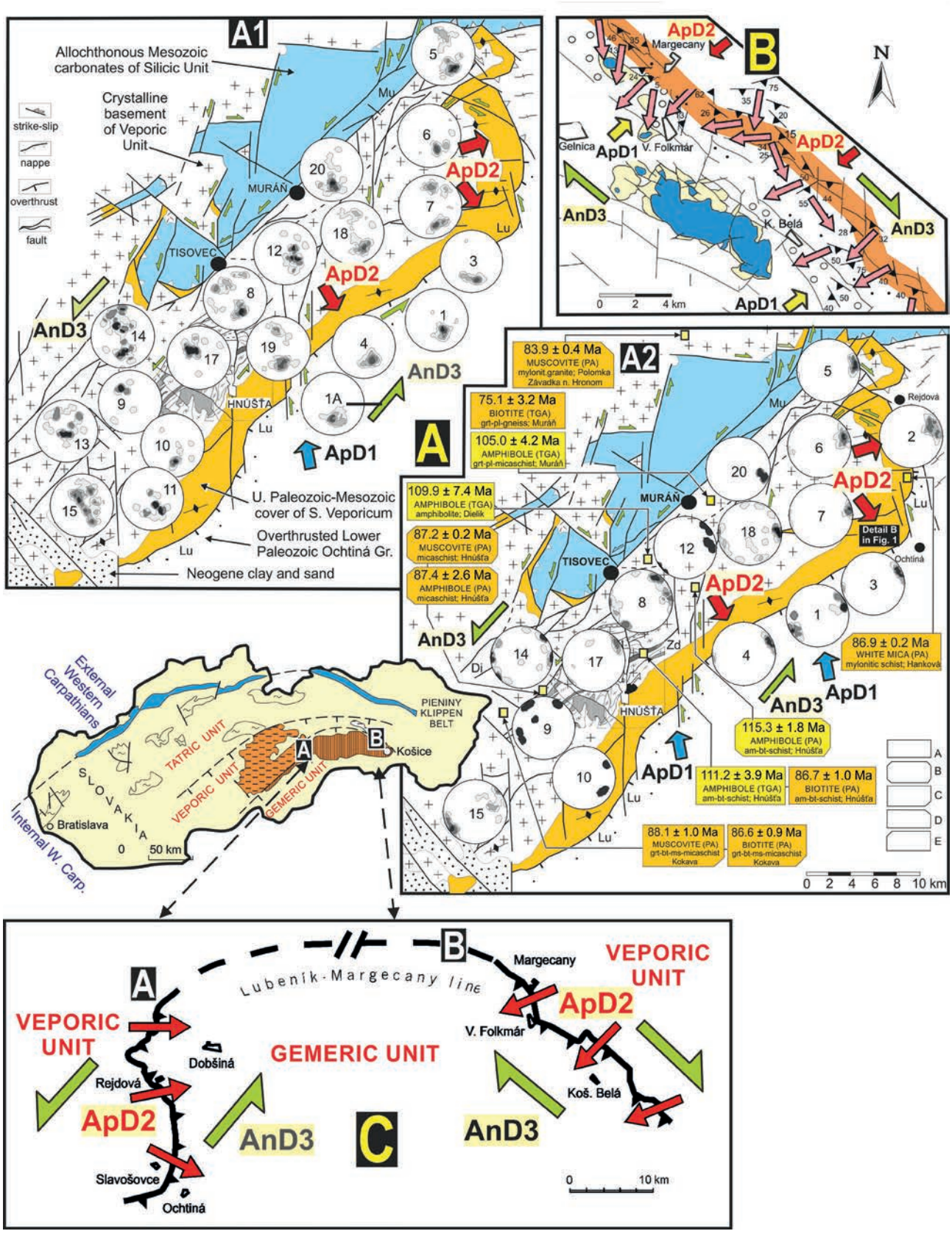
A1
Allochthonous Mesozoic carbonates of Silicic Unit
Crystalline basement of Veporic Unit
strike-slip
nappe
overthrust
fault
MURÁŇ
TISOVEC
HNÚŠTA
Mu
Lu
ApD1
ApD2
AnD3
U. Paleozoic-Mesozoic cover of S. Veporicum
Overthrusted Lower Paleozoic Ochtiná Gr.
Neogene clay and sand
B
Margecany
Gelnica
V. Folkmár
K. Belá
N
0 2 4 km
A2
83.9 ± 0.4 Ma
MUSCOVITE (PA)
mylonit.granite; Polomka Závadka n. Hronom
75.1 ± 3.2 Ma
BIOTITE (TGA)
grt-pl-gneiss; Muráň
105.0 ± 4.2 Ma
AMPHIBOLE (TGA)
grt-pl-micaschist; Muráň
109.9 ± 7.4 Ma
AMPHIBOLE (TGA)
amphibolite; Dielik
87.2 ± 0.2 Ma
MUSCOVITE (PA)
micaschist; Hnúšťa
87.4 ± 2.6 Ma
AMPHIBOLE (PA)
micaschist; Hnúšťa
Rejdová
Ochtiná
Detail B in Fig. 1
Zd
Di
86.9 ± 0.2 Ma
WHITE MICA (PA)
mylonitic schist; Hanková
115.3 ± 1.8 Ma
AMPHIBOLE (PA)
am-bt-schist; Hnúšťa
111.2 ± 3.9 Ma
AMPHIBOLE (TGA)
am-bt-schist; Hnúšťa
86.7 ± 1.0 Ma
BIOTITE (PA)
am-bt-schist; Hnúšťa
88.1 ± 1.0 Ma
MUSCOVITE (PA)
grt-bt-ms-micaschist Kokava
86.6 ± 0.9 Ma
BIOTITE (PA)
grt-bt-ms-micaschist Kokava
A
B
C
D
E
0 2 4 6 8 10 km
External Western Carpathians
Internal W. Carp.
PIENINY KLIPPEN BELT
TATRIC UNIT
VEPORIC UNIT
GEMERIC UNIT
Košice
Bratislava
SLOVAKIA
0 50 km
Lubeník-Margecany line
VEPORIC UNIT
GEMERIC UNIT
Dobšiná
Rejdová
Slavošovce
Ochtiná
V. Folkmár
Koš. Belá
0 10 km

Fig. 15. Kinematics of oroclinal bending of the W. Carpathians demonstrated on AnD3 bend of the ApD1c / ApD2 thrust / unroofing zone between Veporic and Gemeric units, forming syneclise at the western part of this contact zone (shown in **C** down in this figure). The revealing that the ApD2 unroofing kinematics is apparently antagonistic in this Paleo-Alpine ApD12 zone – in western syneclisis segment of this zone the unroofing is generally to E and SE (cf. **A1, A2, C**), but in eastern segment of this zone is the opposite – towards the SW (**B, C**). In earlier reconstructions, this bending was interpreted to be a product of the ApD3 shearing (e.g. Németh et al., 2012), but a new reconstruction of kinematics of Alpine processes in this zone magnifies the role of younger Neo-Alpine AnD3 shearing as a reason of present oroclinal bending. This principle applies also in other bended segments of the whole Carpathian belt. General tectonic situation is shown in this figure by pale-yellow schematic map of W. Carpathians situated in center left position. Oroclinal bending of the W. Carpathians was produced by AnD3 displacements along conjugate systems of sinistral (NE–SW) and dextral (NW–SE) shear zones (Németh et al., 2001), being visualized in **C** by green half arrows. Figure in part **A** (**A1** – mesoscopic foliation, **A2** – mesoscopic linear structures, including $^{40}Ar/^{39}Ar$ dating of synkinematic white micas) documents also ApD2 unroofing kinematics revealed from the 1990s by structural geologists in the western contact zones (**A1;** cf. Hók et al., 1993; Madarás et al., 1996; Németh et al., 2004) and being dated by $^{40}Ar/^{39}Ar$ ApD2 tectonometamorphic white micas (**A2)**. Authors of geochronological data are indicated by rectangles in right down bar in A2: A – Maluski in Kováčik et al. (1996), B – Kováčik and Maluski (1995), C – Maluski et al. (1993), D – Dallmeyer et al. (1993), E – Dallmeyer et al. (1996). TGA represent total gas age, PA plateau age. The role of Cenozoic conjugate shear zones kinematics in oroclinal bending of the Internal W. Carpathians became known when revealing generally opposite ApD2 unroofing kinematics in the eastern part of the Veporic-Gemeric contact zone by Németh et al. (2001); shown in segment **B** (right up in the figure).

1a) is a principal problem of the evolution of whole Alpine-Carpathian orogenic belt, including the role of Neo-Alpine subduction (AnD1a), magmatism / volcanism (AnD2? + 4?), as well as Neo-Alpine shearing (AnD3) in formation of this bend. In further text we will try to address this challenge.

AnD0 continental breakup and rifting phase

The AnD0 rifting phase of Neo-Alpine evolution encompasses two events: (1) the Middle Jurassic ($AnD0_V$) continental breakup, leading to origin of the Alpine Tethys related South Penninic-Váhic Ocean (Late Bajocian–Early Bathonian; Oravic evolution). This continental breakup is contemporaneous with Jurassic ApD1s subduction of the elongated Meliatic oceanic basin located on the opposite – southern side of orogenic belt, having ApD1s subduction slab dipping south (i.e. away of orogenic belt), and (2) the Early Cretaceous ($AnD0_M$) rifting and continental breakup, leading to opening of orogen parallel Magura Ocean as continuation of the North Penninic zone (cf. Plašienka, 2003, 2018). This Early Cretaceous process was coeval with the Paleo-Alpine ApD1c collision acting in south located zone of Internal Western Carpathians with generally north-vergent ApD1c nappe stacking including also sequences of Meliatic oceanic domain (cf. Plašienka, 1997). By this way the zone of Internal W. Carpathians became the axial zone of orogenic belt. We must emphasize that according our reconstructions (cf. l.c.), the course of elongated Neo-Tethys Meliatic ocean was nearly equatorial (E–W), correspondingly as the course of previous Variscan Paleo-Tethys Rakovec basin, as well as the youngest – Neo-Alpine Oravic and Magura basins. **Parallelism of suture zones is one of characteristic features of polyorogenic evolution.**

The contradicting synchronous convergent vs. divergent kinematics in parallel Alpine zones represents another paradox, occurring in polyorogenic zones and being traditionally interpreted as a consequence of subduction slab pull. In our particular case it would relate to the Meliatic oceanic crust subduction slab pull southward. **The slab pull concept here forces again to problem of existing hot line (ECMB) below the spreading zone at Meliata Ocean (ApD0),** occurring between Rakovec suture zone in the North and later zone of Meliata subduction slab in the South. If so, when Meliata ocean in W. Carpathians was closed by subduction, this hot line was still active beneath the Variscan + Paleo-Alpine suture zones and this is demonstrated by Late Cretaceous south-vergent ApD2 unroofing of MAp2 overheated Veporic basement nappe by the same hot line. This process is documented in previous subchapters. **The configuration looked as follows: in direction from the south northward – (1) Meliata subduction slab dipping south, (2) zone of collision stack and accretion prism nappes, being overheating by hot line and (3) more to the north acting new AnD0 Oravic and Magura spreading zones. This configuration indicates that new AnD0 spreading could not be driven by a subduction slab pull, but again by the same (Variscan / Paleo-Alpine / Neo-Alpine) hot line.**

Here presented interpretation of the role of elongated subequatorial–course convectional heat related to ECMCC (hot line), driving the polyorogenic cycles geodynamics of Intra-Pangea subequatorial type is a novel contribution to current global plate tectonic concepts.

AnD1 collision

According present interpretations by numerous authors (see references in first paragraphs of subchapter 4.3), the AnD1 convergence generally accounts the southward polarity of AnD1a subduction of the flysch zone between

the southern margin of European Platform and the ALCAPA (Alpine-Carpathian-Pannonian) zone. In the territory of W. Carpathians this subduction caused individualization and strong AnD1 north-vergent deformation of the Pieniny Klippen Belt, built dominantly of carbonatic sequences of the southern margin of AnD0 flysch basin. The complex Neo-Alpine AnD1c collisional events of Late Cretaceous to Middle Eocene age were caused by northward drift of the Adriatic microplate (Plašienka, 2018). Similar to other orogenic belts, the convergent folding in the External Western Carpathians (ECW in Fig. 1B) commenced in their internal parts and progressed in time towards their foreland (Oszczypko, 2006). From the end of Paleogene the AnD1c collision, acting at the Pieniny Klippen Belt / Magura Basin boundary, has progressed more externally and completed it was in early Miocene – early Burdigalian in the northern part of the Krosno flysch basin (Fig. 1B). During Early and Middle Miocene the Polish Carpathian Foredeep developed as a peripheral foreland basin in front of advancing Carpathian orogenic wedge (l.c.). The development of this Foredeep can be related with AnD2 / MAn2 thermal processes and gradual uplift of collided zone of External Western Carpathians.

AnD2 post-collisional events

The former AnD1 subduction-related structures were overprinted by the AnD2 gravitational collapse normal faults (Zuchiewicz et al., 2002; Tokarski et al., 2006). These faults bound intramontane basins, being filled with Neogene sediments. The postcollisional MAn2 thermal processes produced Neogene magmatism and superficially very vigorous volcanism. We interpret the MAn2 magmatism and volcanism again as a consequence of the input of convectional mantle heat from the ECMCC.

The Miocene to Quaternary volcanism in the Western Carpathians (and s.l. the Circum-Pannonian region) contributes to understanding of the youngest evolutionary stage of Eastern / Southern Carpathians arc (syneclisis) evolution. The volcanic products of Miocene to Quaternary age were divided into sequence of volcanic suites linked to Neo-Alpine post-convergent (AnD2?, AnD4?) magmatogenic events (cf. Lexa & Konečný, 1998): The **areal type silicic volcanism** and later **andesite volcanism** have terminated with **alkali basalt volcanics related to post-convergence extension environment** (AnD4). Authors (l.c.) emphasize that the compositional difference between areal-type and arc-type andesite volcanics is negligible and these suites were divided on the basis of spatial distribution and temporal evolution. Arc type andesite volcanics are interpreted to be the proof of deep reaching subduction. Their position and timing indicate that subduction has reached the magma generation depth when it was nearly vertical and reached its final stage of tear-off (Konečný et al., 2002). According to our interpretation the nearly vertical position of AnD1a subduction slab and tear-off were caused by the positioning of subduction slab against to descending convection current of ECMCC flow. The Cenozoic flysch belt subduction initiation to opposite (northward) direction was not possible because of the barrier effect of European Platform crystalline basement (cf. Fig. 1B). Exceptionality of this subduction process is magnified also by the fact of "imperfection" of supposed Neo-Alpine Klippen Belt subduction process, which took place earlier in more southern parallel zone than the Magura basin subduction (cf. Lexa & Konečný, 1998, and Fig. 1 part I in Németh et al., 2016).

AnD3 origin of oroclinal bend of Western Carpathians

The conjugate NW-SE and NE-SW (AnD3) systems of Alpine shear zones in the Western Carpathians were first discovered by Grecula et al. (1990) in the region of Gemeric Unit. Later the importance of dextral NW-SE trending and sinistral NE-SW trending shear zones was emphasized also by other authors. Their structural research was focused on principal Tertiary shear zones, displaying the inconsistences / shifts in the course of individual lithological strips. Into this category of XD3 shear zones of brittle / brittle-ductile kinematics we do not account moderately inclined brittle-ductile / ductile shear zones related to XD1 thrusting and XD2 unroofing. Younger re-activation / overprint of these XD12 discontinuities by younger AnD3 shear zones is clearly decipherable by overprinting relations (cf. Fig. 14A). The research of kinematics of AnD3 shear zones has contributed to explanation of convex oroclinal bending of W. Carpathians (cf. Fig. 1B and 15C). Principal information about AnD3 shear zones is available in works dealing with following topics: AnD3 reactivation of ApD12 contact zone of Gemeric and Veporic units – Gazdačko (1994), Németh et al. (2001), Farkašovský et al. (2023), Transgemeric shear zone – Lexa et al. (2003), Pohorelá shear zone – Hók and Hraško (1990), Madarás et al. (1994), Muráň fault – Marko (1993), Pelech and Kronome (2019), Gerátová et al. (2022), Sinec shear zone – Németh et al. (2004), Mýto-Tisovec fault – Marko and Vojtko (2006), northern part of Internal W. Carpathians – Vojtko et al. (2010, 2015). Modern review of tectonic evolution of W. Carpathians, including topics of Cenozoic AnD3 conjugate system of shear zones provide works by Kováč et al. (2002), Kováč and Plašienka (2002), Marko et al. (2017), Plašienka (2018) and Bezák et al. (2023).

AnD4 regional faults of pure-shear kinematics of sub-equatorial and submeridian courses

Besides the arched course of the individual mountain ranges (Fig. 1B), the Western Carpathians provide spectacular morphological evidences of a net of subequatorial

and submeridian trending faults, cross-cutting older tectonic and morphological elements. These overprinting relations demonstrate that these subequatorial and submeridian prevailingly pure-shear type faults with dominant vertical kinematics (uplifts and subsidences) of rock sequences bordered by them, represent a product of the youngest orogenic phase – AnD4 – present in the Western Carpathians. Besides regional faults and frequent morphological evidences (e.g. course of valleys), the AnD4 brittle disintegration of older structures and lithology are well observable also at the outcrop scale. Several faults of submeridian course (e.g. the Zázrivá-Budapest fault, Central Slovakian fault zone, a.o.) cross the whole Western Carpathians and represent regional reflection on E-W trending extension related to MCMCCs. The post-AnD3 N-S coursing transcrustal discontinuities can produce the pathways for Miocene volcanism. The N-S trending volcanic range of the Slanské vrchy Mts in the eastern part of W. Carpathians can serve as an exemplary case of linearly situated range of Middle / Upper Miocene andesite volcanoes, spatially contradicting to their relation with eventual continental or island arc volcanism of subduction related AnD1s process (cf. Bacsó, 2023).

5 Geodynamic considerations leading to birth of hypothesis of the New Global Tectonics 2.0

5.1 Columnar mantle plumes (mantle diapirs) vs. convection currents of subequatorial-course mantle bulge (ECMB), subequatorial-course mantle convection currents (ECMCCs), submeridian-course mantle convection currents (MCMCCs) and their interconnections

The origin of new rift zones and mid-oceanic ridges was traditionally interpreted as a consequence of the lithosphere breaks due to the pull of descending slabs in subduction zones (e.g. Jacobs, 1992).

The research by several authors from the 1970s has described within the globe the differing number of the mantle plumes (mantle diapirs). Even that time they were interpreted to be a driving force of global geodynamics. Morgan (1971, 1972) in his pioneering works defined 20 plume localities. Burke and Wilson (1976) distinguished altogether 122 hot spots (superficial indications of mantle plumes), being active during the last 10 million years. From this number, altogether 53 were located in oceanic basins, 24 on or near mid-ocean ridges and 69 on continents. Altogether 25 hot spots defined in Africa represented the greatest concentration revealed within the continent. The hot spots were revealed in relatively regular net on the globe. **The rift zone origin due to heat generated by several mantle plumes having generally linear arrangement** was presented by Dewey and Burke (1974) on example of N-S located series of rift-rift-rift (r-r-r) junctions in continental crust. They represented the initiation of rift divergence, leading to South-Atlantic-type advanced rifting stage. This important outcome emphasizes, that several hot spots with generally linear position of submeridian course can cause a special type of continental breakup and become a rift zone. New principal interpretation appeared in work by Courtillot et al. (2003), distinguishing altogether 49 hot spots with anchoring of their mantle plumes in depths of 500 km and 2 850 km. In subequatorial plane two antipodal domes of mantle upwelling are shown in this work (l.c.) – below the central Pacific Ocean and Africa (Fig. 4 ibid; used slightly modified in Fig. 16 of our interpretation). Based on results of finite frequency tomography, the deep mantle plumes catalogue by Montelli et al. (2006) states 17 mantle plumes originating at least below the upper mantle and 4 plumes reaching only to middle mantle. Only the Eifel and Seychelles plumes are unambiguously confined to cross-cut only the upper mantle. Starting plumes are visible in the lowermost mantle beneath South of Java, East of Solomon, and in the Coral Sea (l.c.). Authors (l.c.) suggest a pulsating behaviour of the Iceland plume due to the substantial disagreement between *P-wave* and *S-wave* images.

Continental breakup in the case of Rodinia and Pangea with relation to mantle convection was comprehensively explained by Pirajno (2000). The pioneering works about mantle convection currents appeared in the 1920s (Schwinner, 1920; Holmes, 1929). Regarding the mantle convection, presently there are available several concepts – interpreting two separate convecting layers above and below 670 km discontinuity, or a whole-mantle convection. Important there were results of the seismic tomography, supporting the idea of flow across the boundary layer between upper and lower mantle (van der Hilst et al., 1997). This concept joints previous ones and is known as "leaky two-layer" theory.

Owing the long-time research and based on works referred above, the author of this contribution prefers a new hypothesis of linear trending sources of convectional heat, being categorized into **(1) subequatorial-course mantle bulge (ECMB) and (2) subequatorial-course mantle convection currents (ECMCCs) / submeridian-course mantle convection currents (MCMCCs; Fig. 16) with existing crossings of subequatorial-course and submeridian-course systems, as well as diagonal interconnections of both systems.** All these categories represent hot lines owing to upwelling mantle currents – they contribute with heat to rifting (XD0), post-collision processes (XD2) and intra-plate processes (XD4). The descending currents – are principal at subduction (XD1s). All principally contribute to lithosphere geodynamics, parallel with existing "classic" **(3) columnar mantle plumes (mantle diapirs),** superficially being expressed by hot spots. **The**

subequatorial-course mantle bulge (ECMB) and parallel – situated in higher latitudes – subequatorial-course mantle convection currents (ECMCCs) are principal for polyorogenic / polymetamorphic / polymetallogenic evolution (cf. Németh, 2002, Fig. 3 ibid; Németh, 2005a, Németh et al, 2016), and in Phanerozoic Eon such evolution seems to be very distinctive in the Alpine-Carpathian-Himalayan belt.

Findings in the Western Carpathians (l.c.) indicate that **the same linear source of subequatorial convectional heat (hot line) acted throughout several orogenic cycles and produced within them the riftogenesis generating the oceanic-type crust, but also contributes to closure of generated elongated basins at convergent collisional evolution and principally contributing to post-collisional evolution and origin of orogen parallel metamorphic core complexes and uplift in the axis of orogenic belt, unroofing and gradual opening of a new generation rift(s). Shift of lithosphere over hot line causes parallel location of products of individual orogenic cycles, i.e. suture zones** (cf. Figs. 10 and 11), which cannot be explained by interpretation of linear arrangement of columnar hot spots (according to rift-rift-rift concept by Dewey and Burke, 1974). **This hot line hypothesis explains well the polyorogenic evolution, but also fits well at reconstruction of polymetamorphic and polymetallogenic events and their products throughout several orogenic cycles** (Németh et al., 2016).

Concerning the source of heat for continual flow of magma within the mantle (the most significantly but indirectly registerable in ECMB, ECMCCs and MCMCCs), presently is well proved the concept of thermonuclear reactions acting in the innermost parts of the Earth which resemble those in the Sun (Fowler, 1984; Herndon, 1996, 2011; Raghavan, 2002; Anisichkin et al., 2005; Schuiling, 2006; Rusov et al., 2007; de Meijer & van Westrenen, 2008; Terez & Terez, 2011, 2013, 2015; Fukuhara, 2016; Sobolev & Bilan 2018; Pawula, 2022; for mantle flow interpretations see also Davis, 2022). According to studies referred above, **the mantle plumes (mantle diapirs) could be parallelized with the eruptions from the Sun, but happening in totally different environment – not in vacuum and zero temperatures, but to glowing mantle environment, so the enormous thermal effect of such eruptions can last millions of years, or even throughout several orogenic cycles.**

When considering the Earth geodynamics and the counter-clockwise rotation of the globe, important aspect is the **difference in rotation of the lithosphere with respect to that in the deep mantle**. Modelling by several authors (e.g. Ricard et al., 1991, Fig. 2 ibid.; Doglioni, 1993; Doglioni, et al., 1999) has resulted into series of vectors, trending generally E–W and depicting the lithosphere movement generally westward with respect to deep mantle. If we express it by the opposite interpretation – the mantle is relatively moving east with respect of the lithosphere moving west (Fig. 3 in Ricard et al., 1991). This interpretation was used in model suggested in this article (Fig. 16) in combination with the model by Courtillot et al. (2003). The different rotation velocity of lithosphere with regard to that of Earth's mantle and core causes that the submeridian Circum-Pangea-type subduction slabs are dipping west very steeply, but dipping moderately to the east. **This kinematics is principal in the Circum-Pangea submeridian-course transcrustal discontinuities, but also inside present Europe – cf. dip of Vrancea subduction slab and its break-off in the Eastern Carpathians** (Sperner et al., 2001)**.** Interesting in Fig. 2 of Courtillot et al. (2003) is the moderate bending of vectors course from their E-W trajectory. In the territory on North America these vectors are so short and unimportant that it can indicate why the continuation of the Intra-Pangea subequatorial polyorogenic belt in North American territory is unclear.

5.2 "Continental drift" vs. drift of lithospheric plates

As generally known, the concept of continental drift by Alfred Wegener (1912 and following outcomes) was not accepted unequivocally, when he as a driving force interpreted the rotation of the Earth. The Russian-American mathematician Paul Sophus Epstein proved that kinematics suggested by Alfred Wegener is not real / possible. Really – continents are not drifting on Earth surface as they are. **Continents are drifting on Earth being passively carried by drifting lithospheric plates.** Hence – instead of continents alone – drifting on our planet are lithospheric plates. This idea was published in the series of principal geodynamic articles by John Tuso Wilson (1965, 1966 and 1967).

Drift of lithospheric plates operates with difficulties, because the whole surface of our planet is covered by lithospheric plates = lithosphere (continental but also oceanic crust). When imagined completed puzzle picture – how some segments can be changed when they appear in wrong position? In the case of lithosphere there is no possibility to uplift those in a "wrong position" and exchange them with others. No subduction and lithospheric collision with imbrication, accretion and nappes stacking are helpful, because oceanic rift zones still produce a new – oceanic – crust. So the coverage of our planet with lithosphere is all the time complete.

At drift of lithospheric plates the oceanic rift zones play relatively passive role. They are products of extension (divergent movement) caused by mantle convection currents. Zone where the mantle convection currents reach the bottom of lithosphere is named as **hot line**. In this uppermost zone the mantle convection zones divide to both sides of the zone and gradually start to descend, in some places contributing to start or progression of subduction. Smaller importance of riftogenesis at lithospheric

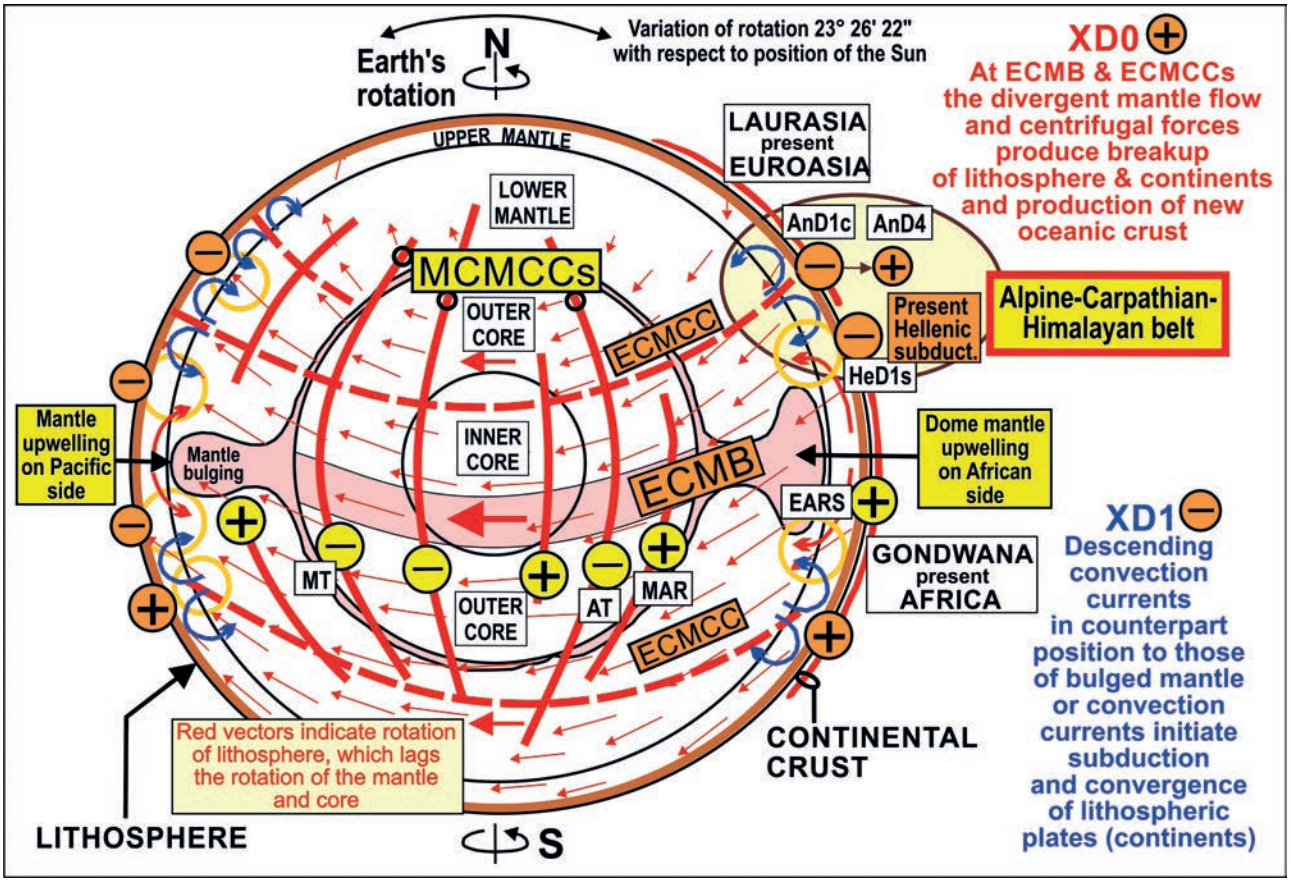

Fig. 16. Model of the global geodynamics based on the concept of polyorogenic zones trending subequatorial and characterized by the case study of the Western Carpathians (positioned on the right side up in this visualization). The concepts by Courtillot et al. (2003; equatorial mantle bulging), as well as Ricard et al. (1991; differential rotation between lithosphere and mantle – red generally E-W trending thin arrows) were used for consideration of subequatorial and submeridian zones. The Earth's geodynamics benefits from thermonuclear reactions corresponding with those in the Sun (references are in the chapter 5.1). For simplification, in this model the mantle plumes (mantle diapirs) are not visualized. The shape of ECMB (pale red) taken from Courtillot et al. (l.c.), shows two principal cases: ECMB beneath the extended continent (Africa) and beneath the globally extended oceanic crust (Pacific). In other places around the wider zone of globe equator the ECMB shapes differ between these two principal shapes. Signs in orange circles (also in Fig. 2) represent rifting (+) or subduction (–) in subequatorial zones and those in yellow circles in submeridian zones. MT – Mariana Trench, AT – Atacama Trench, MAR – Mid-Atlantic Ridge, EARS – East African Rift System.

plates displacement and orogenesis s.l. ("mountain building") is highlighted in XD labelling by number ZERO = XD0.

Convergent subduction processes lead at polyorogenic evolution to collision (XD1c) and "mountain building". As we demonstrate in present paper, this happens dominantly at zones of subequatorial direction. Zones of submeridian direction have many times smaller frequency of collision events.

The drift of lithospheric plates author of this paper explains by the shifts along transform faults / shear zones. Within individual orogenic cycles they are labelled as XD3 phase, but they may be acting throughout several orogenic cycles, especially at polyorogenic case indicated by this article (e.g. ApAnHeD3 – continual activity of some shear (transform) faults during several orogenic cycles – here Paleo-Alpine, Neo-Alpine and Hellenic ones). The importance of transform faults was firstly revealed by John Tuso Wilson (1965). These simple shear-type faults = transform faults / zones are extremely frequent in the lithosphere (up to decameter mutual distance, or decipherable by steeply dipping cleavage zones even at the outcrop scale), so the lithosphere is disintegrated by them to microplates or rock blocks. Because the transform / shear faults dominantly develop in conjugate system of two preferable directions NW–SE (dextral shear) and NE–SW (sinistral shear), the lateral shifts allow in long time perspective the drift of lithospheric plates / microplates / rock blocks. Transversal courses of transform / shear faults are caused by the different displacement length along the equator and equator parallel zones in higher latitudes at the rotation of the Earth. In this point author provides also explanation of the reason of origin of subequatorial weakened zones with located mantle convection currents

(ECMMC), which are developed also due to differing subequatorial displacement paths of lithosphere at rotation of the Earth. The supreme order discontinuities in lithosphere (ECMMCs), produced by the Earth's rotation within on the Earth's crust, are projected depthward and activating / allowing mantle convection currents. Principal at origin of different – global N-S trending discontinuities there are the differences inbetween physical parameters, rheology and the rotation kinematics of individual zones of the Earth (core, mantle, crust) producing a stress field contributing to N-S trending lithosphere / continents fracturing. The minor role there may play also uneven (undulated) base of lithosphere, which is interpreted under continental crust and differs from that at the base of oceanic crust. Because the ascending and descending submeridian mantle currents are present at rifts, but also subduction zones (cf. Fig. 16), it underlines the interconnection of tectonic processes in the lithosphere with the processes in the Earth's mantle.

At all interpretations we must have in mind that new discontinuities are preferably developing within older / already existing discontinuities, but above described global geodynamic rules are valid in polyorogenic zones as well as in all places within the globe, differing only by their size and importance, regarding on latitude and position where they act.

6 Concluding summary

The presentation of individual orogenic cycles and their phases in the case of the Western Carpathians, being part of polyorogenic Alpine-Carpathian-Himalayan belt, has been in this paper extended to global considerations. The W. Carpathians with a distinct zonal setting and symmetric moderate north convex oroclinal bending, as well as the small width in transverse direction only of ca 200 km represent an ideal study area of the geodynamic processes in polyorogenic belt.

As the drivers of polyorogenic evolution, but also of all global processes there are interpreted the linear sources of convectional heat – the subequatorial-course mantle bulge (ECMB), subequatorial-course mantle convection currents (ECMCCs), submeridian-course mantle convection currents (MCMCCs), and at some special cases also their interconnections. The mantle plumes (mantle diapirs) play a secondary role in global geodynamics. As demonstrated by numerous cited studies, all here listed mantle ascents are products of a permanent heat production by thermonuclear reactions in the innermost zones of the Earth. The shape and course of linear-course mantle ascents and related descends are a product of Earth's rotation (ECMB + ECMCCs), but probably also of uneven base of lithosphere under continents in meridian direction (at MCMCCs). All linear-course mantle ascents and descents can contribute to rifting as well as subduction. The concept of a slab pull is not understood here as the dominant at global geodynamics, especially due to revealing mega- or gigapophyroclasts of heavy rigid rounded blocks of HP-HT rocks (glaucophanites, metagabbros, peridotites) being exhumed by reversal rotation movement in the subduction slab. This synsubduction exhumation requires compression – and this is in contradiction with an interpretation of extension at subduction slab pull concept.

The multiple switch between divergence and convergence at polyorogenic zones of subequatorial direction, producing multiple continental breakup alternating with collision

Dominant in global geodynamics and in multiple equatorially directed polyorogenic continental breakups is a mantle convection. The positioning of convection currents is influenced by the rotation of the Earth. The supreme importance mantle convection belt has a subequatorial ring shape – being defined as a subequatorial-course mantle bulge (ECMB). Parallel with ECMB there exist also several subequatorial-course mantle convection currents (ECMCCs), being developed in weakened zones (in lithophere discontinuities), produced by different length of rotation pathes in parallel zones being developed in different latitudes. If no other aspects are considered – an extension produced by the rotation driven centrifugal forces contributes also to origin of subequatorial-course mantle convection currents and related equator parallel XD0 disintegration (breakup) of the lithosphere in polyorogenic zones and divergent wandering of disintegrated parts generally towards the north in northern hemisphere and towards the south in southern hemisphere. The start of the opposite XD1 convergent drift of disintegrated parts depends on relation of their weight and decrease of centrifugal forces in more distant zones from the equator: Reaching the critically distant position from the equator the centripetal forces start to act on the XD0 displaced parts of continental crust, and the former disintegrated parts at XD1 tend to collide owing the action of these centripetal forces.

Processes producing continental breakup by submeridian-course convection currents (MCMCCs)

The Western Carpathians as a part of polyorogenic belt of subequatorial direction do not provide good conditions for investigation of submeridian trending crust disintegration. Despite – long, regional scale faults of meridian course are present also in this territory (as well as in the whole European continent), encompassing also vertical uplift and subsidence of local mountain ranges related to the youngest orogenic cycle (in the Western Carpathian territory AnD – with very instructively developed AnD3 and AnD4 phases; cf. Németh et al., 2023). This young evolution was well deciphered also in other parts of European continent by Cloeting et al., 2005, 2007, and references herein.

The concept of the net rotation of the lithosphere with respect to deep mantle, as presented by Ricard et al. (1991) and later further elaborated by Doglioni (1993) and Doglioni et al. (1991, 1999, 2006) was included into our considerations and resulting model (Fig. 16). The delay of lithosphere rotation (in Fig. 16 shown by thin, generally equator parallel arrows, pointing west) and the differences inbetween physical parameters, rheology and the rotation kinematics of individual zones of the Earth (core, mantle, crust) produce a stress field contributing to N-S trending lithosphere / continents fracturing. Originating global scale N-S trending discontinuities are used for mantle uprise and the meridian-course mantle convection currents (MC-MCCs) originate by this way. Secondarily they contribute to continental breakup of submeridian direction – e.g. recent activity in the East African Rift System represents an embryonal phase of a new Wilson cycle, in the distant future probably reaching the mature stage of Mid-Atlantic ridge-type. Typical example of active subduction along the submeridian-course zone is represented by the Atacama subduction (cf. Figs. 2 and 16). The concept of eastward migration of the mantle relative to the lithosphere (Ricard et al., 1991, Fig. 3 ibid.) explains well the reason of steepening of the dip of subduction slabs dipping west and their shallow dip in cases when they are dipping east. Within Carpathian chain the first of these cases was interpreted (and proved) e.g. in Vrancea zone in the Eastern Carpathians.

Further non-regularities are common, too, being caused by the principle of preferred establishing of younger discontinuities on older ones, but also the common microplates / blocks shifts and rotation (preferably during XD3 phase), as well as the lithospheric plates / continents rotation due to thermal effect of columnar-type mantle plumes and related mantle flows. All these aspects must be taken into account when considering products of any orogenic phase in any region.

Role of transform / shear faults at drift of lithospheric plates on Earth's surface

The lithospheric plates are limited by rift zones, subduction zones and transform faults. The whole surface of the Earth is covered by lithospheric plates. At their drift – indicated by the drift of continents carried by the drifting lithospheric plates, the rift and subduction zones play a minor role if the divergence rates at the rift zones correspond with rates of subduction on the opposite side of lithospheric plate, or the rate differences are small. Therefore principal at the drift of lithospheric plates are the subvertical transform / shear faults which build a dense net on the Earth's surface, segmenting lithospheric plates (as well as their carried continents) to smaller plates / microplates / rock blocks, allowing them to migrate by sliding one next to the other.

Combining above presented interpretation of (A) a global geodynamic importance of hot lines (ECMB, ECMCCs and MCMCCs), with (B) lateral displacements along a dense net of transform / shear faults, being principal for global scale drift of lithospheric plates (bearing continents), together with further principles of plate tectonics provide a basis for establishing of a new hypothesis of New Global Tectonics 2.0. To become a theory, this hypothesis requires a detail study of mutual interaction between linear mantle convection currents and columnar mantle plumes, regarding their genetic relations and kinematic consequences on lithospheric plates displacement. This study will become easier now because of available numerous scientific studies proving the existence of thermonuclear reactions in innermost zones of the Earth, producing heat for all geodynamic processes in the Earth.

Acknowledgements

Author expresses his thanks to Ministry of Environment of the Slovak Republic for funding numerous scientifically contributing regional geological and metallogenetic projects, as well as for the research possibilities on EC Horizon 2020, Horizon Europe and UNESCO/IUGS IGCP bases. Comments of three anonymous reviewers contributed much to improvement of primary manuscript. This paper is also a contribution of the State Geological Institute of Dionýz Štúr (SGUDS), Slovakia, for the EC – CINEA HORIZON-CL5-2021-D3-D2 project 101075609 Geological Service for Europe (GSEU) within WP6 – Geological framework for the European geological data & information system, as well as for the EuroGeoSurveys Geological Mapping and Modelling Expert Group.

References

Anisichkin, V. F., Bezborodov, A. A. & Suslov, I. R., 2005: Nuclear fission chain reactions of nuclides in the Earth's core over billions of years. *Atomic Energy, 98, 5, 352–360.*

Asch, K., 2005: The 1 : 5 Million International Geological Map of Europe and Adjacent Areas. *Hannover, BGR.*

Bacsó, Z., 2023: The Brehov volcanogenic and stratabound base metal and gold deposit (Eastern Slovakia): Position and genetic relations in the Internal Carpathian-Alpine Cenozoic metallogenetic belt. *Mineralia Slovaca, 55, 1, 27–52.*

Bajaník, Š., Hanzel, V., Ivanička, J., Mello, J., Pristaš, J., Reichwalder, P., Snopko, L., Vozár, J. & Vozárová, A., 1983: Vysvetlivky ku geologickej mape Slovenského rudohoria-východná časť v mierke 1 : 50 000. *Bratislava, Geologický ústav Dionýza Štúra, 1–223* (in Slovak with extended English summary).

Barski, M., Matyja, B. A., Segit, T. & Wierzbowski, A., 2012: Early to Late Bajocian age of the "black flysch" (Szlachtowa Fm.) deposits: implications for the history and geological structure of the Pieniny Klippen Belt, Carpathians. *Geological Quartnary, 56, 3, 391–410.* doi: 10.7306/gq.1030.

Bezák, V., 2002: Hercynian and Alpine strike-slip tectonic – a dominant element of tectonic development of the Inner Western Carpathians. *Geologica Carpathica, 53, 6–8.*

Bezák, V., Bielik, M., Marko, F., Zahorec, P., Pašteka, R., Vozár, J. & Papčo, J., 2023: Geological and tectonic interpretation of the new Bouguer gravity anomaly map of Slovakia. *Geologica Carpathica. 74, 2, 109–122*.

Bielik, M., Kováč, M., Kučera, I., Michalík, P., Šujan, M. & Hók, J., 2002: Neo-Alpine linear density boundaries (faults) detected by gravimetry. *Geologica Carpathica, 53, 4, 235–244.*

Birkenmajer, K., 1986: Stages of structural evolution of the Pieniny Klippen Belt, Carpathians. *Studia Geologica Polonica, 88, 7–32.*

Birkenmajer, K., 1988: Exotic Andrusov ridge: its role in plate-tectonic evolution of the West Carpathians foldbelt. *Studia Geologica Polonica, 91, 7, 37.*

Birkenmajer, K. & Oszczypko, N., 1989: Cretaceous and Palaeogene Lithostratigraphic units of the Magura Nappe, Krynica Subunit, Carpathians. *Annales Societatis Geologorum Poloniae, 59, 145–181.*

Bogusz, J., Jarosiński, M. & Wnuk, K., 2011: Regional 2.5D model of deformations in Central Europe from GNSS observations: General assumptions of project. *Reports on Geodesy, 2, 91, 59–66.*

Bogusz, J., Brzezinski, A., Kosek, W. & Nastuda, J., 2015: Earth rotation and geodynamics, *Geodesy and Cartography, 64, Spec. Iss., 51–84.*

Broska, I. & Uher, P., 2001: Whole-rock chemistry and genetic typology of the West Carpathian, Variscan Granites. *Geologica Carpathica, 52, 2, 79–90.*

Broska, I. & Kubiš, M., 2018: Accessory minerals and evolution of tin-bearing S-type granites in the western segment of the Gemeric Unit (Western Carpathians). *Geologica Carpathica, 69, 5, 483–497.*

Cambel, B., Bagdasarjan, G. P., Gukasjan, R. Ch. & Veselský, J., 1989: Rb-Sr geochronology of leucocratic granitoid rocks from the Spissko-gemerske rudohorie Mts. and Veporicum. *Geologický zborník – Geologica Carpathica, 40, 323–332.*

Cieszkowski, M., Golonka, J., Krobicki, M., Slaczka, A., Oszczypko, N., Waskowska, A. & Wendorff, M., 2009: The Northern Carpathians plate tectonic evolutionary stages and origin of olistoliths and olistostromes. *Geodinamica Acta 22, 1–3, 101–126.* DOI: 10.3166/ga.22.101-126.

Cloetingh, S., Ziegler, P. A., Beekman, F., Andriessen, P. A. M., Matenco, L., Bada, G., Garcia-Castellanos, D., Hardebol, N., Dèzes, P. & Sokoutis, D., 2005: Lithospheric memory, state of stress and rheology: neotectonic controls on Europe's intraplate continental topography. *Quaternary Science Reviews, 24, 241–204.*

Cloetingh, S. A. P. L., Ziegler, P. A, Bogaard, P. J. F., Andriessen, P. A. M., Artemieva, I. M., Bada, G., van Balen, R. T., Beekman, F., Ben-Avraham, Z., Brun, J.-P., Bunge, H. P., Burov, E. B., Carbonell, R., Facenna, C., Friedrich, A., Gallart, J., Green, A. G., Heidbach, O., Jones, A. G., Matenco, L., Mosar, J., Oncken, O., Pascal, C., Peters, G., Sliaupa, S., Soesoo, A., Spakman, W., Stephenson, R. A., Thybo, H., Torsvik. T., de Vicente G., Wenzel, F., Wortel, M. J. R. & TOPO-EUROPE Working Group, 2007: TOPO-EUROPE: The geoscience of coupled deep Earth-surface processes. *Global and Planetary Change, 58, 1–118.*

Courtillot, V., Davaille, A., Besse, J. & Stock, J., 2003: Three distinct types of hotspots in the Earth's mantle. *Earth and Planetary Science Letters, 205, 295–305.*

Csontos, L. & Vörös, A., 2004: Mesozoic plate tectonic reconstruction of the Carpathian region. *Palaeogrphy, Palaeoclimatolgy, Palaeoecology, 210, 1–56.*

Dallmeyer, R. D., Neubauer, F. & Putiš, M., 1993: $^{40}Ar/^{39}Ar$ mineral age controls for the Pre-Alpine and Alpine tectonic evolution of nappe complexes in the Western Carpathians. In: Pitoňák, P. and Spišiak, J. (eds.): Pre-Alpine Events in the Western Carpathians' Realm. *Proceedings of Conference, Stará Lesná, 13–20.*

Dallmeyer, R. D., Neubauer, F., Handler, R., Fritz, H., Muller, W., Pana, D. & Putiš, M., 1996: Tectonothermal evolution on the inner Alps and Carpathians: Evidence from $^{40}Ar/^{39}Ar$ mineral and whole-rock data. *Eclogae geologicae Helvetiae, 89, 1, 203–227.*

Dallmeyer, R. D., Németh, Z. & Putiš, M., 2005: Regional tectonothermal events in Gemericum and adjacent units (Western Carpathians, Slovakia): Contribution by the $^{40}Ar/39Ar$ dating. *Slovak Geological Magazine, 11, 2–3, 155–163.*

Davies, G. F., 2022: Stories from the Deep Earth. How scientists figured out what drives tectonic plates and mountain building. *Springer Nature Switzerland AG, 1–202*.

de Meijer, R. J. & van Westrenen, W., 2008: The feasibility and implications of nuclear georeactors in Earth's core-mantle boundary region. *South African Journal of Science, 104, 3, 111–118.*

Demko, R. & Hraško, Ľ., 2013: Ryolitové teleso Gregová pri Telgárte. *Mineralia Slovaca, 45, 161–174* (in Slovak with English summary).

Dewey, J. F. & Burke, K., 1974: Hot spots and continental break-up: Implications for collisional orogeny. *Geology, 2, 57–60.*

Doglioni, C., 1993: Geological evidence for a global tectonic polarity. *Journal of the Geological Society (London), 150, 991–1002.*

Doglioni, C., Moretti, I. & Roure, F., 1991: Basal lithospheric detachment, eastward mantle flow and Mediterranean geodynamics: A discussion. *Journal of Geodynamics, 13, 1, 47–65.*

Doglioni, C., Harabaglia, P., Merlini, S., Mongelli, F., Peccerillo, A. & Piromallo, C., 1999: Orogens and slabs vs. their direction of subduction. *Earth-Science Reviews, 45, 167–208.*

Doglioni, C., Cuffaro, M. & Carminati, E., 2006: What moves slabs? *Bolletino di Geofisica Teorica ed Applicata, 47, 3, 227–247.*

Domeier, M., Van der Voo, R. & Torsvik, T. H., 2012: Paleomagnetism and Pangea: The road to reconciliation. *Tectonophysics, 514–517, 14–43.*

Evans, D. A. D. & Mitchell, R. N., 2011: Assembly and breakup of the core of Paleoproterozoic-Mesoproterozoic supercontinent Nuna. *Geology, 39, 5, 443–446.*

Finger, F., Broska, I., Haunschmid, B., Hraško, Ľ., Kohút, M., Krenn, E., Petrík, I., Riegler, G. & Uher, P., 2003: Electron-microprobe dating of monazites from Western Carpathian basement granitoids: Plutonic evidence for an important Permian rifting event subsequent to Variscan crustal anatexis. *Int. J. Earth Sci. (Geologische Rundschau), 92, 86–98.*

Fowler, W. A., 1984: Experimental and theoretical nuclear astrophysics: the quest for the origin of the elements. Lecture delivered on December 8, 1983, on the occasion of the

presentation of the 1983 Nobel Prize in Physics. *Reviews of Modern Physics, 56, 2, I, 149–179.*

Foulger, G. R., 2010: Plates vs. plumes: A geological controversy. *Blackwell, Willey, 1–362.*

Fukuhara, M., 2016: Possible generation of heat from nuclear fusion in Earth's inner core. *Nature, Scientific Reports, 6, 37740.* DOI: 10.1038/srep37740.

Gawęda, A., Szopa, K., Golonka, J., Chew, D. & Waśkowska, A., 2021: Central European Variscan Basement in the Outer Carpathians: A case study from the Magura Nappe, Outer Western Carpathians, Poland. *Minerals, 11, 256.* https://doi.org/10.3390/min11030256.

Gazdačko, Ľ., 1994: Polyfázový deformačný vývoj východnej časti stykovej zóny gemerika a veporika. *Mineralia Slovaca., 26, 6, 387–398* (in Slovak with English summary).

Gerátová, S., Vojtko, R., Lačný, A. & Kriváňová, K., 2022: The structural pattern and tectonic evolution of the Muráň fault revealed by geological data, fault-slip analysis, and paleostress reconstruction (Western Carpathians). *Geologica Carpathica, 73, 1, 43–62.*

Girbacea, R. & Frisch, W., 1998: Slab in the wrong place: Lower lithospheric mantle delamination in the last stage of the Eastern Carpathian subduction retreat. *Geology, 26, 611–614.*

Golonka, J., Krobicki, M., Oszczypko, N., Ślączka, A. & Słomka, T., 2003: Geodynamic evolution and palaeogeography of the Polish Carpathians and adjacent areas during Neo-Cimmerian and preceding events (latest Triassic–earliest Cretaceous). In: McCann, T. & Saintot, A. (eds.): Tracing Tectonic Deformation Using the Sedimentary Record. *The Geological Society of London, Special Publications, 208, 138–158.*

Golonka, J., 2011: Evolution of the Outer Carpathian Basins. In: Bąk, M., Kaminski, M. A. & Waśkowska, A. (eds.): Integrating Microfossil Records from the Oceans and Epicontinental Seas. *Grzybowski Foundation Special Publication, 17, 3–14.*

Golonka, J., Krobicki, M. & Waśkowska, A., 2018: The Pieniny Klippen Belt in Poland. *Geology, Geophysics & Environment, 44, 1, 111–125.* http://dx.doi.org/10.7494/geol.2018.44.1.111.

Göğüş, O. H., Pysklywec, R. N. & Faccenna, C., 2016: Postcollisional lithospheric evolution of the Southeast Carpathians: Comparison of geodynamical models and observations. *Tectonics, 35, 1205–1224.* doi:10.1002/2015TC004096.

Grecula, P., 1982: Gemerikum – segment riftogénneho bazénu Paleotetýdy. *Bratislava, Alfa, 1–263* (in Slovak with extended English summary).

Grecula, P., Návesňák, D., Bartalský, B., Gazdačko, Ľ., Németh, Z., István, J. & Vrbatovič, P., 1990: Shear zones and arc structure of Gemericum, the Western Carpathians. *Mineralia Slovaca, 22, 97–110.*

Grecula, P. (ed.), Abonyi, A., Abonyiová, M., Antaš, M., Bartalský, B., Bartalský, J., Dianiška, I., Drnzík, E., Ďuďa, R., Gargulák, M., Gazdačko, Ľ., Hudáček, J., Kobulský, J., Lörinz, L., Macko, J., Návesňák, D., Németh, Z., Novotný, L., Radvanec, M., Rojkovič, I., Rozložník, L., Rozložník, O., Varček, C. & Zlocha, J., 1995: Mineral deposits of the Slovak Ore Mountains. Vol. 1. *Bratislava, Geocomplex, 1–829.*

Grecula, P., Hovorka, D. & Putiš, M. (eds.), 1997: Geological evolution of the Western Carpathians. *Bratislava, Mineralia Slovaca – Monogr., 1–370.*

Grecula, P. (ed.), Kobulský, J., Gazdačko, Ľ., Németh, Z., Hraško, Ľ., Novotný, Ľ. & Maglay, J., 2009: Geological map of the Spiš-Gemer Ore Mts., 1 : 50 000. *Bratislava, State Geological Institute of Dionýz Štúr.*

Grecula, P. & Kobulský, J., 2011: Vysvetlivky ku geologickej mape Spišsko-gemerského rudohoria 1 : 50 000. *Bratislava, State Geological Institute of Dionýz Štúr* (in Slovak with English summary).

Herndon, J. M., 1996: Substructure of the inner core of the Earth (nuclear fission / chondrite / oxidation state / seismology / composition). *Proc. Natl. Acad. Sci. USA, Geophysics, 93, 646–648.*

Herndon, J. M., 2011: Geodynamic basis of heat transport in the Earth. *Current Science, 101, 11, 1440–1450.*

Heron, P. J., Lowman, J. P. & Stein, C., 2015: Influences on the positioning of mantle plumes following supercontinent formation. *Journal of Geophysical Research, Solid Earth, 120, 3628–3658.*

Hide, R., Clayton, R. W., Hager, B. H., Spieth, M. A. & Woorhies, C. V., 1993: Topographic core-mantle coupling and fluctuations in the Earth's rotation: Relating Geophysical Structures and Processes. *The Jeffreys Volume Geophysical Monograph, 76, IUGG Volume 16, 107–120.*

Hók, J. & Hraško, Ľ., 1990: Deformačná analýza západnej časti pohorelskej línie. *Mineralia Slovaca, 22, 1, 69–80* (in Slovak with English summary).

Hók, J., Kováč, P. & Madarás, J., 1993: Extenzná tektonika západného úseku styčnej zóny gemerika a veporika. *Mineralia Slovaca, 25, 3, 172–176* (in Slovak with English summary).

Hók, J., Pelech, O., Teťák, F., Németh, Z. & Nagy, A., 2019: Outline of the geology of Slovakia (W. Carpathians). *Mineralia Slovaca, 51, 1, 31–60.*

Holmes, A., 1929: A review of the continental drift hypothesis. *The Mining Magazine, April 1929.*

Hovorka, D., Ivan, P. & Spišiak, J., 1984: Nappe with the amphibolite metamorphites in the Inner Western Carpathians – its position, origin and interpretations. *Mineralia Slovaca, 16, 1, 73–86.*

Hraško, Ľ., Bezák, V. & Molák, B., 1997: Postorogénne peraluminózne dvojsľudné granity a granitové porfýry v kohútskej zóne veporika (oblasť Klenovec – Zlatno). *Mineralia Slovaca, 29, 2, 113–135* (in Slovak with English summary).

Hraško, Ľ., Határ, J., Huhma, H., Mäntäri, I., Michalko, J. & Vaasjoki, M., 1999: U/Pb zircon dating of the Upper Cretaceous granite (Rochovce type) in the Western Carpathians. *Krystalinikum, 25, 163–171.*

Hraško, Ľ., Németh, Z. & Konečný, P., 2024: Variscan lithotectonic units in the Suchý massif of the Strážovské vrchy Mts, Western Carpathians – products of sedimentary, tectonometamorphic and granite forming processes. *Mineralia Slovaca, 56, 1, 3–50.* https://doi.org/10.56623/ms.2024.56.1.1.

Huang, Z., Yuan, C., Long, X., Zhang, Y. & Du, L., 2019: From breakup of Nuna to assembly of Rodinia: A link between the Chinese Central Tianshan Block and Fennoscandia. *Tectonics, 38, 4378–4398.* https://doi.org/10.1029/2018TC005471.

IERS, 2023: Measuring the irregularities of the Earth`s rotation. *Frankfurt am Main, Germany, Central Bureau of the International Earth Rotation and Reference Systems Service (IERS) hosted by the Federal Agency for Cartography and Geodesy (BKG) (9th May 2023).* https://www.iers.org/IERS/EN/Science/EarthRotation/EarthRotation.html.

Irving, E., 1977: Drift of the major continental blocks since the Devonian. *Nature, 270* (*5635), 304–309.*

Ivan, P., 1996: Problems of geodynamic evolution and geological structure of the Paleozoic Gemeric Unit (Inner Western Carpathians) as inferred by magmatic rock study. *Slovak Geological Magazine, 3–4, 239–243.*

Ivan, P., 2002: Relics of the Meliata ocean crust: Geodynamic implications of mineralogical, petrological and geochemical proxies. *Geologica Carpathica, 53, 4, 245–256.*

Ivan, P., Méres, Š. & Sýkora, M., 2009: Magnesioriebeckite in red cherts and basalts (Jaklovce Fm., of the Meliatic Unit, Western Carpathians): An indicator of initial stage of the high-pressure subduction metamorphism. *Mineralia Slovaca, 41, 4, 419–432* (in Slovak with English summary).

Ivan, P. & Méres, Š., 2012: The Zlatník Group – Variscan ophiolites on the northern border of the Gemeric Superunit (Western Carpathians). *Mineralia Slovaca, 44, 1, 39–56.*

Janák, M., Plašienka, D., Frey, M., Cosca, M., Schmidt, S. Th., Lupták, B. & Méres, Š., 2001a: Cretaceous evolution of a metamorphic core complex, the Veporic unit, Western Carpathians (Slovakia): P-T conditions and in situ $^{40}Ar/^{39}Ar$ UV laser probe dating of metapelites. *J. metamorphic Geol., 19, 197–216.*

Janák, M., Cosca, M., Finger, F., Plašienka, D., Koroknai, B., Lupták, B. & Horváth, P., 2001b: Alpine (Cretaceous) metamorphism in the Western Carpathians: P-T-t paths and exhumation of the Veporic core complex. *Geologisch--Paläontologische Mitteilungen Innsbruck, 25, 115–118.*

Jurewicz, E., 2005: Geodynamic evolution of the Tatra Mts. and the Pieniny Klippen Belt (Western Carpathians): problems and comments. *Acta Geologica Polonica, 55, 3, 295–338.*

Knapp, J. H., Knapp, C. C., Raileanu, V., Matenco, L., Mocanu, V. & Dinu, C., 2005: Crustal constraints on the origin of mantle seismicity in the Vrancea zone, Romania: The case for active continental lithospheric delamination. *Tectonophysics, 410, 311–323.* doi:10.1016/j.tecto.2005.02.020.

Kohút, M., Kovach, V. P., Kotov, A. B., Salnikova, E. B. & Savatenkov, V. M., 1999: Sr and Nd isotope geochemistry of Hercynian granitic rocks from the Western Carpathians – implications for granite genesis and crustal evolution. *Geologica Carpathica, 50, 477–487.*

Kohút, M., Nabelek, P. & Recio, C., 2001: Stable isotopes. In: Petrík, I., Kohút, M. & Broska, I. (eds.): Granitic plutonism of the Western Carpathians. Monograph. *Bratislava, Veda, 33–35.*

Kohút, M. & Recio, C., 2002: Sulphur isotope study of selected Hercynian granitic and surrounding rocks from the Western Carpathians (Slovakia). *Geologica Carpathica, 53, 3–13.*

Kohút, M., Uher, P., Putiš, M., Ondrejka, M., Sergeev, S., Larionov, A. & Paderin, I., 2009: SHRIMP U-Th-Pb zircon dating of the granitoid massifs in the Malé Karpaty Mountains (Western Carpathians): Evidence of Meso--Hercynian successive S- to I-type granitic magmatism. *Geologica Carpathica, 60, 5, 345–350.*

Kohút, M., 2012: Genesis of the Gemeric granites in the light of isotope geochemistry: Separated facts from myth. *Mineralia Slovaca, 44, 1, 89.*

Kohút, M., Stein, H., Uher, P., Zimmerman, A. & Hraško, Ľ., 2013a: Re-Os and U-Th-Pb dating of the Rochovce granite and its mineralization (Western Carpathians, Slovakia). *Geologica Carpathica, 61, 1, 71–79.*

Kohút, M., Trubač, J., Novotný, L., Ackerman, L., Demko, R., Bartalský, B. & Erban, V., 2013b: Geology and Re-Os molybdenite geochronology of the Kurišková U-Mo deposit (Western Carpathians, Slovakia). *Journal of Geosciences, 58, 271–282.*

Konečný, V., Kováč, M., Lexa, J. & Šefara, J., 2002: Neogene evolution of the Carpatho-Pannonian region: An interplay of subduction and back-arc diapiric uprise in the mantle. *EGS Spec. Publ. Ser., 1, 165–194.*

Kovách, A., Svingor, E. & Grecula, P., 1979: Nové dáta o gemerických granitoch. *Mineralia Slovaca, 11, 71–77* (in Slovak with English summary).

Kovách, A., Svingor, E. & Grecula, P., 1986: Rb/Sr isotopic ages of granitoide rocks from the Spiš-Gemer metalliferous Mts., West Carpathians, Eastern Slovakia. *Mineralia Slovaca, 18, 1–14.*

Kováč, M., 2000: Geodynamický, paleogeografický a štruktúrny vývoj karpatsko-panónskeho regiónu v miocéne: Nový pohľad na neogénne panvy Slovenska. *Bratislava, VEDA, 1–202* (in Slovak).

Kováč, M. & Plašienka, D., 2002: Geological structure of the Alpine-Carpathian-Pannonian junction and neighbouring slopes of the Bohemian Massif. *Bratislava, Comenius Univ., 1–45.*

Kováč, M., Bielik, M., Hók, J., Kováč, P., Kronome, B., Labák, P., Moczo, P., Plašienka, D., Šefara, J. & Šujan, M., 2002: Seismic activity and neotectonic evolution of the Western Carpathians (Slovakia). *EGU Stephan Mueller Special Publication, Series 3, 167–184.*

Kováčik, M. & Maluski, H., 1995: Alpine reactivation of the Eastern Veporic basement metamorphites (Western Carpathians). *Terra Nova, 7, Abstract suppl. 1, 45.*

Kováčik, M., Kráľ, J. & Maluski, H., 1996: Metamorhic rocks in the Southern Veporicum basement: their Alpine metamorphism and thermochronologic evolution. *Mineralia Slovaca, 28, 185–202.*

Kozur, H. & Mock, R., 1995: First evidence of Jurassic in the Folkmár Suture Zone of the Meliaticum in Slovakia and its tectonic implications. *Mineralia Slovaca, 27, 201–307.*

Krobicki, M., Golonka, J. & Aubrecht, R., 2003: Pieniny Klippen Belt: General geology and geodynamic evolution. In: Golonka, J. & Lewandowski, M. (eds.): Geology, geophysics, geothermics and deep structure of the West Carpathians and their basement. *Warszawa, Institute of Geophysics, Polish Academy of Sciences. monographic vol. M-28 (363), 25–33.*

Krystyn, L., Lein, R. & Gawlick, H.-J., 2008: How many Tethyan Triassic oceans? *Berichte Geol. B.-A., 76.*

Levin, B. W., Sasorova, E. V., Steblov, G. M., Domanski, A. V., Prytkov, A. S. & Tsyba, E. N., 2017: Variations of the Earth's rotation rate and cyclic processes in geodynamics. *Geodesy and Geodynamics, 8, 206–212.*

Lexa, J. & Konečný, V., 1998: Geodynamic aspects of the Neogene to Quaternary volcanism. In: Rakús, M. (ed.): Geodynamic development of the Western Carpathians. *Bratislava, GS SR, Dionýz Štúr Publ., 219–240.*

Lexa, O., Schulman, K. & Ježek, J., 2003: Cretaceous collision and indentation in the West Carpathians: View based on structural analysis and numerical modelling. *Tectonics, 22, 6, 1066.*

Liu, L., Chao, B. F., Sun, W. & Kuang, W., 2016: Assessment of the effect of three-dimensional mantle density heterogeneity on Earth rotation in tidal frequencies. *Geodesy and Geodynamics, 7, 396–405.* http://dx.doi.org/10.1016/j.geog.2016.09.002.

Ludwiniak, M., Śmigielski, M., Kowalczyk, S., Łoziński, M., Czarniecka, U. & Lewińska, L., 2019: The intramontane Orava Basin – evidence of large-scale Miocene to Quaternary sinistral wrenching in the Alpine-Carpathian-Pannonian area. *Acta Geologica Polonica, 69, 339–386.*

Madarás, J., Putiš, M. & Dubík, B., 1994: Structural characteristics of the middle part of the Pohorelá tectonic zone; Veporicum, Western Carpathians. *Mineralia Slovaca, 26, 177–191* (in Slovak with English summary).

Madarás, J., Hók, J., Siman, P., Bezák, V., Ledru, P. & Lexa, O., 1996: Extension tectonics and exhumation of crystalline basement of the Veporicum unit (Central Western Carpathians). *Slovak Geological Magazine, 3–4, 179–183.*

Maheľ, M., 1981: Island character of the Klippen Belt; Váhicum – continuation of Southern Penninicum in West Carpathians. *Geologický zborník – Geologica Carpathica, 32, 3, 293–305.*

Maheľ, M., 1986: Geologická stavba československých Karpát. Časť 1: Paleoalpínske jednotky. *Bratislava, Veda, 1–503.*

Maluski, H., Rajlich, P. & Matte, P., 1993: ^{40}Ar-^{39}Ar dating of the lnner Carpathians Variscan basement and Alpine mylonitic overprint. *Tectonophysics, 223, 313–337.*

Marko, F., 1993: Kinematics of Muráň fault between Hrabušice and Tuhár village. In: Rakús, M. & Vozár, J. (eds.): Geodynamický model a hlbinná stavba Západných Karpát. *Konferencie, sympóziá, semináre. Bratislava, Geol. Úst. D. Štúra, 253–261.*

Marko, F., 2024: Neo-Alpine fault controlled crustal blocks dynamics recorded by distribution of the Internal Western Carpathians Neogene basins and core mountains. *Mineralia Slovaca, 56, 2, 132–142.*

Marko, F. & Vojtko, R., 2006: Structural record and tectonic history of the Mýto – Tisovec fault (Central Western Carpathians). *Geologica Carpathica,* 57*, 211–221.*

Marko, F., Sigdel, A., Bielik, M., Bezák, V., Mojzeš, A., Madarás, J., Papčo, J., Siman, P., Acharya, S. & Fekete, K., 2020: A comparison of Cenozoic Neo-Alpine tectonic evolution of the Western Carpathian and Himalayan orogenic belts (Slovakia – Nepal). *Mineralia Slovaca, 52, 2, 63–82.*

Marko, F., Andriessen, P. A. M., Tomek, Č., Bezák. V., Fojtíková, L., Bošanský, M., Piovarči, M. & Reichwalder, P., 2017: Carpathian Shear Corridor – A strike-slip boundary of an extruded crustal segment. *Tectonophysics, 703–704, 119–134.*

Mello, J., Reichwalder, P. & Vozárová, A., 1998: Bôrka nappe: high-pressure relic from the subduction-accretion prism of the Meliata ocean (Inner Western Carpathians, Slovakia). *Slovak Geological Magazine, 4, 4, 261–273.*

Mello, J. & Ivanička, J. (eds.), Grecula, P., Janočko, J., Jacko st., S., Elečko, M., Pristaš, J., Vass, D., Polák, M., Vozár, J., Vozárová, A., Hraško, Ľ., Kováčik, M., Bezák, V., Biely, A., Németh, Z., Kobulský, J., Gazdačko, Ľ., Madarás, J. & Olšavský, M., 2008: General geological map of the Slovak Republic 1 : 200 000, Map sheet 37 – Košice. *Bratislava, Ministry of Environment of the Slovak Republic – Geological Institute of Dionýz Štúr.*

Mock, R., Sýkora, M., Aubrecht, R., Ožvoldová, L., Kronome, B., Reichwalder, P. & Jablonský, J., 1998: Petrology and petrography of the Meliaticum near the Meliata and Jaklovce villages, Slovakia. *Slovak Geological Magazine, 4, 223–260.*

Molčan Matejová, M., Potočný, T., Plašienka, D. & Aubrecht, R., 2025: Palaeoenvironmental interpretation of chaotic complexes of the Meliata Unit (Western Carpathians, Slovakia): new data from biochronology, lithostratigraphy and geochemistry. *Ofioliti, 50, 1, 17–36.*

Montelli, R., Nolet, G., Dahlen, F. A. & Masters, G., 2006: A catalogue of deep mantle plumes: New results from finite frequency tomography, *Geochem. Geophys. Geosyst., 7, Q11007*. doi:10.1029/2006GC001248.

Morel, P. & Irving, E., 1981: Paleomagnetism and the evolution of Pangea. *Journal of Geophysical Research, 86 (B3), 1858–1872.*

Morgan, W. J., 1971: Convection plumes in the lower mantle. *Nature, 230, 42–43.*

Morgan, W. J., 1972: Deep mantle convection plumes and plate motions. *Bulletin of American Association of Petroleum Geologists, 56, 202–213.*

Németh, Z., 2002: Variscan suture zone in Gemericum: Contribution to reconstruction of geodynamic evolution and metallogenetic events of Inner Western Carpathians. *Slovak Geological Magazine, 8, 3–4, 247–257.*

Németh, Z., 2005a: Geodynamic evolution of Gemericum and neighbouring Veporicum in the frame of two-phase divergence and convergence. *Mineralia Slovaca, 37, 3, 202–204.*

Németh, Z., 2005b: Paleopiezometry: Tool for determination of differential stresses for principal ductile shear zones of Gemericum, Western Carpathians. *Slovak Geological Magazine, 11, 2–3, 185–193.*

Németh, Z., 2018: Geodynamic background of the origin of Variscan and Paleo-Alpine metamorphic core complexes in the Western Carpathians and their metallogenetic importance. *XXI Int. Congress of the CBGA, Salzburg, Austria, September 10–13, 2018, Abstracts, p. 211.*

Németh, Z., 2021: Lithotectonic units of the Western Carpathians: Suggestion of simple methodology for lithotectonic units defining, applicable for orogenic belts world-wide. *Mineralia Slovaca, 53, 2, 91–90.*

Németh, Z., Gazdačko, Ľ., Návesňák, D. & Kobulský, J., 1997: Polyphase tectonic evolution of the Gemericum (the Western Carpathians) outlined by review of structural and deformation data. In: Grecula, P., Hovorka, D. & Putiš, M. (eds.), 1997: Geological evolution of the Western Carpathians. *Bratislava, Mineralia Slovaca – Geocomplex, 215–224.*

Németh, Z., Putiš, M. & Grecula, P., 2001: Generovanie oblúkovitého rozhrania gemerika s veporikom z pohľadu kinematiky alpínskeho extenzného odstrešovania. *Geologické práce, Správy, 105, 65–66* (in Slovak).

Németh, Z., Prochaska, W., Radvanec, M., Kováčik, M., Madarás, J., Koděra, P. & Hraško, Ľ., 2004: Magnesite and talc origin in the sequence of geodynamic events in Veporicum, Inner Western Carpathians, Slovakia. *Acta Petrologica Sinica, 20, 4, 837–854.*

Németh, Z., Radvanec, M., Kobulský, J., Gazdačko, Ľ., Putiš, M. & Zákršmidová, B., 2012a: Allochthonous position of the Meliaticum in the North-Gemeric zone (Inner Western Carpathians) as demonstrated by paleopiezometric data. *Mineralia Slovaca, 44, 1, 57–64.*

Németh, Z., Radvanec, M., Gazdačko, Ľ. & Kobulský, J., 2012b: Variscan tectonic setting vs. Alpine overprint in Gemericum (Inner Western Carpathians): Their role in the recent distribution of tectonic units in the eastern part of the territory as expressed in significant localities. *Mineralia Slovaca, 44, 1, 8–15.*

Németh, Z., Putiš, M. & Hraško, Ľ., 2016: The relation of metallogeny to geodynamic processes – the natural prerequisite for the origin of mineral deposits of public importance (MDoPI): The case study in the Western Carpathians, Slovakia. *Mineralia Slovaca, 48, 119–135.*

Németh, Z., Maglay, J., Petro, Ľ., Stercz, M., Grega, D., Pelech, O. & Gaál, Ľ., 2023: Neo-Alpine uplift and subsidence zones in the Western Carpathians: Product of kinematic activity on Cenozoic AnD3 (NW-SE and NE-SW) and AnD4 (E-W – subequatorial and N-S – submeridian) regional faults. *Mineralia Slovaca, 55, 2, 103–116.* https://doi.org/10.56623/ms.2023.55.2.1.

Ondrejka, M., Li, X.-H., Vojtko, R., Putiš, M., Uher, P. & Sobocký, T., 2018: Permian A-type rhyolites of the Muráň Nappe, Inner Western Carpathians, Slovakia: in-situ zircon U-Pb SIMS ages and tectonic setting. *Geologica Carpathica, 69, 2, 187–198.*

Ondrejka, M., Vojtko, R., Putiš, M., Chew, D. M., Olšavský, M., Uher, P., Nemec, O., Drakou, F., Molnárová, A. & Spišiak, J., 2022: Permian A-type rhyolites of the Drienok Nappe, Inner Western Carpathians, Slovakia: Tectonic setting from in-situ zircon U-Pb LA-ICP-MS dating. *Geologica Carpathica, 73, 2, 123–136.*

Oszczypko, N., 2006: Late Jurassic-Miocene evolution of the Outer Carpathian fold-and-thrust belt and its foredeep basin (Western Carpathians, Poland). *Geological Quaterly, 50, 1, 169–194.*

Pawula, A., 2022: Discourse on the evolution of the Earth. *Environment and Pollution, 11, 1, 65–78.*

Pelech, O., Vozárová, A., Uher, P., Petrík, I., Plašienka, D., Šarinová, K. & Rodionov, N., 2017: Late Permian volcanic dykes in the crystalline basement of the Považský Inovec Mts. (Western Carpathians): U-Th-Pb zircon SHRIMP and monazite chemical dating. *Geologica Carpathica, 68, 6, 530–542.*

Pelech, O. & Kronome, B., 2019: Structural analysis in the wider zone of Muráň fault between Šumiac and Tisovec. *Geologické práce, Správy, 134, 33–48* (in Slovak with English summary).

Petrík, I. & Kohút, M., 1997: The evolution of granitoid magmatism during the Hercynian orogen in the Western Carpathians. In: Grecula, P., Hovorka, D. & Putiš, M. (eds.): Geological evolution of the Western Carpathians. *Bratislava, Mineralia Slovaca, Monograph., 235–252.*

Picha, F. J., Stráník, Z. & Krejčí, O., 2006: Geology and hydrocarbon resources of the Outer Western Carpathians and their foreland, Czech Republic. In: Golonka, J. & Picha, F. J. (eds.): The Carpathians and their foreland: Geology and hydrocarbon resources. *Amer. Assoc. Petrol. Geol. Memoir, 84, 49–175.*

Pirajno, F., 2000: Ore deposits and mantle plumes. *Springer--Science-Business-Media, B. V., 1–546.*

Plašienka, D., 1997: Cretaceous tectonochronology of the Central Western Carpathians, Slovakia. *Geologica Carpathica, 48, 2, 99–111.*

Plašienka, D., 2003: Dynamics of Mesozoic pre-orogenic rifting in the Western Carpathians. *Mitt. Österr. Geol. Gesell., 94, 79–98.*

Plašienka, D., 2012: Jurassic syn-rift and Cretaceous syn-orogenic, coarse-grained deposits related to opening and closure of the Váhic (South Penninic) Ocean in the Western Carpathians – an overview. *Geological Quaterly, 56, 4, 601–628.*

Plašienka, D., 2018: Continuity and episodicity in the early Alpine tectonic evolution of the Western Carpathians: How large-scale processes are expressed by the orogenic architecture and rock record data. *Tectonics, 37, 2029–2079.* https://doi.org/10.1029/ 2017TC004779.

Plašienka, D., Grecula, P., Putiš, M., Kováč, M. & Hovorka, D., 1997a: Evolution and structure of the Western Carpathians: an overview. In: Grecula, P., Hovorka, D. & Putiš, M. (eds.): Geological evolution of the Western Carpathians. *Bratislava, Mineralia Slovaca – Monograph., 1–24i.*

Plašienka, D., Putiš, M., Kováč, M., Šefara, J. & Hrušecký, I., 1997b: Zones of Alpidic subduction and crustal underthrusting in the Western Carpathians. In: Grecula, P., Hovorka, D. & Putiš, M. (eds.): Geological evolution of the Western Carpathians. *Bratislava, Mineralia Slovaca – Monograph., 35–42.*

Plašienka, D., Janák, M., Lupták, B., Milovský, R. & Frey, M., 1999: Kinematics and metamorphism of a Cretaceous Core Complex: the Veporic Unit of the Western Carpathians. *Phys. Chem. Earth (A), 24, 8, 651–658.*

Plašienka, D. & Soták, J., 2015: Evolution of Late Cretaceous--Palaeogene synorogenic basins in the Pieniny Klippen Belt and adjacent zones (Western Carpathians, Slovakia): Tectonic controls over a growing orogenic wedge. *Annales Societatis Geologorum Poloniae, 85, 43–76.*

Plašienka, D., Bučová, J. & Šimonová, V., 2020: Variable structural styles and tectonic evolution of an ancient backstop boundary – the Pieniny Klippen Belt of the Western Carpathians. *International Journal of Earth Sciences, 109, 4, 1355–1376*. https://doi.org/10.1007/s00531-019-01789-5.

Potočný, T., Jeřábek, P. & Plašienka, D., 2023: Subduction – exhumation cycle recorded by calcite deformation microstructures: blueschist-facies metacarbonates and kinematic implications for deformation of the Meliata Unit (West Carpathians). *International Journal of Earth Sciences, 112, 2097–2117*. https://doi.org/10.1007/s00531-023-02344-z.

Potočný, T., Molčan Matejová, M., Méres, Š. & Plašienka, D., 2025: Th-U-Pb dating of euhedral monazites in radiolarian-bearing deposits: implications for the tectono-stratigraphic evolution of the Meliatic mélange in the Western Carpathians. *Journal of the Geological Society, 182, jsg2024-230.* https://doi.org/10.1144/jgs2024-230.

Putiš, M., 1992: Variscan and Alpidic nappe structures of the Western Carpathian crystalline basement. *Geologica Carpathica, 43, 369–380.*

Putiš, M., 1994: South Tatric-Veporic basement geology: Variscan nappe structures; Alpine thick-skinned and extensional tectonics in the Western Carpathians (Eastern Low Tatra Mountains, Northwestern Slovak Ore Mountains). *Mitt. Österr. geol. Gesell., 86, 83–99.*

Putiš, M., Sergeev, S., Ondrejka, M., Larionov, A., Siman, P., Spišiak, J., Uher, P. & Paderin, I., 2008: Cambrian-Ordovician metaigneous rocks associated with Cadomian fragments in the West-Carpathian basement dated by SHRIMP on zircons: a record from the Gondwana active margin setting. *Geologica Carpathica, 59, 3–18.*

Putiš, M., Ivan, P., Kohút, M., Spišiak, J., Siman, P., Radvanec, M., Uher, P., Sergeev, S., Larionov, A., Méres, Š., Demko, R. & Ondrejka, M., 2009a: Metaigneous rocks of the West-Carpathian basement, Slovakia: indicators of Early Paleozoic extension and shortening events. *Bull. Soc. géol. France, 180, 461–471.*

Putiš, M., Frank, W., Plašienka, D., Siman, P., Sulák, M. & Biroň, A., 2009b: Progradation of the Alpidic Central Western Carpathians orogenic wedge related to two subductions: constrained by $^{40}Ar/^{39}Ar$ ages of white micas. *Geodinamica Acta, 22, 31–56.*

Putiš, M., Radvanec, M., Sergeev, S., Koller, F., Michálek, M., Snárska, B., Koppa, M., Šarinová, K. & Németh, Z., 2011: Metamorphosed succession of cherty shales with basalt and diastrophic breccia in olistolith of the Meliatic Jurassic accretion wedge near Jaklovce (Slovakia), date on zircon (U-Pb SIMS SHRIMP). *Mineralia Slovaca, 43, 1, 1–18* (in Slovak with English summary).

Putiš, M., Li, J., Ružička, P., Ling, X. & Nemec, O., 2016: U/Pb SIMS zircon dating of a rhyolite intercalation in Permian siliciclastics as well as a rhyodacite dyke in micaschists (Infratatricum, W. Carpathians). *Mineralia Slovaca, 48, 135–144.*

Putiš, M., Koller, F., Li, X.-H., Li, Q.-L., Larionov, A., Siman, P., Ondrejka, M., Uher, P., Németh, Z., Ružička, P. & Nemec, O., 2019a: Geochronology of Permian-Triassic tectono-magmatic events from the Inner Western Carpathians and Austroalpine units. *Proceedings, Smolenice, October 9.–11., 2019, Geologica Carpathica, 70.*

Putiš, M., Danišík, M., Siman, P., Nemec, O., Tomek, Č. & Ružička, P., 2019b: Cretaceous and Eocene tectono-thermal events determined in the Inner Western Carpathians orogenic front Infratatricum. *Geological Quarterly, 63, 2, 248–274.*

Putiš, M., Soták, J., Li, Q-L., Ondrejka, M., Li, X-H., Hu, Z., Ling, X., Nemec, O., Németh, Z. & Ružička, P., 2019c: Origin and age determination of the Neotethys Meliata Basin ophiolite fragments in the Late Jurassic-Early Cretaceous accretionary wedge mélange (Inner Western Carpathians, Slovakia). *Minerals, 9, 652.* doi:10.3390/min9110652.

Putiš, M., Ondrejka, M., Nemec, O., Li, Q-L., Chew, D., Li, X-H., Madarás, J., Németh, Z., Spišiak, Z., Siman, P. & Ružička, P., 2024: The Western Carpathians Variscan Orogen: A collage of post-Cadomian Cenerian, and Paleotethyan complexes from the Gondwana-derived terranes (a new concept). In: Hudáčková, N., Nemec, O. & Ruman, A. (eds.): Environmental, structural and stratigraphical evolution of the Western Carpathians: 13th ESSEWECA Conference, Abstract Book, 3rd–4th December 2024, *Bratislava, Slovakia, 57–61.*

Radvanec, M., 1994: Crystallization sequence under partial crust melting in extensive regime on the example of granite generation in Ochtiná and Rochovce area (Western Carpathians). *Mineralia Slovaca, 26, 6, 373–386.*

Radvanec, M., 1999: Eklogitizované klinopyroxenické gabro s retrográdnou metamorfózou v pumpellyitovo-aktinolitovej fácii na vrchu Babiná a Ostrá (gemerikum). *Mineralia Slovaca, 31, 5–6, 467–484* (in Slovak with English summary).

Radvanec, M., 2000: P-T dráha exhumácie ultravysokotlakovo metamorfovaného peridotitu neďaleko Jakloviec na severe gemerika a na lokalite Skalka pri Sedliciach na sever od pruhu Branisko – Čierna hora. *Mineralia Slovaca, 32,* 5, *439–458* (in Slovak with English summary).

Radvanec, M., 2005: Prehnit-pyroxenit na lokalite Danková. *Mineralia Slovaca, 37, 3, 353–357.*

Radvanec, M., Konečný, P., Németh, Z. & Grecula, P., 2007: P-T-t dráha a lokálne anatektické tavenie metapelitu s prímesou psamitického kremeňa vo variskej metamorfóze gemerika. *Mineralia Slovaca, 39, 1–44* (in Slovak with extended English summary).

Radvanec, M., Konečný, P., Ondrejka, M., Putiš, M., Uher, P. & Németh, Z., 2009: Granity gemerika ako indikátor extenzie kôry nad neskorovariskou subdukčnou zónou a pri ranoalpínskej riftogenéze (Západné Karpaty): interpretácia podľa veku monazitu a zirkónu datovaného metódou CHIME a SHRIMP. *Mineralia Slovaca, 41, 4, 381–394* (in Slovak with English summary).

Radvanec, M., Németh, Z. & Bajtoš, P. (eds.), 2010: Magnesite and talc in Slovakia – Genetic and geoenvironmental models. Monograph. *Bratislava, State Geological Institute of Dionyz Štúr, 1–189.*

Radvanec, M., Németh, Z., Kráľ, J. & Pramuka, S., 2017: Variscan dismembered metaophiolite suite fragments of Paleo-Tethys in Gemeric unit, Western Carpathians. *Mineralia Slovaca, 49, 1, 1–48.*

Radvanec, M. & Németh, Z., 2018: Variscan epidote-eclogite, blueschists and pumpellyite-actinolite facies Cpx/Sr-rich epidote-metagabbro blocks exhumed in Carboniferous, with Permian amphibolite facies overprint (Gemeric unit, Western Carpathians). *Mineralia Slovaca, 50, 1, 55–99.*

Raghavan, R. S., 2002: Detecting a nuclear fission reactor at the center of the Earth. *arXiv.org, Ithaca, U.S.A., 1–5.*

Rakús, M. (ed.), 1998: Geodynamic development of the Western Carpathians. *Bratislava, Geological Survey of Slovak Republic, Dionýz Štúr Publishers, 1–290.*

Ricard, Y., Doglioni, C. & Sabadini, R., 1991: Differential rotation between lithosphere and mantle: A consequence of lateral mantle viscosity variations. *Journal of Geophysical Research, 96, B5, 8407–8415.*

Richards, M. A., Ricard Y., Lithgow-Bertelloni, C., Spada, G. & Sabadini, R., 1997: An explanation for Earth's long-term rotational stability. *Science, 275, 372–375.*

Roland, N. W., 1976: Tektonisches Standardnetze und Beanspruchungspläne für Erde und Mars. *Geologische Rundschau, 65, 17–33.*

Rusov, V. D., Pavlovich, V. N., Vaschenko, V. N., Tarasov, V. A., Zelentsova, T. N., Bolshakov, V. N., Litvinov, D. A., Kosenko, S. I. & Byegunova, O. A., 2007: Geoantineutrino spectrum and slow nuclear burning on the boundary of the liquid and solid phases of the Earth's core. *Journal of Geophysical Research, 112, B09203, 1–16.* doi:10.1029/2005JB004212.

Schlögl, J., Soták, J., Suan, G., Šamajová, L., Šimonová, V., Teťák, F. & Vozár, J., 2021: Structure, composition and tectonic evolution of the Pieniny Klippen Belt – Central Western Carpathians contiguous zone (Kysuce and Orava regions, NW Slovakia). *Bratislava, Comenius University, 1–148.*

Schmid, S. M., Bernoulli, D., Fügenschuh, B., Matenco, L., Schefer, S., Schuster, R., Tischler, M. & Ustaszewski, K., 2008: The Alpine-Carpathian-Dinaridic orogenic system:

correlation and evolution of tectonic units. *Swiss J. Geosci., 101, 139–183.*

Schmid, S. M., Fügenschuh, B., Koumov, A., Mațenco, L., Nievergelt, P., Oberhänsli, R., Pleuger, J., Schefer, S., Schuster, R., Tomljenovic, B., Ustaszewski, K. & van Hinsbergen, D. J. J., 2020: Tectonic units of the Alpine collision zone between Eastern Alps and western Turkey. *Gondwana Research, 78, 308–374.*

Schuiling, R. D., 2006: Is there a Nuclear Reactor at the Center of the Earth? *Earth, Moon, and Planets, 99, 33–49.* DOI 10.1007/s11038-006-9108-4.

Schwinner, R., 1920: Vulkanismus und Gebirgsbildung. Ein Versuch. *Zeitschrift Vulkanologie, 5, 175–230.*

Sikora, W., 1971: Esquisse de la tectogénèse de la zone des Klippes des Pieniny en Pologne d'après de nouvelles donnés géologiques. *Rocz. Pol. Tow. Geol., 41, 1, 221–239.*

Sikora, W., 1974: The Pieniny Klippen Belt (Polish Carpathians). In: Maheľ, M. (ed.): Tectonics of the Carpathian-Balkan regions. *Bratislava, Geological Institute of Dionýz Štúr, 177–180.*

Skupien, P. & Vašíček, Z., 2008: Western Carpathians in the territory of the Czech Republic. *Geologia, 34, 3/1, 139–149.*

Smolárik, M. & Németh, Z., 2015: Talc genesis related on tectonometamorphic evolution: Preliminary results from the Gemerská Poloma deposit (Gemericum, Western Carpathians). *Proceedings of Mineralogical-petrological conference Petros 2015, Bratislava, Comenius Univ., 54–57.*

Sobocký, T., Ondrejka, M., Uher, P., Mikuš, T. & Konečný, P., 2020: Monazite-group minerals and xenotime-(Y) in A-type granitic rocks: chemical composition and in-situ Th-U-total Pb EPMA dating (Velence Hills, Hungary). *Acta Geologica Slovaca, 12,* 2, *89–106.*

Sobolev, V. V. & Bilan, N. V., 2018: Physical conditions of the 'light' core formation and thermonuclear heat source deep inside the Earth. *Naukovyi Visnyk NHU, 5, 13–23.*

Sperner, B., Lorenz, F., Bonjer, K., Hettel, S., Müller, B. & Wenzel, F., 2001: Slab break-off – abrupt cut or gradual detachment? New insights from the Vrancea Region (SE Carpathians, Romania). *Terra Nova, 13, 172–179.*

Spišiak, J., Hovorka, D. & Ivan, P., 1985: Klátovská skupina – reprezentant metamorfitov amfibolitovej fácie Vnútorných Západných Karpát. *Geologické práce, Správy, 82, 205–220.*

Stille, H., 1924: Grundfragen der vergleichenden Tektonik. *Verlag von Gebrüder Borntraeger.*

Szabó, S., Novotný, L., Bartalský, B. & Jurík, I., 2014: Nové poznatky o geologickej stavbe ložiska Košice I – Kurišková. *Mineralia Slovaca, 46, 59–68* (in Slovak with extended English summary).

Tang, G.-J., Cawood, P. A., Wyman, D. A., Wang, Q. & Zhao, Z.-H., 2017: Evolving mantle sources in postcollisional early Permian-Triassic magmatic rocks in the heart of Tianshan Orogen (western China). *Geochemistry, Geophysics, Geosystems, 18, 4110–4122.* https://doi.org/10.1002/2017GC006977.

Tauson, L. B., Kozlov, V. D., Cambel, B. & Kamenický, L., 1977: Geochemistry and the problem of ore-bearing capacity of the Gemeride granites of Slovakia. *Geologický zborník – Geologica Carpathica, 28, 261–267* (in Russian with English abstract).

Terez, E. I. & Terez, I. E., 2011: Thermonuclear processes in the core is the main source of energy of geodynamic evolution and degassing of the Earth. *Bulletin of the Crimean Astrophysical Observatory, 107, 103–112.*

Terez, E. I. & Terez, I. E., 2013: Thermonuclear reaction as the main source of the Earth's energy. *International Journal of Astronomy and Astrophysics, 3, 362–365.* http://dx.doi.org/10.4236/ijaa.2013.33040.

Terez, E. I. & Terez, I. E., 2015: Fusion reactions as the main source of the Earth's internal energy. *Herald of the Russian Academy of Sciences, Vol. 85, 2, 163–169.*

Tokarski, A., Świerczewska, A., Zuchiewicz, W., Márton, E., Hurai, V., Anczkiewicz, A., Michalik, M., Szeliga, W. & Rauch-Włodarska, M., 2006: Conference Excursion 1: Structural development of the Magura Nappe (Outer Carpathians): From subduction to collapse. *GeoLines, 20, 145–164.*

Tomek, Č., 1993: Deep crustal structure beneath the central and inner West Carpathians. *Tectonophysics, 226, 417–431.*

Uhlig, V., 1890: Ergebnisse geologischer Aufnahmen in den westgalizischen Karpathen, II. Der pieninische Klippenzug. *Jahrbuch der k.-k. geologischen Reichsanstalt, 40, 3–4, 559–824.*

van Hinsbergen, D. J. J., Torsvik, T. H., Schmid, S. M., Mațenco, L. C., Maffione, M., Vissers, R. L. M., Gürer, D. & Spakman, W., 2020: Orogenic architecture of the Mediterranean region and kinematic reconstruction of its tectonic evolution since the Triassic. *Gondwana Research, 81, 79–229.*

Villasenor, G., Catlos, E. J., Broska, I., Kohút, M., Hraško, Ľ., Aguilera, K., Etzel, T. M., Kyle, J. R. & Stockli, D. F., 2021a: Evidence for widestread mid-Permian magmatic activity related to rifting following the Variscan orogeny (Western Carpathians). *Lithos, 390–391.* https://doi.org/10.1016/j.lithos.2021.106083.

Villasenor, G., Catlos, E.J ., Broska, I., Kohút, M., Hraško, Ľ., Aguilera, K., Etzel, T. M., Kyle, J. R. & Stockli, D. F., 2021b: Western Carpathian mid-Permian magmatism: Petrographic, geochemical and geochronological data. *Data in Brief, 36.*

Vojtko, R., Tokárová, E., Sliva, Ľ. & Pešková, I., 2010: Cenozoic palaeostress field reconstruction and revised tectonic history in the northern part of the Central Western Carpathians (the Spišská Magura and Tatra Mountains). *Geologica Carpathica, 61, 211–225.* https://doi.org/10.2478/v10096-010-0012-5.

Vojtko, R., Králiková, S., Kriváňová, K. & Vojtková, S., 2015: Lithostratigraphy and tectonics of the eastern part of the Veporské vrchy Mts. (Central Western Carpathians). *Acta Geologica Slovaca, 7, 113–127.*

Vozár, J., Ebner, F., Vozárová, A., Haas, J., Kovács, S., Sudar, M., Bielik, M. & Peró, Cs. (eds.), 2010: Variscan and Alpine terranes of the Circum-Pannonian region. *Bratislava, Geological Institute, Slovak Academy of Sciences, 7–233.*

Vozárová, A., Šmelko, M., Paderin, I. & Larionov, A., 2012: Permian volcanics in the Northern Gemericum and Bôrka Nappe system: U-Pb zircon dating and the implications for geodynamic evolution (Western Carpathians, Slovakia). *Geologica Carpathica, 63, 3, 191–200.*

Vozárová, A., Rodionov, N., Vozár, J., Lepekhina, E. & Šarinová, K., 2016: U-Pb zircon ages from Permian volcanic rocks and tonalite of the Northern Veporicum (Western Carpathians). *Journal of Geosciences, 61, 221–237.*

Vozárová, A., Šarinová, K., Rodionov, N. & Vozár, J., 2020: Zircon U-Pb geochronology from Permian rocks of the Tribeč Mts. (Western Carpathians, Slovakia). *Geologica Carpathica, 71, 3, 374–287.*

Vozárová, A., Rodionov, N., Šarinová, K. & Vozár, J., 2021: U-Pb zircon ages from Permian volcanites of the Čierna Hora Mts. (Western Carpathians, Slovakia): Regional tectonic implications. *Geologica Carpathica, 72, 5, 361–372.*

Wallace, R. E. (ed.), 1990: The San Andreas Faul System, California. *U.S. Geological Survey Proofessional Paper, 1515, 1–283.*

Wegener, A., 1912: Die Entstehung der Kontinente. *Geologische Rundschau, 3, 276–292.* https://doi.org/10.1007/BF02202896.

Wilson, C. R., 1995: Earth rotation and global change. *Reviews of Geophysics, Supplement, 225–229.*

Wilson, J. T., 1965: A new class of faults and their bearing on continental drift. *Nature, 207, 4995, 343–347.* doi:10.1038/207343a0.

Wilson, J. T., 1966: Did the Atlantic close and then re-open? *Nature, 211, 5050, 676–681*.

Wilson, J. T., 1967: C. Convection currents and continental drift. XIII. Evidence from ocean islands suggesting movement in the Earth. *Proceedings from the Symposium on continental drift, Montevideo, Uruguay (1967), 143–167.*

Wilson, R. W., Houseman, G. A., Buiter, S. J. H., McCaffrey, K. J. W. & Doré, A. G., 2019: Fifty years of thee Wilson Cycle concept in plate tectonics: an overview. *Geological Society, London, Special Publications, 470, 1–17.* https://doi.org/10.1144/SP470-2019-58.

Xu, Ch. & Sun, W., 2012: Co-seismic Earth's rotation change caused by the 2012 Sumatra earthquake. *Geodesy and Geodynamics, 3, 4, 28–31*.

Zhang, S., Li, Z.-X., Evans, D. A. D., Wu, H., Li, H. & Dong, J., 2012: Pre-Rodinia supercontinent Nuna shaping up: A global synthesis with new paleomagnetic results from North China. *Earth and Planetary Science Letters, 353–354, 145–155.*

Zhao, G., Wang, Y., Huang, B., Dong, Y., Li, S., Zhang, G. & Yu, S., 2018: Geological reconstructions of the East Asian blocks: From the breakup of Rodinia to the assembly of Pangea. *Earth-Science Reviews, 186, 262–286.*

Geodynamika polyorogenetických zón na príklade vývoja Západných Karpát

Dôkazmi o polyorogenetickom vývoji alpsko-karpatsko-himalájskej zóny (**obr. 1A, 2**) sú sporadické relikty paralelných sutúrnych zón so subekvatoriálnym (približne východno-západným) priebehom. Polyorogenéza, t. j. sekvencia viacerých po sebe nasledujúcich orogenetických (Wilsonových) cyklov, bola v tejto zóne najlepšie zdokumentovaná v Západných Karpatoch, pre ktoré je charakteristická symetrická oblúkovitá stavba, v strednej časti vyklenutá na sever (**obr. 1A, B**). Navyše, Západné Karpaty sa vyznačujú výraznou zonálnosťou a unikátnym detailným stupňom preskúmanosti.

V doterajších interpretáciách boli niektoré sutúrne zóny v Z. Karpatoch interpretované ako relikty zaoblúkových bazénov skorších „hlavných" oceánskych bazénov a s nimi súvisiacich subdukčných procesov. Tento sumarizujúci článok aplikovaním zjednodušujúcej prezentačnej metodiky *XD labelling* (Németh, 2021; **obr. 3**) zdôrazňuje doloženú existenciu troch kompletných orogenetických („horotvorných") cyklov v Z. Karpatoch. Pri tejto metodike premenná *X* vyjadruje názov orogenetického cyklu – napr. v prípade Z. Karpát variského – **VD** (paleozoický vývoj Z. Karpát), paleoalpínskeho – **ApD** (mezozoický vývoj Z. Karpát) a neoalpínskeho – **AnD** (generálne kenozoický vývoj Z. Karpát so začiatkom v závere mezozoika). Procesy a produkty pokadómskej cenerijskej orogenézy nie sú v tomto článku prezentované pre ich stále prebiehajúci výskum. Číselné vyjadrenie za symbolom *XD* pri konkrétnom orogenetickom cykle uvádza jeho konkrétnu orogenetickú fázu. Symbol **XD0** označuje divergentnú riftogénnu etapu vývoja, a to: **0a** – subfázu začiatku riftogenézy ešte na kontinentálnej kôre súvisiacu s regionálnou extenziou, **0b** – stenčovanie kontinentálnej kôry, **0c** – prebiehajúcu riftogenézu už s produkciou oceánskej kôry. **XD1** označuje proces konvergencie – **XD1s** subdukciu, **XD1o** obdukciu a **XD1c** kolíziu. Orogenetické cykly **XD0** a **XD1** tvoria základ orogenetického (platňovo-tektonického) cyklu, ktorý bol podľa prác J. T. Wilsona zo šesťdesiatych rokov minulého storočia nazvaný aj Wilsonov cyklus. J. T. Wilson sa považuje za zakladateľa koncepcie platňovej tektoniky, ktorá platí dodnes.

Množstvo nových poznatkov, ktoré boli získané v ostatných desaťročiach predovšetkým z Vnútorných Západných Karpát, iniciovalo potrebu rozšírenia klasického orogenetického (Wilsonovho) cyklu o ďalšie tri orogenetické fázy. Tým bol definovaný tzv. **rozšírený orogenetický cyklus** (Németh, 2021), v ktorom sú ku klasickému Wilsonovmu cyklu pridané fázy pokolíznych vnútroplatňových procesov: **XD2** – pokolízne odstrešovanie v dôsledku prehrievania a výzdvihu osi orogenetickej zóny teplom z horúcej línie (ako dôsledku subekvatoriálneho plášťového konvekčného prúdenia = *subequatorial-course mantle convection current* – **ECMCC**), **XD3** – označuje zvýšenú aktivitu párového systému strižných zón smeru SZ – JV (pravostranný strih) a SV – JZ (ľavostranný strih), **XD4** – obdobie zvýšenej regionálnej extenzie spôsobujúce vznik regionálnych zlomov (lineamentov) vyznačujúcich sa kinematikou čistého strihu a nezriedka presahujúcich hranice jednotlivých regiónov či dokonca štátov. Orogenetická fáza XD4 predznamenávala začiatok nového orogenetického cyklu. Genetickú a sukcesívnu spätosť orogenetických fáz XD3 a XD4 doložili Németh et al. (2023). Metodika *XD labelling* je veľmi vhodná na časové/evolučné zaraďovanie litotektonických jednotiek, ich rozhraní, ale aj na sukcesívne zaraďovanie metamorfných/rekryštalizačných prepisov horninových súborov s využitím indexu *MX* a pri zachovaní ďalších detailov ako pri *XD* indexovaní.

Ťažisko článku pozostáva z prehľadnej sumarizácie prejavov jednotlivých orogenetických cyklov a ich fáz v súslednom poradí od variského cez paleoalpínsky po neoalpínsky orogenetický cyklus. Text je doplnený výpovednými obrázkami prevažne tektonického a geodynamického charakteru (**obr. 4 – 15**). Dôraz kladie na vysvetlenie, prečo autor ani jeden z analyzovaných pretiahnutých bazé-

nov s oceánskou kôrou v jeho osi nepovažuje za produkt zaoblúkovej extenzie, ale za novo vygenerovaný bazén v dôsledku extenzie nad lineárnym zdrojom konvekčného tepla (horúcou líniou, ECMCC). V záverečných kapitolách *5. Geodynamické úvahy vedúce k zrodeniu hypotézy novej globálnej tektoniky 2.0* a *6. Záverečné zosumarizovanie* autor prehľadnou formou približuje inovatívne interpretácie, ktoré prináša tento článok. Zároveň poskytuje námety na ďalšie bádanie, ktoré môžu posunúť súčasné znalosti z problematiky geodynamiky:

1. Súčasný astrofyzikálny výskum viacerých autorov (Fowler, 1984; Herndon, 1996, 2011; Raghavan, 2002; Anisichkin et al., 2005; Schuiling, 2006; Rusov et al., 2007; de Meijer a van Westrenen, 2008; Terez a Terez, 2011, 2013, 2015; Fukuhara, 2016; Sobolev a Bilan, 2018; Pawula, 2022) potvrdzuje existenciu kontinuálnych termonukleárnych reakcií vo vnútorných zónach Zeme, ktoré korešpondujú s reakciami prebiehajúcimi na Slnku. Tieto reakcie vo vnútorných zónach Zeme prispievajú energiou k udržovaniu vysokej teploty plášťových hmôt a ich konvekčnému prúdeniu globálneho rozsahu. V našej interpretácii ide o **subekvatoriálne plášťové vydutie** (generálne v smere V – Z v oblasti rovníka v dôsledku rotácie Zeme) = *subequatorial-course mantle bulge* ECMB, o paralelné **subekvatoriálne plášťové konvekčné prúdenie** (vo vyšších zemepisných šírkach) = *subequatorial-course mantle convection current* ECMCC a **submeridiánne plášťové konvekčné prúdenie** (generálne v smere S – J) = *submeridian-course mantle convection current* MCMCC), ale aj o plášťové diapíry (*mantle plumes* v klasickom chápaní, ktorých prejavom na zemskom povrchu sú *hot spots*, tzv. horúce škvrny). Plášťové diapíry *(mantle plumes)* môžu byť „vnútrozemskou verziou“ erupcií na povrchu Slnka (erupcie, na rozdiel od jadra Zeme, sú tam do prostredia vákua a teploty absolútnej nuly).
2. Na situovanie lineárnych zón globálneho plášťového konvekčného prúdenia (ECMB, ECMCCs a MCMCCs) má dominantný vplyv rotácia Zeme a zaostávanie rotácie zemskej kôry oproti rotácii plášťa Zeme v zmysle koncepcií autorov Ricard et al. (1991; obr. 2 ibid.), Doglioni (1993), Doglioni et al. (1999) a Courtillot et al. (2003). V súlade s týmito skoršími prácami sa autor tohto článku stotožňuje s názorom, že určujúcim faktorom geodynamiky Zeme je konvekčné prúdenie v plášti a nie „ťah subdukujúcej studenej oceánskej kôry“ *(subduction slab pull)*. Všeobecne je známe, že „studená“ oceánska kôra je hrubá asi 3 km (ale hrúbka horúcich plášťových hmôt pod ňou je niekoľko tisíc kilometrov) a ponáranie oceánskej kôry v subdukčných zónach je spôsobené prúdením plášťa, a nie ponáranie tenkej oceánskej kôry spôsobuje prúdenie plášťových hmôt a súvisiaci pohyb litosférických platní. Vo svete aj na Slovensku (**obr. 13**) je známych veľa prípadov tzv. synsubdukčne exhumovaných blokov vysokotlakovo metamorfovaných hornín. V podmienkach Západných Karpát tieto bloky zaobleného až dokonale guľovitého tvaru pochádzajú z plášťovej litosféry a bázy kontinentálnej kôry (metagabrá; Radvanec, 1999; Radvanec a Németh, 2018) alebo reprezentujú peridotit (Radvanec, 2000). Tieto exhumované bloky vysokotlakovo metamorfovaných hornín guľovitého tvaru (**obr. 13**) reprezentujú megaporfyroklasty. Keďže ide o horniny s vysokou mernou hmotnosťou, ich pohyb v subdukčnom kanáli proti prúdu subdukovaného mäkkého a spravidla nespevneného materiálu vyžaduje výrazne kompresné prostredie, nie extenziu, ktorá je hlavným faktorom interpretácie *subduction slab pull*.
3. Možnosť pohybu kontinentov po povrchu Zeme („kontinentálny drift“) v zmysle interpretácie A. Wegenera (1912 a následné práce) vyvrátil P. S. Epstein, matematik rusko-amerického pôvodu. Kontinenty ako také sa po povrchu Zeme nemôžu presúvať. Presúvajú sa litosférické platne a niektoré z nich na sebe nesú kontinenty. Túto zásadu vyjadril John Tuso Wilson (1965, 1966, 1967) vo svojich principiálnych prácach, ktoré položili základy platňovej tektoniky. Z histórie geovied je zaujímavá skutočnosť, že A. Wegener v dvadsiatych rokoch minulého storočia pôsobil ako profesor na univerzite v Grazi (Rakúsko) synchrónne s profesorom R. Schwinnerom, ktorý sa zaoberal konvekčným prúdením v plášti. Keby boli obaja profesori vzájomne komunikovali, mohli svoje koncepcie zjednotiť. Tým by boli položili základy platňovej tektoniky o približne štyri desaťročia skôr ako J. T. Wilson. Paralelne s pomerne komplikovaným vysvetlením pohybov litosférických platní kombináciou divergencie v riftových zónach, konvergencie v subdukčných zónach a bočných posunov na transformných zlomoch (Wilson, 1965) autor tohto článku prezentuje možnosť výrazne jednoduchšieho vysvetlenia pohybu litosférických platní po povrchu Zeme: početnosť a hustota distribúcie transformých zlomov (strižných zón) je oveľa vyššia, než bolo v minulosti známe. Dlhoročné terénne výskumy vo Vnútorných Západných Karpatoch, doložené aj geofyzikálnym profilovaním (Grecula et al., 1990), dokumentovali bočné posuny na stovkách zlomov párového (konjugovaného) systému strižných zón smeru generálne SZ – JV (pravostranné posuny) a SV – JZ (ľavostranné posuny). Týmto spôsobom sú litosférické platne pomerne husto segmentované na mikroplatne či bloky hornín, ktoré majú možnosť vzájomnými bočnými posunmi meniť vzájomnú konfiguráciu a takto prispievať k vzniku ohybov *(orogenic bend)* v priebehu horninových pruhov, či dokonca celých orogenetických zón. Najmarkantnejším prejavom takýchto ohybov sú tzv. syneklízy – dvojité ohyby v tvare písmena S. Sú známe z Karpát (dvojitý ohyb priebehu Západných Karpát, Východných Karpát a Južných Karpát), Himalájí (v ich východnom zakončení), ale aj z priebehu západnej časti kontaktnej zóny gemerika s veporikom (**obr. 1, 2 a 15C**). Vzájomný pohyb litosférických platní či mikroplatní uvedenou kinematikou sa dominantne viaže na orogenetické či polyorogenetické zóny; v kratonizovaných častiach Zeme je stabilita litosférických platní s pomerne hrubou lifosférou budovanou kryštalinikom výrazne vyššia.

Inovatívne aspekty geodynamiky Zeme uvedené v bodoch 1, 2 a 3 predstavujú vhodné témy na ďalší komplexný výskum a následné potvrdenie či vyvrátenie hypotézy, ktorú autor článku nazval *Nová globálna tektonika 2.0*. V každom prípade, poznatky získané mnohými desiatkami vysoko erudovaných bádateľov zo Západných Karpád výrazne obohacujú vedy o Zemi v celosvetovom meradle.

Doručené / Received: 2. 12. 2024
Prijaté na publikovanie / Accepted: 17. 12. 2024

Mineralia Slovaca, Web ISSN 1338-3523, ISSN 0369-2086, https://doi.org/10.56623/ms.2024.56.2.2
56, 2 (2024), 143 – 152, © Authors 2024. CC BY 4.0

Neo-Alpine fault controlled crustal blocks dynamics recorded by distribution of the Internal Western Carpathian Neogene basins and core mountains

FRANTIŠEK MARKO

Comenius University in Bratislava, Faculty of Natural Sciences,
Department of Geology and Paleontology, Ilkovičova 6, 842 15 Bratislava, Slovakia; frantisek.marko@uniba.sk

Abstract: In the Miocene epoch, the crust of eastward escaping Carpathian units was segmented by faults to independently moving tectonic blocks. Contemporaneously with invasion of the Carpathian units to the subducting oceanic embayment situated in the North European platform, syntectonic sedimentation took place on these moving tectonic blocks. The Neogene basins of the Internal Western Carpathians (IWC) reflect basin basement movement activity and can be from the point of view of their position in the orogen, basement dynamics and tectonic style divided to three geodynamic types: i) Large Middle Miocene-Pliocene back-arc, thermal-subsidence basins related to the mantle upwelling, ii) Early-Middle Miocene inter-arc fault-controlled basins, or their rotated and tilted remnants situated inside the Carpathian Shear Corridor (CSC) – a boundary strike-slip shear zone of extruded IWC crustal segment; iii) tectonically separated parts of disintegrated Internal Western Carpathian Early Miocene-Pliocene molasse basin, situated within strongly deformed peri-Klippen and Klippen zone, representing strike-slip tectonic interface between mutually rotated Internal and External Western Carpathian domains. The crustal block dynamics is reflected simultaneously in the core mountains distribution. The youngest core mountains (AFT age 9–22 Ma) are geneticaly related to and situated inside the CSC, which was interrupted by northward shifted tectonic block, explaining the outstanding position of the Malá Fatra Mts.

Key words: faults, block dynamics, Neogene basins, core mountains, Internal Western Carpathians

Graphical abstract

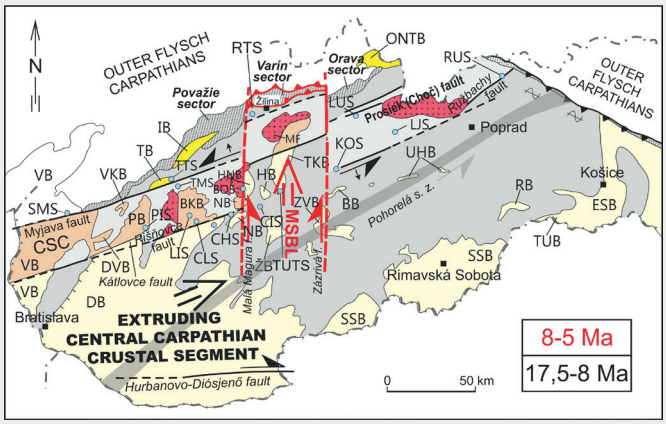

Highlights

- Paper deals with the Internal Western Carpathians blocks Miocene dynamics recorded in distribution of Neogene sedimentary basins and core mountains.
- As the prominent tectonic block boundary is regarded herein the Carpathian Shear Corridor (CSC), representing the northern sinistral tectonic interface of extruding Internal Carpathian crustal block.
- The division of Neogene basins to three geodynamic types is discussed, based on basement activity and indication of the Late Miocene interruption of the Carpathian Shear Corridor by Mid-Slovakian block shift towards the north.

Introduction

The Western Carpathian branch of Tethyan Alpides (Schmid et al., 2008; Minár et al., 2011) is composed of two tectonically juxtaposed prominent tectonic superunits of the Internal and External Western Carpathians (sensu Biely et al., 1996; Bezák et al., 2004). This principal tectonic division of the Western Carpathians is derived from the youngest Neo-Alpine (mostly Miocene) tectonic processes, when the flysch accretionary prism of the External Western Carpathians and the Pieniny Klippen Belt (PKB) structure were created due to the collision of the Internal Western Carpathians (IWC) block with the European platform. Internal Western Carpathians consist of the crustal basement thrust sheets with their sedimentary cover and superimposed detached superficial Mesozoic nappe units formed during the Paleo- and Meso-Alpine (Middle / Late Cretaceous up to the Early Paleogene) period. The crustal basement nappe units are composed of Variscan crystalline complexes and Upper Paleozoic and Mesozoic cover formations. The sedimentary basins with Upper Cretaceous and Paleogene flysch sequences represent the Meso-Alpine formations and Neogene sedimentary basins and neovolcanic complexes represent the Neo-Alpine formations superimposed on the Paleo- and Meso-Alpine nappe system.

Faulting had an important role during the Neo-Alpine tectonic evolution of Carpatho-Pannonian area (e.g. Grecula et al., 1990; Csontos et al., 1992; Csontos & Nagymarosy, 1998). Especially, in the process of individual detached blocks invasion into the future Carpathian realm controlled by strike-slip faults (Golonka et al., 2006). The shape of the Carpathian orogenic belt was constrained by the pre-collision shape of thin crust embayment – flysch basin inside the stable North European Platform (NEP). In the area of Eastern Alps, the progress of the orogenic front advancement stopped due to collision and Alpine units were pushed-up and juxtaposed to the southern margin of the Bohemian massif by Apulia microplate propagation to the north. Meanwhile, after frontal collision of Alpine orogenic belt with the European foreland, the Carpatho-Pannonian units escaped eastward to the bay of subducting thin quasioceanic crust (Ratschbacher et al., 1991; Nemčok, 1993; Fodor, 1995; Nemčok et al., 1998; Sperner et al., 2002; Kováč et al., 2018). Oceanic embayment in the North European platform was the depositional area for the Paleogene Magura basin flysch sediments (Oszczypko et al., 2015). In the Carpathian loop the active collisional front progressively moved from the west to the east (e.g. Jiříček, 1979; Matenco & Bertotti, 2000) due to oblique collision. During subduction of underlying thin crust beneath progressing Internal Western Carpathians, sediments of the Magura basin were scraped off and transformed to the structure of diachronous External Carpathian accretionary prism, consisting of rootless compressional flysch nappes and duplexes. These were arranged in a thin-skinned thrust system transfered to high-angle thrusts along the Pieniny Klippen Belt (PKB) boundary. The western segment of the PKB structure in between the External and Internal Carpathians was finally formed as the transpressional flower structure (e.g. Plašienka et al., 2020). In front of the flysch accretionary prism, fore-arc fore-land basin was created due to loading of pile of flysch nappes. Contemporaneously, the Internal Carpathian micro-plate, broken to several decoupled fragments that underwent large translations, rotations and smaller blocks also uplifts and subsidences due to tilting (e.g. Grecula & Roth, 1977; Jurewicz, 2005; Németh et al., 2023). It resulted in development of specific morpho-tectonic features as alternating intramontane basins (halfgrabens) and asymmetric horsts (core mountains), structural bendings due to strike-slip movements, fan-shaped tectonic structures and robust Miocene volcanic activity (Lexa & Konečný; 1998), which are all representing peculiarities of the Western Carpathians.

Dynamic evolution of the Western Carpathians resulted in a genetical variability of the Neogene sedimentary basins. Depending upon their geodynamic position in the orogen they were already described as fore-arc, inter-arc and back-arc basins and were recognized as basins formed by lithospheric extension – thermal subsidence, flexure and strike-slip related basins (Vass, 1979, 1998; Fodor et al., 1999; Kováč et al., 1997, 2017; Kováč, 2000). In the following, we focus to description and geodynamic evaluation of the Internal Western Carpathian basins in respect to IWC blocks movement activity.

The nature and tectonic zonation of the Internal Western Carpathian Neogene basins and young core mountains distribution related to crustal blocks dynamics

The process of Neo-Alpine tectonic evolution is reflected in the character of sedimentary depositions. The Western Carpathian Neogene basins are syn-orogenic and except of the foredeep basin, they are piggy-back in nature, because they were created on fluently moving Internal Carpathian crustal segments. The basins evolved, and some or part of them were subsequently deformed, even destroyed due to the basin inversion and erosion. This evolution is reflected in distribution, tectonic and age diversity of the Neogene sedimentary complexes.

Miall (1984) specifies the following principal criteria used in plate-tectonics related basin classification: (1) basin position relative to the plate margin; (2) character of the plate margin dynamics related to convergece, divergence and strike-slip, and (3) geotectonic type of crust (continetal, ocean, thick, thin,…). Depending upon basins geotectonic position there are in the Western Carpathians fore-arc basins in front of the orogenic belt because of roll-over down-warping of the over-riding External Carpathians flysch nappe units, large back-arc basins in the Internal Western Carpathians formed by lithospheric extension, and there are also many smaller intra-mountain (intramontane), intra-arc fault-controlled basins (Vass, 1979, 1998; Royden et al., 1982; Čech, 1988; Kováč et al., 1989, 1997, 1998, 2017, 2018; Kováč, 2000; Janočko et al., 2003). Some recent occurrences of Neogene sediments are only relics of inverted and eroded basins. The Western Carpathian Neo-Alpine orogenic belt has no classic volcanic arc, and volcanites, except of Vihorlat and Popriečny Mts., which occur inside the escaped micro-plate of Internal Western Carpathians. This is why the further major classification is based upon basin position relative to the progressing margin of the Internal Western Carpathians, what is the contact zone inbetween the Internal and External Carpathians – the Pieniny Klippen Belt. All basins south of the PKB, situated inside the moving Internal Western Carpathians are in back-arc or inter-arc position and basins north of the PKB are in fore-arc position.

The Vienna basin has an outstanding tectonic position among the Western Carpathians basins. It covers Alpine-Carpathian junction structure / area as well as contact zone of External and Internal Western Carpathians (PKB).

The Vienna basin is long-living depocentre of Neogene sedimentation with a complex history and it comprisizes both back-arc as well as fore-arc parts. The Vienna basin is genetically related to tectonic separation of the Eastern Alpine and Western Carpathian branches of Alpine orogenic belt (Tari et al., 2021). Basin as a whole was defined as a pull-apart basin (Royden, 1985) controlled by NW-SE sinistral strike-slip faults and N-S normal faults, creating depocenters of sedimentation. Sediments of the Slovakian part of the Vienna basin, situated on relatively thick crust (Čech, 1984, 1988; Royden, 1985; Wessely, 1988; Jiříček & Tomek, 1981; Tomek & Thon, 1988), cover the contact zone of Internal and External Western Carpathians, and the basin was classified as inter-mountain and inter-block, repectively (Čech, 1988), inter-arc sensu Miall (1984). The basin portion south of the PKB is in back-arc position and its basement is formed by IWC or Austro-Alpine units. The part of the Vienna basin situated north of the PKB is in fore-arc position and its basement is formed by flysch units of External Carpathians accretionary wedge. The middle part of the Vienna basin is affected by the strike-slips within the Carpahian Shear Corridor (Marko et al., 2017). The Early-Middle Miocene sequences of the Vienna basin, situated south of PKB, are strongly affected by escape of Central Carpathian Crustal Segment (CCCS; see Fig. 1) to the east. This model clarifies the origin of the Vienna basin isostatic imbalance (Tomek, pers. com.), caused by continued Central Carpathian Crustal Segment (CCCS) rapid escape during the Neo-Alpine period. Eastward motion of CCCS caused E-W extension at the back of escaping segment accommodated by N-S normal faulting and fast subsidence in the Vienna basin, as well N-S normal faulting in the Malé Karpaty Mts.

The Neogene basins of the Western Carpathians have been geodynamically classified to four types (Bezák et al., 2004); thermal extensional, shear (related to strike-slip faulting), post-collisional and piggy-back ones. Below we moderately moddify this division and we specify distribution of defined basin types in respect to prominent fault block boundaries.

The **Internal Western Carpathian Neogene basins** can be from the viewpoint of tectonic style, position in orogenic belt and the basin substratum block dynamics divided into three geodynamic types (Fig. 1). These are listed from south to north and numbered (1), (2) and (3) below:

(1) Large **Middle Miocene-Pliocene back-arc basins** related to the great Pannonian basin (thermal extensional basins sensu Bezák et al., 2004), which occupy territories of thin crust (Bielik et al., 2010; Tomek, 1993), characterized by high density gravity field (Pašteka et al., 2017) and high heat flow (Majcin et al., 2017). These include the southern part of the Vienna basin and Danube basin (e.g. Šujan et al., 2023), South Slovakian and East Slovakian basins (including Turňa basin), which represent peripheral depressions of the great Pannonian basin, situated south of the Carpathian Shear Corridor. The formation of the Neogene back-arc basins in the Carpathian orogenic system was driven by subduction of quasi-oceanic thin crust beneath the moving Internal Carpathian continental plate (as expressed in Stegena et al., 1975; Horváth & Royden, 1981; Jiříček & Tomek, 1981; Doglioni et al., 1991). This geodynamic process led to oblique continental collision (CC type) of the Carpathians with foreland, gradually progressing from the west to the east. The origin and subsidence of the great Pannonian basin (Bergerat, 1989; Tari et al., 1992; Horváth, 1993) and its peripheral depressions are related to the Pannonian mantle diapir activity (Van Bemmelen, 1972; Stegena et al., 1975; Mc Kenzie, 1978; Vass, 1979; Horváth & Royden, 1981; Royden et al., 1982) and also to its marginal satellite diapirs (Vass, 1979; Čech, 1988; Pospíšil, 1980). In addition to the thermal-controlled slow subsidence concept, Horváth and Royden (1981) and Royden (1985) submitted the fault-controlled pull-apart model of rapid subsidence of some local depocentres of sedimentation of the Pannonian depositional system. The NE-SW trending sinistral strike-slip master faults were here considered as the dominant responsible structures. These works inspired also some followers to describe strike-slip tectonics in the Western Carpathians Neogene basins (as in Pospíšil, 1990; Fodor, 1995; Decker & Pereson, 1996; Hrušecký et al., 1996; Kováč et al., 1989; Marko et al., 1991, 2012, 2017).

The southern part of the Vienna basin and the Danube basin are situated at the periphery of the great Pannonian basin. Subsidence of the Pannonian basin, situated on thinner crust in comparison to the Vienna basin, is connected with **Pannonian mantle diapir collapse accompanied by extensive Pliocene volcanic activity**.

The Horná Nitra, Handlová, southern part of Turiec, Žiar, Zvolen, Banská Bystrica, Upper Hron valley and Rožňava intra-mountain basins are isolated and related to the Danube and South Slovakian basins. These are the remnants of peripheral embayments-spurs of large basins into IWC shore preserved by the fault-controlled subsidence of individual blocks and some of them represent local depressions filled by volcano-sedimentary and lacustrine depositions (Konečný et al., 2003).

(2) The second geodynamic type of basins encompasses the isolated **Early-Middle Miocene intra-mountain fault-controlled basins including the strike-slip basins** (wrench furrows sensu Montenat et al., 1987), shear basins respectively (sensu Bezák et al., 2004), or their remnants situated in the Carpathian Shear Corridor (CSC). This emphasises the role of ENE-WSW strike-slip faults in the north-western part of the Western Carpathians during Neo-Alpine tectonic evolution, and it led to definition of ENE-WSW Carpathian Shear Corridor as the strike-slip

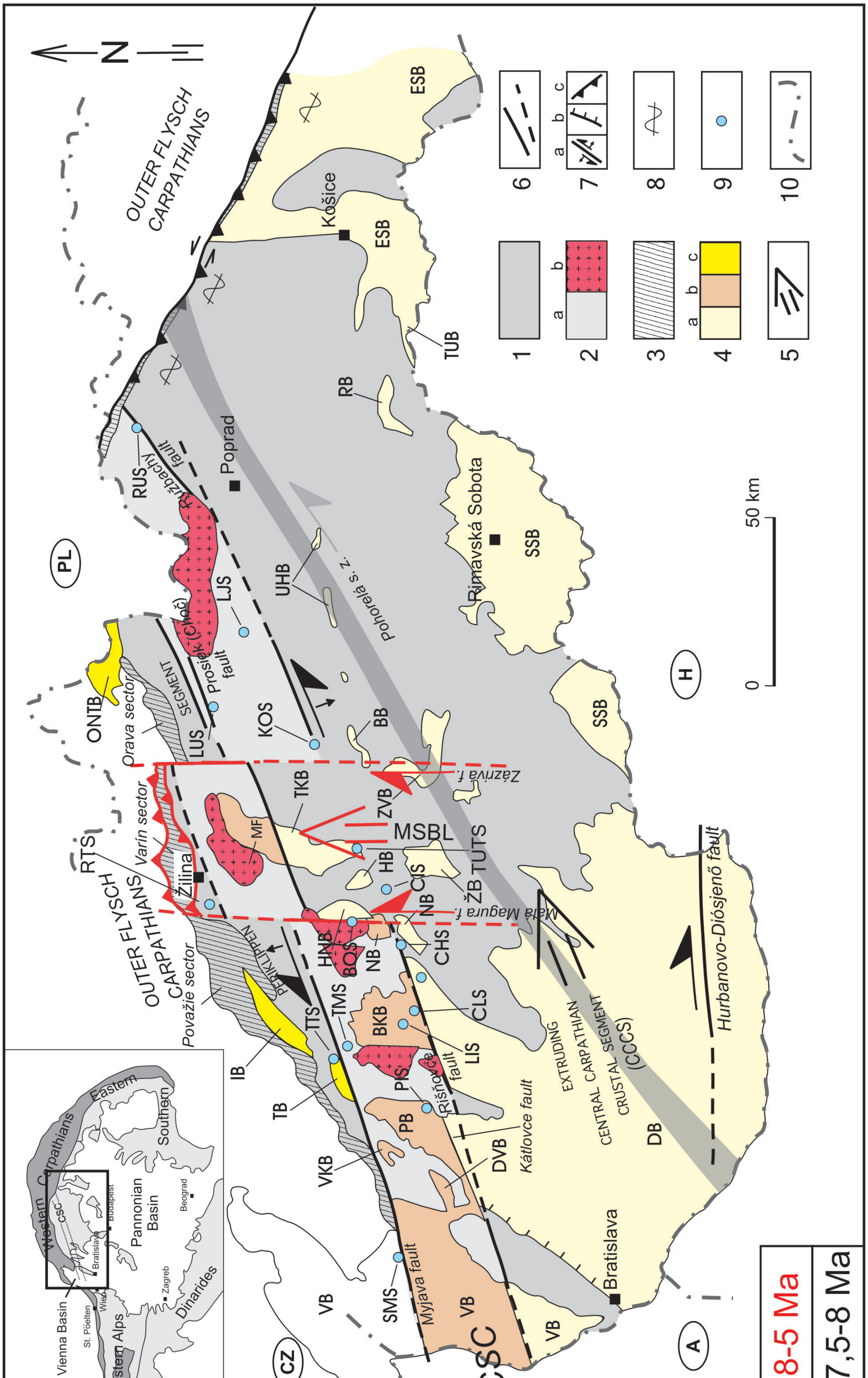
8-5 Ma
17,5-8 Ma
OUTER FLYSCH CARPATHIANS
OUTER FLYSCH CARPATHIANS
Orava sector
Varín sector
Považie sector
SEGMENT
PL
CZ
A
H
Košice
Poprad
Žilina
Bratislava
Rimavská Sobota
ESB
TUB
RB
UHB
SSB
ONTB
LUS
LJS
KOS
BB
TKB
ZVB
MSBL
TUTS
HB
ŽB
NB
CHS
BOS
HNB
RTS
MF
RUS
IB
TB
TTS
TMS
BKB
CLS
LIS
PS
PB
DVB
DB
VKB
SMS
VB
CSC
PERIKLIPPEN
Prosiek (Choč) fault
Ružbachy fault
Pohorelá s. z.
Zázrivá f.
Malá Magura f.
Rišňovce fault
Kátlovce fault
Myjava fault
Hurbanovo-Diósjenő fault
EXTRUDING CENTRAL CARPATHIAN CRUSTAL SEGMENT (CCCS)
0
50 km
Vienna Basin
St. Pöelten
Wien
Bratislava
Eastern Alps
Zagreb
Dinarides
Western
Carpathians
Eastern
Southern
Pannonian Basin
Budapest
Beograd
CsC
1
2
3
4
5
6
7
8
9
10
a
b
c

boundary of an extruded Central Carpathian Crustal Segment of Internal Western Carpathians (Marko et al., 2017). Within this ca 50 km wide shear zone there are situated the middle part of the Vienna basin, the depocenters of sedimentation of the northern spurs of the Danube basin (Piešťany bay depression, Bánovce depression, e.g. Marko, 2012; Hók et al., 2016) and the majority of intra-mountain basins (Dobrá voda, Vaďovce, northern part of Nováky, Horná Nitra and northern part of Turiec basins). Intense strike-slip shearing, block rotation and tilting occurred inside the CSC during the Lower-Middle Miocene evolution. This is reflected in the tectonic style of the Neogene half-grabens, alternating with tilted and rotated horsts of the outer core mountain belt – a basin and range-like structure. The CSC was a very dynamic environment for sedimentation and / or disintegration of existing basins, and there is an evidence that the CSC operated as a dextral shear zone and strike-slip basins (Kingston et al., 1983), developed inside the shear zone (CSC) in the Early Miocene stages (Kováč et al., 1989). After en-bloc counter clock wise (CCW) rotation of the Western Carpathians Internides (Balla, 1984), the CSC was re-oriented to ENE-WSW course and commenced operation as a sinistral strike-slip boundary of the eastwardly escaping Central Carpathian Crustal Segment. The Early Miocene deposits within the CSC were disintegrated by CCW block rotations and tilting during the long lasting and intense sinistral shearing, and contemporary the new, Middle-Late Miocene tecto-sedimentary cycle continued in localy developed depressions.

From the distribution of young core mountains (pushed-up and exhumed at ca 20–9 Ma ago (Kráľ, 1977; Danišík et al., 2010; Králiková et al., 2014a, b; Marko et al., 2017), which are geneticaly and spatialy related to CSC, it can be considered, that the Carpathian Shear Corridor was after its Upper Miocene sinistral strike-slip activity cut and interrupted by the N-S oriented Malá Magura and Zázrivá tear faults, rimming Mid-Slovakian upper crustal block (MSBL). This segment of CSC, rimmed by mentioned boundary strike-slip faults (Kováč & Hók, 1993), was ca 20 km shifted to the north approximately 8–5 Ma ago (Fig. 1, highlighted in red). This event resulted in push-out of the exhumed Malá Fatra Mts. core with Turiec basin to the north. This shift is a reason of contrasting compressional tectonic style in frontal part of displaced Mid-Slovakian Block (Haško & Polák, 1979; Marko et al., 2005; Plašienka et al., 2016) and E-W orientation of the Varín sector of PKB in contrast with the strike-slip style and NE-SW orientation of neighbouring Považie and Orava sectors of PKB. The geodynamic reason / drive of such extreme northward shift of the Mid-Slovakian block is going to be discussed in currently prepared paper (Marko, in prep.). dealing with Neo-Alpine tectonic evolution of the Western Carpathians internides. It seems to be gravitational structure – slide of the upper crustal packet due to robust volcanic activity in the Central Slovakian area related to a mantle plume.

(3) The third geodynamic type encompass the Trenčín, Ilava and Orava-Nowy Targ **basins situated north of CSC inside the intensively deformed Pieniny Klippen Belt and peri-Klippen zone and affected by its dynamics**. The Klippen zone represents strike-slip tectonic zone – suture dividing converging and mutually rotating / shifting External and Internal Western Carpathian terranes (Marschalko, 1979; Birkenmajer, 1986; Plašienka, 2018).

The largest Orava-Nowy Targ basin was interpreted as the fresh water molasse intramontane (Žytko et al., 1989; Zuchiewicz, 2002; Ludwiniak et al., 2019). fault controlled pull-apart basin (Nemčok & Lexa, 1990; Baumgart-Kotarba, 2001; Pomianowski, 2003; Zuchiewicz, 2010) with maximum thickness of Karpatian-

Fig. 1. Distribution and tectonic zonation of the Internal Western Carpathian Neogene sedimentary basins and young core mountains related to Middle (in black) and Late Miocene (in red) dynamics of crustal segments and blocks propagation. 1 – Internal Western Carpathians (in the frame of general map located upper left); 2 – a) Pre-Neogene units in Carpathian Shear Corridor (CSC), b) crystalline mountain cores uplifted and exhumed (22–9 Ma AFT ages) due to CSC activity; 3 – Pieniny Klippen Belt; 4 – Inner Western Carpathian Neogene sedimentary basins: a) Middle-Late Miocene to Pliocene back-arc basins related to the great Pannonian basin (thermal basins) and small fault controlled intramountain basins, b) Early-Middle Miocene basins genetically and spatially related to the Carpathian Shear Corridor (shear basins), c) fragmented Early Miocene basins situated within the Pieniny Klippen Belt zone and peri-Klippen zone; 5 – Movement tendencies of Internal Western Carpathians crustal segments and blocks; 6 – Main block-boundary faults, existing and supposed; 7 – Fault kinematics: a) strike-slip, b) normal, c) reverse; 8 – Neo-Alpine folds; 9 – Prominent thermal mineral water resources related to boundary-faults and structure of the Carpathian Shear Corridor; 10 – Slovak Republic state border, Numbers in frames in left down corner indicate the dominant periods of activity on faults in scheme coloured red and black. Abreviations: BB – Banská Bystrica basin, BKB – Bánovská kotlina basin, DB – Danube basin, DVB – Dobrá voda basin, ESB – East Slovakian basin, HB – Handlová basin, HNB – Hornonitrianska kotlina basin, IB – Ilava basin, MF – Malá Fatra Mts., MSBL – Mid-Slovakian block, NB – Nováky basin, ONTB – Orava-Nowy Targ basin, PB – Piešťanský záliv basin, RB – Rožňava basin, SSB – South Slovakian basin, TB – Trenčín basin, TKB – Turčianska kotlina basin, TUB – Turňa basin, UHB – Upper Hron valley basin, VB – Vienna basin, VKB – Vaďovská kotlina basin, ŽB – Žiar basin, ZVB – Zvolen basin; Thermal mineral water spa and springs / wells: CIS – Cigeľ, BOS – Bojnice, CHS – Chalmová, CLS – Chudá Lehota, KOS – Korytnica, LIS – Libichava, LJS – Liptovský Ján, LUS – Lúčky-kúpele, PIS – Piešťany, RTS – Rajecké Teplice, RUS – Ružbachy, SMS – Smrdáky, TMS – Trenčianske Mitice, TTS – Trenčianske Teplice, TUS – Turčianske Teplice.

Badenian-Sarmathian-Pliocene formations reaching 950 m (Watycha, 1976; Nagy et al., 1996; Potfaj, 2003; Lój et al., 2009).

The Trenčín and Ilava basins are filled with Eggenburgian to Pliocene sediments. The upper parts of the Trenčín, Ilava and the Orava-Nowy Targ basins have facially and lithologically identical sedimentary fill of the same latest Pannonian age – lacustrine clays with lignite intercalations overlain by fluvial sands and gravels (Biely et al., 1996).

Discussion

It is not excluded that formerly at least the Trenčín and Ilava, but maybe also Orava-Nowy Targ basins created one depocentre of molasse sedimentation in the early stages of the Carpathian Neo-Alpine evolution prior to the CCW en-bloc rotation of the Internal Western Carpathians, which are part of ALCAPA micro-plate (Balla, 1984). This basin could be in the process of ALCAPA CCW rotation disintegrated into the Trenčín, Ilava and perhaps also Orava-Nowy Targ parts, which were separated and dextrally displaced to the recent position, because ALCAPA CCW rotation should be in the Klippen and peri-Klippen zone accommodated by intensive dextral shearing inbetween the External and Internal Western Carpathians domains. If the Orava-Nowy Targ basin was a part of former unite molasses basin, we have to calculate with extreme ca 140 km dextral displacement along PKB zone, what represents the recent distance between Orava-Nowy Targ and Ilava basins.

In herein presented tectonic concept, the Carpathian Shear Corridor (CSC) operated as a prominent strike-slip boundary of the extruding Central Carpathian Crustal Segment (CCCS; Fig. 1). Boundary dislocations of CSC could be indicated also by occurences of thermal mineral water sources (Smrdáky, Piešťany, Trenčianske Teplice, Libichava, Chalmová, Chudá Lehota, Bojnice, Cigeľ, Turčianske Teplice, Korytnica, Lúčky-spa, Liptovský Ján, Ružbachy), which are apparently spatialy and geneticaly related to the structure of the Carpathian Shear Corridor. Deep reach of dynamic boundary faults of the Carpathian Shear Corridor could have been utilized as pathways for migration of water coming from deep thermal sources.

The Carpathian Shear Corridor, which represents the principal topic of this paper, is a conspicuous structure in morpho-tectonic surface architecture. Nevertheless, the most prominent crustal discontinuity named Pohorelá shear zone was interpreted by Bezák et al. (2023) in the new Bouger gravity anomaly map south of CSC. This tectonic interface is indicated also by magnetotelluric data (Bezák et al., 2020) and roughly corresponds the Vepor deep range fault formerly delineated by geophysicists and represents the strike-slip tectonic contact of gravitationally contrasting crustal segments (Bezák et al., 2023, and citations mentioned there). Pohorelá shear zone and CSC seems to be geneticaly related, they have similar course and strike-slip kinematics. This is why the Pohorelá shear zone, fault respectively, is drawn in Fig. 1 as well. While CSC accomodated significant Neo-Alpine progress of Carpathians crustal segments, the noticeable coeval activity of the Pohorelá shear zone has not been proven, it seems to be older structure.

Conclusions

The geodynamic approach to the Internal Western Carpathian Neogene basins, outlined in this paper of conceptual discussion character, could contribute to understanding of the nature and distribution of Neogene sediments and core mountains (Fig. 1). The extrusion concept of the Internal Western Carpathians (IWC) Neo-Alpine Miocene tectonic evolution emphasizes the role of faults during the step-wise extrusion of the Carpathian crustal segments. The rigid upper crust of progressing IWC was broken to independently moving blocks which filled the complex shaped oceanic embayment in the foreland plate. The prominent strike-slip faults, combined with thrusts and extensional faults controlled the occupation of the NEP embayment by individual Internal Carpathian and Pannonian blocks.

Character and distribution of Neogene sedimentary basins reflects tectonic processes realized during the formation of Western Carpathian structure. Contemporaneously with the progress in Carpathian orogenesis, the Neogene sedimentary basins were formed on the moving basement. In this light, the Miocene sedimentary sequences of the Internal Western Carpathian Neogene basins represent the syn-orogenic products of syn-tectonic sedimentation. Internal Carpathian Neogene sedimentary basins belong into the following three geodynamic types based on basin position relative to the progressing crustal segments margins:

1. Large back-arc basins related to the Pannonian basin system genetically connected with the activity of the Pannonian mantle diapir and its satellites and remnants of their intramontane embayments – spurs being fingered into IWC shore.
2. Strike-slip fault-controlled basins situated inside boundary shear zone (Carpathian Shear Corridor) of extruded IWC crustal segment, arranged in basin-and-range like structure, due to rotation and tilting of blocks in this dynamic strike-slip shear zone.
3. Isolated basins situated within the Klippen and peri-Klippen zone, which represent the separated parts of tectonicaly disintegrated molasse basin of Internal Western Carpathians due to Early-Middle Miocene extensive strike-slip shearing in highly strained zone between Inner and Outer Western Carpathian domains.

Young core mountains (uplifted and exhumed ca 20–9 Ma ago) are evidently spatialy related to CSC. They emerged due to strike-slip dynamics of this shear zone. It can be considered, that the Carpathian Shear Corridor was

after its Upper Miocene sinistral strike-slip activity cut and interrupted by N-S trending Malá Magura and Zázrivá tear faults, rimming the Mid-Slovakian upper crustal block (MSBL). This segment of CSC was shifted ca 20 km to the North approximately 8–5 Ma ago. This event resulted in push-out of the already exhumed Malá Fatra core Mts. with the Turiec basin to the north and is the reason of contrasting compressional tectonic style of the PKB Varín sector in contrast with the strike-slip style and NE-SW orientation of neighbouring Považie and Orava sectors of PKB.

Acknowledgements

This work was supported by the Slovak Research and Development Agency under contracts No. APVV-21-0159 and Vega 1/0107/23.

References

Balla, Z., 1984: The Carpathian loop and the Pannonian basin: a kinematic analysis. *Geoph. Trans., 30, 313–353.*

Baumgart-Kotarba, M., 2001: Continuous tectonic evolution of the Orava Basin (Norther Carpathians) from Late Badenian to present day? *Geologica Carpathica, 52, 103–110*.

Bergerat, F., 1989: From pull-appart to the rifting processes: The formation of the Pannonian basin. *Tectonophysics, 157, 271–280*.

Bezák, V., Bielik, M., Marko, F., Záhorec, P., Pašteka, R., Vozár, J. & Papčo, J., 2023: Geological and tectonic interpretation of new Bouguer gravity anomaly map of Slovakia, *Geologica Carpathica, 74, 2, 109–122*.

Bezák, V., Broska, I., Ivanička, J., Reichwalder, P., Vozár, J., Polák, M., Havrila, M., Mello, J., Biely, A., Plašienka, D., Potfaj, M., Konečný, V., Lexa, J., Kaličiak, M., Žec, B., Vass, D., Elečko, M., Janočko, J., Pereszlényi, M., Marko, F., Maglay, J. & Pristaš, J., 2004: Tectonic map of Slovak republic 1 : 500 000. Ed. V. Bezák. *Bratislava*, *Štátny geologický ústav Dionýza Štúra.*

Bezák, V., Pek, J., Vozár, J., Majcin, D., Bielik, M. & Tomek, Č., 2020: Geoelectrically distinct zones in the crust of the Western Carpathians: A consequence of Neogene strike-slip tectonics, *Geologica Carpathica, 71, 1, 14–23*. DI 10.31577/GeolCarp.71.1.2, UT WOS:000519627300002.

Bielik, M., Tášárová, Z. A., Vozár, J., Zeyen, M., Gutterch, A., Grad, M., Janik, T., Wybraniec, S., Götze, H.-J. & Dérerová, J., 2010: Gravity and seismic modeling in the Carpathian-Pannonian Region. In: Vozár, J. et al. (eds.): Variscan and Alpine terranes of the Circum-Pannonian Region. *Bratislava, Geological Institute, SAS, 202–233*.

Biely, A. (ed.), Bezák, V., Elečko, M., Gross, P., Kaličiak, M., Konečný, V., Lexa, J., Mello, J., Nemčok, J., Potfaj, M., Rakús, M., Vass, D., Vozár, J. & Vozárová, A., 1996: Explanations to geological map of Slovakia (1 : 50 000). *Bratislava, MŽP SR – GS SR, Výd. D. Štúra, 76 pp*. (in Slovak).

Birkenmajer, K., 1986: Stages of structural evolution of the Pieniny Klippen Belt, Carpathians. *Studia Geologica Polonica, 88, 7–32*.

Csontos, L. & Nagymarosy, A., 1998: The mid-Hungarian line: a zone of repeated tectonic inversion. *Tectonophysics, 297, 51–71*.

Csontos, L., Nagymarosy, A., Horváth, F. & Kováč, M., 1992: Tertiary evolution of the intra-Carpathian area: a model. *Tectonophysics, 208, 221–241*.

Čech, F., 1988: Dynamics of the Neogene Carpathian Basins in relation to Deep Structure, Crustal type and Fuel Deposits. *Západné Karpaty, Sér. Geológia, 12, 293 pp*.

Čech, F., 1984: The Vienna basin: Problems of its genesis and type. *Geologický Zborník – Geologica Carpathica, 35, 6, 667–682*.

Danišík, M., Kohút, M., Broska, I. & Frisch, W., 2010: Thermal evolution of the Malá Fatra Mountains (Central Western Carpathians): insights from zircon and apatite fission track thermochronology. *Geologica Carpathica, 61, 19–27*.

Decker, K. & Pereson, H., 1996: Tertiary kinematics in the Alpine-Carpathian-Pannonian system: links between thrusting, transform faulting and crustal extension. In: Wessely, G. & Liebl, S. (eds.): Oil and Gas in Alpidic Thrustbelts and Basins of Central and Eastern Europe. *EAGE Special Publication, 5, 69–77*.

Doglioni, C., Moretti, I. & Roure, F., 1991: Basal lithospheric detachement, eastward mantle flow and mediterranean geodynamics: a discussion. *J. of Geodyn*., *13, 3, 47–65*.

Fodor, L., 1995: From transpression to transtension: Oligocene-Miocene structural evolution of the Vienna basin and the East Alpine-West Carpathians junction. *Tectonophysics, 242, 151–182*.

Fodor, L., Csontos, L., Bada, G., Györfi, L. & Benkovics, L., 1999: Tertiary tectonic evolution of the Pannonian Basin system and neighbouring orogens: a new synthesis of paleostress data. In: Durand, B., Jolivet, L., Horváth, F. & Sérane, M. (eds.): The Mediterranean Basins: Tertiary extension within the Alpine Orogen. *Geol. Soc. London*, *Spec. Publ*., *156, 295–334*.

Golonka, J., Gahagan, L., Krobicki, M., Marko, F., Oszczypko, N. & Slaczka, A., 2006: Plate tectonic evolution and paleogeography of the Circum-Carpathian region. In: Golonka, J. & Pícha, F. (eds.): The Carpathians and their foreland: Geology and hydrocarbon resources. Monography. *Amer. Assoc. Petrol. Geol. Memoir, 84, 11–46*.

Grecula, P. & Roth, Z., 1978: Kinematický model Západních Karpat v souborném řezu. *Sborník geologických věd – Geologie (Praha), 32, 49–70*.

Grecula, P., Návesňák, D., Bartalský, B., Gazdačko, Ľ., Németh, Z., Ištván, J. & Vrbatovič, P., 1990: Shear zones and arc structure of Gemericum, the Western Carpathians. *Mineralia Slovaca, 22, 2, 97–110.*

Haško, J. & Polák, M., 1979: Explanations to geological map of Kysucké vrchy and Kriváň part of Malá Fatra Mts. in the scale 1 : 50 000. *Bratislava, Štátny geologický ústav Dionýza Štúra* (in Slovak).

Hók, J., Kováč, M., Pelech, O., Pešková, I., Vojtko, R. & Králiková, S., 2016: The Alpine tectonic evolution of the Danube basin and its northern periphery (southwestern Slovakia). *Geologica Carpathica, 67, 495–505*.

Horváth, F., 1993: Towards a mechanical model for the formation of the Pannonian basin. *Tectonophysics, 226, 333–357*.

Horváth, F. & Royden, L., 1981: Mechanism of the formation of the Intra-Carpathian basins: a review. *Earth Evol. Sci., 3–4, 307–316*.

Hrušecký, I., Šefara, J., Masaryk, P. & Lintnerová, O., 1996: The structural and facies development and exploration potential of the Slovak part of the Danube basin. In: Wessely, G. & Liebl, W. (eds.): Oil and Gas in Alpidic thrust-belts and basins of Central and Eastern Europe. *EAGE Spec. Publ., 5, 417–429*.

Janočko, J., Vass, D., Kováč, M., Konečný, V. & Lexa, J., 2003: Tectono-sedimentary evolution of Western Carpathian Tertiary basins: An overview. *Mineralia Slovaca, 3–4, 35, 161–168*.

Jiříček, R., 1979: Tectogenetic development of the Carpathian arc in the Oligocene and Neogene. In: Maheľ, M. (ed.): Tectonical profiles through the West Carpathians. *Bratislava, Geol. Inst. Dionýz Štúr, 205–214* (in Czech).

Jiříček, R. & Tomek, Č., 1981: Sedimentary and structural evolutionof the Vienna basin. *Earth. Evol. Sci., 3–4, 195–204*.

Jurewicz, E., 2005: Geodynamic evolution of the Tatra Mts. and the Pieniny Klippen Belt (Western Carpathians). *Acta Geol. Pol*., *55, 3, 295–338*.

Kingston, D. R., Dishroon, C. P. & Wiliams, P. A., 1983: Global basin classification system. *Amer. Assoc. Petrol. Geol. Bull., 67, 12, 2175–2193*.

Konečný, V., Lexa, J. & Šimon, L., 2003: Geologic structure and evolution of intravolcanic depressions in the area of Neogene volcanism in Central Slovakia. *Mineralia Slovaca, 35, 3–4, 255–290.*

Kováč, M., 2000: Geodynamic, paleogeographic and structural evolutionof Carpatho-Pannonian region in the Miocene: a new view on Neogene basins of Slovakia. *Bratislava, VEDA*, *203 pp*. (in Slovak).

Kováč, M., Bielik, M., Lexa, J., Pereszlényi, J., Šefara, J., Túnyi, I. & Vass, D., 1997: The Western Carpathian intramountane basins. In: Grecula, P., Hovorka, D. & Putiš, M. (eds.): Geological evolution of the Western Carpathians. *Bratislava, Mineralia Slovaca – Monograph., 43–64*.

Kováč, P. & Hók, J., 1993: The Central Slovak fault system – the field evidence of a strike-slip. *Geologica Carpathica, 49, 3, 155–159*.

Kováč, M., Baráth, I., Holický, I., Marko, F. & Tunyi, I., 1989: Basin opening in the Lower Miocene strike-slip zone in the SW part of the Western Carpathians. *Geologický Zborník – Geologica Carpathica, 10, 1, 37–62*.

Kováč, M., Márton, E., Kľučiar, T. & Vojtko, R., 2018: Miocene basin opening in relation to the north-eastward tectonic extrusion of the ALCAPA Mega-Unit. *Geologica Carpathica, 69, 254–263*.

Kováč, M., Márton, E., Oszczypko, N., Vojtko, R., Hók, J., Králiková, S., Plašienka, D., Kľučiar, T., Hudáčková, N. & Oszczypko-Clowes, M., 2017: Neogene palaeogeography and basin evolution of the Western Carpathians, Northern Pannonian domain and adjoing areas. *Global and Planetary Change, 155, 133–154.*

Kováč, M., Nagymarosy, A., Oszczypko, N., Slaczka, A., Csontos, L., Maruteanu, M., Matenco, L. & Márton, M., 1998: Palinspastic reconstruction of the Carpathian-Pannonian region during the Miocene. In: Rakús, M. (ed.): Geodynamic development of the Western Carpathians. *Bratislava, Geol. Surv. Slov. Rep., 189–217*.

Králiková, S., Vojtko, R., Andriessen, P., Kováč, M., Fügenschuh, B., Hók, J. & Minár, J., 2014a: Late Cretaceous – Cenozoic thermal evolution of the northern part of the Central Western Carpathians (Slovakia): revealed by zircon and apatite fission track thermochronology. *Tectonophysics, 615–616, 142–153*.

Králiková, S., Vojtko, R., Sliva, Ľ., Minár, J., Fügenschuh, B., Kováč, M. & Hók, J., 2014b: Cretaceous-Quaternary tectonic evolution of the Tatra Mts (Western Carpathians): constraints from structural, sedimentary, geomorphological, and fission track data. *Geologica Carpathica, 65, 4, 307–326*.

Kráľ, J., 1977: Fission track ages of apatites from some granitoid rocks in West Carpathians. *Geologický Zborník – Geologica Carpathica, 28, 269–276*.

Lexa, J. & Konečný, V., 1998: Geodynamic aspect of the Neogene to Quaternary volcanism. In: Rakús, M. (ed.): Geodynamic development of the Western Carpathians. *Bratislava, Geol Surv. Slovak Rep., 219–240*.

Lój, M., Madej, J., Porzucek, S. & Zuchiewicz, W., 2009: Monitoring geodynamic processes using geodetic and gravimetric methods: An example from the Western Carpathians (South Poland). *Geologia, Kwartalnik AGH, 35, 2, 217–247*.

Ludwiniak, M., Śmigielski, M., Kowalczyk, S., Łoziński, M., Czarniecka, U. & Lewińska, L., 2019: The intramontane Orava Basin – evidence of large-scale Miocene to Quaternary sinistral wrenching in the Alpine-Carpathian-Pannonian area. *Acta Geologica Polonica, 69, 339–386*.

Majcin, D., Král, M., Bilčík, D., Šujan, M. & Vranovská, A., 2017: Deep geothermal sources for electricity production in Slovakia: thermal conditions. *Contrib. to Geophys. Geod., 47, 1, 1–22*, doi:10.1515/congeo-2017-0001.

Marko, F., 2012: Cenozoic stress field and fault activity of northern margin of Danube basin (Western Carpathians, Slovakia). *Mineralia Slovaca, 44, 3, 213–230* (in Slovak).

Marko, F., Andriessen, P. A. M., Tomek, Č., Bezák, V., Fojtíková, L., Bošanský, M., †Piovarči, M. & Reichwalder, P., 2017: Carpathian Shear Corridor – a strike-slip boundary of an extruded crustal segment. *Tectonophysics, 703–704, 119–134*.

Marko, F., Fodor, L. & Kováč, M., 1991: Miocene strike-slip faulting and block rotation in Brezovské Karpaty Mts. (Western Carpathians). *Mineralia slovaca, 23, 3, l89–200*.

Marko, F., Vojtko, R., Plašienka, D., Sliva, Ľ., Jablonský, J., Reichwalder, P. & Starek, D., 2005: A contribution to the tectonics of the Periklippen zone near Zázrivá (Western Carpathians). *Slovak Geological Magazine, 11, 1, 37–43*.

Marschalko, R., 1979: Considerations about Pienide flysch basins and their substratum in the Creatceous and Paleogene (West Carpthians). Czechoslovak geology and tectonics. *Bratislava, Veda, 103–114*.

Matenco, L. & Bertotti, G., 2000: Tertiary tectonic evolution of the external East Carpathians (Romania). *Tectonophysics, 316, 255–286*.

McKenzie, D. P., 1978: Some remarks on the development of sedimentary basins. *Eart Planet. Sci. Lett., 40, 25–32*.

Mial, A. D., 1984: Principles of Sedimentary Basin Analysis. *New York – Berlin – Heidelberg – Tokyo, Springer, 490 pp*.

Minár, J., Bielik, M., Kováč. M., Plašienka, D., Barka, I., Stankoviansky, M. & Zeyen, 2011: New morphostructural

subdivision of the Western Carpathians: An approach integrating geodynamics into targeted morphometric analysis. *Tectonophysics, 502, 156–174.*

Montenat, Ch., Ott D'Estvou & Masse, P., 1987: Tectonic--sedimentary characters of the Betic Neogene Basins evolving in a crustal transcurrent shear zone (SE Spain). *Soc. Nat. Elf Aquitaine, Pau, France, 1–22.*

Nagy, A., Vass, D., Petrik, F. & Pereszlényi, M., 1996: Tectogenesis of the Orava Depression in the light of latest biostratigraphic investigations and organic matter alteration study. *Slovak Geological Magazine, 1, 49–58*.

Nemčok, M., 1993: Transition from convergence to escape: field evidence from the West Carpathians. *Tectonophysics, 217, 117–142*.

Nemčok, M. & Lexa, J., 1990: Evolution of the basin and range structure around Žiar Mountain range. *Geologický Zborník – Geologica Carpathica, 41, 229–258*.

Nemčok, M., Pospíšil, L., Lexa, J. & Donelick, R. A., 1998: Tertiary subduction and slab break-off model of the Carpathian-Pannonian region. *Tectonophysics, 295, 307–340*.

Németh, Z., Maglay, J., Petro, Ľ., Stercz, M., Grega, D., Pelech, O. & Gaál, Ľ., 2023: Neo-Alpine uplift and subsidence zones in the Western Carpathians: Product of kinematic activity on Cenozoic AnD3 (NW-SE and NE-SW) and AnD4 (E-W – subequatorial and N-S – submeridian) regional faults. *Mineralia Slovaca, 55, 2, 103–116.*

Oszczypko, N., Slaczka, A., Oszczypko-Clowes, M. & Olszewska, B., 2015: Where was the Magura Ocean? *Acta Geologica Polonica, 65, 3, 319–344*.

Pašteka, R., Záhorec, P., Kušnirák, D. Bošanský, M. Papčo, J., Szalaiová, V., Krajňák ,M., Marušiak, I., Mikuška, J. & Bielik, M., 2017: High resolution Slovak Bouguer gravity anomaly map and itsenhanced derivative transformations: new possibilities for interpretation of anomalous gravity fields. *Contr. to Geoph. and Geodesy, 47, 2, 81–94*.

Plašienka, D., 2018: The Carpathian Klippen Belt and types of its klippen – an attempt at a genetic classification. *Mineralia Slovaca, 49, 1, 1–24*.

Plašienka, D., Bučová, J. & Šimonová, V., 2020: Variable structural styles and tectonic evolution of an ancient backstop boundary – the Pieniny Klippen Belt of the Western Carpathians. *Int. Journal of Earth Sci., 109, 4, 1355–1376*.

Plašienka, D., Jósza, Š., Gedl, P. & Soták, J., 2016: Structure of the eastern part of the Varín sector of the Pieniny Klippen Belt – unraveling the puzzle. In: Šujan M. (ed.): Environmental, Structural and Stratigraphical Evolution of the Western Carpathians: 10th ESSEWECA Conference, Abstract book, 1st–2nd December 2016, *Bratislava, Slovakia, 76–77*.

Pomianowski, P., 2003: Tectonics of the Orawa-Nowy Targ basin-results on computer analysis of gravimetric and geoelectric data. *Prezeglad Geologiczny, 51, 6, 498–506* (in Polish).

Pospíšil, L., 1980: Interpretation of gravity field in thze East Slovakian Neogene area. Sbor. ref. z odb. semin. Výskum hlubinné geologické stavby *Československa*, *Liblice, 59–66* (in Czech).

Pospíšil, L., 1990: Contemporaneous possibilities of shear zones identification in Western Carpathian area. *Mineralia Slovaca, 22, 1, 19–31* (in Czech).

Potfaj, M., 2003: Geology of the Slovakian part of the Orava – an overview. In: Golonka, J. & Lewandowski, M. (eds.): Geology, geophysics, geothermics and deep structure of the West Carpathians and their basement. *Publication of the Institute of Geophysics, Polish Academy of Sciences*, Monographic Volume, *M-28, 363, 51–56*.

Ratschbacher, L., Frisch, W., Linzer, H. G. & Merle, O., 1991: Lateral extrusion in the Eastern Alps. Part II: Structural analysis. *Tectonics, 10, 2, 257–271*.

Royden, L. H., 1985: The Vienna Basin – a thin-skinned pull--apart basin. In: Biddle, K. & Bilick, N.-Ch. (eds.): *SEMP Spec. Publ., 37, 319–338*.

Royden, L. H., Horváth, F. & Burchfield, B. C., 1982: Transform faulting extension and subduction in the Pannonian region. *Geol. Soc. Amer. Bull. (New York), 93.*

Schmid, S. M., Bernoulli, D., Fugenschuh, B., Matenco, L., Schefer, S., Schuster, R., Tischler, M. & Ustaszewski, K., 2008: The Alpine-Carpathian-Dinaridic orogenic system: correlation and evolution of tectonic units. *Swiss Journal of Geosciences, 101, 1, 139–183*.

Sperner, B., Ratschbacher, L. & Nemčok, M., 2002: Interplay between subduction retreat and lateral extrusion: Tectonics of the Western Carpathians. *Tectonics, 21, 6, 1051–1074*.

Stegena, L., Géczy, B. & Horváth, F., 1975: Late cenozoic evolution of the Pannonian Basin. *Tectonophysics, 26, 71–90*.

Šujan, M., Chyba, A., Rószová, B., Braucher, R., Šujan, M., Šipka, F. & Šipka, F., ASTER TEAM, 2023: Surviving from transgression to regression of Lake Pannon: Fan deltas of the Nemčiňany Fm. persisted across the rifting until the post-rift stage of the Danube Basin, western Slovakia. *Geologica Carpathica, 76, 6, 469–488.*

Tari, G., Bada, G., Beidinger, A., Csizmeg, J., Danišík, M., Gjerazi, I., Grasemann, B., Kováč, M., Plašienka, D., Šujan, M. & Szafián, P., 2021: The connection between Alps and the Carpathians beneath the Pannonian basin: Selective reactivation of Alpine nappe contacts during Miocene extension. *Global and Planetary Change, 197, 103401.*

Tari, G., Horváth, F. & Rumpler, J., 1992: Styles of extension in the Pannonian basin. *Tectonophysics, 208, 303–319*.

Tomek, Č., 1993: Deep crustal structure beneath the central and inner West Carpathians. *Tectonophysics, 226, 417–431*.

Tomek, Č. & Thon, A., 1988: Interpretation of Seismic Reflection Profiles from the Vienna Basin, the Danube Basin and the Transdanubian Depression in Czechoslovakia. *Amer. Assoc. Petrol. Geol. Memoir, 45, 171–182*.

Van Bemmelen, R.W., 1972: Geodynamic models – Development in Geotectonics, 2. *Amsterdam – London – New York, Elsevier, 267 pp*.

Vass, D., 1998: Neogene geodynamic development of the Carpathian arc and associated basins. In: Rakús, M. (ed.): Geodynamic development of the Western Carpathians. *Bratislava, GS SR, Dionýz Štúr Publishers, 155–188*.

Vass, D., 1979: Genesis of inner-molasse basins in West Carpathians in light of leading function of mantle in Earth`s crust development. Czechosl. Geology and global tectonics. *Bratislava, Veda, 183–197*.

Watycha, L., 1976: Neogene of Orawa-Nowy Targ basin. *Kwartalnik Geologiczny, 20, 575–587* (in Polish).

Wessely, G., 1988: Structure and Development of the Vienna Basin in Austria. In: Royden, L. H. & Horváth, F. (eds.): The Pannonian basin. A study in basin evolution. *Amer. Assoc. Petrol. Geol. Memoir, 45, 333–346.*

Zuchiewicz, W., 2002: Neotectonics, morphotectonics, seismotectonics – state of researche and perspectives for the future: introduction. *Folia Quaternaria, 73, 5–12*.

Zuchiewicz, W., 2010: Neotectonics of the Polish Carpathians and Carpathian's foredeep. *Kraków, Wydawnictwa AGH, 234 pp.* (in Polish).

Žytko, K., Gucik, S. Rylko, W., Osczypko, N., Zajac, R., Garlicka, L., Nemčok, J., Eliáš, M., Menčík, E., Dvořák, J., Stránik, Z., Rakús, M. & Matejovská, O., 1989: Geological map of the Western Outer Carpathians and their foreland withouth Quaternary formations. In: D. Poprawa & J. Nemčok (eds.): Geological Atlas of the Outer Western Carpathians and their Foreland, 1 : 500 000. *Warszawa, Państwowy Instytut Geologiczny*.

Neoalpínska geodynamika kôrových segmentov ohraničených zlomami, dokumentovaná na príklade západokarpatských neogénnych bazénov a distribúcie jadrových pohorí

V neoalpínskej fáze orogenézy Západných Karpát dôležitú úlohu zohrali zlomy. Kontinentálna kôra kriedovo konsolidovaných vnútrokarpatských jednotiek bola zlomami vyšších rádov segmentovaná na samostatne sa pohybujúce bloky, ktoré extrudovali do zálivu subdukujúcej oceánskej kôry, situovaného v severoeurópskej platni (Ratschbacher et al., 1991; Doglioni et al., 1991). Po kolízii vnútrokarpatských jednotiek/blokov s predpolím (Český masív) v zóne pieninského bradlového pásma a kolmatovaní pribradlového segmentu Vnútorných Karpát sa aktívnym severným smernoposunovým rozhraním bloku pohybujúceho sa na VSV (CCCS) stal karpatský strižný koridor (CSC; Marko et al., 2017). Je dominantným dynamickým tektonickým rozhraním v miocéne (obr. 1).

V práci diskusného charakteru je navrhnutá tektonická kategorizácia neogénnych sedimentárnych bazénov vzhľadom na špecifickú dynamiku neoalpínskych blokov tvoriacich ich podložie. Podľa tohto kritéria už definované geodynamické typy vnútrokarpatských bazénov (Čech, 1984, 1989; Vass, 1979, 1998; Kováč, 2000; Janočko, 2003; Bezák et al., 2004) klasifikovaných na základe kritérií teórie platňovej tektoniky (pozícia bazénu vzhľadom na okraj platní/mikroplatní, tektonický režim platňových okrajov a geotektonický typ kôry/litosféry; napr. Mial, 1984) môžeme zaradiť do troch kategórií vymenovaných z juhu na sever: **1.** rozsiahle strednomiocénne až pliocénne zaoblúkové extenzné bazény vznikajúce termálnou subsidenciou vzťahujúce sa na veľký panónsky bazén. Sú vyvinuté na tenkej kôre (Pašteka et al., 2017) s vysokým tepelným tokom (Majcin et al., 2017) vlyvom aktivity plášťového diapíru a jeho satelitov (Vass, 1979; Čech, 1988; Pospíšil, 1990); **2.** izolované rotované a tiltované spodno- až strednomiocénne vnútrohorské bazény situované v zóne karpatského strižného koridoru (CSC) spojené so zlomovou smernoposunovou tektonikou – bazény strižných zón (napr. Montenat et al., 1987); **3.** bazény situované v zóne bradlového pásma a pribradlovej zóne, ktoré sú pravdepodobne smernými posunmi, pravostranne separovanými segmentmi molasového bazénu čela vnútrokarpatského bloku. To podporuje predpokladanú významnú rotáciu vnútrokarpatského bloku, ktorý je súčasťou bloku ALCAPA (Balla, 1984) vzhľadom na jednotky Vonkajších Karpát (napr. Marschalko, 1979).

Špecifikom Západných Karpát sú mladé jadrové pohoria (FT veky 22 – 9 mil. rokov) s exhumovaným kryštalinikom (Kráľ, 1977; Danišík et al., 2010; Králiková et al., 2014a, b; Marko et al., 2017) striedajúce sa s „halfgrabenmi“ neogénnych bazénov (štruktúra *basin and range*; napr. Nemčok a Lexa, 1990). Tento štýl stavby je vyvinutý v karpatskom strižnom koridore. Považujeme ho za dôsledok smernoposunovej dynamiky tejto strižnej zóny. Z konfigurácie mladých jadrových pohorí sa dá usúdiť, že CSC bol po jeho strednomiocénnej aktivite prerušený vysunutím stredoslovenského bloku (MSBL) ohraničeného zázrivským a malomagurským zlomom na sever (obr. 1). V tomto bloku sa nachádza aj jadrové pohorie Malá Fatra, ktoré bolo spolu s priľahlou Turčianskou kotlinou vysunuté na sever. Tento koncept vysvetľuje umiestnenie tohto mladého jadrového pohoria mimo kurzu miocénnej strižnej zóny CSC a zároveň vysvetľuje kontrastný kompresný tektonický štýl varínskeho segmentu bradlového pásma v porovnaní so susednými segmentmi, ktoré majú smernoposunový štýl. Príčinu vysunutia stredoslovenského bloku na sever nepoznáme, ale predpokladáme, že mohlo ísť o gravitačný fenomén spôsobený vyklenutím kôry v dôsledku subvulkanických intrúzií v kremnicko-štiavnickej vulkanickej oblasti a následného skĺznutia bloku na sever pozdĺž zlomov laterálnych rámp.

Dominantné stredno- až vrchnomiocénne rozhranie blokov CSC je ohraničené severnou a južnou okrajovou zlomovou zónou. Predpokladáme, že tieto rozhrania sú strmé, majú hlboký dosah a umožňujú migráciu podzemnej vody a fluíd s. l. do veľkej hĺbky, ich mineralizáciu a ohrev. Distribúcia významných minerálnych prameňov a studní termálnej minerálnej vody západnej časti Západných Karpát ukazuje, že sa priestorovo viažu na okrajové zlomy karpatského strižného koridoru. To zároveň indikuje existenciu týchto okrajových zlomov.

Doručené / Received: 10. 7. 2024
Prijaté na publikovanie / Accepted: 17. 12. 2024

Mineralia Slovaca, Web ISSN 1338-3523, ISSN 0369-2086, https://doi.org/10.56623/ms.2024.56.2.3
56, 2 (2024), 153 – 164, © Authors 2024. CC BY 4.0

Geochemical constraints on the petrogenesis of Patharkhola gneiss, Kumaun Lesser Himalaya, India

HARITABH RANA[1,4], HAREL THOMAS[1], JYOTI BIDOLYA[1], AMAN SONI[1], RISHABH BATRI[1], SATYAM SHUKLA[1], KAVITA DEVI[2] and ALINA KARKI[3]

[1]Department of Applied Geology, Dr. Harisingh Gour Vishwavidyalaya,
Sagar A Central University Sagar (M.P.) 470003, India;
harelthomas@gmail.com; hthomas@dhsgsu.edu.in
[2]Department of Geology, Mizoram University, Tanhril, Aizawl 796004, Mizoram, India
[3]Central Department of Geology, Tribhuvan University (TU), Kirtipur, Kathmandu, Nepal
[4]Geological Survey of India, Dehradun, Uttarakhand

Abstract: A new set of geochemical and mineralogical data of gneisses from the Patharkhola region of the Dudhatoli syncline, Kumaun Lesser Himalaya is discussed to elucidate their petrogenesis and tectonic environment of India. These Patharkhola gneisses exhibit foliated texture and are primarily composed of K-feldspar ($KAlSi_3O_8$) and plagioclase ($NaAlSi_3O_8$) with perthite ($(K,Na)AlSi_3O_8$), biotite ($K(Mg,Fe)_3AlSi_3O_{10}(F,OH)_2$), muscovite ($KAl_2(AlSi_3O_{10})(OH)_2$), and tourmaline ($(Na(Mg,Fe,Mn,Li,Al)_3Al_6[Si_6O_{18}](BO_3)_3(O,OH,F)_4$) as accessory minerals. They exhibit $SiO_2 > 70$ % with average $K_2O/Na_2O = 1.31$ % while Nb, V, Zr, La, and Eu show strong negative anomalies normalized to Post Archean Australian Shale (PAAS). The chondrite-normalized rare earth element (REE) concentrations of light rare earth elements (LREE) to heavy rare earth elements (HREE) exhibit varying ratios, ranging from 4.8 to 10.6 for (La/Yb)N. Additionally, there is a significant europium (Eu) anomaly, with Eu/Eu* ratios between 0.3 and 0.6. The authors have done Post Archean Australian Shale (PAAS) normalization as well as chondrite normalization separately and dealt with the variation in both normalizations.
The ratios of Al_2O_3/TiO_2 (82–112), Th/Sc (1.3–9.4), and Eu/Eu* (0.3–0.6) suggest that the precursor materials of these gneisses were felsic in nature. Based on the petrological and geochemical characteristics of the studied gneisses, it is proposed that the Patharkhola gneisses formed in an active continental margin, where the sediments originated from felsic sources.

Key words: geochemistry, petrogenesis, gneiss, Almora, Patharkhola, Himalaya

Graphical abstract

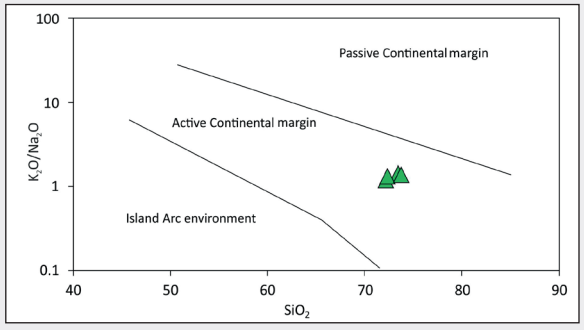

Highlights

- The Patharkhola gneisses exhibit elevated levels of SiO_2, potassic elements, and LREE/HREE (La/Yb) N ratios between 4.8–10.6 along with Eu/Eu* ratios falling between 0.3–0.6 with Th/Sc ratios between 1.3–9.4. These geochemical characteristics suggest that the gneisses are derived from felsic sediments.
- The Patharkhola gneisses are believed to be developed in an environment characterized by an arc type setting, where sediments rich in silt and clay are found in close proximity to the area.

Introduction

Around 55 million years ago, a significant event occurred when the Indian and Asian tectonic plates collided, leading to the formation of the majestic Himalayan mountain range. This geological wonder stretches along the entire northern boundary of India and serves as a remarkable example of intercontinental collision in Earth's geological history. Notable scientific studies conducted by Molnar and Tapponnier (1975), Valdiya (1980a, b, 1988), Yin (2006), and Webb (2011, 2013) have offered valuable insights into the complex processes that shaped this iconic mountain belt. The collision of these continents causes continental shortening, which results in the arrangement of Himalayan rocks through various thrust systems. Key thrust systems include the Main Central Thrust (MCT), Main Boundary Thrust (MBT), and Himalayan Frontal Thrust (HFT) (Srivastava & Mitra, 1994). The MCT forms the northern boundary of the Lesser Himalayan rocks, while the MBT marks the southern boundary.

The tectonics of the Lesser Himalaya have been studied extensively (Gansser, 1964; Valdiya, 1980a, b, 1988; Joshi et al., 2017, 2019; Rana, 2023; Rana & Thomas, 2018, 2023; Rana et al., 2023a, b; Thomas, T. & Thomas, H., 2003). Research by Mehdi et al. (1972), Saxena and Rao (1975), Agarwal (1994), Srivastava and Mitra (1996), and Bhattacharya (1999, 2000) has provided insights into the structural setup of the Lesser Himalayan rocks. In contrast, Ghosh et al. (1974), Srivastava and Mitra (1996), and Joshi

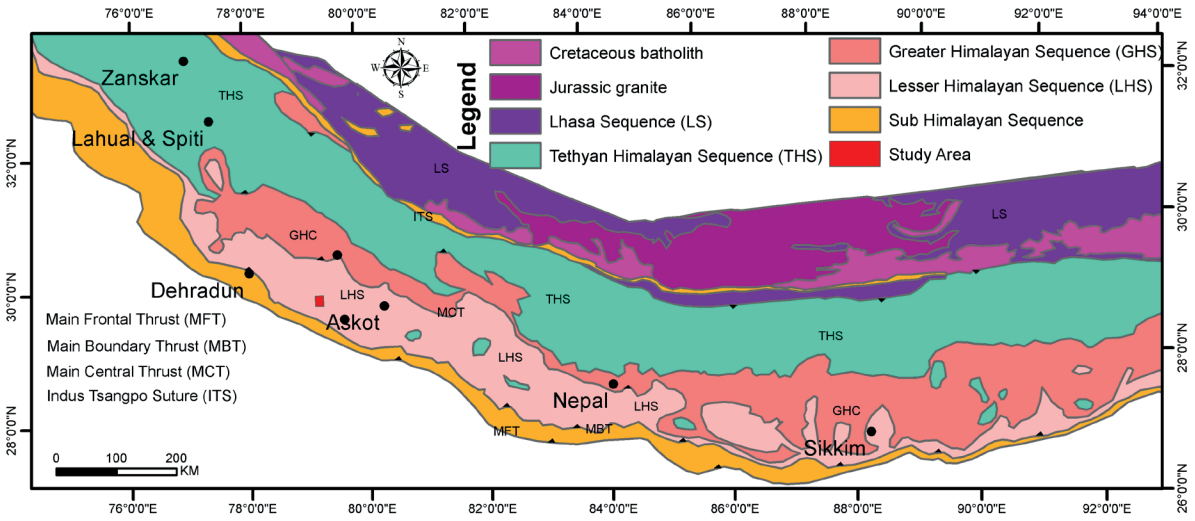

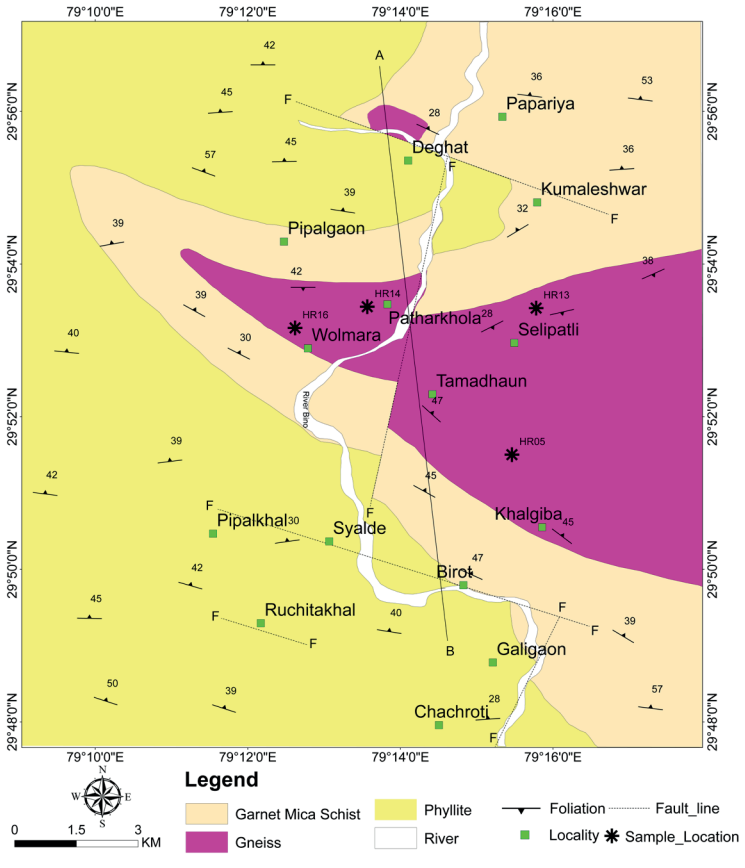

Fig. 1. Detail geological map around Patharkhola, Kumaun Lesser Himalaya, Uttarakhand, India (modified after Thomas & Thomas, 1992). Location of this detail map in regional map is shown in upper picture.

and Tiwari (2009) have explored the metamorphic history of the Almora Crystallines.

The central part of the Almora nappe exhibits a variety of deformation patterns and polyphase metamorphism, as documented by Gairola and Joshi in 1978. The Munsiari gneisses of the Almora Group in the Lesser Himalaya have been dated to approximately 1,830 ± 200 million years old (Bhanot et al., 1977). Islam et al. (2005) classified the Proterozoic granitoids of the Lesser Himalaya into two clusters: an older cluster ranging from 2,200 to 1,800 million years old, and a younger cluster from 1,400 to 1,200 million years old.

Although various studies have proposed different ages for the rocks in this region, there is a lack of extensive research focusing on their geochemical investigation. Kohn et al. (2010) utilized U-Pb dating to suggest an age of 1,830 ± 50 million years. In contrast, Mandal et al. (2016) proposed an age of 1,878 ± 2.4 million years for the augen gneisses discovered in the Askot area.

Geological settings

Numerous tectonic movements have shaped the geological structure of the Lesser Himalayan rocks, resulting in a complex arrangement. In the Patharkhola area, the exposed rocks belong to the Dudhatoli Group (Rana & Thomas, 2018). This group is part of the "Inner Schistose Series" or the "Metamorphic and Crystalline Nappe Tectonic Zone" of the Lesser Himalaya, which constitutes a distinct structural unit that has undergone multiple deformations and polyphase metamorphism. The authors have discussed the geochemical constraints of the gneisses found in

Patharkhola. Regarding the metamorphism of the Almora Group rocks, these have experienced at least two phases of deformation, characterized by well-developed F1 and F2 folds. The older S1 schistosity planes, which were formed during D1 deformation, are defined by muscovite and biotite flakes along with inequant quartz; these have been affected by tight to isoclinal folds (F2). The S2 schistosity planes, which developed parallel to the crenulation cleavages during D2 deformation, are defined by the mica flakes. Four metamorphic zones have been identified: chlorite-biotite, garnet-biotite, kyanite-biotite, and sillimanite-K-feldspar (Joshi & Tiwari, 2001). Rana (2023), Rana et al. (2023a, b) Rana and Thomas (2023), noted that the rocks of Patharkhola exhibit a clockwise pressure-temperature path characteristic of the Barrovian zone of metamorphism, with temperatures ranging from 350 °C to 600 °C and pressures between 3.3 to 6.5 kilobars. In the Kumaun and Garhwal regions, there are two significant outliers of crystalline rocks. The southern outlier is known as the Garhwal nappe, while the northern outliers are referred to as the Dudhatoli-Almora Nappe. The Dudhatoli Crystallines extend from Garhwal in the west-northwest to Kumaun in the east-southeast. In 1972, Mehdi et al. classified the Mandhali, Chandpur, and Nagthat Formations, along with the Dudhatoli-Almora Crystallines, as part of the newly established Dudhatoli Group. The Dudhatoli-Almora Crystallines form the uppermost horizon of this group and are believed to be of Precambrian age.

Gneisses can be observed between Wolmara village and Patharkhola, where they come into contact with garnet-bearing schists ($Mg_3Al_2Si_3O_{18}$). These foliated gneisses have a medium grain size and are characterized by their hardness and compactness. They contain abundant biotite ($K(Mg,Fe)_3AlSi_3O_{10}(F,OH)_2$) and muscovite ($KAl_2(AlSi_3O_{10})(OH)_2$), which contribute to their foliation. Ad-

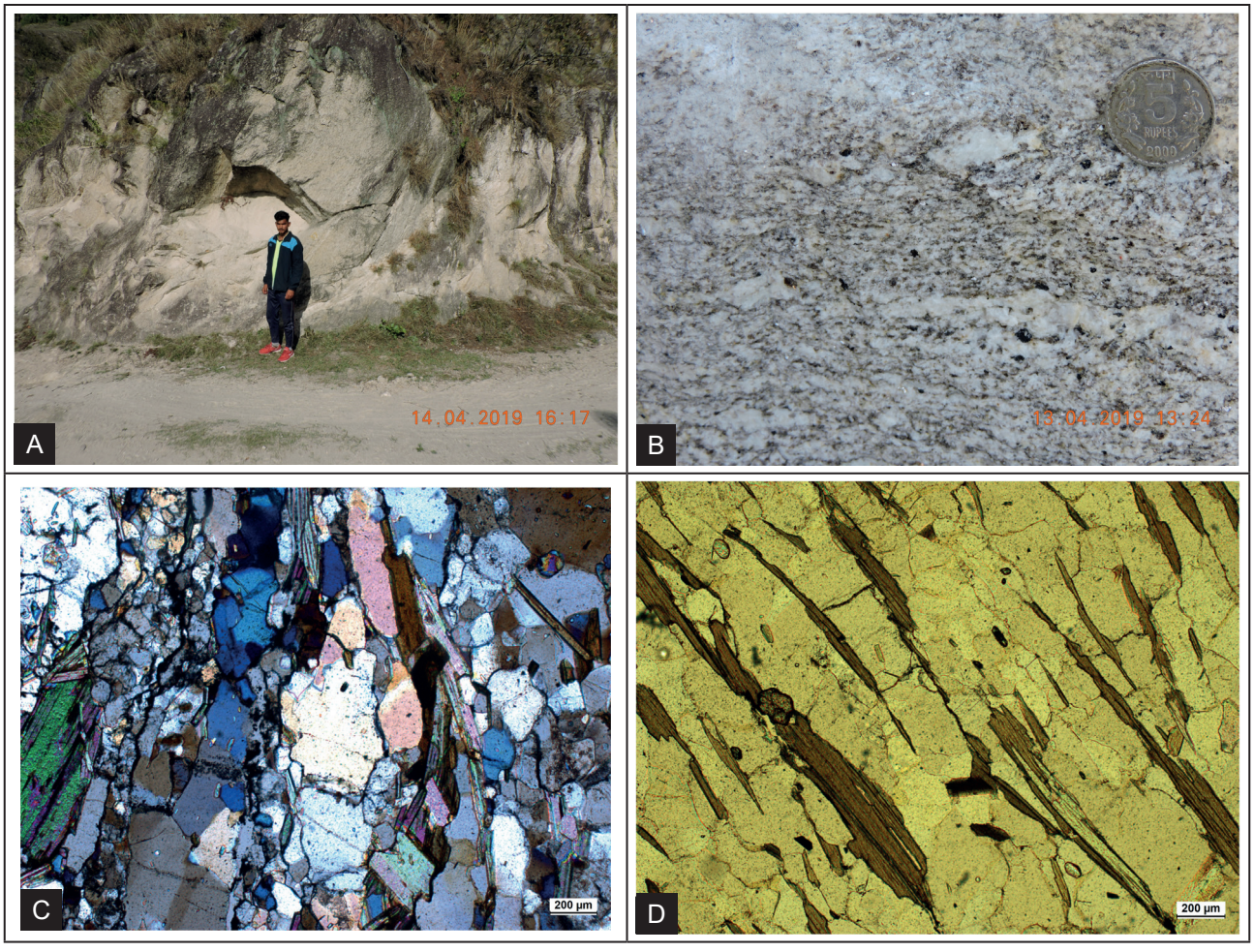

Fig. 2. Representative field and microscopic photographs of Patharkhola gneiss presented in this study: A – Foliated gneiss exposed at road section of Patharkhola village. B – Freshly cut foliated gneiss showing quartz, feldspar and phyllosilicates. C – Foliated gneiss showing biotite-muscovite-quartz-feldspar assemblage. D – Foliated gneiss showing alternated bands of phyllosilicates and quartzo-feldspathic layer in plane polarised light.

ditionally, porphyroblasts of feldspar ($KAlSi_3O_8$) can be found within these gneisses. Notably, near the Tamadhaun Primary School and around Khalgiba village, randomly oriented tourmaline ($Na(Mg,Fe,Mn,Li,Al)_3Al_6[Si_6O_{18}](BO_3)_3(O,OH,F)_4$) laths measuring 3 to 4 cm in length have been observed (Rana & Thomas, 2018).

Analytical methods

Thin section petrographic studies have been carried out with polarizing microscope having mounted photo camera. Whole-rock major oxides and trace element concentrations were determined by using pressed pellets on a wavelength dispersive X-Ray Fluorescence (WD-XRF) Bruker S8 Tiger at the Wadia Institute of Himalayan Geology (WIHG), Dehradun. Loss on Ignition (LOI) for every sample was determined by heating silica crucible containing 5 mg rock powder of each sample at 950 °C. XRF technique analytical precision for both major and trace elements lies within ± 2–3 % and ± 5–6 %, respectively (Saini et al., 2007). The rare earth elements (REEs) of the representative volcanic rocks were analysed using Inductively Coupled Plasma Mass Spectrometry (ICP-MS, ELAN DRC-E, Perkin Elmer), strictly following the open digestion method at WIHG, Dehradun. Approximately 100 mg of powdered sample was measured with the help of an electronic weighing balance, which is treated with a mixture of 10 ml distilled acids (HF: HNO_3) in the ratio of 1 : 2. The crucibles made of Teflon containing acid treated samples were put on a hot plate heating at ~200 °C for a few hours. About ~2 ml of perchloric acid ($HClO_4$) was added, and the entire mixture was left to evaporate until dry. After the samples were turned into a thick brown paste form, 10 ml of 1 : 1 HNO_3

Tab. 1

Major, trace and REE of Patharkhola Gneiss of Kumaon Lesser Himalaya

Sample No.	HR05	HR13	HR14	HR16	Sample No.	HR05	HR13	HR14	HR16
SiO_2	72.2	73.46	72.31	73.36	Sc	2	2	4	1
Al_2O_3	15.63	15.36	15.79	15.3	V	11	11	15	10
Fe_2O_3	2.02	1.9	2.55	1.96	Cr	808	967	8 192	857
FeO	1.8	1.69	2.27	1.74	Co	252	127	1 169	459
MnO	0.03	0.03	0.06	0.03	Ni	934	989	8 665	839
MgO	0.26	0.23	0.24	0.23	Cu	2	7	18	9
Cao	0.62	0.64	0.66	0.69	Zn	82	50	41	54
Na_2O	3.83	3.36	3.6	3.43	Ga	21	14	17	16
K_2O	4.53	4.82	4.72	4.68	Rb	460	323	323	303
TiO_2	0.19	0.15	0.14	0.17	Sr	49	81	73	84
P_2O_5	0.27	0.26	0.28	0.26	Y	41	32	32	31
Total	99.58	100.21	100.35	100.51	Zr	71	57	59	64
K_2O/Na_2O	1.182	1.434	1.311	1.364	Nb	26	14	15	15
Na_2O/Al_2O_3	0.245	0.218	0.227	0.224	Ba	160	210	196	221
Rare Earth Elements					Pb	32	39	36	41
La	1.579	2.671	0.717	2.747	Th	17	5	5	7
Ce	5.776	5.412	36.882	16.406	U	4.7	1.1	2.2	BDL
Pr	0.717	1.144	5.019	2.913					
Nd	2.747	4.344	17.709	10.848					
Sm	0.847	1.397	4.88	3.192					
Eu	0.077	0.283	0.823	0.582					
Gd	0.674	1.445	5.513	3.47					
Tb	0.098	0.293	0.998	0.647					
Dy	0.42	1.56	4.964	3.398					
Ho	0.06	0.242	0.759	0.517					
Er	0.133	0.475	1.504	1.024					
Tm	0.019	0.063	0.191	0.131					
Yb	0.106	0.399	1.09	0.683					
Lu	0.014	0.05	0.15	0.093					
REE total	13.267	19.778	81.19	43.73					
LREE/HREE	14.6	5.41	9.25	7.08					
La/Eu	20.2	9.43	22.55	14.77					
Eu/Lu	5.5	5.66	5.48	6.25					

*BDL = Below detection limit

was added, and the samples were kept on the hot plate for another 10 minutes. The final solution is left up to 100 ml in a volumetric flask and ready for REE analysis.

Petrography

The gneisses found in Patharkhola exhibit a medium to coarse-grained texture when examined under a microscope. These rocks are primarily composed of feldspar, including both potassium feldspar ($KAlSi_3O_8$) and plagioclase ($NaAlSi_3O_8$), and they are devoid of garnet. Other minerals present in the gneisses include perthite ($(K,Na)AlSi_3O_8$), biotite ($K(Mg,Fe)_3AlSi_3O_{10}(F,OH)_2$), muscovite ($KAl_2(AlSi_3O_{10})(OH)_2$), secondary muscovite, and tourmaline ($Na(Mg,Fe,Mn,Li,Al)_3Al_6[Si_6O_{18}](BO_3)_3(O,OH,F)_4$). The gneissosity of these rocks is characterized by alternating layers of quartzo-feldspathic material and mica. In some portions muscovite and biotite are noticeably aligned, giving an appearance of lepidoblastic texture. Furthermore, the gneisses display compositional layering and foliation.

Following mineral assemblages has been observed:

a) Quartz-K-feldspar-Plagioclase-Muscovite-Sericite,

b) Biotite-Muscovite-Quartz-K-Feldspar.

The majority quartz grains display characteristics ranging from xenoblastic to subidioblastic. These grains often feature sutured edges, showing bulging boundaries and the pinning of adjacent grains. The undulose extinction observed in the grains indicates that they have experienced ductile deformation followed by recrystallization.

It is common to observe undistorted quartz grains containing tiny sericite inclusions that exhibit strain-free extinction. Additionally, there are flattened and elongated quartz grains that display undulose extinction. K-feldspars are predominantly perthitic in nature, with patches occurring both at the core and rim of the grains. In some instances, the K-feldspar undergoes alteration, resulting in sericitization which is primarily observed at the boundaries between grains.

Plagioclase feldspars are typically observed as subidioblastic grains, exhibiting albite type twinning in most areas and mechanical twinning in a few areas. The measured extinction angles on these grains range from An_{16} to An_{38}, indicating that the plagioclase is of the oligoclase to andesine variety. The foliation is defined by the preferred alignment of brownish biotite lepidoblasts, which display light brown to dark brown pleochroism commonly associated with muscovite. Additionally, a second generation of biotite can be observed, forming an angular relationship with the earlier biotite and defining a major foliation.

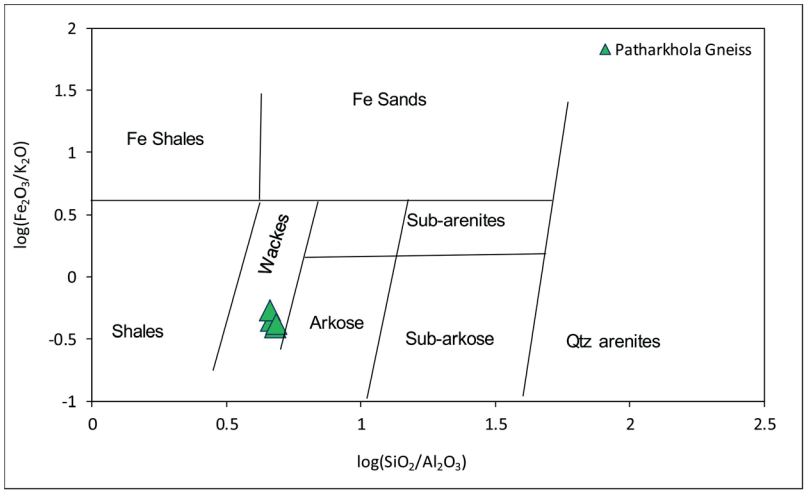

a)

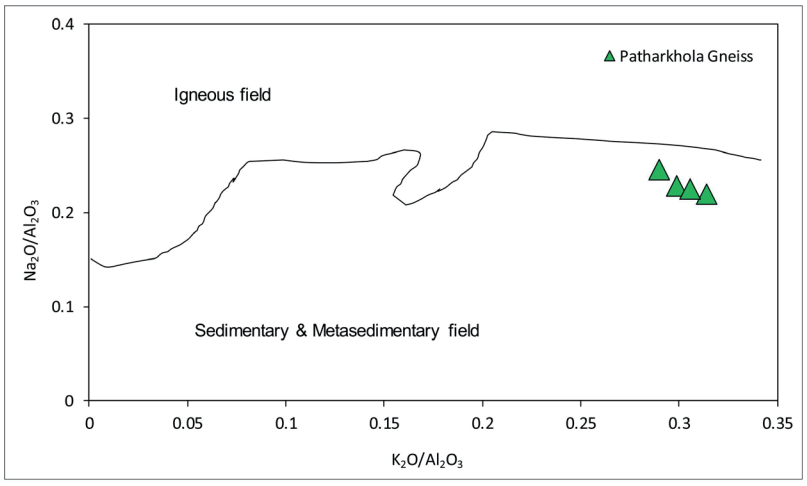

b)

Fig. 3. a – Log (SiO_2/Al_2O_3) versus log (Fe_2O_3/K_2O) after Herron (1988). **b** – K_2O/Al_2O_3 versus Na_2O/Al_2O_3 after Garrels and Mackenzie (1971) for classifications of Patharkhola gneiss of Kumaon Lesser Himalaya.

Fig. 3c. Harker Variation diagrams of SiO_2 versus other major oxides of Patharkhola gneisses, Kumaon Lesser Himalaya.

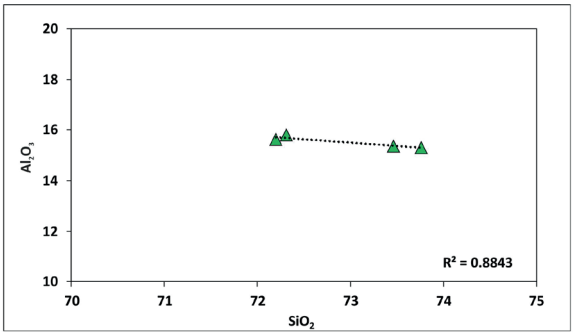
Al2O3
SiO2
R² = 0.8843

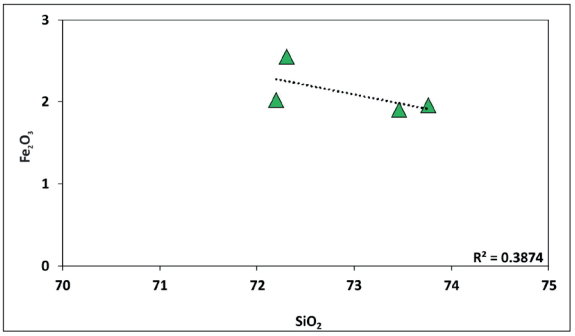
Fe2O3
SiO2
R² = 0.3874

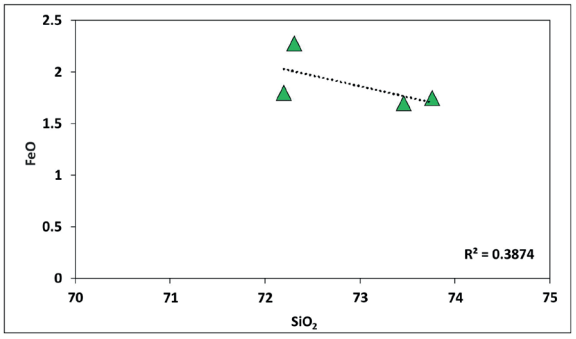
FeO
SiO2
R² = 0.3874

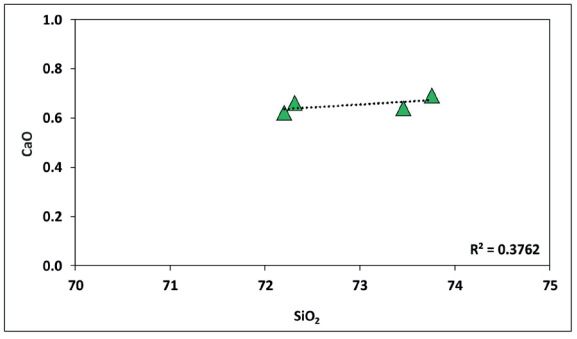
CaO
SiO2
R² = 0.3762

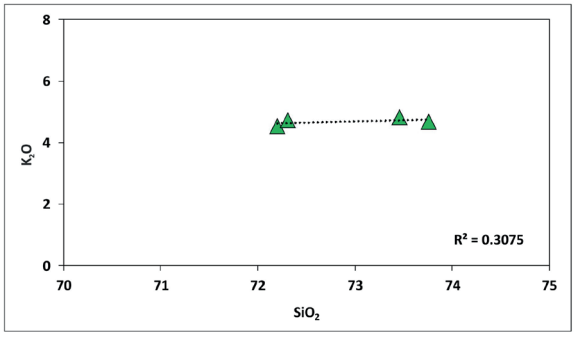
K2O
SiO2
R² = 0.3075

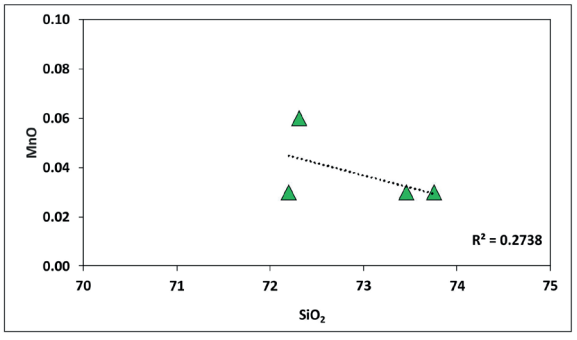
MnO
SiO2
R² = 0.2738

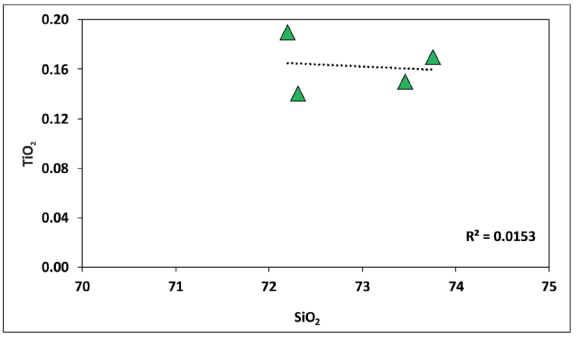
TiO2
SiO2
R² = 0.0153

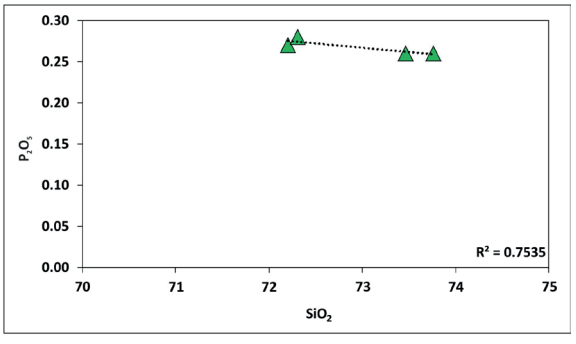
P2O5
SiO2
R² = 0.7535

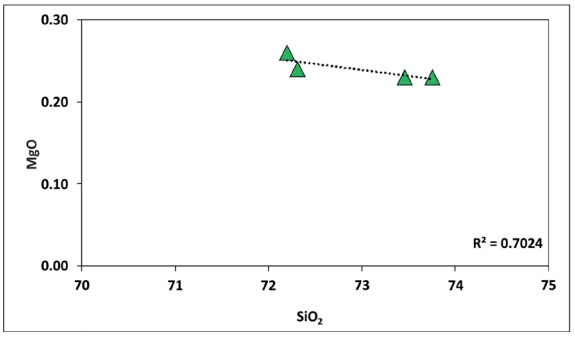
MgO
SiO2
R² = 0.7024

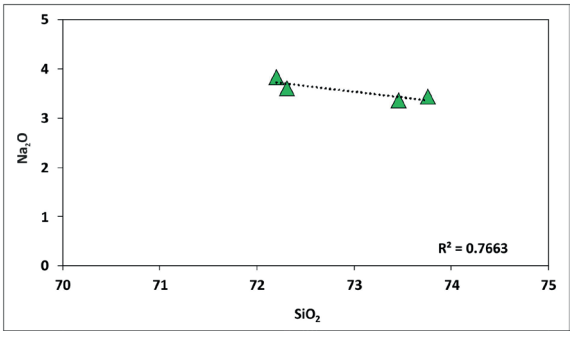
Na2O
SiO2
R² = 0.7663

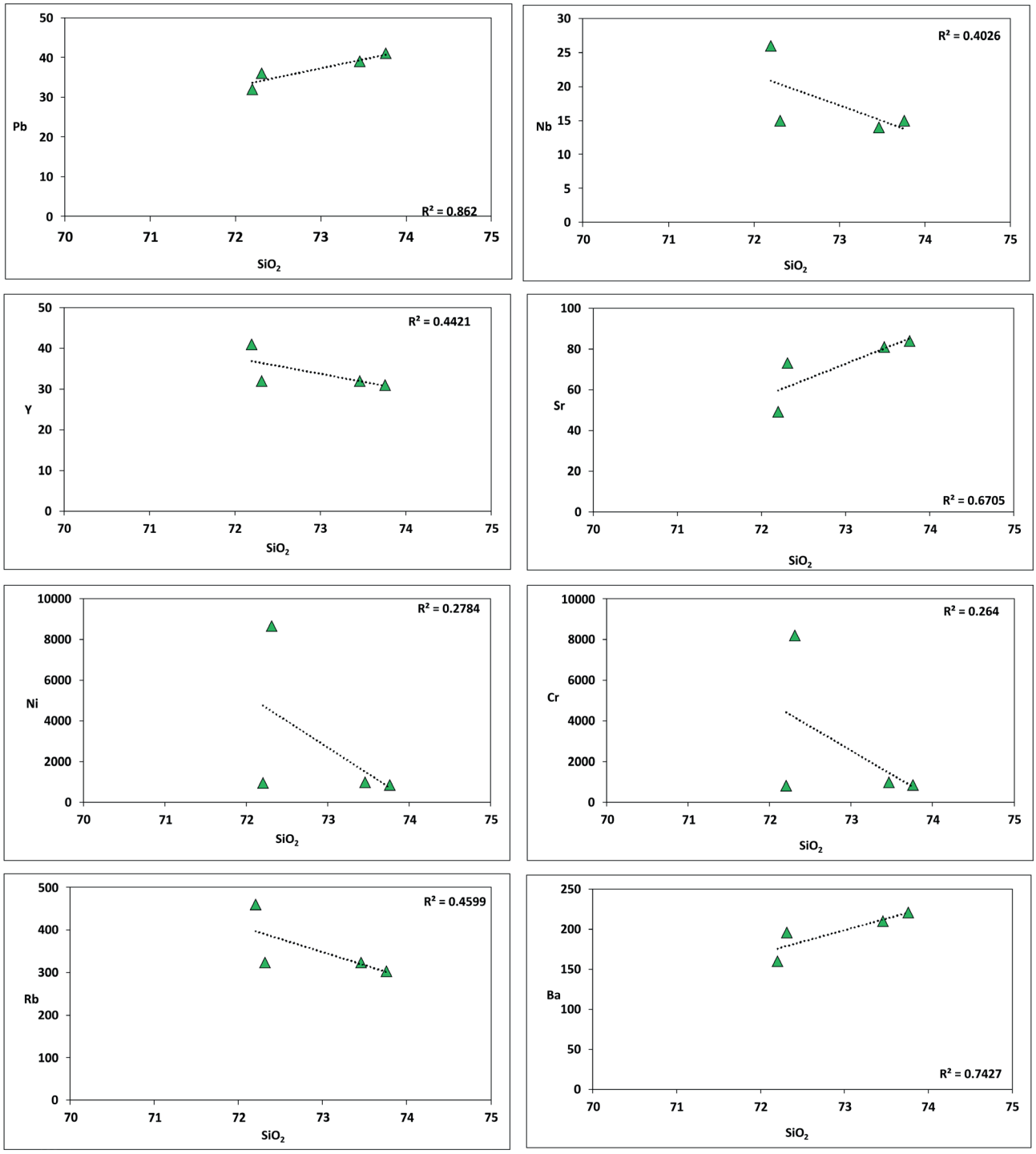

Fig. 3d. Harker variation diagrams of SiO_2 versus trace elements of Patharkhola gneisses, Kumaun Lesser Himalaya.

Geochemical characteristics of Patharkhola gneiss

The findings of the four chosen gneissic rocks, including major oxides, trace elements and REE, have been presented in Tab. 1. The content of SiO_2 ranges from 72.20 % to 73.76 %, while the content of Al_2O_3 ranges from 15.30 % to 15.79 %. It is worth noting that all four selected samples have a SiO_2 content exceeding 70 %. The average content of Na_2O and K_2O in the gneiss is 3.56 % and 4.69 % respectively. Generally, the Patharkhola gneisses exhibit a higher potassium enrichment than sodium. The average K_2O/Na_2O ratio for these rocks is 1.31 %. The TiO_2 content in the rocks varies from 0.03 % to 0.06 %.

The FeO/MgO ratio ranges from 6.91 % to 9.45 % for these rocks.

Herron (1988) established a classification system for the origin of terrigenous sediments based on logarithmic ratios of SiO_2/Al_2O_3 versus Fe_2O_3/K_2O. By plotting the Patharkhola gneiss on the Herron classification plot (Fig. 3a), it can be determined that the investigated gneiss belongs to the wacke type that indicates the gneiss has originated from a source with a silty to clayey composition. The presence of high SiO_2 concentration in the samples within the wacke field suggests a significant contribution of quartz debris in the sedimentary environment. The relationship between K_2O/Al_2O_3 and Na_2O/Al_2O_3 has effectively distinguished between sedimentary and igneous rocks, as demonstrated by Garrels and Mackenzie in 1971. It is clear that all samples fall within the specified range for sedimentary rock, as depicted in Fig. 3b. In the Harker variation diagram, SiO_2 exhibits regression values greater than 0.5 for Al_2O_3, P_2O_5, MgO, and Na_2O. Despite these regression values exceeding 0.5, all the major oxides display a nearly horizontal or inverse trend with SiO_2, as shown in Fig. 3c. The significant presence of K_2O, in conjunction with Al_2O_3, indicates an enrichment of mica and chlorite concentration. Furthermore, the behaviour of trace elements in the gneissic assemblages has been examined using variation diagrams, with the plot of SiO_2 against trace elements depicted in Fig. 3d.

Sedimentary processes have a significant impact on the composition of alkali and alkaline earth elements. This is mainly due to their high solubility in aqueous solutions and their transportation as dissolved phases from the source to the deposition sites. Throughout the processes of weathering, transportation, and diagenesis, elements like Ti, Al, and HFSE can easily dissolve in high-temperature aqueous solutions without being fractionated relative to each other.

The Patharkhola gneisses exhibit an Al_2O_3/TiO_2 ratio ranging from 82 to 112, which suggests that they originated from felsic source rocks. In order to determine the composition of the provenance, characteristics of trace

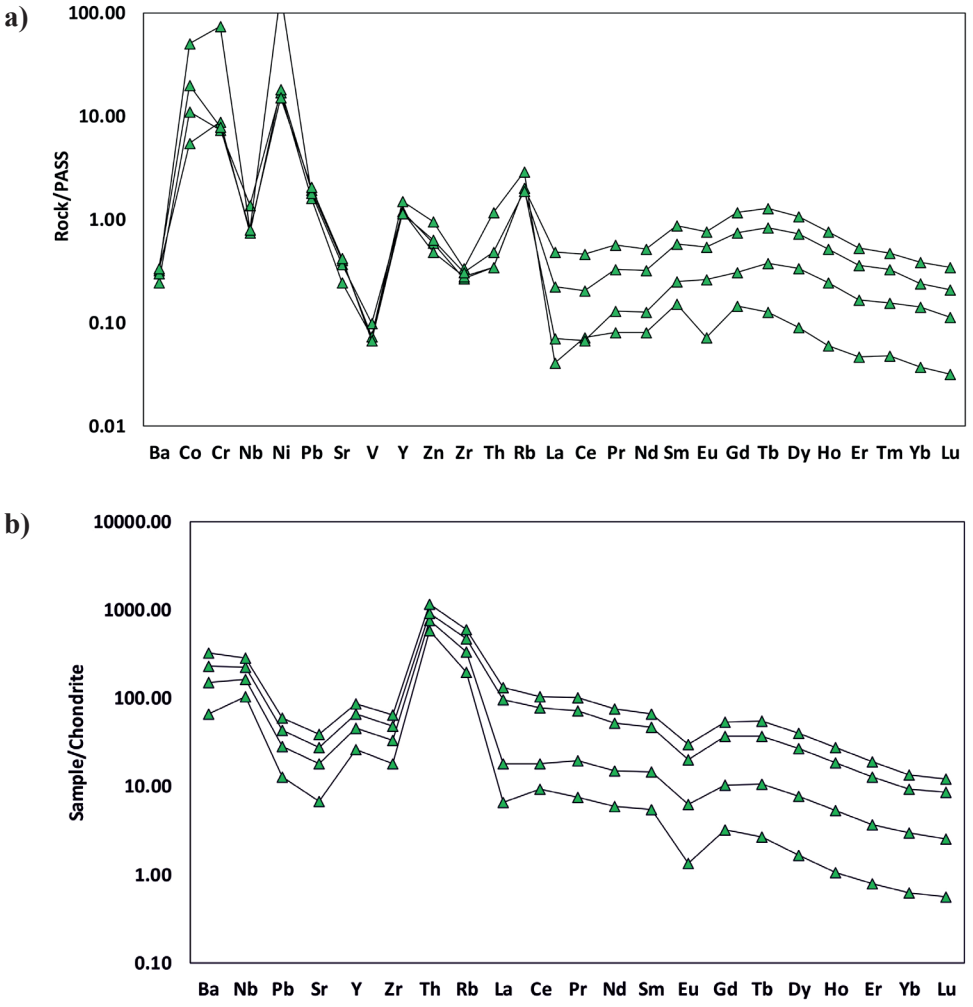

Fig. 4. a – REE Rock/PAAS normalized plot (Taylor & McLennan, 1985); **b** – REE chondrite normalized plot (Sun and McDonough 1989) of Patharkhola gneisses, Kumaon Lesser Himalaya.

elements such as REE, Cr, Co, Sc, and Th are studied, as they remain immobile under surficial conditions and have a short residence time in aqueous phases (Taylor & McLennan, 1985). These elements are commonly transported from the source to the depositional sites in terrigenous sediments. Felsic sources typically contain high concentrations of highly incompatible elements like REE and Th. The Th/Sc and Eu/Eu* ratios of felsic-derived sediments range from 0.8 to 20.5 and 0.4 to 0.9, respectively (Cullers & Podkovyrov, 2000). The Th/Sc (1.3–9.4) and Eu/Eu* (0.3–0.6) values of the Patharkhola gneisses fall within the range of felsic source sediments, indicating that these gneisses originated from felsic sedimentary sources.

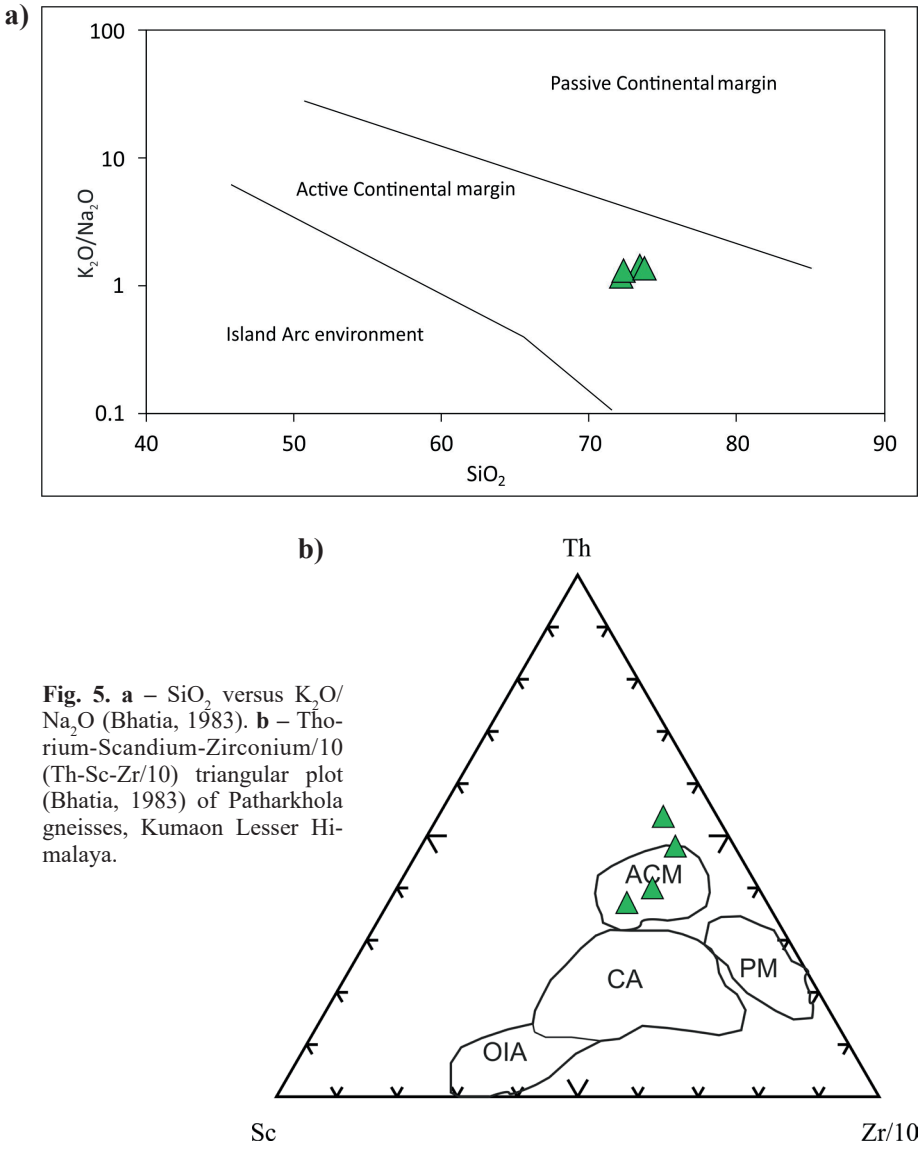

Fig. 5. a – SiO_2 versus K_2O/Na_2O (Bhatia, 1983). **b** – Thorium-Scandium-Zirconium/10 (Th-Sc-Zr/10) triangular plot (Bhatia, 1983) of Patharkhola gneisses, Kumaon Lesser Himalaya.

The Eu anomaly and REE patterns are important indicators for examining the characteristics of source rocks (Altrin et al., 2013). It is considered that high LREE/HREE ratios and negative Eu anomalies are typically associated with felsic sources, while flat REE patterns with fewer Eu anomalies are associated with mafic sources. In the case of the Patharkhola gneisses, the data shows fractionated trends with high LREE/HREE ratios (La/Yb)N ranging from 4.8 to 10.6, as well as Eu/Eu* values ranging from 0.3 to 0.6, which further support the presence of felsic sources.

The elements Nb, Y, Ni, Cr, and Rb exhibit a negative correlation, while Ba, Sr, and Pb show a positive correlation in relation to SiO_2. The content of Nb ranges from 14 to 26 ppm, with an average of 17.5 ppm, which is slightly lower than the content in Post Archean Australian Shale (PAAS) at 19 ppm. In the multi-element diagram normalized to PAAS, the gneisses from Patharkhola exhibit strong negative anomalies of Nb, V, Zr, La, and Eu. On the other hand, Cr, Ni, Y, and Rb show enrichment relative to PAAS. The total REE (ΣREE) content in the gneisses ranges from 13.26 to 81.19 ppm. The chondrites-normalized REE concentrations display varying LREE/HREE ratios (La/Yb)N, ranging from 4.8 to 10.6. The authors have done Post Archean Australian Shale (PAAS) normalization as well as chondrite normalization separately and dealt with the variation in both normalizations. The REE patterns are fractionated, with highly enriched LREE and fractionated HREE, featuring a prominent Eu anomaly with an Eu/Eu* anomaly range of 0.3–0.6. In terms of trace elements, Ba, Sr, V, Zn, and Zr in the Patharkhola gneiss exhibit low concentrations compared to PAAS.

The gneisses rare earth data was standardized to chondrites, as documented by Sun and McDonough in 1989. An interesting observation reveals that the light rare earth elements (LREE) exhibit steeper patterns, characterized by a La/Eu ratio of 16.73. In contrast, the heavier rare earth elements (HREE) display a less pronounced trend, with an Eu/Lu ratio of 5.72.

Tectonic implications

The role of geochemistry as a sensitive indicator in determining the origin of sedimentary and metasedimentary rocks, as well as providing insights into the tectonic setting of their deposition, has been extensively explored in scientific literature. Esteemed researchers such as Bhatia (1983), Bhatia and Crook (1986), Roser and Korsch (1986), Madukwe et al. (2015), and Grizelj et al. (2017) have significantly contributed to our understanding of this subject matter. Their studies have consistently demonstrated the importance of geochemical analysis in unraveling the provenance and tectonic history of these rocks.

Geochemical study is crucial in understanding the tectonic setting of ancient depositional sedimentary environments. Through the analysis of geochemical data, various discriminant diagrams have been developed to determine the tectonic setting in which sediments were deposited. For instance, the classification plot of SiO_2 versus K_2O/Na_2O, introduced by Bhatia and Crook in 1986, indicates that the protolith of Patharkhola gneisses was formed in an active continental margin. Another diagram, the triangular plot of Zr/10, Sc, and Th proposed by Bhatia in 1983, also confirms that the Patharkhola gneisses belong to an active continental margin.

Almora pelitic gneisses from Askot klippe have shown similar geochemical characteristics as of Patharkhola gneisses. The Eu/Eu* anomaly for Almora pelitic gneisses from Askot shows 0.15–0.54 having similar pronounced negative Eu anomaly. Negative Nb anomaly for both of these Patharkhola gneiss and Almora gneiss (Das et al., 2019) along with the garnet mica schist of Patharkhola (Rana et al., 2023b) Rana and Thomas (2023) shows similar sedimentation and metamorphism conditions.

Conclusion

The Patharkhola gneisses from Almora Dudhatoli Group of Kumaun Lesser Himalaya have shown the following characteristics:

The gneisses are composed of quartz, predominantly K-feldspar and minor amount of Na-plagioclase with mica group of minerals that represent pelitic assemblage. SiO_2 and Al_2O_3 total around 87–88 % with average Na_2O and K_2O values are 3.56 and 4.69 % respectively.

LREE/HREE ratios $(La/Yb)_N$ ranging from 4.8 to 10.6 showing notable enrichment of LREE and fractionated HREE, along with a prominent Eu anomaly (Eu/Eu* anomaly = 0.3–0.6).

Based on the petrological and geochemical characteristics, it is concluded that Patharkhola gneisses were formed in an active continental margin originating from felsic sources.

The rocks of Patharkhola formed during the Paleo-Proterozoic period in an arc-type setting where in between the arc and Indian continental plate, simultaneously the rifting of back-arc basin followed by the receiving of sediments both from the arc and the continental crust leads to the formation of lesser Himalayan rocks.

Acknowledgements

The authors thank the Head of Department of Applied Geology, Dr. Harisingh Gour Vishwavidyalaya, Sagar (M.P.) and the Department of Science and Technology, New Delhi, India, for providing facilities as including PURSE-Phase-II for conducting present research work. The authors express sincere thanks to the reviewers, Dr. Martin Radvanec (State Geological Institute of Dionyz Stur, Slovakia) and Dr. Ondrej Nemec (Comenius University, Slovakia) for their critical and constructive reviews which significantly improved the focus and clarity of the manuscript.

References

Agarwal, K. K., Jahan, N. & Agarwal, A., 2010: Modification of fold geometry in Almora crystalline shear zone, Lesser Himalaya, India. *Journal of the Geological Society of India*, *75, 411–414.*

Agarwal, A., Agarwal, K. K., Bali, R., Prakash, C. & Joshi, G., 2016: Back-thrusting in Lesser Himalaya: Evidences from magnetic fabric studies in parts of Almora crystalline zone, Kumaun Lesser Himalaya. *Journal of Earth System Science*, *125*, *873–884*.

Bhanot, V. B., Singh, V. P., Kansal, A. K. & Thakur, V. C., 1977: Early Proterozoic Rb-Sr whole-rock age for central crystalline gneiss of Higher Himalaya, Kumaun. *Geol. Soc. India, 18, 2, 90–91.*

Bhatia, M. R., 1983: Plate tectonics and geochemical composition of sandstones. *Journal of geology, 91, 6, 611–627.*

Bhatia, M. R. & Crook, K. A., 1986: Trace element characteristics of greywackes and tectonic setting discrimination of sedimentary basins. *Contr. Mineral. Petrology, 92, 2, 181–193.*

Cullers, R. L. & Podkovyrov, V. N., 2000: Geochemistry of the Mesoproterozoic Lakhanda shales in southeastern Yakutia, Russia: implications for mineralogical and provenance control, and recycling. *Precambrian Research*, *104, 1–2, 77–93.*

Das, B. P., Joshi, M. & Kumar, A., 2019: Tectonochemistry and p-t Conditions of Ramgarh and Almora Gneisses from Askot Klippe, Kumaun Lesser Himalaya. *Acta Geologica Sinica – English Edition, 93, 2, 322–343.*

Gairola, V. K. & Joshi, M., 1978: Structure of a part of Dudatoli Almora crystalline thrust sheet around Thalisain, district Pauri Garhwal – Structure d'une partie de la nappe charriée cristalline de Dudatoli-Almora dans la région de Thalisain, district de Pauri Garhwal Himal. *Geology, 8, 1, 379–39.*

Ghose, A., Chakrabarti, B. & Singh, R. K., 1974: Structural and metamorphic history of the Almora group, Kumaun Himalaya, Uttar Pradesh. *Geology*, *4*, *171–174*.

Grizelj, A., Peh, Z., Tibljaš, D., Kovačić, M. & Kurečić, T., 2017: Mineralogical and geochemical characteristics of

Miocene pelitic sedimentary rocks from the south-western part of the Pannonian Basin System (Croatia): Implications for provenance studies. *Geosci. Frontiers, 8, 1, 65–80.*

Herron, M. M., 1988: Geochemical classification of terrigenous sands and shales from core or log data. *Journal of Sedimentary Research*, *58*, *5, 820–829*.

Islam, R., Ahmad, T. & Khanna, P. P., 2005: An overview on the granitoids of the NW Himalaya. *Him. Geol., 26, 1, 49–60.*

Joshi, M. & Tiwari, A. N., 2001: Metamorphic evolution of the Almora Nappe along the Chhara-Someshwar transect, Kumaun Himalayan. In 'Geology and Natural Environment of the Lesser Himalaya: Present Status and Strategy for the Next Two Decades', *Abstr. vol. Nainital, 6–7.*

Joshi, M. & Tiwari, A. N., 2007: Folded metamorphic reaction isograds in the Almora Nappe, Kumaun Lesser Himalaya: Field evidence and tectonic implications. *Neu. Jb. Geol. Paläont., Abh., 215–225.*

Joshi, M. & Tiwari, A. N., 2009: Structural events and metamorphic consequences in Almora Nappe, during Himalayan collision tectonics. *J. Asian Earth Sci., 34, 3, 326–335.*

Joshi, M. & Tiwari, A. N., 2004: Quartz C-axes and metastable phases in the metamorphic rocks of Almora Nappe: evidence of pre-Himalayan signatures. *Current Sci., 87, 995–998.*

Joshi, G., Agarwal, A., Agarwal, K. K., Srivastava, S. & Valdivia, L. A., 2017: Microstructures and strain variation: Evidence of multiple splays in the North Almora Thrust Zone, Kumaun Lesser Himalaya, Uttarakhand, India. *Tectonophysics, 694, 239–248.*

Joshi, M., Kumar, A., Ghosh, P., Das, B. P. & Devi, P. M., 2019: North Almora Fault: a crucial missing link in the strike slip tectonics of western Himalaya. *J. Asian Earth Sci., 172, 249–263.*

Kohn, M. J., Paul, S. K. & Corrie, S. L., 2010: The lower Lesser Himalayan sequence: A Paleoproterozoic arc on the northern margin of the Indian plate. *Bulletin*, *122, 3–4,* 323–335.

Mackenzie, F. T. & Garrels, R. M., 1971: Evolution of sedimentary rocks. *New York, Norton.*

Madukwe, H. Y., Obasi, R. A., Fakolade, O. R. & Bassey, C. E., 2015: Provenance, tectonic setting and source-area weathering of the coastal plain sediments, South West, Nigeria. *Sci. Res. J., 3, II, 20–31.*

Mandal, S., Robinson, D. M., Kohn, M. J., Khanal, S., Das, O. & Bose, S., 2016: Zircon U-Pb ages and Hf isotopes of the Askot klippe, Kumaun, northwest India: Implications for Paleoproterozoic tectonics, basin evolution and associated metallogeny of the northern Indian cratonic margin. *Tectonics*, *35, 4, 965–982.*

Mehdi, S. H., Kumar, G. & Prakash, G., 1972: Tectonic evolution of eastern Kumaun Himalaya: a new approach. *Himalayan Geol., 2, 481–501.*

Molnar, P. & Tapponnier, P., 1975: Cenozoic Tectonics of Asia: Effects of a Continental Collision: Features of recent continental tectonics in Asia can be interpreted as results of the India-Eurasia collision. *Science, 189, 4201, 419–426.*

Rana, H. & Harel, T., 2018: Geology of the Patharkhola area, Almora District, Uttarakhand (India): with special reference to the lithology and field relation. *Bull. Depart. Geol., 1–6.* DOI: https://doi.org/10.3126/bdg.v20i0.20716.

Rana, H., 2023: Petrography and Petrogenesis of rock around Patharkhola area, District Almora, Uttrakhand. *Unpublished Ph.D. thesis, pp. 218.*

Rana, H., Harel, T., Aman, S. & Satyam, S., 2023a: Petrochemistry of Phyllites from Patharkhola, Lesser Kumaun Himalaya with Reference to Tectonic Implications. *Earth and Planetary Science*, *2, 2, 1–9*. https://doi.org/10.36956/eps.v2i2.842.

Rana, H., Harel, T. & Rishabh, B., 2023b: Geochemical characteristics and tectonic interpretation of garnet mica schists of Patharkhola area in Kumaun Lesser Himalaya Uttarakhand Himalaya, India. *Mineralia Slovaca, 55, 2, 133–142.* DOI: https://doi.org/10.56623/ms.2023.55.2.3.

Rana, H. & Harel, T., 2023: Structural, Micro-Structural and Thermal Characterizations of Natural Garnet of Regions of Patharkhola from the State of Uttarakhand of India. *BPAS-Geology, 42F, 1, 1–9.* DOI:10.48165/bpas.2023.42 F.1.1.

Roser, B. P. & Korsch, R. J., 1986: Determination of tectonic setting of sandstone-mudstone suites using SiO_2 content and K_2O/Na_2O ratio. *Journal of geology, 94, 5, 635–650.*

Saini, N. K., Mukherjee, P. K., Khanna, P. P. & Purohit, K. K., 2007: A proposed amphibolite reference rock sample (AM-H) from Himachal Pradesh. *Geological Society of India*, *799–802*.

Srivastava, P. & Mitra, G., 1994: Thrust geometries and deep structure of the outer and lesser Himalaya, Kumaon and Garhwal (India): Implications for evolution of the Himalayan fold-and-thrust belt. *Tectonics, 13, 1, 89–109.*

Srivastava, P. & Gautam, M., 1996: Deformation mechanisms and inverted thermal profile in the North Almora Thrust mylonite zone, Kumaon Lesser Himalaya, India. *Journal of structural geology, 18, 1, 27–39*.

Sun, S. S. & McDonough, W. F., 1989: Chemical and isotopic systematics of oceanic basalts: implications for mantle composition and processes. *Geol. Soc., London, Spec. Publ., 42, 1, 313–345.*

Taylor, S. R. & McLennan, S. M., 1985: The Continental Crust: its Composition and Evolution. *Oxford, Blackwell Scientific Publication, pp. 312.*

Thomas, T. & Thomas, H., 1992: Fold flattening and strain studies in a part of Almora Crystalline Zone, around Tamadhaun Kumaun Himalaya. *Indian Mining and Engineering Jour., 5–7.*

Thomas, T. & Thomas, H., 2003: Fourier Shape of The Fold Developed around Tamadhaun, District Almora Using a Computer Programm. *Gond. Geol. Magz., Advances in Precambrian of Central India, Spec. Vol., 7, 169–176.*

Valdiya, K. S., 1980a: Stratigraphic scheme of the sedimentary units of the Kumaun Lesser Himalaya. *Stratigraphy and correlations of the lesser Himalayan formations, 72, 48.*

Valdiya, K., 1980b: Geology of Kumaun lesser Himalaya. *W. I. H. G., 291–295.*

Valdiya, K. S., 1988: Tectonics and evolution of the central sector of the Himalaya. *Phil. Trans. Roy. Soc. London. Ser. A, Mathem. Phys. Sci., 326, 1589, 151–175.*

Verma, S. P. & Armstrong-Altrin, J. S., 2013: New multi-dimensional diagrams for tectonic discrimination of silici-

clastic sediments and their application to Precambrian basins. *Chemical Geology*, *355*, *117–133.*

Whitney, D. L. & Evans, B. W., 2010: Abbreviations for names of rock-forming minerals. *American mineralogist*, *95, 1, 185–187.*

Webb, A. A. G., Yin, A., Harrison, T. M., Célérier, J., Gehrels, G. E., Manning, C. E. & Grove, M., 2011: Cenozoic tectonic history of the Himachal Himalaya (northwestern India) and its constraints on the formation mechanism of the Himalayan orogen. *Geosphere, 7, 4, 1013–1061.*

Webb, A. A. G., 2013: Preliminary balanced palinspastic reconstruction of Cenozoic deformation across the Himachal Himalaya (northwestern India). *Geosphere, 9, 3, 572–587.*

Yin, A., 2006: Cenozoic tectonic evolution of the Himalayan orogen as constrained by along-strike variation of structural geometry, exhumation history, and foreland sedimentation. *Earth Sci. Rev., 76, 1–131.*

Geochemické charakteristiky petrogenézy rúl oblasti Patharkhola z kumaunských Malých Himalájí v Indii

Himalájska horská reťaz vznikla kolíziou indickej a ázijskej litosférickej platne pred zhruba 55 miliónmi rokov (Molnar a Tapponnier, 1975; Valdiya, 1980a, b, 1988; Yin, 2006; Webb, 2011, 2013). Tektoniku Malých Himalájí – zóny situovanej južne od hlavného hrebeňa Himalájí – intenzívne skúmali Gansser (1964), Mehdi et al. (1972), Thomas a Thomas (1992, 2003), Agarwal et al. (2010, 2016), Joshi et al. (2017, 2019), Rana (2023), Rana a Thomas (2018, 2023) a Rana et al. (2023a, b). Práce autorov Ghosh et al. (1974), Srivastava a Mitra (1996) a Joshi a Tiwari (2004, 2007, 2009) priniesli nové poznatky o metamorfnej histórii kryštalického masívu Almora, ktorého geochemické charakteristiky sú náplňou tejto štúdie.

Minerálne zloženie skúmaných rúl paleoproterozoického veku z oblasti Patharkhola – kremeň, dominantne draselné živce a sľudy – indikuje pelitický protolit rulových metamorfitov. SiO_2 a Al_2O_3 majú zastúpenie 87 – 88 %. Hodnoty Na_2O a K_2O sú 3,56 a 4,69 %. Pomery LREE/HREE (La/Yb)N v rozsahu 4,8 – 10,6 spolu s anomáliou Eu/Eu* (0,3 – 0,6) a Th/Sc (1,3 – 9,4) indikujú, že protolitom týchto rúl boli felzitické sedimenty. Ich primárna pozícia sa spája s prostredím vulkanického oblúka s blízkou prítomnosťou sedimentov bohatých na silt a íl.

Doručené / Received: 2. 8. 2024
Prijaté na publikovanie / Accepted: 17. 12. 2024

Mineralia Slovaca, Web ISSN 1338-3523, ISSN 0369-2086, https://doi.org/10.56623/ms.2024.56.2.4
56, 2 (2024), 165 – 180, © Authors 2024. CC BY 4.0

A comparative study of decision tree and support vector machine methods for gold prospectivity mapping

MOHAMMAD EBDALI[1] and ARDESHIR HEZARKHANI[2]*

[1, 2]Amirkabir University of Technology, Department of Mining Engineering, Tehran, Iran; ardehez@aut.ac.ir

Abstract: Elements geochemical anomalies mapping is one of the main goals of geochemical investigations. Since the field studies are time-consuming and costly, the data processing, applying machine learning methods could be applied, which is less expensive, faster, and more accurate. In this study, two machine learning methods, including decision tree algorithm and support vector machine, were applied for gold prospectivity mapping. To reach this aim, silver, copper, lead and zinc values were used as input variables. The comparison of the analytical results obtained from the two mentioned methods confirms that the DT (decision tree) model has sufficient accuracy and better performance than the SVM (support vector machine) model for preparing gold prospectivity mapping in the studied area.

Key words: decision tree, machine learning, mineral prospectivity mapping, support vector machine

Graphical abstract

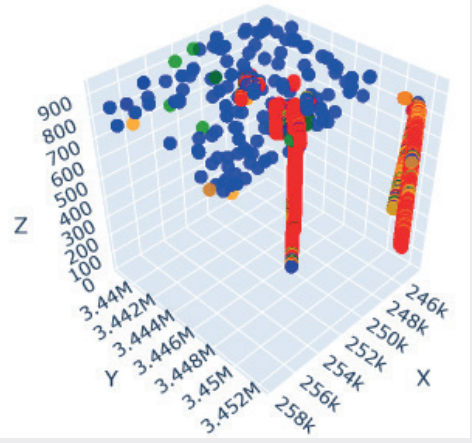

Highlights

- Two machine learning methods, including decision tree algorithm and support vector machine, were applied for gold prospectivity mapping. To reach applicable results, the silver, copper, lead and zinc values were used as input variables.
- The comparison of the analytical results obtained from the two machine learning methods confirms that the DT (decision tree) model has sufficient accuracy and better performance than the SVM (support vector machine) method for preparing gold prospectivity mapping in the studied area.

1 Introduction

New techniques for estimating and evaluating variables have been created from research conducted over an extended period. New techniques like machine learning algorithms are used to address the issue of variable estimation (Dutta et al., 2010). These algorithms learn how data is related by using the examples provided to them. The attraction of these non-linear estimators is their capability to function like a black box. By providing sufficient data to these algorithms and subsequently educating them, they have the ability to grasp the connection between the input data, like sample coordinates, and the output data, such as the ore grade at specific points. With this approach, there is no need to take into account assumptions regarding linearity for components, coefficients, or relationships (Zhang et al., 2024). Machine learning algorithms are categorized into supervised learning methods and unsupervised learning methods (Chatterjee et al., 2010b; Jafrasteh et al., 2018). Both main categories have various techniques and algorithms which are utilized, based on the specific problem and the type and amount of data available. Decision tree is a commonly applied tool and technique for data mining proficiency. This method can be very beneficial in situations where the volume of data is extremely large. Data mining involves discovering valuable knowledge that is hidden and unknown within databases. There are two main categories of data mining methods: descriptive and predictive. Clustering is among the most well-known descriptive techniques, while classification is considered one of the most crucial predictive techniques. The clustering perspective is crucial in data mining for analysing large amounts of data and samples with different characteristics,

ORCID Nos. of authors: Mohammad Ebdali (http://orcid.org/0009-0002-4114-1611), Ardeshir Hezarkhani (http://orcid.org/0000-0002-1149-3440)

as it involves important methods and techniques (Anderberg, 1973). Data is clustered in the clustering method by maximizing similarity within groups and minimizing it between groups. The process of classification involves identifying data categories or concepts in order to create a model that can predict the categories of unknown objects. A classifier is a function that learns to assign a data item to a specific category from a set of predefined categories. Decision Tree, Bayes classifier, and Neural Network are a few popular classification techniques. A decision tree can generate easy-to-understand explanations of the connections within a set of data and is useful for tasks involving classification and prediction. This decision-making framework can be implemented through mathematical and computational methods that aid in categorizing and summarizing a dataset (Tsai & Yen-Jiun, 2009). Among the varied and effective methods in the artificial intelligence field for estimating and evaluating grades are artificial neural networks (Chatterjee et al., 2010a, b; Guo, 2010; Li et al., 2010; Mahmoudabadi et al., 2009; Nezamolhosseini et al., 2017; Samanta et al., 2005; Sayadi & Shahrabadi, 2008; Tahmasebi & Hezarkhani, 2010, 2012; Tsai & Yen-Jiun, 2009), neural fuzzy inference (Tahmasebi & Hezarkhani, 2010), random forest (Jafrasteh et al., 2018), and support vector machine (Maleki et al., 2014; Matías et al., 2004; Tenorio et al., 2015). In mining engineering, artificial neural networks are used not only for grade estimation, but also for tasks like blast network dimension estimation (Amnieh et al., 2012), processing factory design (Kotake et al., 2002; Singh et al., 2013), geological classification (Thuijsman, 1995), remote sensing data classification (Miller, 1995; Wang, 2005), and identifying failure models in Underground Mining (Lee & Sterling, 1992; Shahin et al., 2008). The decision tree algorithm, the foundation of the random forest algorithm, has been extensively utilized in geological and remote sensing applications as a successful classifier (Jhonnerie et al., 2015; Krishna et al., 2018; Masoumi et al., 2017).

Support vector machine, a supervised learning technique, is utilized for both classification and regression purposes. The SVM classifier operates by linearly classifying the data. It aims to choose the plain that has a higher confidence margin. Utilizing nonlinear programming techniques, the optimal line for the data is determined by solving the equation, as these methods are commonly used for solving constrained problems. Prior to the linear division, the data is transformed into a higher dimensional space using the kernel function to enable the machine to classify the data with high complexity. To address the issue of dealing with high dimensions, Lagrange's duality theorem is employed to convert the original minimization problem into a dual form. This new form involves a kernel function, a simpler version of the complex function phi that maps to the high-dimensional space by multiplying the phi function's vector. Various types of kernel functions, such as exponential, polynomial, and sigmoid kernels, can be utilized. Despite being newer than the artificial neural network method, the support vector machine method has quickly gained popularity due to its robust mathematical foundation (Kecman, 2001, 2004; Smola & Schölkopf, 2004). This technique is commonly employed in pattern recognition software, such as spatial data analysis (Dutta et al., 2010), creating natural radioactivity maps (Pozdnoukhov, 2005), estimating arsenic levels in bedrock from river sediments using support vector machine method (Twarakavi et al., 2006), identifying alteration zones linked to mineralization (Abbaszadeh et al., 2013, 2015; Soliman & Mahmoud, 2012), and classification of remote sensing images (Moorthi et al., 2011; Soliman & Mahmoud, 2012; Soliman et al., 2012). This approach has also been applied in determining the grade of slate deposits (Matías et al., 2004), glacial type platinum (Tenorio et al., 2015), gold (Chatterjee et al., 2010a), and iron (Maleki et al., 2014) in the grade estimation field. Hence, in this study, decision tree algorithm and support vector machine were applied to conduct gold prospectivity mapping.

2 Geological setting of the study area

The Janja area is located in Sistan and Paluchestan province. The region is situated in a flat sandy plain with sparse vegetation and few rock outcrops (Fig. 1), with altitudes ranging from 800 to 900 m a. s. l.

The research area is a section of the Zabul-Zahedan-Saravan subregion. This subregion is included in the flysch basin located in eastern Iran, commonly known as the eastern Iranian mountains. The region of the province contains a deep oceanic bedrock that is overlaid with a thick series of flysch deposits of Late Cretaceous-Oligocene age. The mentioned basin is believed to have originated after a collision within the continent between the Lot block to the west and the Afghan block to the east, following with formation of oceanic crust and ophiolitic complexes. While much of the crust has been lost in Neo-Alpine subduction zone, remnants can be seen along deep, longitudinal faults like the Nehbandan fault in the area. According to the geologic map of the area (Fig. 2), the Cretaceous Flysch (Kuf) is the oldest and most prominent solidified unit. This flysch is made up of alternating beds of grey to green greywackes and calcareous lichens. The majority of calcareous lichens displays a light green, weathered color, with occasional beds of fine-grained greywackes. In multiple areas of the region, thick beds of calcareous lichen (Kumr) units are visible. These limestone lichens are associated with the Cretaceous flysch and, in terms of lithology, are identical to the lower formations, however, they are consistently found below a layer of volcaniclastic sediments. The thickness of unit varies, reaching up to

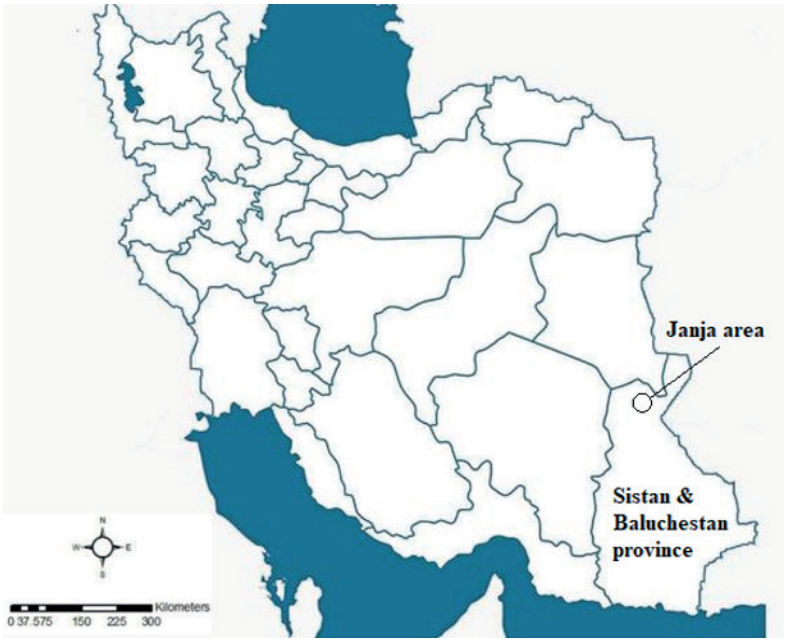

Fig. 1. Geographical location map of Janja area.

536 meters in the eastern part of the ophiolitic belt. The Sefidabe Formation (KPs) is one of the largest units found in the Janja area, particularly in the central and eastern parts of the zone. This structure is primarily made up of a series of volcaniclastic and pyroclastic deposits, which are divided into lower and upper sections in some areas. The bottom section (KPs1) is made up of thin to medium layers of volcaniclastic material, along with some volcanic flows, clastic sediments, and limestones. The upper section displays characteristics of stratified volcanic and pyroclastic rocks with pale green lichen layers alternated. In the north, these units are hundreds of meters thick, but their thickness decreases quickly towards the east and west. In certain areas, these units appear to be similar to Kuf sediments.

3 Data and methods

3.1 Sampling operation

Considering the extent of exploration and the dense waterway network in the area, a sampling system was developed for gathering geochemical and heavy mineral samples. This system consists of 285 geochemical samples and 59 heavy mineral samples from waterways (Fig. 3).

Alongside collecting samples from the sediment of waterways, 18 trenches were excavated on the surface where polymetallic veins are exposed, as well as in the area where intense operations were conducted. It was tried to design the trenches perpendicular to the trend of the veins based on the outcrops of the veins. Additionally, 16 boreholes

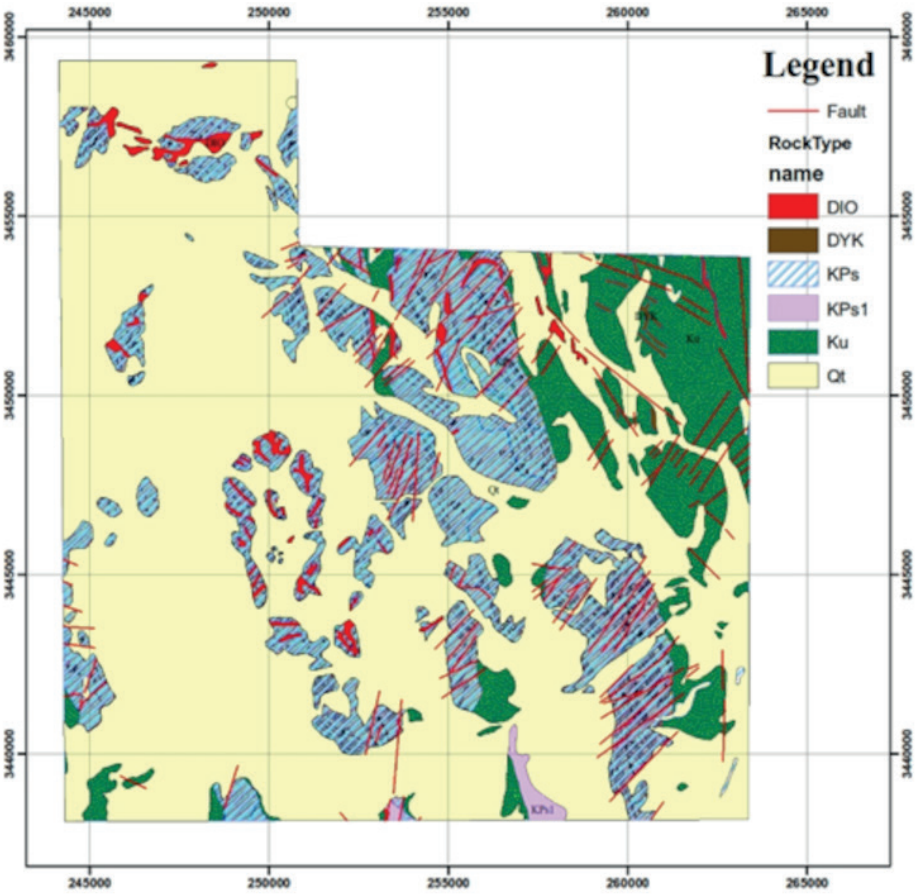

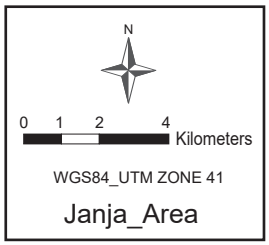

Fig. 2. Geological map of Janja area.

were drilled for polymetallic mineralization in the region. A combined total of 3 754 samples were gathered from trenches and boreholes excavated in the area.

3.2 Decision tree algorithm

The decision tree algorithm belongs among the most commonly used data mining algorithms. In data mining, the decision tree serves as a predictive model that is applicable for regression and classification models. If used for regression, it is termed a regression tree; if for classification, it is known as a classification tree. A set of binary decisions is used by the decision tree to carry out multi-stage classifications. Every choice separates a collection of pixels into two categories according to a set of logical conditions. A tree may contain any quantity of decision nodes. Information from various origins and categories can be utilized in constructing a decision tree (Zaremotlagh & Hezarkhani, 2017). Decision trees are effective methods for predicting and clarifying the connection between certain measurements and a target variable. The decision tree algorithm was utilized in this study to pinpoint potential mining locations. The decision tree picks a variable with a high information value to identify the promising range (equation [1]). The effectiveness of the chosen variable is assessed by utilizing equation [2] and the entropy reduction criterion (Zhang et al., 2019).

$$E(t) = \sum_{j}^{} p(j \mid t) Logp(j \mid t) p, \quad [1]$$

Where $E(t)$ is the entropy criterion – the relative frequency of class j in node t. Hence, the information gain for every split is calculated in the following manner:

$$GAIN_{Split} = E(p) - \sum_{i=1}^{k} \frac{ni}{n} E(j), \quad [2]$$

Where $E(p)$ is the overall entropy at parent node and is the sum of weighted entropy at each child node. The parent node is divided into k components and the number of records in the component is i. This maximizes the similarity and difference between the data sets in nodes (Shirali, 2016). In the decision tree framework, the forecast generated by the tree is described as a set of rules. Every route from the starting point to a last branch of the decision tree represents a rule, and ultimately, the leaf is marked with the category that contains the highest number of data entries. A feature selection criterion is a method to choose

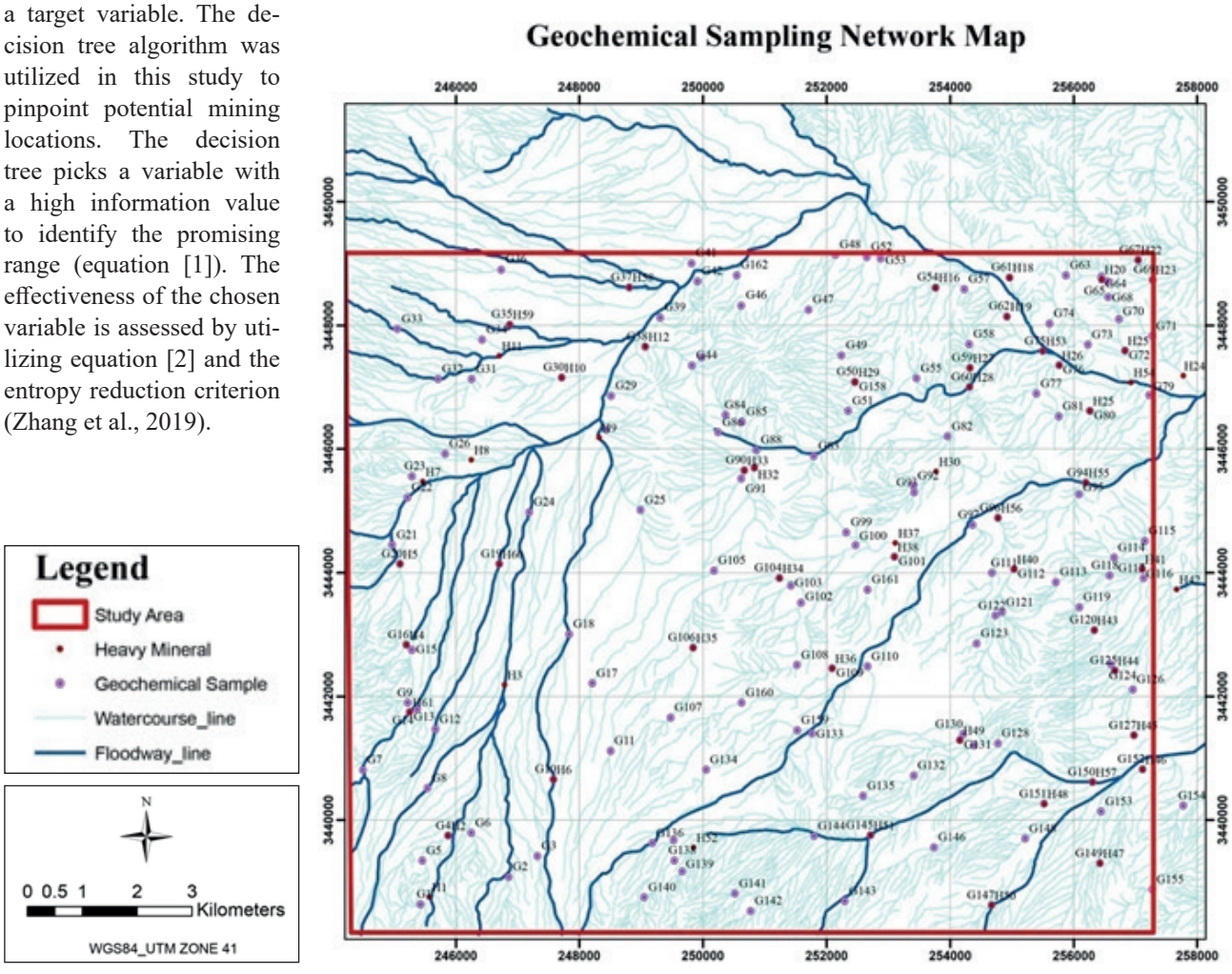

Fig. 3. Geochemical sampling network of waterway sediments in Janja area.

the best branch point criterion that separates the labeled classes in training data. Two popular methods for selecting features are the Gini coefficient and entropy index. The Gini index is a statistical metric employed to gauge the spread of data within a dataset. This index is determined by utilizing equation [3]:

$$Gini = 1 - \Sigma p^2, \quad [3]$$

Where p is the probability of occurrence of a particular class in the set. The Gini index is utilized in the decision tree algorithm to evaluate how similar the subsets formed by a feature are in terms of their composition. A lower Gini index makes a feature better for splitting data into more uniform subsets. The decision tree algorithm utilizes the Gini index to pick the feature that leads to the most significant decrease in the Gini index of the set. This indicates that the chosen characteristic results in the greatest level of uniformity in the subsets that are formed. Entropy plays a crucial role in machine learning, particularly in the development of decision trees. Entropy quantifies the level of instability or uncertainty in a dataset. This concept may aid in understanding how information is spread out in a set of data and how it can be used to properly split the data when constructing a decision tree. In order to determine entropy, we need first to determine the likelihood of each class appearing in the dataset. Next, these probabilities are used in determining the overall entropy, as outlined in equation [4]:

$$Entropy = -\Sigma(p(x)\ log_2\ p(x)), \quad [4]$$

Where $p(x)$ is the probability of occurrence of each class. The entropy value shows the level of instability or complexity present in the data. Entropy is utilized in decision trees to determine the best feature to split at each node. The objective is to choose the feature that results in the most significant decrease in entropy, ensuring that the partitioned data is more consistent and capable of making more precise forecasts. Pruning plays a crucial role in optimizing decision trees. Pruning involves removing sub-nodes from the decision tree, which is in contrast to splitting. When constructing a decision tree, several branches represent abnormalities in the training data resulting from outliers or noise. In some tree creation algorithms, pruning is is considered a part of the algorithm. While in other cases, pruning is solely employed to address the issue of overfitting. Several methods use statistical criteria to remove less reliable branches. Pruned trees are often smaller and less complicated, making them simpler to comprehend. Pruned trees generally have a quicker and more accurate performance in classifying test data compared to unpruned trees. Two popular methods are used for cutting trees. In the initial stages of constructing a tree, pre-pruning involves frequently stopping to prune the tree. As soon as a stop is created, the node transforms into a leaf. The post pruning method is the second case. It removes subtrees from a full-grown tree. Pruning a subtree involves removing branches at a node and replacing them with a leaf node. The size of the decision tree is another crucial parameter. A simpler decision tree is more communicative and transparent. Hence, the accuracy of the tree is significantly impacted by its level of complexity. Typically, the complexity of a tree is assessed by one of the following criteria: the total number of nodes, total number of leaves, tree depth, and number of features used.

3.3 Support vector machine

Support vector machines represent type of generalized linear models that rely on a linear combination of features to make decisions regarding classification and regression. Support vector machines, like artificial neural networks, have the ability to estimate multivariate functions with any desired level of precision and are suitable for representing various nonlinear and intricate procedures (Wu et al., 2018). Support vector regression, a form of support vector machine, is used for estimation across different issues. This approach involves educating algorithms and relies on the support vector machine classifier method, which is more comprehensive than the aforementioned method (Smola & Schölkopf, 2004). The method of support vector regression, rooted in statistical learning theory and focused on minimizing structural risk, was originally presented by Vapnik in the 1990s (Matías et al., 2004). In a regression model, it is essential to determine the relationship between the dependent variable y and a group of independent variables x (Smola & Schölkopf, 2004). This technique is applicable for predicting and classification problems involving two or more categories (Martínez-Ramón & Christodoulou, 2022). The aim of these issues is to create a classification standard that is effective for samples that have not been harvested and also has strong generalizability. The optimal hyperplane is defined as the linear separating plain with the largest margin and equal distance from the nearest points, with the goal of extending the boundary to cover all potential ranges. Typically, in linear classification tasks, a weight like W needs to be taken into account for a vector like X in order for this weight to effectively categorize the vectors into their correct classes. The optimal separator plate is chosen based on equation [5] (Abe, 2005; Tran et al., 2005).

$$\mathbf{w}^T x + b = 0, \quad [5]$$

Where $\mathbf{w}$ is the weight matrix; $\mathbf{T}$ is the output of the weighting matrix; x is the vector and b is the bias constant. The inner multiplication is used to express the relationship between vector x and weight $\mathbf{w}$. In the context

of the Support Vector Machine algorithm, the equation [5] typically represents a decision boundary. In other words, 0 (the numeral zero) indicates the decision boundary itself, which separates different classes in the feature space. The points that lie on this boundary satisfy the equation [5]:

- Positive Class: For instances of the positive class (e.g., class +1), the expression $\mathbf{w}^T x + b = 0 > 0$.
- Negative Class: For instances of the negative class (e.g., class –1), the expression $\mathbf{w}^T x + b = 0 < 0$.

A set of points is optimally separated by a plain based on the conditions that they are accurately classified in their respective classes. The maximum distance between the nearest points of each data class to the separating plain is shown in Fig. 4 (Sánchez, 2003; Tran et al., 2005). Therefore, it is necessary to calculate the parameters **w** and in order to meet the two specified conditions. To address this issue and regulate the precision of the data, equation [6] is formulated for the margin (Huang et al., 2006).

$$\mathbf{w}^T x + b = 0 = \begin{cases} x \le 1 & for \quad y_i = -1 \\ x \ge 1 & for \quad y_i = 1 \end{cases}, \qquad [6]$$

Where the y_i represents the class label for the i^{th} training example. In this case, it can take on values of −1 or 1, which correspond to two classes. Typically, $y_i = 1$ might represent the positive class and = −1 the negative class.

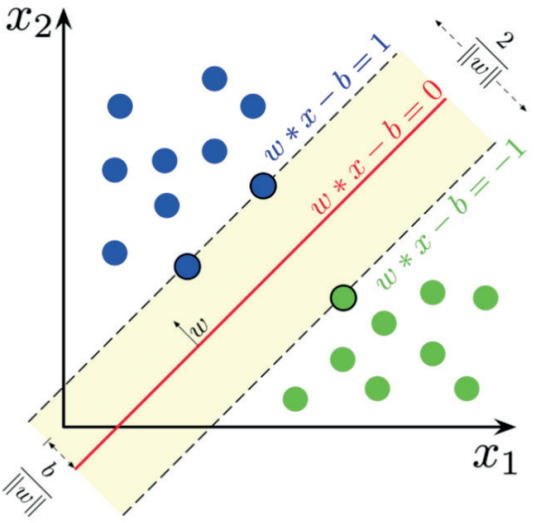

Fig. 4. Optimal separator plate and margins.

To find the ideal separation boundary with the right margin, the goal is to maximize the distance between both margins. Formula [7] illustrates the method for determining and optimizing the separation distance of these two thresholds (Martínez-Ramón & Christodoulou, 2022).

$$d(w, b; x) = \frac{|(\mathbf{w}^T x + b - 1) - (\mathbf{w}^T x + b + 1)|}{\|w\|} = \frac{2}{\|w\|}, [7]$$

Where $d(w, b; x)$ represents the distance from a point (given by the feature vector) to the decision boundary defined by $\mathbf{w}^T x + b = 0$. The constants 1 and −1 represent specific thresholds that define the margins for the separated classes. Typically, the decision boundary is set to equal 0 (the numeral zero), while the margins are defined as 1 and −1. The $\|w\|$ is called a soft function. According to the results obtained from equation [7], the goal is to maximize the desired margin (Abe, 2005; Huang et al., 2006; Martínez-Ramón & Christodoulou, 2022; Merler & Jurman, 2006; Sánchez, 2003). Occasionally in the linear system, there are situations where multiple data points are missing (Fig. 5). In this situation, the error function is necessary in order to attain an excellent separating plane. Equation [8] (Bishop & Nasrabadi, 2006; Wang, 2005) displays this function.

$$F(\xi) = \sum_{i=1}^{N} \xi i, \qquad [8]$$

Where the function $F(\xi)$ measures the total error resulting from the slack variables , which correspond to misclassified instances or instances that fall outside the margin. Put differently, ξi represents the classification error value. The data placed in the margin is the significant feature in Fig. 5. This data is used by the vector machine to accurately classify the data (Van Der Heijden et al., 2005; Wang, 2005).

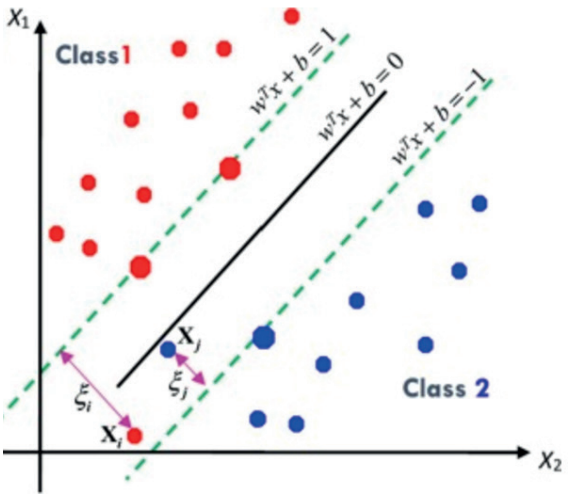

Fig. 5. A linear integral system with error rate ξi (Zhang et al., 2019).

Hence, equation [9] represents the optimization problem in non-separable linear systems. The vector **w** determines the hyper plain of the generalized optimal isolator through equation [9] (Bishop & Nasrabadi, 2006).

$$M in_{\mathbf{w},b} = \frac{1}{2}\mathbf{w}^T\mathbf{w} + C\sum_{i=1}^{N}\xi i, S.t \quad yi\,(\mathbf{w}^T x_i + b) \ge 1 - \xi i \qquad [9]$$

Where $M\ in_{w,b}$ denotes the objective function that is attempted to be minimized $\frac{1}{2}\mathbf{w}^{T}\mathbf{w}$ during the training of the model. It represents the total loss that needs to be minimized – represents the regularization component of the objective function. It is often associated with maximizing the margin, the factor of $\frac{1}{2}$ is used for mathematical convenience, particularly when taking derivatives, $\sum_{i=1}^{N}$ ξi represents the total slack variable penalties for all training samples, N is the total number of training samples in the dataset, and ξi is the slack variable corresponding to the i^{th} training example. The ξi measures the extent to which the i^{th} example falls within the margin or is misclassified. If ξi = 0, the example is correctly classified; if ξi > 0, it is either misclassified or lies within the margin. The y_i is the class label of the i^{th} training example, which takes values of 1 or −1. It indicates which class the example belongs to. The x_i is the feature vector of the i^{th} training sample. Each component of this vector corresponds to a feature of that sample. The constraint $y_i(\mathbf{w}^{T}x_i + b) \geq 1 - \xi i$ ensures that each training example is correctly classified with a margin of at least 1 minus the slack variable. For a correctly classified point ($y_i = +1$), the condition requires that the output of the decision function $\mathbf{w}^{T}x_i + b$ is at least 1. For misclassified points or those near the margin (when ξi > 0), it provides leeway by allowing a margin of less than 1. The parameter C is the interaction coefficient to maximize margins and minimize performance error. In cases such as this one, Lagrange multipliers are utilized, appearing as Lagrange multipliers in equation [10] in the latest correlation involving α, β (Wang, 2005).

$$Lp\ (\mathbf{w},\ b,\ \xi,\ \alpha,\ \beta) = \frac{1}{2}\ \mathbf{w}^{T}\ \mathbf{w} + C\ \sum_{(i=1)}^{N}\xi_i - \sum_{(i=1)}^{N}\alpha_i \{y_i\ [\mathbf{w}^{T}\ x_i + b] - 1 + \xi_i\ \} - \sum_{(i=1)}^{N}\ \beta_i\ \xi_i \qquad [10]$$

Where α_i is Lagrange multiplier associated with the constraints of the SVM optimization problem. Each corresponds to the i^{th} training example and measures how much the corresponding constraint contributes to the Lagrangian. Non-zero indicates that a data point is either a support vector or on the margin and β_i is Lagrange multipliers associated with the slack variables ξ_i. Each β_i represents the penalty associated with the i^{th} slack variable. A non-zero β_i indicates that there is some violation of the minimum margin requirement.

The fundamental issue of equation [10] can be converted into a dual problem by dual classical Lagrange. Equation [11] defines the dual aspect of this relationship.

$$Max\mathbf{W}(\alpha,\beta) = Max_{\alpha,\beta}(M\ in_{w,b,\xi}L(\mathbf{w},b,\xi,\alpha,\beta), \qquad [11]$$

Setting the derivative of equation [11] with respect to **W** and equal to zero yields the values of equations [12]:

$$\begin{cases} \dfrac{\partial L}{\partial \mathbf{w}} = o \quad then \quad \mathbf{w} = \sum_{i=1}^{N}\alpha_i\ \beta_i\ \mathrm{x}_i \\ \dfrac{\partial L}{\partial b} = o \quad then \quad \mathbf{w} = \sum_{i=1}^{N}\alpha_i\ \mathrm{y}_i = o\ , \\ \dfrac{\partial L}{\partial \xi} = o \quad then \quad \alpha_i\ + \beta_i = C \end{cases} \qquad [12]$$

Equation [11] can be used to express the relationships in the form of equation [13] to derive the basic equation of the vector machine in the linear integral state (Wang, 2005).

$$MaxL_d\ (\alpha) = \sum_{i=1}^{N}\ \alpha_i - \frac{1}{2}\ \sum_{i=1}^{N}\ y_i\ y_i\ \alpha_i\ \alpha_i x_i^{T}\ x_i, \qquad [13]$$

$$S.t = \begin{cases} o \leq \alpha_i \leq C \\ \sum_{i=1}^{N}\ \alpha_i\ y_i = o \end{cases}$$

It is evident that the linearly separable system functions in the same way as the linearly separable system. The only thing that sets them apart is the adjustment of the boundaries of the Lagrange coefficients. The parameter C must be established in these systems in order to determine the classifier's extra capacity. Typically, a vector such as x in a higher-dimensional space is represented as a linear vector machine in a higher space (also known as a feature space) depicted in Fig. 6, with the input space still being nonlinear.

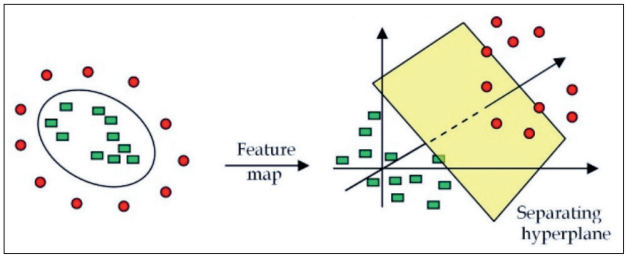

Fig. 6. Data classification in higher space.

It is important to mention that Table 1 displays the most frequently utilized kernel functions for linear inseparable problems.

Tab. 1

The prevailing kernel functions employed in linearly inseparable issues

Type	Kernel function
Linear	K(x_i,x_j)=$\gamma x_i\ x_j$
Polynomial	$K(x_i\ x_j) = (\gamma x_i\ x_j + r)^{d}, \gamma > o^{\circ}$
RBF	$K(x_i\ x_j) = exp\{-\gamma\|\|x_i - x_j\|\|^{2}\}, \gamma > o^{\circ}$
Sigmoid	$K(x_i\ x_j) = \tanh(\gamma x_i\ x_j + r), \gamma > o^{\circ}$

4 Results and analysis

4.1 Gold grade estimation using decision tree algorithm

Regarding this matter, the data extracted from geochemical samples and the analysis results from exploratory boreholes were evaluated in relation to outlier values, number of communities, and normality. Next, this information was sent to Python 3.11 software to create a model of potential gold mineralization areas, using factors such as rock type, alteration zones, and silver, copper, lead, and zinc values as independent variables. The model building process involves two phases: training the model and assessing its accuracy, which will be detailed further. To prepare the model for training, the dataset was split randomly into two sets in a 70 : 30 ratio. Training involved 70 % of the data while the remaining 30 % was used for validation during model evaluation. In order to prevent overfitting during modeling, the pruning technique was applied before the tree was allowed to grow, aiming to decrease complexity. In order to achieve this goal, the confidence factor, which ranges from 0 to 1, was utilized. This study utilized a confidence factor of 0.95 to prune the decision tree. The scikit-learn library's classifier decision tree was employed to develop and utilize a decision tree for data categorization purposes. This class constructs a decision tree using the CART algorithm. The decision tree is constructed using the CART algorithm through recursive and alternating divisions. Once the model is in place, it might not function effectively, therefore tweaking the corresponding hyperparameters is necessary to achieve the intended results. Some of the decision tree hyperparameters are as follows:

1. The minimum number of samples in each node to create branching and tree growth.
2. The least number of leaves that show the results of decisions.
3. Maximum depth of tree (number of rows).
4. The largest number of components that are randomly considered in the posterior direction of the tree.
5. Tree node evaluation indices to analyse the information obtained from different nodes for the purpose of branching, for example Gini coefficient and entropy.

Fig. 7. Correlation diagram between the variables of Janja dataset.

By applying various hyperparameters, the model was eventually fine-tuned to its optimal state. In this framework, the model requires a minimum of 5 samples in each node for tree development, a minimum of 3 leaves, a maximum tree depth of 4, and uses the entropy index as the appropriate criterion. Furthermore, because the 3rd and 4th categories of gold hold greater significance in terms of discovery, a weighting method was implemented for these classes. This description assigned weights of 0.2, 0.2, 0.3, and 0.3 to classes 1,

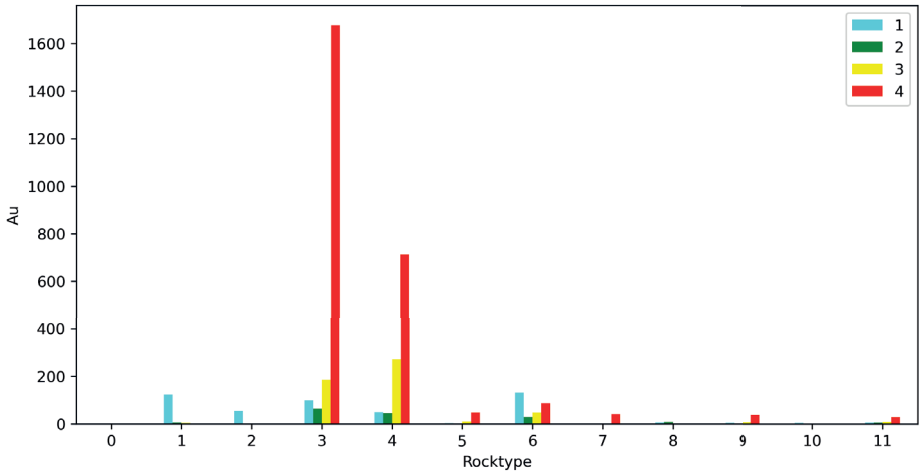

Fig. 8. The quantity of gold found in various rock types in the Janja area (3 – diorite, 4 – hornfels, 6 – schist, 7 – clay).

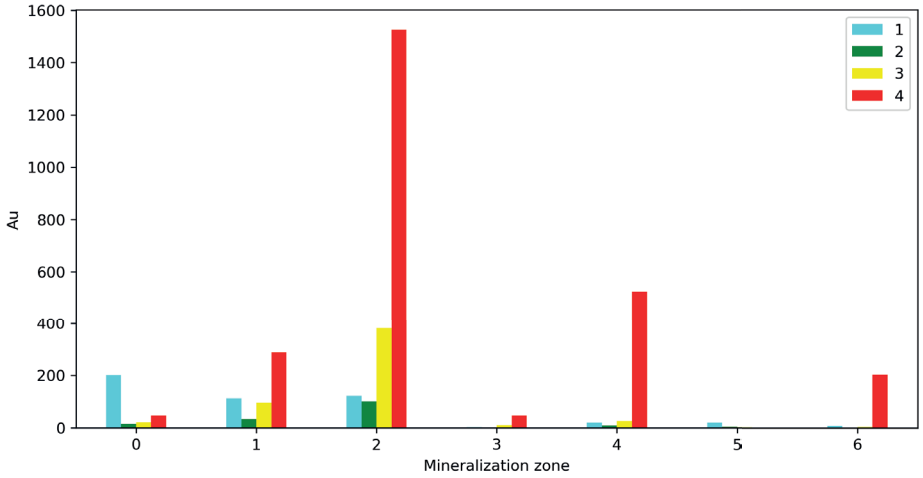

Fig. 9. The quantity of gold found in various alteration zones in the Janja area, specifically in zones 12 (propylitic) and 17 (potassic).

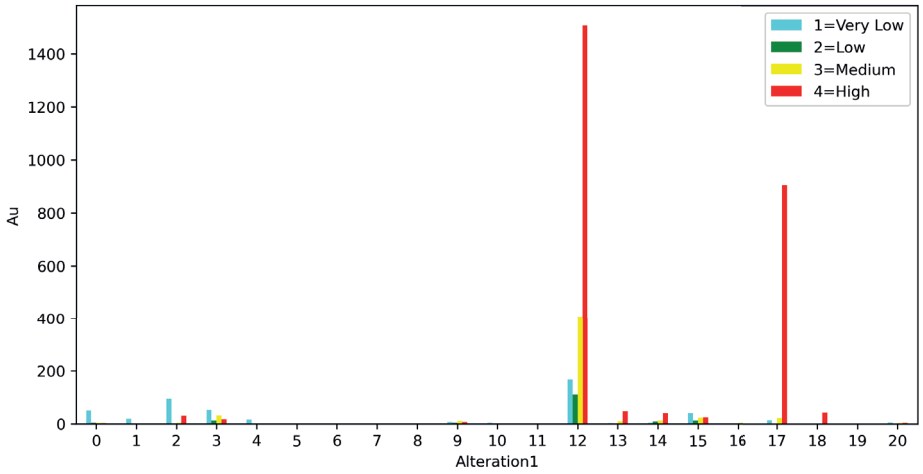

Fig. 10. The quantity of gold in different mineralization zones in the Janja area, including zones 2 (hypogene), 4 (oxyhypogene), and 1 and 6 (supergene and oxidation zones).

2, 3, and 4, respectively. According to the results of this algorithm depicted in Fig. 7, the correlation between gold and type 1 alteration stands at 0.597, with type 2 alteration at 0.575, with mineralization zone at 0.393, with the type of mineralization host rock at 0.049, and with silver, copper, lead and zinc show no relation. The types of variables such as alteration type 1 and type 2, mineralization zone, and rock type have been discussed in a broad manner, with each having distinct variations. The correlation of each type with mineralization will vary accordingly.

It is worth noting that diorite, hornfels, amphibole-rich schist, and clay are the most effective in gold particle deposition, as shown in Fig. 8.

Furthermore, Fig. 9 illustrates the presence of gold particles increasing in areas with propylitic, potassic, clay, siliceous, iron oxide III, and chlorite alterations, in descending order.

Another factor that influences the buildup of gold particles, specifically the mineralization zone, was also examined, with the outcomes displayed in Fig. 10. According to the results of the decision tree model, the hypogene mineralization zone followed by the oxyhypogene zone will be given higher priority for gold particle accumulation. In the following stage, the oxidation and oxysupergen areas provide ideal conditions for the gold particles to be deposited.

Ultimately, the decision tree algorithm is employed to showcase the three-dimensional model of the area under study, as depicted in Fig. 11. Indeed, the identification of potential mineral-rich zones can be achieved through the utilization of this algorithm.

Evaluating the accuracy of a classifier is crucial once it has been constructed. Using test data is more beneficial for evaluating the precision of a classifier. After constructing the model with the training data, it is important to assess its accuracy in predicting the class label of the samples using the test data. The classifier's accuracy on test samples is determined by the number of samples correctly classified by the model. Certainly, the error rate can be computed in place of accuracy. Another crucial aspect revolves around the cross validation of data, which is essential for assessing the efficacy of machine learning models and relies on where the model gathers the necessary training information from within the dataset. In the specific model, the sensitivity of the model to this issue was also assessed by assigning values of 5 and 10 for this criterion. Ultimately, the model that was achieved underwent evaluation. During the model assessment, the following metrics were calculated: overall accuracy (91.7 %), prediction accuracy for positive cases (91.9 %), coverage of positive samples (91.7 %), and F1 score (91.8 %).

4.2 Gold grade estimation using support vector machine method

The radial basis function (RBF) is chosen as the kernel function to assess the grade of Janja polymetallic deposit through the support vector machine classification method. The RBF kernel transforms the samples in a nonlinear manner to a space with higher dimensions. In contrast to other kernel types, this kernel encounters fewer computational issues and can effectively handle data sets with high dimensions. Additionally, this kernel function has a lower number of parameters when compared to functions like polynomial functions, ultimately decreasing the model's complexity (Hsu et al., 2003; Lin et al., 2008). The effectiveness of a model using the support vector machine technique heavily relies on the parameters chosen for the model. In order to achieve a model with strong generalization abilities, it is important to carefully decide on the model parameters. Selecting the best parameters for the model can impact its performance quality; hence, a model with incorrect parameters might yield undesirable outcomes (Kecman, 2004; Oliver & Webster, 2014). In order to find the best parameters for the model – such as C, γ, and kernel type, a network search approach was employed, utilizing a 10-point cross-validation. This approach involves setting up a uniform grid in

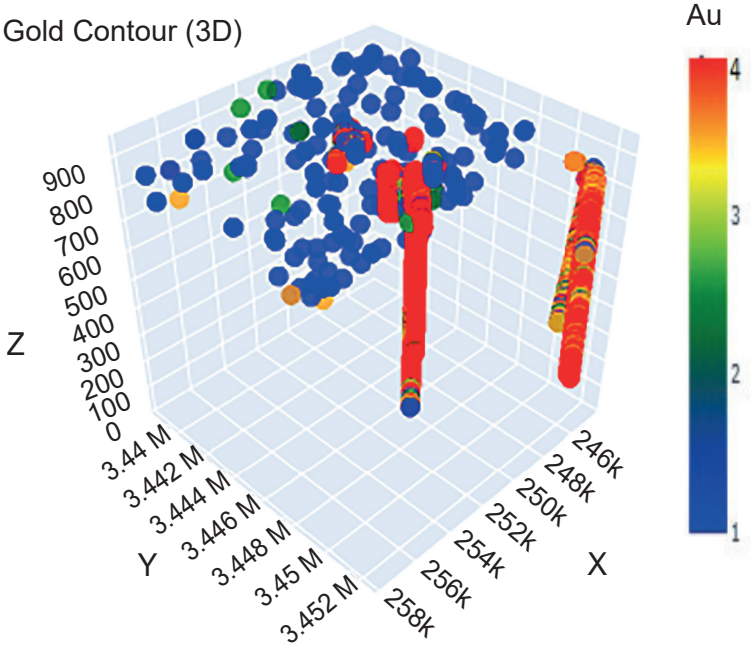

Fig. 11. Three-dimensional diagram of promising mineral areas of the studied region.

the parameter space that needs to be explored, followed by assessing all grid points in order to identify the best overall point. Ultimately, the grid search will identify the best possible point among all points within the grid for the specified parameter. The network search method begins by creating a large network in the parameter space and gradually defines smaller networks as it approaches the optimal point, ultimately converging towards the overall optimal point in the parameter space (Hsu et al., 2003). Table 2 displays the range of values to search for each model parameter. The primary concept of this approach is to identify the best parameters of the model in order to minimize the model error. As stated, the cross-validation method is utilized in conjunction with the network search method for this purpose. During k-fold validation, the training set is initially partitioned into k equal-sized subsets. Each subset is tested in consecutive order by the model trained based on the remaining k-1 subsets. Thus, each individual sample in the training set is calculated only one time. Therefore, the accuracy of cross-validation will be the proportion of correctly predicted data. Indeed, the RMSE error value is achieved for the specified parameters in every test subset through the implementation of cross-validation technique. The mean RMSE for each of the k test subsets is shown as a way to evaluate the model's performance. This introduces the optimal parameters of the model as those that result in the lowest RMSE. Another benefit of using cross-validation is its ability to address the issue of overfitting in the model (Che & Hu, 2008; Hsu et al., 2003).

Tab. 2

The search interval for each of the model parameters in estimating gold grade

Support vector machine model parameter	Search range
C	{0.01, 0.1, 1, 10, 100}
γ	{0.01, 0.1, 0.2, 0.3}
Kernel	{Linear, Polynomial, RBF}

Table 3 displays the best C and γ parameters, as well as the kernel type, determined through a grid search method using 10-fold cross-validation. Once the model's best parameters were chosen and the lowest error from cross-validation was achieved, the entire training dataset (90 % of the total data) was used to train the optimal model. The process of training the model was carried out using Python 3.11 software. Following the training phase using the best parameters, the support vector machine model's effectiveness and efficiency were assessed using the test data (10 % of the overall dataset).

Tab. 3

Optimal values of C, γ and Kernel parameters applying the gird search method based on cross-validations that is divided into 10 folds

Optimal parameters of the model	The optimal value of the parameter
C	1
γ	0.1
Kernel	RBF

SVM methods have been employed in order to improve the accuracy of gold grade predictions. To achieve this goal, the dataset needs to be separated into training and testing sets. The input data consisted of the silver, copper, lead, and zinc values with gold value being the output data. This network underwent training using various combinations of training and testing data, including ratios of 90/10, 80/20, 70/30, 60/40, and 50/50. The results that were obtained can be found in table 4. It was found that the best scenario involved using 90 % of the data for training and 10 % for testing.

Tab. 4

Impact of varying selection ratios of training and testing data on support vector machine algorithm

Training / testing [%]	Accuracy [%]	RMSE
90/10	82	0.917
80/20	80	0.964
70/30	76.8	0.949
60/40	76.5	0.923
50/50	76.3	0.911

Following the calculation of the training and testing data ratio, visual patterns were generated using three-dimensional diagrams to show the correlation between the actual and predicted values of gold. Furthermore, within these illustrations, gold anomaly regions were depicted in pairs based on the concentration of the input elements. Since gold has a stronger correlation with copper compared to silver, lead, and zinc, pairs of input elements are first examined before drawing diagrams to represent anomalies of gold, as shown in Fig. 12.

5 Conclusions

Today, the implementation of variable estimation is a recent approach that has facilitated the decision-making process in various fields of study. Estimating the

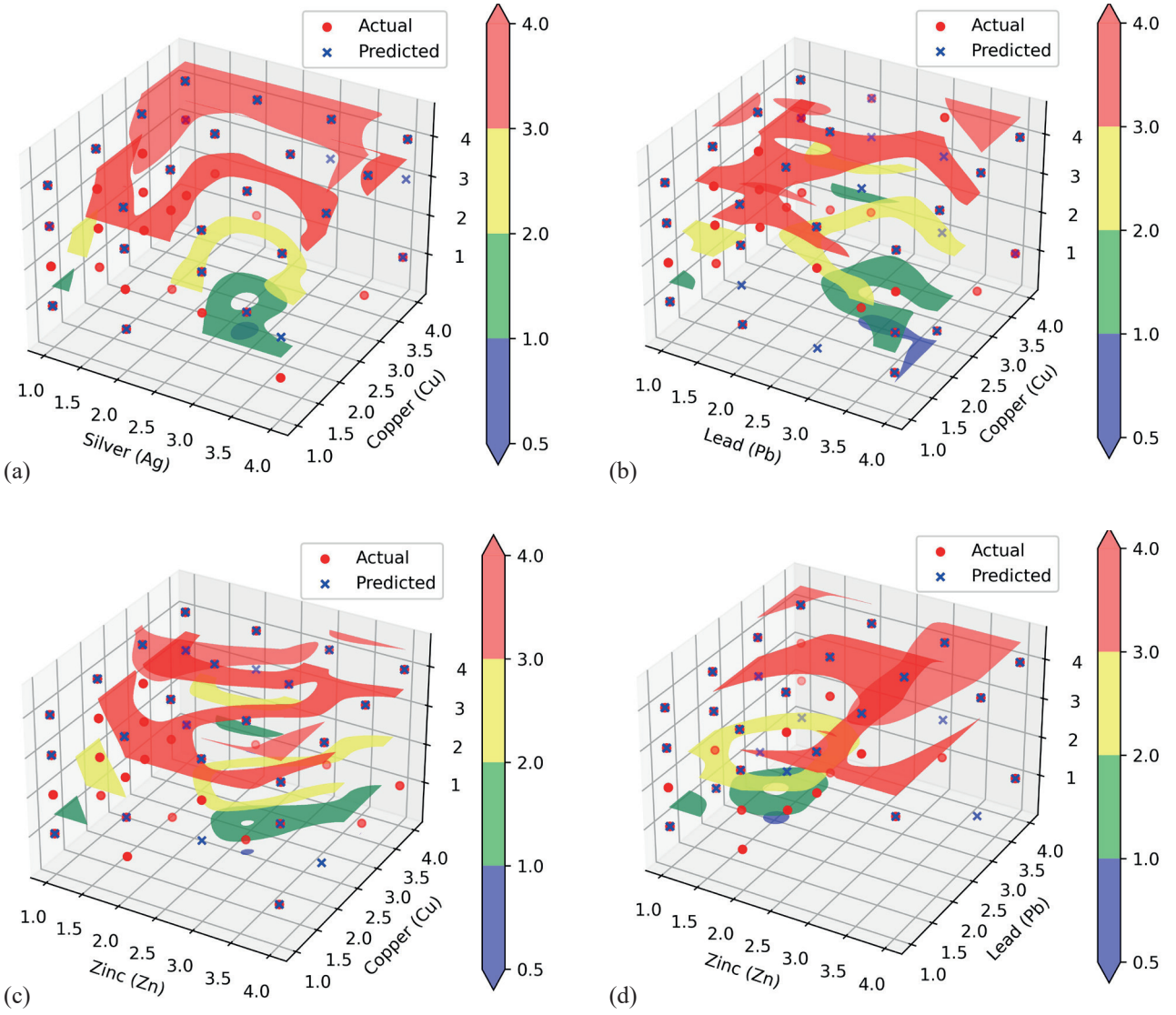

Fig. 12. 3D diagram of gold anomaly zones based on grade of: a) silver and copper, b) lead and copper, c) zinc and copper, and d) zinc and lead.

grade of mineral deposits is a crucial aspect of evaluating them in geosciences. There exist several techniques to determine this crucial factor. Years of thorough research have resulted in the creation of innovative techniques for estimating variable amount in the deposit. One of the methods available is the decision tree algorithm, which is a simple and powerful machine learning algorithm suitable for classification and regression tasks. It can be easily understood and is capable of processing many different types of data. Nonetheless, it is susceptible to overfitting and may be unreliable. Although they have limitations, decision trees are utilized in many fields, making them a useful tool for analysing data and making predictions. If the data includes logical conditions or is divided into various categories, the decision tree algorithm is the appropriate selection. Using different classification algorithms is recommended when dealing with an excessive amount of numerical variables in the data. By utilizing the decision tree algorithm, it is evident that diorite, hornfels, amphibole-rich schist, and clay show the highest potential for gold particle deposition. Diorite plays a significant role in rock formations containing gold deposits and is considered the source rock. Indeed, the thermal engine is situated within the diorite rock, causing the hydrothermal solutions to move due to the heat produced. Hornfels does not play a significant role in gold mineralization due to its low porosity, which results in poor permeability to hydrothermal fluids, preventing mineralization in this rock. When pyrite crystals are found in schist or clay, it indicates the presence of either pyrite or

its phantom form representing gold. This shows that gold has been displaced within the sulfur phase due to shifts in oxidation-reduction conditions. The gold particles are typically found in reducing environments like clay minerals and schists, where they can be released from complexes and precipitated due to hydrothermal activity, making these rocks favorable hosts for gold. The producer may consist of diorite while the host rock can be composed of clay and schist rocks. Hence, it is recommended to obtain a thin sample from the schists and use electric charge to determine if gold particles are present. Additionally, it is important to determine the phase of any gold particles found in the schist sections: Is it in the crystallization phase or in the mineralogical phase like pyrite or chalcopyrite? Furthermore, there has been a build-up of gold particles in the alteration zones of propylenic, potassic, clay, siliceous, iron III oxide and chlorite in descending order. It is important to point out that the propylitic and argillic alteration zones possess geochemical attributes required for the accumulation of gold. Mineralization is favored in the propylitic zone of hydrothermal systems due to its high oxidation levels and acidic environment. Atmospheric waters also have a part to play. This area is optimal for disrupting gold compounds. In the potassic zone, temperatures exceeding 450 degrees Celsius prevent gold complexes from breaking unless they are already enclosed in pyrite and chalcopyrite. However, typically, the area high in potassium does not have a significant amount of gold deposits, whereas the surrounding propylitic and argillic zones are rich in gold because gold complexes are the final phase to deteriorate and, if they bond, they stay firm even in colder temperatures. In other words, gold complexes either do not enter the game or come until the end of the game. The accumulation of gold particles in the mineralization zones was also investigated. According to the decision tree model's results, the hypogene mineralization zone followed by the oxyhypogene will be given higher priority for the aggregation of gold particles. In the following stage, the oxidation and oxysupergen regions are conducive zones for the accumulation of gold particles. Indeed, the hypogene mineralization area corresponds to potassic and phyllic modification. The propylitic zone has a similar level of oxidation as the hypogene zone, but actually displays more argillic characteristics. The supergene zone includes clay minerals, iron oxide, and chlorite, with siliceous alteration also being part of the argillic zone. Indeed, there is a high concentration of gold in the hot section of the mine, which goes against the low gold mineralization found in Sarcheshme and Songun mines in Iran. In those mines, gold is mostly deposited in the cold areas near the mass and in veins of types 4 and 5, which contain pyrite, anhydrite, and calcite. In conclusion, the decision tree algorithm can accurately pinpoint mineral-rich areas with a high success rate of 92 %, as demonstrated in the relevant section where the diagram was displayed.

Another effective and powerful machine learning technique is the support vector machine method, employed for predicting the gold quality in Janja region. Firstly, the support vector machine method was used to determine the best values for the model parameters, followed by the implementation of the final model with these optimal parameters. The assessment of the model indicates that it will be effective in predicting the gold grade, which is a crucial factor in assessing the quality of the deposit. The primary objective of this study is to develop a method for predicting the gold grade based on its distinct characteristics and properties. Due to the limited amount of data in numerous instances, analysing it can be challenging and expensive. However, usually during the initial phases of research, analysis, and forming conclusions and decisions should be made according to the limited data available. Appropriate estimation and forecasting methods are necessary for this task. This research aimed to forecast the gold grade quantity and accompanying anomaly ranges in Janja polymetallic deposit by utilizing statistical techniques and support vector machine algorithm. It can be observed that the support vector machine technique is able to accurately predict the distribution of gold grades within a certain range. Hence, it is possible to conclude that employing support vector machine techniques in geochemical research on low grade and dispersed elements like gold not only saves time and money but also identifies patterns by interpolating between inputs and outputs while reducing the error between predicted and actual values. The results of deposit modeling indicate that it has been successful in predicting the gold grade. Moreover, the economic analysis and mine design can be carried out using the resulting grade model.

Acknowledgement

The completion of this research paper would not have been possible without the support and guidance by Professor Ardeshir Hezarkhani, Amirkabir University of Technology. His dedication and overwhelming attitude towards helping his students is solely responsible for completing this research paper. The encouragement and insightful feedback were instrumental in accomplishing this task.

Authors would also like to express a gratitude to experts from the State Geological Institute of Dionýz Štúr (SGUDS, Slovak Geological Survey) for their constructive criticism and valuable feedback, enhancing the quality of this paper. We also consider it our duty to express our gratitude to the esteemed reviewers, Professor Ladislav Vizi (SGUDS) and an anonymous reviewer for their valuable comments, improving the scientific level of this paper.

References

Abbaszadeh, M., Hezarkhani, A. & Soltani-Mohammadi, S., 2013: An SVM-based machine learning method for the separation of alteration zones in Sungun porphyry copper deposit. *Geochemistry*, 73, 545–554.

Abbaszadeh, M., Hezarkhani, A. & Soltani-Mohammadi, S., 2015: Classification of alteration zones based on whole-rock geochemical data using support vector machine. *Journal of the Geological Society of India*, 85, 500–508.

Abe, S., 2005: Support vector machines for pattern classification. *London, Springer.*

Amnieh, H. B., Siamaki, A. & Soltani, S., 2012: Design of blasting pattern in proportion to the peak particle velocity (PPV): Artificial neural networks approach. *Safety Science*, 50, 1913–1916.

Anderberg, M. R., 1973: The broad view of cluster analysis. *Cluster analysis for applications*, 1, 1–9.

Bishop, C. M. & Nasrabadi, N. M., 2006: Pattern recognition and machine learning. *New York, Springer.*

Chatterjee, S., Bandopadhyay, S. & Machuca, D., 2010a: Ore grade prediction using a genetic algorithm and clustering based ensemble neural network model. *Mathematical Geosciences*, 42, 309–326.

Chatterjee, S., Bandopadhyay, S. & Machuca, D., 2010b: Ore Grade Prediction Using a Genetic Algorithm and Clustering Based Ensemble Neural Network Model. *Mathematical Geosciences*, 42, 309–326.

Che, X. L. & Hu, L., 2008: Grid resource prediction approach based on Nu-Support Vector Regression. In: *International Conference on Machine Learning and Cybernetics*, IEEE, 778–783.

Dutta, S., Bandopadhyay, S., Ganguli, R. & Misra, D., 2010: Machine Learning Algorithms and Their Application to Ore Reserve Estimation of Sparse and Imprecise Data. *Journal of Intelligent Learning Systems & Applications*, 2, 86–96.

Guo, W. W., 2010: A novel application of neural networks for instant iron-ore grade estimation. *Expert Systems with Applications*, 37, 8729–8735.

Hsu, C. W., Chang, C. C. & Lin, C. J., 2003: A practical guide to support vector classification. *Department of Computer Science, National Taiwan University*, 1396–1400.

Huang, T. M., Kecman, V. & Kopriva, I., 2006: Kernel based algorithms for mining huge data sets. *Heidelberg, Springer.*

Jafrasteh, B., Fathianpour, N. & Suárez, A., 2018: Comparison of machine learning methods for copper ore grade estimation. *Computational Geosciences*, 22, 1371–1388.

Jhonnerie, R., Siregar, V. P., Nababan, B., Prasetyo, L. B. & Wouthuyzen, S., 2015: Random forest classification for mangrove land cover mapping using Landsat 5 TM and ALOS PALSAR imageries. *Procedia Environmental Sciences*, 24, 215–221.

Kecman, V., 2001: Learning and soft computing: support vector machines, neural networks, and fuzzy logic models. *MIT press.*

Kecman, V., 2004: Support vector machines basics. School of Engineering, *University of Auckland.*

Kotake, N., Suzuki, K., Asahi, S. & Kanda, Y., 2002: Experimental study on the grinding rate constant of solid materials in a ball mill. *Powder Technology*, 122, 101–108.

Krishna, G., Sahoo, R. N., Pradhan, S., Ahmad, T. & Sahoo, P. M., 2018: Hyperspectral satellite data analysis for pure pixels extraction and evaluation of advanced classifier algorithms for LULC classification. *Earth Science Informatics*, 11, 159–170.

Lee, C. & Sterling, R. L., 1992: Identifying probable failure modes for underground openings using a neural network. *International journal of rock mechanics and mining sciences & geomechanics abstracts*, 29, 1.

Li, X. L., Xie, Y. L., Guo, Q. J. & Li, L. H., 2010: Adaptive ore grade estimation method for the mineral deposit evaluation. *Mathematical and Computer Modelling*, 52, 1947–1956.

Lin, S. W., Lee, Z. J., Chen, S. C. & Seng, T. Y., 2008: Parameter determination of support vector machine and feature selection using simulated annealing approach. *Applied soft computing*, 8, 1505–1512.

Mahmoudabadi, H., Izadi, M. & Bagher Menhaj, M., 2009: A hybrid method for grade estimation using genetic algorithm and neural networks. *Computational Geosciences*, 13, 91–101.

Maleki, S., Ramazi, H. R. & Moradi, S., 2014: Estimation of Iron concentration by using a support vector machineand an artificial neural network-the case study of the Choghart deposit southeast of Yazd, Yazd, Iran. *Geopersia*, 4, 201–212.

Martínez-Ramón, M. & Christodoulou, C., 2022: Support vector machines for antenna array processing and electromagnetics. *Springer Nature.*

Masoumi, F., Eslamkish, T., Abkar, A. A., Honarmand, M. & Harris, J. R., 2017: Integration of spectral, thermal, and textural features of ASTER data using Random Forests classification for lithological mapping. *Journal of African Earth Sciences*, 129, 445–457.

Matías, J. M., Vaamonde, A., Taboada, J. & Gonzalez-Manteiga, W., 2004: Support vector machines and gradient boosting for graphical estimation of a slate deposit. *Stochastic Environmental Research and Risk Assessment*, 18, 309–323.

Merler, S. & Jurman, G., 2006: Terminated ramp-support vector machines: a nonparametric data dependent kernel. *Neural Networks*, 19, 1597–1611.

Moorthi, S. M., Misra, I., Kaur, R., Darji, N. P. & Ramakrishnan, R., 2011: Kernel based learning approach for satellite image classification using support vector machine. *IEEE recent advances in intelligent computational systems,* 107–110.

Nezamolhosseini, S. A., Mojtahedzadeh, S. H. & Gholamnejad, J., 2017: The application of artificial neural networks to ore reserve estimation at choghart iron ore deposit. *Analytical and Numerical Methods in Mining Engineering*, 73–83.

Oliver, M. A. & Webster, R., 2014: A tutorial guide to geostatistics: Computing and modelling variograms and kriging. *Catena,* 113, 56–69.

Pozdnoukhov, A., 2005: Support vector regression for automated robust spatial mapping of natural radioactivity. *Automatic mapping algorithms,* 57.

Samanta, B., Ganguli, R. & Bandopadhyay, S., 2005: Comparing the predictive performance of neural networks with ordinary kriging in a bauxite deposit. *Mining Technology*, 114, 129–139.

Sánchez, A. V. D., 2003: Advanced support vector machines and kernel methods. *Neurocomputing*, 55, 5–20.

Sayadi, A. R. M. M. & Shahrabadi, H., 2008: Reserve Evaluation of Esfordi Phosphate Mine using Geostatistical and Artificial Neural Network, *Scientific Quarterly Journal of Geosciences*, 18, 102–109.

Shahin, M. A., Jaksa, M. B. & Maier, H. R., 2008: State of the art of artificial neural networks in geotechnical engineering. *Electronic Journal of Geotechnical Engineering*, 8, 1–26.

Shirali, R., 2016: Classification trees and rule-based modeling using the C5. 0 algorithm for self-image across sex and race in St. Louis. *St. Louis, Washington University.*

Singh, V., Banerjee, P. K., Tripathy, S. K., Saxena, V. & Venugopal, R., 2013: Artificial neural network modeling of ball mill grinding process. *J. Powder Metall. Min.*, 2, 106.

Smola, A. J. & Schölkopf, B., 2004: A tutorial on support vector regression. *Statistics and computing*, 14, 199–222.

Soliman, O. S. & Mahmoud, A. S., 2012: A classification system for remote sensing satellite images using support vector machine with non-linear kernel functions. In: *8th International Conference on Informatics and Systems (INFOS)*, BIO-181, IEEE.

Soliman, O. S., Mahmoud, A. S. & Hassan, S. M., 2012: Remote sensing satellite images classification using support vector machine and particle swarm optimization. In: *Third International Conference on Innovations in Bio-Inspired Computing and Applications*, IEEE, 280– 285.

Tahmasebi, P. & Hezarkhani, A., 2010: Application of adaptive neuro-fuzzy inference system for grade estimation; case study, Sarcheshmeh porphyry copper deposit, Kerman, Iran. *Australian Journal of Basic and Applied Sciences*, 4, 408–420.

Tahmasebi, P. & Hezarkhani, A., 2012: A hybrid neural networks-fuzzy logic-genetic algorithm for grade estimation. *Computers & geosciences*, 42, 18–27.

Tenorio, V. O., Bandopadhyay, S., Misra, D., Naidu, S. & Kelley, J., 2015: Support vector machines applied for resource estimation of underwater glacier-type platinum deposits. *Application Of Computers an d Operations Research in the Mineral Industry*, 18, 309–323.

Thuijsman, F., 1995: Artificial neural networks: an introduction to ANN theory and practice. *Springer Science & Business Media.*

Tran, Q. A., Li, X. & Duan, H., 2005: Efficient performance estimate for one-class support vector machine. 26, no. 8. *Pattern Recognition Letters*, 26, 1174–1182.

Tsai, C. F. & Yen-Jiun, C., 2009: Earnings management prediction: a pilot study of combining neural networks and decision trees. *Expert Systems with Applications*, 36, 7183–7191.

Twarakavi, N. K., Misra, D. & Bandopadhyay, S., 2006: Prediction of arsenic in bedrock derived stream sediments at a gold mine site under conditions of sparse data. *Natural Resources Research*, 15, 15–26.

Van Der Heijden, F., Duin, R. P., De Ridder, D. & Tax, D. M., 2005: Classification, parameter estimation and state estimation: an engineering approach using MATLAB. *John Wiley*.

Wang, L. (ed.), 2005: Support vector machines: theory and applications. *Springer Science & Business Media.*

Wu, W., Li, A. D., He, X. H., Ma, R., Liu, H. B. & Lv, J. K., 2018: A comparison of support vector machines, artificial neural network and classification tree for identifying soil texture classes in southwest China. *Computers and Electronics in Agriculture*, 144, 86–93.

Zaremotlagh, S. & Hezarkhani, A., 2017: The use of decision tree induction and artificial neural networks for recognizing the geochemical distribution patterns of LREE in the Choghart deposit, Central Iran. *Journal of African Earth Sciences*, 128, 37–46.

Zhang, S., Carranza, E. J. M., Fu, C., Zhang, W. & Xiang, Q., 2024: Interpretable Machine Learning for Geochemical Anomaly Delineation in the Yuanbo Nang District, Gansu Province, China. *Minerals,* 14, 5.

Zhang, S., Xiao, K., Carranza, E. J. M. & Yang, F., 2019: Maximum entropy and random forest modeling of mineral potential: Analysis of gold prospectivity in the Hezuo-Meiwu district, west Qinling Orogen, China. *Natural Resources Research*, 28, 645–664.

Porovnávacia štúdia počítačových metodík rozhodovacieho stromu a podporného vektora na mapovanie perspektív zlatonosnosti

Mapovanie geochemických anomálií je jedným z hlavných cieľov geochemického výskumu. Keďže terénne štúdie sú časovo náročné a nákladné, veľkou pomocou pri hodnotení získaných údajov je ich spracovanie metodikami počítačového spracovania, hlavne algoritmom rozhodovacieho stromu (*Decision Tree*; DT). Je to jednoduchý a výkonný nástroj pri strojovom učení, vhodný na klasifikačné a regresné úlohy. Poskytuje lacnú, rýchlu a pomerne presnú alternatívu spracovania získaných údajov. Okrem algoritmu DT článok prezentuje aj podporný vektorový nástroj (*Support Vector Machine*; SVM). Obe metodiky boli aplikované pri mapovaní perspektívy zlata v oblasti Janja vo východnom Iráne. Porovnanie analytických výsledkov získaných z týchto dvoch metód potvrdzuje, že model DT má dostatočnú presnosť a viac správnych výsledkov ako model SVM. Má to vplyv na proces prípravy a projektovania ďalších fáz prieskumu a mapovania perspektívy zlata študovanej oblasti.

Skúmaná oblasť Janja v provinciách Sistan a Balúčistan (východný Irán) sa vyznačuje charakteristickou piesočnatou rovinou v nadmorskej výške 800 – 9 000 m, riedkou vegetáciou, ale aj malou odkrytosťou skalného podložia (obr. 1). Skúmaná oblasť zahŕňa subregión Zábul – Zahedan – Saravan. Flyšové sekvencie majú vrchnokriedový až oligocénny vek. Vznik tejto zóny sa interpretuje zrážkou litosférických mikroplatní, ktorá bola spojená s exhumáciou ofiolitových komplexov. V centrálnej a východnej časti zóny vystupuje formácia Sefidabe (označenie KPs na obr. 2). Je to jedna z najrozsiahlejších jednotiek v oblasti Janja. Pozostáva z vulkanických a pyroklastických sekvencií, ktorých prítomnosť zohrala úlohu pri vzniku miestnej zlatorudnej mineralizácie. Vzhľadom na rozsah prieskumu a hustú sieť vodných tokov sa v oblasti realizoval systematický odber 285 geochemických vzoriek a 59 vzoriek ťažkých minerálov z vodných tokov (obr. 3). Popri odbere vzoriek z vodných tokov sa vzorkovanie robilo aj na povrchu v miestach odkrytosti polymetalických žíl.

Aplikácia algoritmu DT dokladá, že diorit a s ním susediace horniny metamorfované teplom, bridlice a zvetraninový plášť (hlina) vykazujú najvyšší potenciál na prítomnosť zlatých častíc. Diorit má tradične významnú úlohu v horninových sekvenciách obsahujúcich ložiská zlata a považuje sa za zdrojovú horninu mineralizácie. Teplo dioritovej magmy napomáha hydrotermálnym procesom. Naopak, kontaktné rohovce v susedstve dioritových telies zohrávajú negatívnu úlohu pri vzniku zlatorudnej mineralizácie pre ich nízku pórovitosť, sťažujúcu prestup hydroteriem a kryštalizačné procesy mineralizácie. Kryštály pyritu nachádzajúce sa v bridlici alebo hline indikujú vyzrážanie zlata zo sulfátovej fázy v dôsledku zmeny oxidačno-redukčných podmienok. Častice zlata sa zvyčajne nachádzajú v redukčnom prostredí, ako sú ílovité minerály a bridlice. Tam sa môžu vyzrážať v dôsledku hydrotermálnej aktivity. Vďaka tomu sú tieto horniny perspektívne na zlatorudnú mineralizáciu. Zdrojovou horninou v prípade výskytov v oblasti Janja je teda diorit a hostiteľským prostredím sú bridlice a zvetraninový plášť. Dôležité je aj zistenie formy výskytu zlata v bridliciach (napr. v pyrite alebo chalkopyrite) a skúmanie propylitizovaných a argilitových alteračných zón. Mineralizácia sa prednostne vyskytuje v propylitickej zóne hydrotermálneho systému v dôsledku vysokej úrovne oxidácie a kyslého prostredia. Úlohu zohráva aj atmosférická voda. Oblasti s vysokým obsahom draslíka však zvyčajne nedisponujú väčším množstvom zlatorudných ložísk. Naopak, susediace okolité propylitické a argilitové zóny sú bohaté na zlatorudnú mineralizáciu. Záver článku prináša hodnotenie, že algoritmus rozhodovacieho stromu (DT) môže určiť oblasti bohaté na vyhľadávanú mineralizáciu s vysokou úspešnosťou.

Doručené / Received: 22. 10. 2024
Prijaté na publikovanie / Accepted: 17. 12. 2024

Mineralia Slovaca, Web ISSN 1338-3523, ISSN 0369-2086, https://doi.org/10.56623/ms.2024.56.2.5
56, 2 (2024), 181 – 194, © Authors 2024. CC BY 4.0

Processing of low-grade phosphate ores of Djebel Onk mine (Algeria) with electrostatic separation method

RAOUNAK BAHOUS[1], ABDELAZIZ IDRES[2], IBTISSEM ZERIRI[3], FARID AIT MERZEG[4,5], FAHEM TIOUR[6], NADIIA DOVBASH[7], AISSA BENSELHOUB*[3] and STEFANO BELLUCCI[8]

[1]Mining Laboratory, Mining Engineering Department, Larbi Tebessi University, Tebessa, Algeria
[2]Laboratory of Mining Resources Valorization and Environment (LAVAMINE), Mining Department, Badji Mokhtar University, Annaba, Algeria
[3]Environmental Research Center (C.R.E); Annaba, Algeria
[4]Research Unit in Physico-Chemical Analyzes of Fluids and Soils (URAPC-FS), Alger, Algeria
[5]Scientific and Technical Research Center in Physical and Chemical Analyses (CRAPC), Tipaza, Algeria
[6]Laboratory of Materials Technology and Process Engineering (LTMGP), Abderahmane Mira University, Bejaia, Algeria
[7]National Scientific Centre «Institute of Agriculture of the National Academy of Agricultural Sciences» Chabany, Ukraine
[8]INFN-Laboratori Nazionali di Frascati, Via E. Fermi 54, 00044 Frascati, Italy
*Corresponding authors: benselhoub@yahoo.fr, raounak.bahous@univ-tebessa.dz

Abstract: Phosphate ore is an important raw material for manufacturing phosphorous fertilizers and chemicals. Although most phosphate resources cannot be marketed directly as raw material, including that from the Djebel Onk mine, due to their low P_2O_5 content and high impurity content. To obtain a quality phosphate concentrate, the enrichment of low-grade phosphate ore is therefore of great necessity. The objective of this research was to explore the use of mixtures consisting of three beige phosphate sub-layers and two black phosphate sub-layers as feed material. The objective of this study was also to identify the chemical composition and mineral phases of the ore by various analysis techniques (X-ray diffraction, X-ray fluorescence, SEM / EDS scanning electron microscope, and optical microscope). Many beneficiation techniques can be used to improve the P_2O_5 content of phosphate ores depending on their characteristics. This technique of electrostatic separation gave excellent results in terms of content and recovery for both calcined and non-calcined beige and black phosphates. The removal of organic matter and calcite is crucial in the phosphate industry, wherefore high-quality phosphoric acid can be produced more economically, while reducing acid consumption. The best-obtained results from the calcination process followed by electrostatic separation from an initial ore with a content of 31.15 % of P_2O_5 were achieved for calcined beige phosphate (under conditions: rotation speed: 30 rpm, electrical voltage: 30 kV), with content of P_2O_5 in concentrate 36.89 % and recovery of 93.91 %. For calcined black phosphate the best results were achieved under conditions: rotation speed: 50 rpm, electrical voltage: 35 kV, with content of P_2O_5 in concentrate 36.65 % and recovery of 93.88 % from an initial ore (with a content of 30.85 % P_2O_5). This study highlights the importance of the calcination treatment before the electrostatic separation operation.

Key words: beige phosphate, black phosphate, low-grade phosphate, calcination, enrichment, electrostatic separation, Djebel Onk mine, Kef Essennoun

Graphical abstract

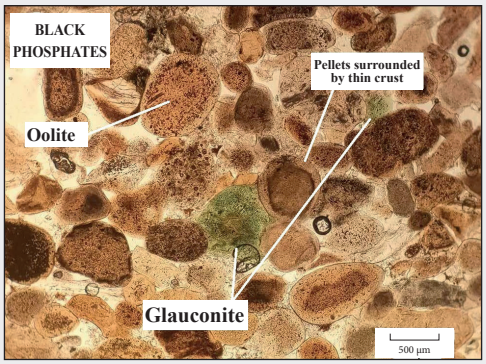

Highlights

- The study focuses on the characterization of treatment by electrostatic separation of low-grade phosphate ore from the Djebel Onk mine (Kef Essennoun – Algeria).
- The originality of presented research resides in the possible application of a combined method for the phosphate ore enrichment by calcination and electrostatic separation, which is an effective strategy for concentrating ore from a sub-arid region. The phosphate ores treated by these processes meet industrial requirements and international standards.

1 Introduction

Phosphorus is an essential element in the agricultural sector, used in the form of fertilizers and animal feed. Algeria has a significant mining industry with vast potential. In terms of Algeria's economy, mining products will certainly dominate the future. Algerian phosphate, notably that of the Tebessa region (Eastern Saharan Atlas) is particularly important, with the Djebel Onk deposit being the largest in the country, estimated at 2.2 billion tons of phosphates (USGS, 2020). The Kef Essennoun deposit is characterized by a thick layer of approximately 35 m of Upper Thanetian phosphorites, divided into three sub-layers according to the P_2O_5 and MgO contents, and is presented in two different forms, one black and the other beige (Kechiched et al., 2016). The phosphate beneficiation industry faces the challenge of economically and efficiently exploitinglow-grade phosphate ores. It is confronted with a decline in the quality of phosphate rocks, unpredictable quantities of gangues, and the need to combine different enrichment techniques (Zafar et al., 1996). Recently, many reports have been published on the improvement of low-grade phosphate ores, using both wet and dry beneficiation techniques (Bada et al., 2012).

This study focuses on the physicochemical and mineralogical characterization of phosphate ore from the Kef Essennoun mine, using various analysis techniques (X-ray diffraction, X-ray fluorescence, SEM / EDS scanning electron microscope, and optical microscope). The objective is to identify the chemical composition and mineral phases of the ore.

Depending on the climatic conditions of the region, a study was carried out to test the possibility of high-tension electrostatic separation treatment on representative samples. This technique gave excellent results in terms of content and recovery for both calcined and non-calcined beige and black phosphate. The process makes it possible, on the one hand, to reduce the volumes of waste and, on the other hand, to protect the environment from the dangers of phosphate waste.

Phosphate ore deposits containing a large amount of carbonates and significant chemical substitutions, respectively in the gangue and throughout the ore, make it difficult to concentrate phosphate elements (Kechiched et al., 2020).

The calcination of phosphate ore is a well-known processing method that increases the phosphorus (P_2O_5) content of the ore (Zieliński et al., 2023).

Natural phosphate is the fundamental component for the manufacture of phosphoric acid and phosphate fertilizers. Kef Essennoun phosphate reacts to heat treatment, which allows the purity of raw and calcined phosphates to be estimated. The P_2O_5 content increased from 28.39 % in the raw phosphate to 31.09 % in the calcined product (Bounemia et al., 2023). At elevated temperatures, fluorapatite can undergo thermal decomposition resulting in changes to its chemical and crystal structure.

Using an electrostatic separator can improve the recovery of minerals, including phosphate. The efficiency of the process allows a content and recovery of 35 % and 90.1 % respectively to be obtained (Stencel et al., 2003).

Electrostatic separation is a method used to sort materials based on their electrical properties. This technique has been applied to various materials, including granular mixtures of different sizes and compositions, such as non-conductive particles, non-conductive and conductive particles, as well as conductive particles (Fig. 3) (Zhu et al., 2023; Bendilmi et al., 2022).

The conductive particles discharge rapidly onto the grounded electrode. Simultaneously, the particles also become charged by electrostatic induction. The electric field extracts the charge carriers from the electrode and transfers them to the particles (Dascalescu et al., 1994; Idres et al., 2016).

It is fascinating to note that electrostatic ore processing offers significant benefits, both in terms of concentrate recovery and reducing stored volumes, and protecting the environment (Tiour et al., 2022; Idres et al., 2017, 2014).

2 Study area

2.1 Geological setting and deposit location

The Djebel Onk phosphate deposit near Bir El Ater (Fig. 1) is located in the transition zone between the eastern part of the Saharan Atlas to the north and the Saharan platform to thesouth.The boundary between these two tectonic units is marked by the southernmost Atlas fault or flexure. The Atlas Mountains belong to the Alpine belt that was formed by the convergence of the Eurasian and African plates during the Miocene period (Notholt, 1980).

The Kef Essennoun phosphate deposit belongs to the Djebel Onk mining field in northeastern Algeria. It is located approximately 10 km southwest of the town of Bir El Ater, 100 km south of the town of Tebessa and 20 km from the Algerian-Tunisian border (Fig. 1; Gadri et al., 2015).

The Kef Essennoun deposit site presents substantial differences with the Gafsa-Metlaoui basin (Tunisian phosphorite basin), Stratiform deposits of marine phosphate are well developed in the northeastern territory of Algeria. These Tertiary phosphate deposits (late Paleocene-early Eocene) belong to the large Mediterranean phosphogenic province, particularly with regard to lithologies and succession, especially in the phosphorite formation. The sedimentary lithologies consist of a 500 m thick succession dating from the Upper Cretaceous (Maastrichtian) to the

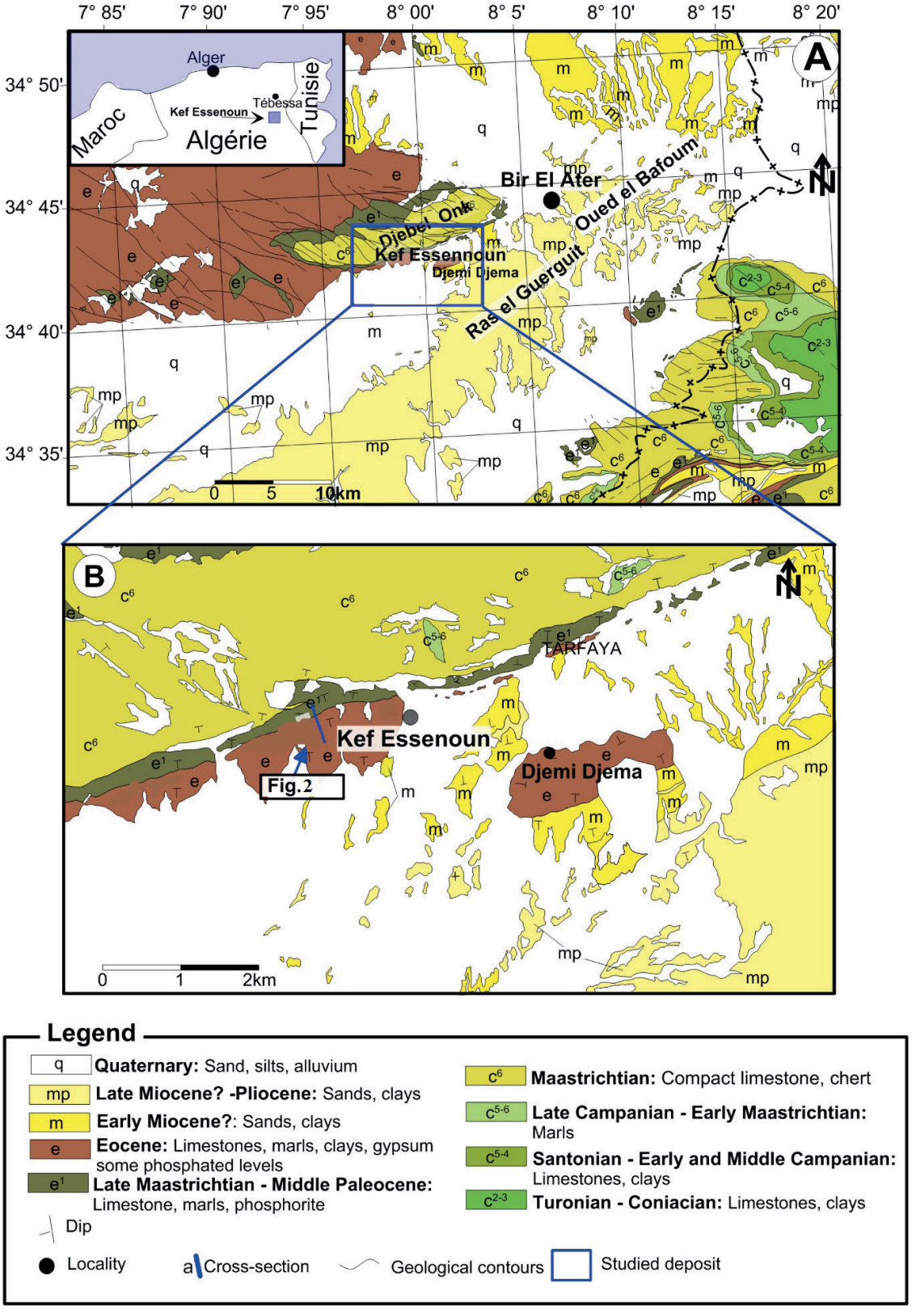

Fig. 1. (A) Geological map of the Djebel Onk mining basin including Kef Essenoun, the studied deposit in southern phosphorites (modified after ORGM, 2000). (B) (Farhaoui et al., 2022).

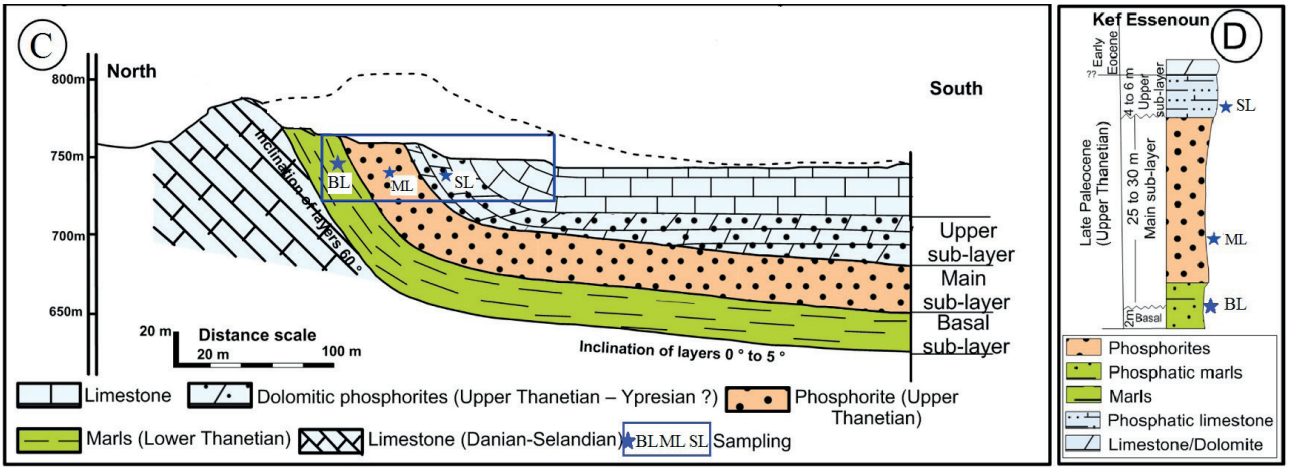

Fig. 2. Simplified geological section of the phosphorite deposit of Kef Essennoun (C); With SL: Somital sub-layer, ML: main sub-layer, BL: The basal sub-layer sample collectionpoints; Simplified lithological column from the Kef Essennoun deposit (D) (Farhaoui et al., 2022).

Middle Eocene (Lutetian) (Farhaoui et al., 2022).

The deposit is characterized by a thick layer (~ 35 m) of Upper Thanetian phosphorites, which is itself divided into three sub-layers known throughout the Djebel Onk district according to the P_2O_5 and MgO contents. From bottom to top, these sub-layers are:

- The basal sub-layer (BL): It is made up of alternating marls, phosphorites, and dolomites, with a thickness of approximately 2 m. The heterogeneous phosphorite grains are cemented by a matrix of marl and clay.
- The main sub-layer (ML): It has a thickness of 25 to 30 m and is exploited for phosphorites. The homogeneous particles of phosphorite are cemented by clay or carbonaceous cement.
- The somitalsub-layer (SL): It consists of a layer of phosphated dolomite with a relatively low P_2O_5 content (16 to 24 %) and a high MgO content (6 to 11 %). Phosphorite particles have heterogeneous particle sizes (Kechiched et al., 2016).

3 Methodology

3.1 Sample preparation

The sampling of the different types of phosphates was carried out on the three sub-layers (somital, main, basal) for beige phosphate, and on the two sub-layers (somital and main) for black phosphate, taken from the different sites. Each phosphate sample weighs 100 kg to ensure its representativeness. In this experimental study, representative samples were taken and subjected to detailed characterization.The sampling points were marked by (Fig. 2) and the samples were labeled, stored in plastic bags, then crushed to a size less than 4 mm, air dried, homogenized, and ground for ease of further handling.

3.2 Physicochemical characterization of the samples

The samples of the three beige phosphate undercoats and the two black phosphate undercoats were mixed separately, with proportions determined according to the length of each layer. Each mixture then underwent a series of operations: homogenization, grinding, quartering, crushing to 4 mm, and sieving using a RETSCH AS200 basic electro-vibrating sieve (Serial No. 22 2504 017 G, Voltage: 230 V, 50 Hz, manufactured in Germany) the vibration amplitude used is equal to 60 and the sieving time is equal to 25 minutes. A quantity of 200 grams of each mixture was crushed in a Retsch ACC brand RM200 mortar grinder (made in Germany); the grinding time is equal to 15 minutes, to carry out the following analyses:

X-ray diffraction (XRD) can identify the mineral phases present in phosphate. This analysis is performed with an OLYMPUS BTX-716Benchtop. The bracket scans from 0° to 55° (2θ angle range) at a speed of 2°/min. The obtained diffractograms are processed using XpertHighScorePlus V3.0d software.

The petrographic analysis of phosphates in the sediments of Kef Essennoun was meticulously carried out by the microscopic examination of thin sections taken at different stratigraphic levels of the deposit.

Determination of major element contents using a Perkin Elmer atomic absorption spectrometer (AAS), model AAnalyst 400; as well as a SEAL Analytical AA3 auto-analyzer (made in the United States). Methods used include automatic spectrophotometry with the Technicon NF U42-201 auto analyzer and the high-performance M4 TORNADO micro-XRF spectrometer.

3.3 Processing of phosphate ore by the combined method of calcination and electrostatic separation

3.3.1 Calcination

The calcination tests are carried out in a muffle furnace from Nabertherm GmbH (manufactured in Germany). A quantity of 100 g of beige phosphate and 100 g of black phosphate are used, with a particle size of (–1 000) µm.

Beige and black phosphates with a particle size (–1 000 + 125) µm are calcined at three different temperatures: 850 °C, 950 °C and 1 050 °C. For each temperature, the calcination duration was 15 minutes. The samples were placed in porcelain crucibles, which were inserted into a preheated muffle furnace. This procedure aims to reduce the content of organic matter contained in the phosphates of Kef Essennoun. After the selected duration, the samples were removed and cooled in a desiccator. The calcined products were then ground in a Retsch AG brand RM200 mortar grinder (manufactured in Germany), for 15 minutes, to obtain a fraction less than 45 µm.

3.3.2 Electrostatic separation

The high-tension separator used in these tests was a Carpco panel type HP16-ll4 model. This device has been specifically designed for high-tension separation studies. Conditions, such as rotor diameters, electrode positions, voltage gradients, polarities, and field shapes, can be varied to study the effects of these variables. Each of the two types of phosphates (black and beige) was subjected to an electrostatic separation operation.The samples were dried under a vacuum between 80 and 100 °C before being introduced into the separator by a vibrating feeder. For each test, 200 g of the representative sample was introduced by a vibrating feeder and transported into the rotor separator, where the particles were subjected to different voltages between the separator electrodes 25, 30 and 35 kV, with different rotation speeds of 30, 40 and 50 rpm.

4 Results and discussions

4.1 Petrographic analysis

The most abundant phosphatic elements appear in the form of rounded to sub-rounded pellets embedded in microsparitic cement with sizes ranging from 150 to 250 µm. These elements are surrounded by a thin, clear cortex; the granules (pel) are slightly rounded and have different colors: white-gray to dark brown in the three different sublayers (Fig. 4).Glauconite grains in the main sublayer of Kef Essennoun are more abundant and have well-rounded shapes, measuring approximately 200 µm. Additionally, other features observed in the thin sections include elongated "C" shaped bone debris.

The exogangue is generally carbonated, showing phosphate grains surrounded by dolomite rhombohedra "A", while the endogangue is present either as a silica grain or as a carbonate, occurring as "A", respectively, as quartz or calcite included in the grains of phosphate and Oolites

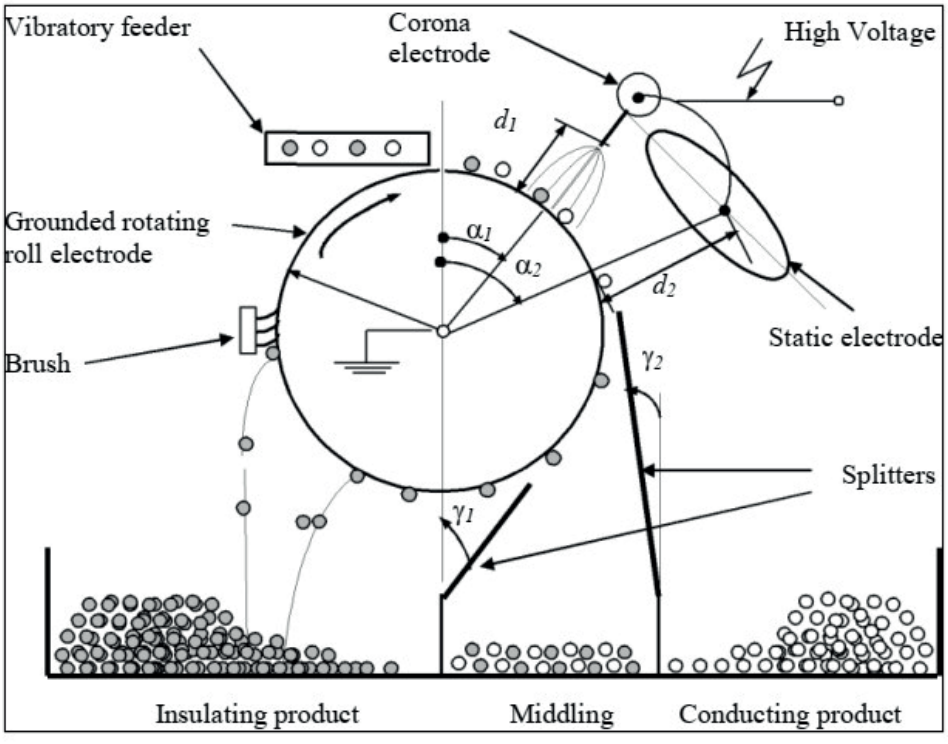

Fig. 3. Loading mechanism in the ring field α_1 and d_1 – angular and radial positions of the corona electrode; α_2 and d_2 – angular and radial positions of the electrostatic electrode; γ_1 and γ_2 – angular positioning of the dividers (Idres et al., 2016).

formed by growth and crystallization of micrometric layers of phosphate “B”, “D” and “E” also show grains of glauconite (Gl) green in color at 500 µm.

Aggregates of small dolomitic “A” rhombohedra constitute the carbonate bonding phase, which generally indicates the beginning of crystallization of the micritic material containing all the impurities of the original mud. The coprolites (Cop) have a cylindrical, elongated morphology “A” and “C”.

4.2 Chemical composition of phosphates

It is interesting to note how analytical techniques have made it possible to reveal relationships between petrographic and mineralogical phases, as well as the particle size distribution and the evolution of chemical contents in minerals. The homogenization method developed for the three sub-layers offers a variety of mixtures meeting the usability criteria. This approach aims to provide a higher quality phosphate concentrate.

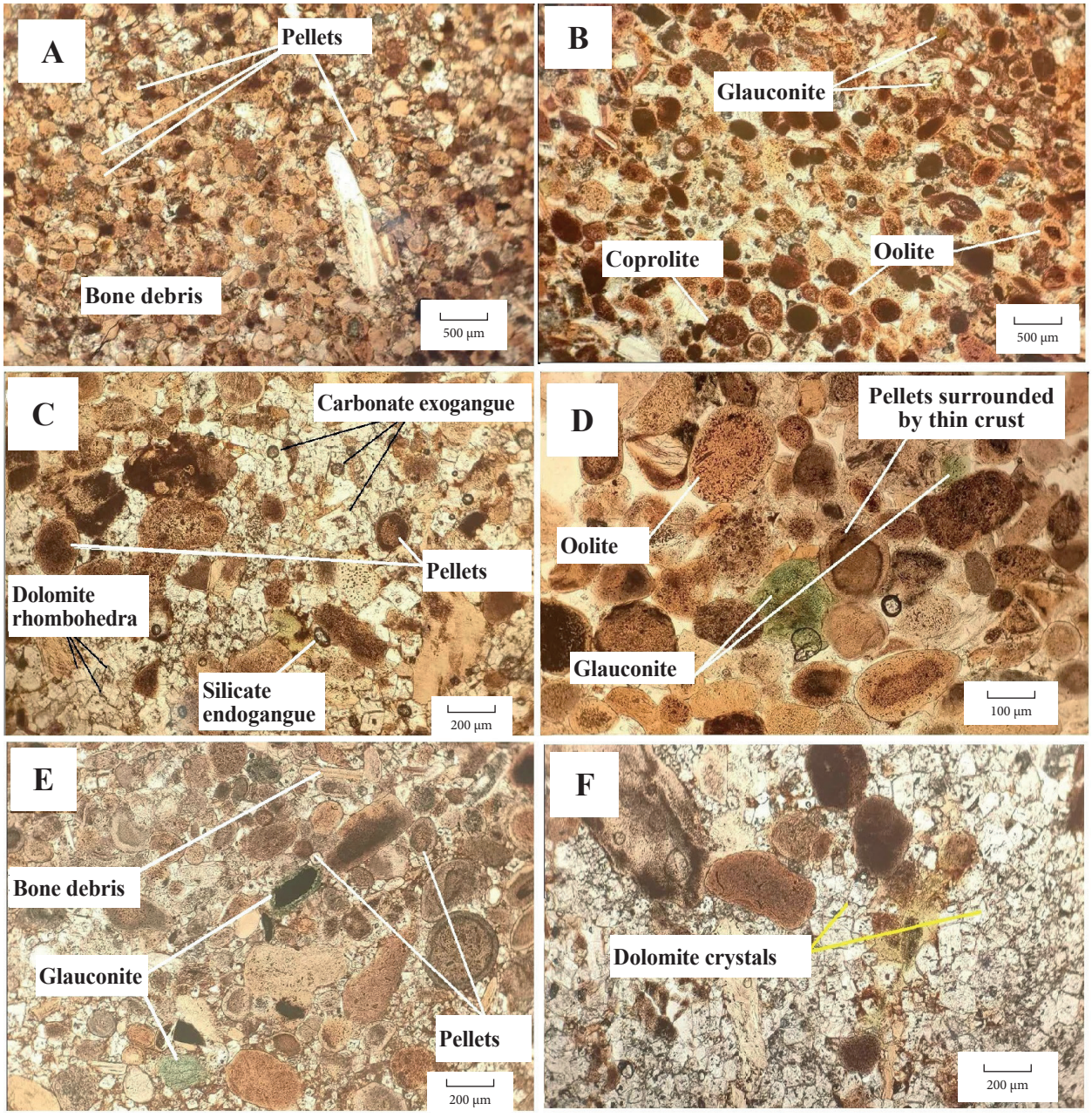

Fig. 4. Microscopic observation (LPNA X10) of the phosphate minerals studied; A, B, C – beige phosphates (somital, main, and basal); D, E – black phosphates (main and somital layer) F – dolomitic phosphates of the summit layer: dolomite crystals; glauconite, Oolite; E – bone debris; coprolite; pellet; organic material.

In our study, a collective homogenization of beige and black phosphates is proposed according to the percentage of reserves, covering the entire deposit. This approach could have a significant impact on the efficiency of mining and on the socio-economic and environmental aspects related to phosphate extraction.

The results of thechemical analysesof the beige and black phosphate samples are presented in tables 1 and 2.

In order to minimize phosphate losses from the Djebel Onk mining complex, the characterization and processing tests will focus on the mixture of the three beige phosphate sub-layers (basal, main, somital), as well as on black phosphate (main and somital).

Tab. 1

Basic chemical composition (P_2O_5, CO_2 and MgO) according to particle size ranges (SL, ML and BL) in beige phosphate

Slices [µm]	P_2O_5 [%]			MgO [%]			CaO [%]			CO_2 [%]		
	SL	ML	BL	SL	ML	BL	SL	ML	BL	SL	ML	BL
> 2 000	17.03	24.74	22.42	4.64	4.44	3.65	28.10	40.82	36.99	20.60	11.04	15.28
–2 000 + 1 000	21.09	23.56	20.96	3.81	2.82	3.98	34.80	38.87	37.88	15.28	12.29	16.61
–1 000 + 500	25.14	24.64	23.31	2.82	2.32	4.98	41.48	40.66	51.15	12.96	11.04	13.32
–500 + 250	25.26	28.51	23.42	2.82	1.33	1.82	41.68	47.04	38.64	10.30	7.31	13.62
–250 + 125	20.00	29.37	24.14	3.64	1.03	1.99	33.00	48.46	46.43	10.96	6.64	8.31
–125 + 63	17.89	23.96	24.66	4.64	1.99	2.98	29.52	39.53	40.69	16.61	8.31	9.97
–63 + 45	16.31	21.41	20.29	4.64	2.98	2.49	26.91	35.33	33.48	15.95	11.63	12.29
–45 + 0	18.75	18.29	16.47	3.98	2.49	2.49	30.94	30.18	27.18	14.62	9.97	11.04

Tab. 2

Basic chemical composition (P_2O_5, CO_2 and MgO) according to particle size ranges (SL and ML) in black phosphate

Classes [mm]	P_2O_5 [%]		MgO [%]		CaO [%]		CO_2 [%]	
	SL	ML	SL	ML	SL	ML	SL	ML
> 2 000	**17.49**	**22.53**	4.47	3.48	28.86	37.17	19.27	14.62
–2 000 + 1 000	**20.17**	**25.53**	3.98	3.98	33.28	42.12	16.94	10.30
–1 000 + 500	**22.71**	**27.45**	3.48	1.66	37.47	45.29	14.62	8.31
–500 + 250	**25.37**	**29.23**	2.82	0.96	41.86	48.23	10.96	7.31
–250 + 125	**26.21**	**26.85**	1.99	1.99	43.25	44.30	14.62	7.64
–125 + 63	**27.34**	**18.85**	1.56	3.32	45.11	31.10	20.60	11.96
–63 + 45	**22.23**	**18.95**	3.65	3.81	36.68	31.26	23.59	13.28
–45 + 0	**27.32**	**16.67**	1.82	2.82	45.08	27.50	23.25	9.96

Tab. 3

Basic chemical composition of particular grain fractions of sub-layer mixture (somital, main, basal) for beige phosphate and for black phosphate (somital and main)

Slices [µm]	Beige phosphate				Black phosphate			
	P_2O_5 [%]	MgO [%]	CaO [%]	CO_2 [%]	P_2O_5 [%]	MgO [%]	CaO [%]	CO_2 [%]
> 2 000	**21.04**	4.24	35.30	15.64	**20.01**	3.98	33.02	16.95
–2 000 + 1 000	**21.87**	3.54	37.18	14.71	**22.85**	3.98	37.70	13.62
–1 000 + 500	**24.36**	3.37	44.43	12.44	**25.08**	2.57	41.38	11.47
–500 + 250	**25.73**	1.99	42.39	10.41	**27.30**	1.89	45.05	9.30
–250 + 125	**25.84**	2.22	42.63	8.63	**26.53**	1.99	43.76	11.13
–125 + 63	**22.17**	3.20	36.58	11.63	**23.53**	2.44	38.11	16.28
–63 + 45	**19.34**	3.37	31.91	13.29	**20.59**	3.73	33.97	18.35
–45 + 0	**17.84**	2.99	29.43	11.88	**22.00**	2.32	36.29	16.61

Tab. 4

Basic chemical composition of sub-layer (somital, main and basal) for beige phosphate and for black phosphate (somital and main)

Beige phosphate				
Sample	Contents [%]			
	P_2O_5	MgO	CO_2	CaO
Somital (SL)	**24.60**	2.58	12.36	39.60
Main (ML)	**27.07**	2.10	9.64	44.66
Basal (BL)	**20.86**	3.32	12.79	34.41
Mixture of the three sub-layers	**27.02**	3.68	9.83	35.40
Slice	**30.20**	2.35	9.60	55.40
Black phosphate				
Somital	**23.05**	3.65	8.64	38.03
Main (ML)	**27.93**	1.94	8.40	46.08
Mixture of the two sub	**26.59**	3.44	9.97	34.83
Slice	**30.8**	2.82	9.30	56.0

*Slice (–1 000 + 125) µm = mixture of three slice fractions (+ 500 µm + 250 µm + 125 µm).

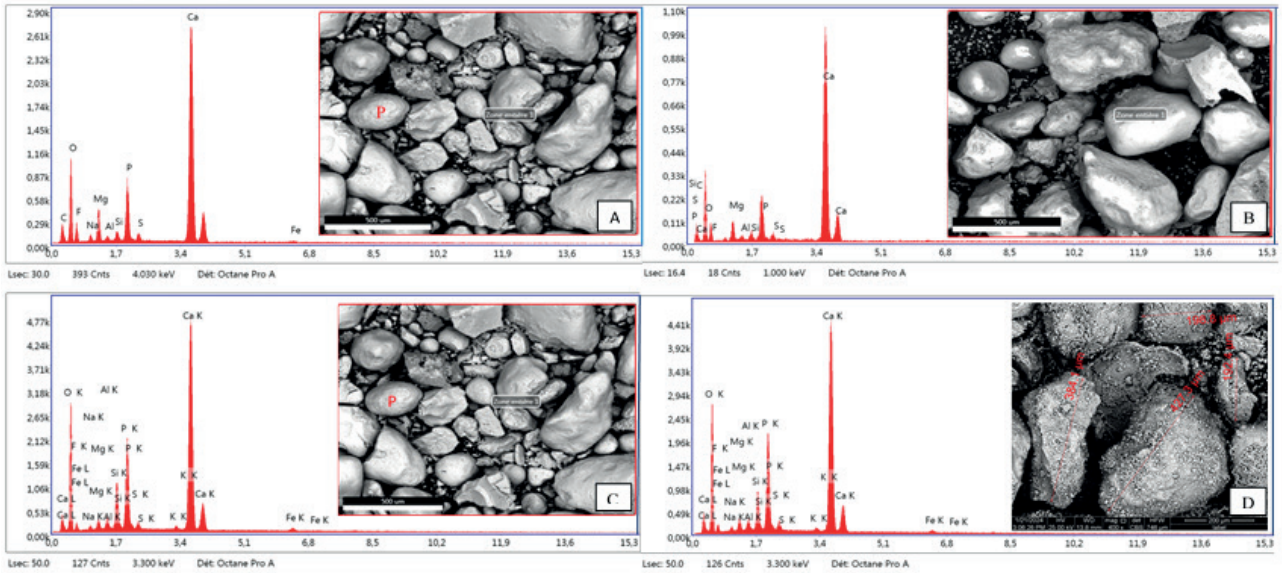

Fig. 5. SEM / EDS observation of beige "A" and black "B" phosphate before calcination and "C" and "D" after calcination (A; B). EDS spectrum showing the abundance of Ca, P and F in the phosphate particles and the high contents of O and Si in the matrix (C; D). EDS analysis showing that the abundance of Ca, O, Si, decrease after calcination. P – pellets, Cop – Coprolite, Ol – Oolite.

The upper sub-layers (somital) of the beige and black phosphates have a P_2O_5 content of 24.60 % and 23.05 %, respectively. The basal sub-layer of the beige phosphate has a P_2O_5 content of 20.86 %. These layers are considered poor ore and are stored near the mine as waste rock.

4.3 Effect of calcination process by sem / eds analysis

Analysis of the sample of beige and black phosphate by SEM is carried out for raw beige phosphate and black phosphate after calcination. The use of SEM / EDS is essential to characterize raw beige and black phosphates,

as well as to evaluate the efficiency of the calcination process.

The obtained EDS spectra for the released phosphate sample show the constituent elements of the released phosphate sample such as C, O, Mg, Al, Si, P, Mo, Ca, and Fe in different ratios. The content of calcium, oxygen, and phosphorus is the highest; however, the EDS spectrum shows that the abundance of Ca, O, and Si is reduced after calcination. The SEM / EDS results before and after calcinations are shown in (Fig. 5).

4.4 X-ray diffraction (XRD)

The mineralogical study carried out by XRD revealed that apatite is a highly substituted francolite, in OH ions (hydroxylapatite) and F ions (fluorapatite). In total, the intensity of the peaks is characteristic of the phosphatic elements and those of the gangue. The results are reported in (Fig. 6).The XRD results shows the presence of fluorapatite and dolomite as main minerals. Apatite, carbonated fluorapatite ($Ca_{10}(PO_4)_5CO_3F_{1,5}(OH)_{0,5}$ as well as the gangue minerals dolomite $CaMg(CO_3)_2$ calcite $CaCO_3$ and quartz SiO_2 have been discovered and form the matrix of the phosphorite grains, however, are present in small quantities. These findings reveal significant differences for the three phosphate sub-layers.

Indeed, the ore of the main layer is the richest in fluorapatite, hydroxylapatite, and the poorest in calcite compared to the two other layers. However, the lower layer is the poorest in phosphate minerals and richest in dolomite compared to the upper and main layers. The presence of dolomite is evident in the upper and lower layers. Quartz is more abundant in the upper layer than in the main and lower layers. Identifying the mineralogical composition and quantity of each mineral in the different phosphate layers can suggest the most appropriate ore processing.

For the gangue minerals, let's note the presence of quartz peaks in small quantities as well as the decrease in dolomite phases and the appearance of CaO and MgO peaks at 2 theta = 37.36° and 42.91° for phosphate.

For black phosphate, it is possible to observe the presence of dolomite peaks in considerable quantity as well as those of quartz and calcite, with the presence of CaO and MgO peaks at 2 theta = 37.36° and 42.90°.These results therefore clearly confirm the presence of phosphate in our samples.

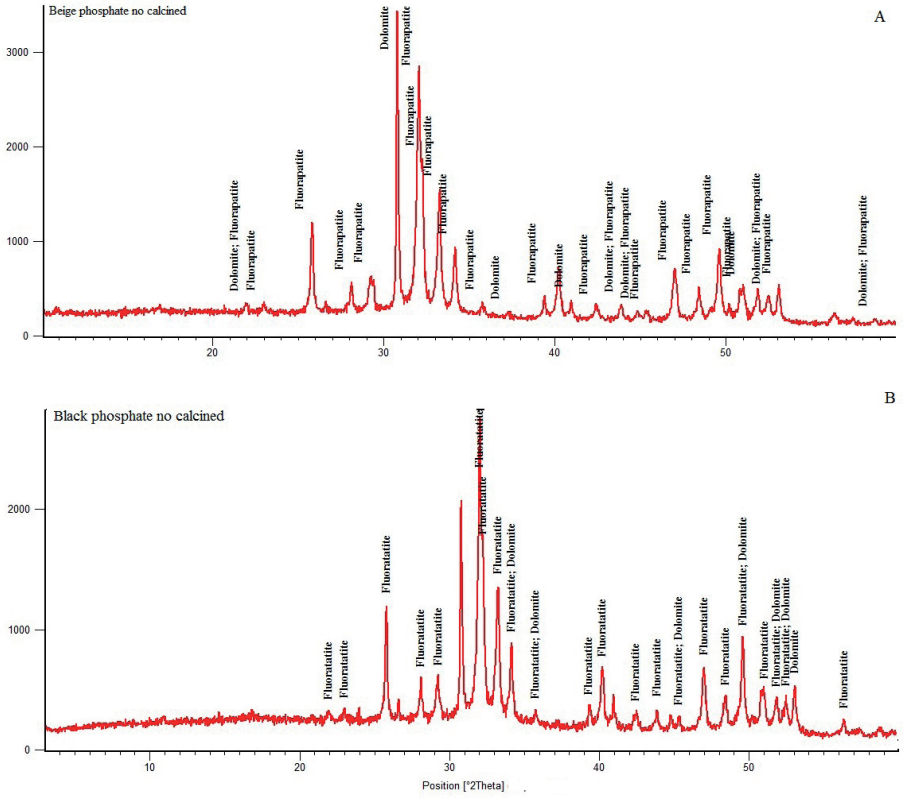

Fig. 6. XRD results of: A – beige phosphate, B – black phosphate (before calcination).

The chemical analysis results of the major elements of the calcination of beige and black phosphates are shown in Tab. 5.

Tab. 5

Results of chemical analysis of the major elements of the calcination of beige and black phosphates

Beige phosphate					
Temperature [°C]	L.O.I [%]	Contents [%]			
		P_2O_5	MgO	CaO	CO_2
0	/	27.02	3.68	35.40	9.97
850	13.61	30.31	3.365	39.70	2.49
950	14.60	31.03	3.979	40.65	1.33
1	15.19	31.15	3.782	40.80	1.00
Black phosphate					
0	/	26.59	3.44	34.83	9.30
850	15.20	26.59	3.448	34.83	9.30
950	16.30	30.79	3.680	40.33	1.49
1	17.37	30.85	3.40	40.41	1.16

Note that with the increase in temperature, the contents of MgO and CaO oxides also increase for beige phosphate (3.78 % and 40.80 %) andfor black phosphate (3.40 % and 40.41 %), respectively. On the other hand, the CO_2 contents gradually decrease until reaching a value of 1 % for beige phosphate and 1.16 % for black phosphate.

The removal of organic matter and calcite is crucial in the phosphate industry. By doing this, high-quality phosphoric acid can be produced more economically, while reducing acid consumption. This fits perfectly into an approach to sustainable development and environmental preservation.

4.5 Treatment using electrostatic separation

Two types of calcined and non-calcined samples were used for the electrostatic separation experiments; with a content of P_2O_5 approximately 31.5 % for beige phosphate and 30.85 % for black phosphate after calcination and 27.02 % and 26.59 % P_2O_5 for beige and black phosphate, in order, without calcination step. A representative sample of the calcination concentrate was prepared for electrostatic separation.

The results of the high-tension electrostatic separation tests (beige and black phosphate calcined and without calcination) are shown in Tabs. 6 and 7.

The best results in X-ray fluo-rescence (XRF) are obtained with the following parameters:

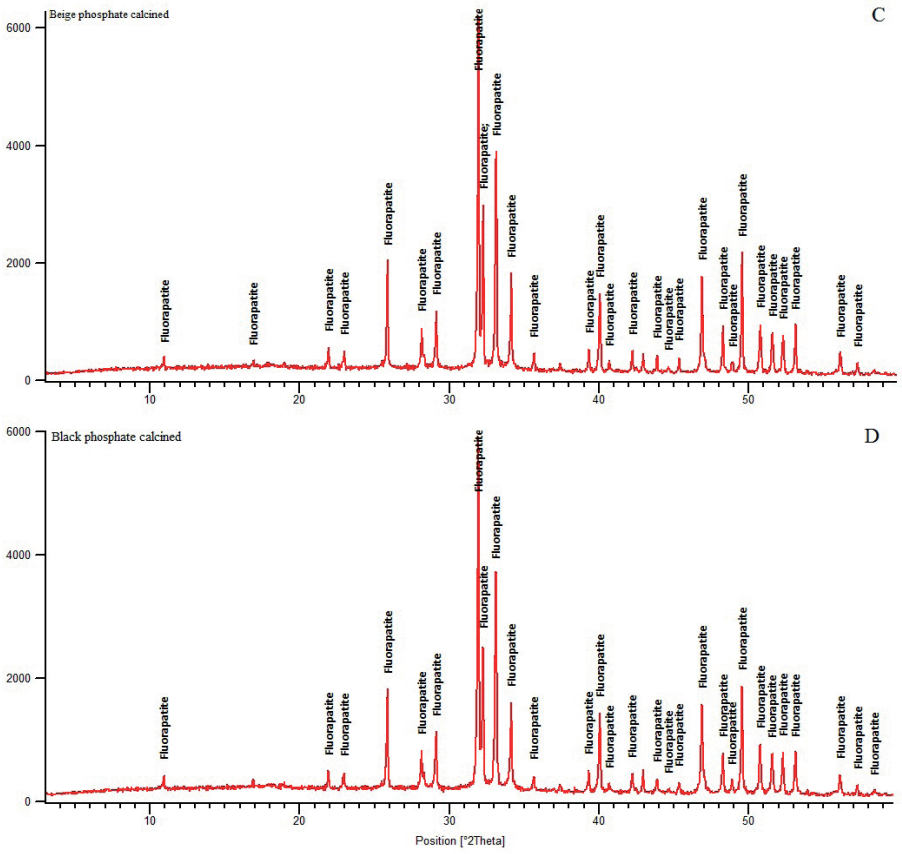

Fig. 7. XRD results of: C – beige phosphate calcined at 1 050 °C, D – black phosphate calcined at 1 050 °C.

Tab. 6

High voltage electrostatic separation test results for non-calcined and calcined beige phosphate

Round / min	Tension [kV]	Conductivity	Non-calcined beige phosphate				Calcined beige phosphate			
			P_2O_5 [%]	MgO [%]	CaO [%]	SiO_2 [%]	P_2O_5 [%]	MgO [%]	CaO [%]	SiO_2 [%]
30	25	conductor	**33.20**	4.42	67.16	6.80	**34.85**	5.05	75.08	6.11
		non-conductor	**28.84**	6.18	53.7	15.06	**26.77**	6.43	68.78	11.56
	30	conductor	**33.22**	4.17	66.28	6.56	**36.89**	4.42	75.85	5.20
		non-conductor	**27.43**	4.85	57.3	17.81	**27.13**	7.08	62.9	9.47
	35	conductor	**29.51**	2.45	60.22	4.94	**28.77**	6.43	68.78	5.56
		non-conductor	**20.84**	4.05	54.3	11.70	**22.33**	8.08	65.90	9.17
40	25	conductor	**32.58**	3.38	65.38	5.49	**32.37**	7.31	75.31	5.84
		non-conductor	**17.81**	6.13	62.36	14.79	**27.15**	8.08	62.9	7.37
	30	conductor	**30.65**	3.32	63.03	5.88	**34.64**	5.20	73.17	5.47
		non-conductor	**24.83**	3.98	58.08	11.05	**26.87**	8.43	63.78	12.56
	35	conductor	**30.24**	3.49	62.5	5.86	**35.56**	4.70	73.83	5.64
		non-conductor	**27.18**	8.17	60.01	11.63	**26.57**	6.46	67.18	11.16
50	25	conductor	**32.95**	4.21	66.43	6.33	**36.68**	6.28	78.15	5.64
		non-conductor	**28.57**	6.33	53.6	14.01	**27.45**	7.08	66.9	9.38
	30	conductor	**30.75**	3.33	60.45	5.34	**30.86**	6.86	71.38	5.34
		non-conductor	**26.94**	5.05	58.44	12.32	**25.94**	7.95	65.44	11.22
	35	conductor	**32.03**	3.29	63.94	5.86	**31.32**	2.20	72.17	5
		non-conductor	**29.60**	6.3	63.36	13.79	**24.33**	5.08	65.9	9.17

Tab. 7

High voltage electrostatic separation test results for non-calcined and calcined black phosphate

Round / min	Tension [kV]	Conductivity	Non-calcined beige phosphate				Calcined beige phosphate			
			P_2O_5 [%]	MgO [%]	CaO [%]	SiO_2 [%]	P_2O_5 [%]	MgO [%]	CaO [%]	SiO_2 [%]
30	25	conductor	**33.77**	3.18	66.89	4.17	**31.85**	7.89	73.47	4.74
		non-conductor	**27.63**	4.95	57.73	16.91	**24.5**	11.08	62.9	9.37
	30	conductor	**35.63**	3.03	69.91	4.23	**33.29**	8.45	76.27	4.79
		non-conductor	**27.5**	4.08	52.9	7.47	**26.53**	9.30	65.12	9.77
	35	conductor	**32.90**	3.03	63.71	3.95	**32.67**	7.07	74.14	6.09
		non-conductor	**17.64**	3.73	41.54	9.35	**26.54**	8.18	64.7	13.06
40	25	conductor	**34.09**	3.53	66.15	4.12	**32.81**	6.97	73.79	4.57
		non-conductor	**26.32**	4.08	53.9	8.41	**25.44**	8.18	68.7	12.16
	30	conductor	**36.06**	3.79	70.37	4.57	**33.52**	10.22	78.97	5.02
		non-conductor	**27.15**	5.08	56.9	9.47	**27.84**	12.18	63.7	14.06
	35	conductor	**35.42**	3.11	69.41	4.27	**29.12**	8.20	70.39	4.79
		non-conductor	**28.15**	4.58	54.9	9.47	**23.60**	9.13	63.36	12.79
50	25	conductor	**34.43**	2.85	67.23	4.38	**33.91**	6.31	71.20	4.7
		non-conductor	**26.5**	5.08	54.9	7.87	**27.93**	5.95	61.73	8.91
	30	conductor	**34.09**	3.46	67.27	4.55	**32.91**	8.62	76.73	5.06
		non-conductor	**25.35**	4.18	53.9	9.47	**17.63**	10.73	41.64	9.75
	35	conductor	**35.31**	3.08	68.16	4.06	**36.65**	9.94	82.16	5.62
		non-conductor	**27.50**	4.48	54.9	8.47	**27.25**	12.58	83.9	9.87

- For calcined beige phosphate and without calcination – rotation speed: 30 rpm, electrical voltage: 30 kV, P_2O_5 content: 36.89 % (calcination) and 33.22 % (without calcination) and recovery: 93.91 % (calcination) and 90.85 % (without calcination).
- For calcined black phosphate – rotation speed: 50 rpm, electrical voltage: 35 kV, P_2O_5 content: 36.63 % and recovery: 93.88 %.
- For black phosphate without calcination – rotation speed: 30 rpm, electrical voltage: 30 kV, P_2O_5 content: 35.65 % and recovery: 91.94 %.

5 Technological scheme of phosphate processing

The obtained treatment results made it possible to develop a treatment scheme for beige and black phosphates from the Kef Essennoun deposit of the Djebel Onk phosphate mining complex (Fig. 8).

X-ray diffraction (XRD) and scanning electron microscopy (SEM / EDS) results confirm that the main mineral phases in the sample are apatites, including fluorapatite, hydroxyapatite, and carbonate fluorapatite. On the other hand, the gangue minerals present include quartz and dolomite.

Calcination breaks down the carbonates into calcium oxide and magnesium oxide and eliminates most of the carbon dioxide (CO_2). The best results of chemical analysis obtained at the temperature 1 050 °C for beige phosphate are content of P_2O_5 31.15 % amount of MgO 3.78 %, and 40.80 % CaO, while for black phosphate was obtained 30.85 % of P_2O_5, 3.40 % MgO and 40.41 % CaO.

The beneficiation of phosphate ore by a combined method of calcination and electrostatic separation is an effective approach to concentrate ore from a sub-arid region. Then, electrostatic separation separates the particles based on their electrical properties, which facilitates the concentration of the phosphate.

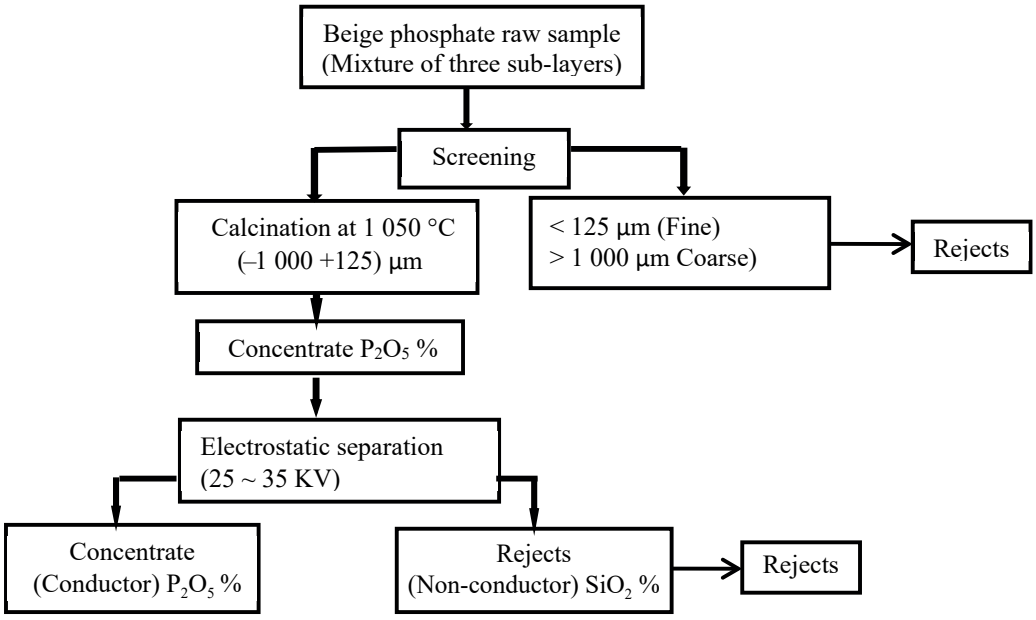

Fig. 8. Technological scheme for processing of Kef-Essennoun phosphate ores by electrostatic separation.

6 Conclusion

The Kef Essennoun deposit has sedimentary origins; it is composed of two types of phosphate: beige and black.

Microscopic observation of thin sections shows that the phosphate ore is mainly composed of phosphate pellets, coprolites, oolites and glauconite, as well as quartz, dolomite and calcite.

Indeed, particle size fractions between 1 000 µm and 125 µm are particularly rich in phosphate and display a significant yield of P_2O_5.

The calcination process allowed us to break down the carbonates into calcium oxide and magnesium oxide and remove most of the carbon dioxide (CO_2).

The best-obtained results from the calcination process followed by electrostatic separation with corona effect from an initial ore with a content of 31.15 % of P_2O_5 were achieved for calcined beige phosphate (rotation speed: 30 rpm, electrical voltage: 30 kV), with content of P_2O_5 in concentrate 36.89 % andrecovery of 93.91 %. For calcined black phosphate (rotation speed: 50 rpm, electrical voltage:

35 kV where content of P_2O_5 in concentrate reached 36.65 % with recovery of 93.88 % from an initial ore with a content of 30.85 % P_2O_5.

Tests of enrichment of calcined and non-calcined beige and black phosphate ore from the Kef Essennoun deposit by a combined method of calcination and electrostatic separation make it possible to obtain very satisfactory results. This study highlights the importance of the calcination treatment before the electrostatic separation operation.

Acknowledgments

The treatment process and characterization analyses were carried out in several scientific research laboratories. The authors of this article would like to thank the Mining Laboratory of Tebessa University; the (LAVAMINE) laboratory of Badji Mokhtar University; the Laboratory of the Djebel Onk Bir Ater Mining Complex, Tebessa; and the Materials Technology and Process Engineering Laboratory (LTMGP) of the University of Bejaia; and the laboratory of the National School of Technology and Engineering of Annaba for the SEM observations, and we would like also to thank the laboratory team (APEEC) of the University of Sidi Bel Abbes. Authors express their thanks for reviewer Alexandra Bekényiová from SGUDS Applied Technology of Raw Materials Processing, Slovakia, as well as one anonymous reviewer'.

References

Bada, S. O., Falcon, L. M., Falcon, R. M. S. & Bergmann, C. P., 2012: Feasibility study on triboelectrostatic concentration of<105 μm phosphate ore. *Journal of the Southern African Institute of Mining and Metallurgy*, 112, 5, 341–345.

Bendilmi, M. S., Zeghloul, T., Ziari, Z., Medles, K. & Dascalescu, L., 2022: Experimental characterization of electric potential uniformity at the surface of polymer plates corona charged by multiple-row needle-type electrodes. *Journal of Electrostatics*, 115, 103656. https://doi.org/10.1016/j.elstat.2021.103656.

Bounemia, L. & Mellah, A., 2021: Characterization of crude and calcined phosphates of Kef Essennoun (Djebel Onk, Algeria). *J. Therm. Anal. Calorim.*, 146, 2049–2057. https://doi.org/10.1007/s10973-020-10167-2.

Dascalescu, L., Morar, R., Iuga, A., Samuila, A., Neamtu, V. & Suarasan, I., 1994: Charging of particulates in the corona field of roll-type electroseparators. *Journal of Physics D: Applied Physics*, 27, 6, 1242. DOI https://doi.org/10.1088/0022-3727/27/6/023.

Ferhaoui, S., Kechiched, R., Bruguier, O., Sinisi, R., Kocsis, L., Mongelli, G. & Laouar, R., 2022: Rare earth elements plus yttrium (REY) in phosphorites from the Tébessa region (Eastern Algeria): Abundance, geochemical distribution through grain size fractions, and economic significance. *Journal of Geochemical Exploration,* 241, 107058. https://doi.org/10.1016/j.gexplo.2022.107058.

Gadri, L., Hadji, R., Zahri, F., Benghazi, Z., Boumezbeur, A., Laid, B. M. & Raïs, K., 2015: The quarries edges stability in opencast mines: a case study of the Jebel Onk phosphate mine, NE Algeria. *Arabian Journal of Geosciences*, 8, 8987–8997. https://doi.org/10.1007/s12517-015-1887-3.

Idres, A., Abdelmalek, C., Bouhedja, A., Benselhoub, A. & Bounouala, M., 2017: Valorization of mining waste from Ouenza iron ore mine (eastern Algeria). *REM--International Engineering Journal*, 70, 85–92. https://doi.org/10.1590/0370-44672016700051.

Idres, A., Bouhedja, A., Bounouala, M. & Benselhoub, A., 2016: New method of electrostatic separation of the oxidized iron ore. *Mining Science*, 23, 33–41. https://DOI10.5277/msc162303http://dx.doi.org/10.5277%2Fmsc162303.

Idres, A., Bounouala, M., Boukelloul, M. L. & Talhi, K., 2014: Study of electrical properties of iron ore in view of electrostatic separation. *International Journal of Mining Engineering and Mineral Processing*, 3, 1, 1–5. DOI: 10.5923/j.mining.20140301.01.

Kechiched, R., Laouar, R., Bruguier, O., Kocsis, L., Salmi--Laouar, S., Bosch, D. & Larit, H., 2020: Comprehensive REE+ Y and sensitive redox trace elements of Algerian phosphorites (Tébessa, eastern Algeria): A geochemical study and depositional environments tracking. *Journal of Geochemical Exploration*, 208, 106396. https://doi.org/10.1016/j.gexplo.2019.106396.

Kechiched, R., Laouar, R., Bruguier, O., Laouar-Salmi, S., Ameur-Zaimeche, O. & Foufou, A., 2016: Preliminary data of REE in Algerian phosphorites: a comparative study and paleo-redox insights. *Procedia Engineering,* 138, 19–29. https://doi.org/10.1016/j.proeng.2016.02.048.

Notholt, A. J., 1980: Economic phosphatic sediments: mode of occurrence and stratigraphical distribution. *Journal of the Geological Society*, 137, 6, 793–805. https://doi.org/10.1144/gsjgs.137.6.0793.

Stencel, J. M., 2003: Pneumatic Transport, Triboelectric Beneficiation for the Florida Phosphate Industry. *Florida, Florida institute of phosphate research*. https://doi.org/02-149-201.

Tiour, F., Idres, A., Ould Hamou, M. & Boutarfa, F., 2022: Characterization and processing of low-grade iron ore from the Khanguet mine by electrostatic separation. *Scientific Bulletin of National Mining University*, 3. https://doi.org/10.33271/nvngu/2022-3/076.

USGS – U.S. Geological Survey, 2020: Mineral Commodity Summaries 2020. *U.S. Geological Survey*, 200 p. https://doi.org/10.3133/mcs2020 (Accessed date: 11/12/2021).

Zafar, Z. I., Anwar, M. M. & Pritchard, D. W., 1996: Innovations in beneficiation technology for low grade phosphate rocks. *Nutrient cycling in agroecosystems*, 46, 135–151. https://doi.org/10.1007/BF00704313.

Zhu, H., Bai, Y., Zu, L., Bi, H. & Wen, J., 2023: Separation of metal and cathode materials from waste lithium iron phosphate battery by electrostatic process separations, 10, 3, 220. https://doi.org/10.3390/separations10030220.

Zieliński, J., Biegun, M., Kaniewski, M., Huculak-Mączka, M. & Hoffmann, J., 2023: Thermal Characteristics of Selected Phosphate Ores and the Effect of Inorganic Salts on Their Calcination. *ACS omega*, 8, 48, 45510–45518. https://DOI: 10.1021/acsomega.3c05573.

Spracovanie fosfátových rúd s nízkym obsahom úžitkovej zložky z bane Djebel Onka (Alžírsko) metódou elektrostatickej separácie

Výskumná práca sa zaoberá problematikou technologického spracovania nízkokvalitných fosfátových rúd z bane Djebel Onk (Alžírsko) metódou elektrostatickej separácie. Cieľom výskumu bolo overiť použitie zmesí pozostávajúcich z troch vzoriek suroviny odobratých zo svetlých (béžových) fosfátových vrstiev (bazálnej, hrubej približne 2 m, hlavnej strednej podvrstvy s hrúbkou asi 25 – 30 m a povrchovej vrstvy, ktorá obsahovala dolomit s nízkym obsahom fosfátov) a dvoch vzoriek suroviny odobratých z čiernych fosfátových podvrstiev povrchovej a hlavnej strednej vrstvy.

Odobraté vzorky boli podrvené na veľkosť zŕn menšiu ako 4 mm, voľne sušené a homogenizované. Pred elektrostatickou separáciou sa skúmané vzorky so zrnitosťou 125 – 1 000 μm kalcinovali pri teplote 850, 950 a 1 050 °C počas 15 minút s cieľom redukcie obsahu organických zložiek vo fosfátoch. Elektrostatická separácia sa realizovala použitím vysokonapäťového separátora typu Carpo HP16-114. Pred elektrostatickou separáciou sa vzorky sušili vo vákuu pri teplote 80 – 100 °C. Na každý test sa použilo 200 g vzorky, ktorá bola podrobená separácii pri napätí 25, 30 a 35 kV s rýchlosťou rotácie 30, 40 a 50 otáčok za minútu.

Chemické a mineralogické zloženie vstupnej suroviny, ako aj produktov technologickej úpravy bolo stanovené použitím rôznych analytických metód (röntgenová difrakčná analýza, röntgenová fluorescencia, SEM/EDS rastrovací elektrónový mikroskop a optický mikroskop).

Na základe uvedených analýz sa na elektrostatickú separáciu zvolili vstupné nekalcinované vzorky a vzorky termicky upravené pri teplote 1 050 °C.

Najvyššia výťažnosť pri použití elektrostatickej separácie v prípade béžového fosfátu sa získala pri kalcinovanej vzorke za týchto podmienok: rýchlosť rotácie 30 otáčok za minútu, elektrické napätie 30 kV. Zo vstupnej kalcinovanej rudy s obsahom 31,15 % P_2O_5 sa separáciou získalo 93,91 % P_2O_5. Z nekalcinovanej vstupnej vzorky s obsahom 33,22 % P_2O_5 sa za rovnakých podmienok získalo 90,85 % P_2O_5.

V prípade čierneho fosfátu po separácii kalcinovanej vstupnej vzorky s obsahom 36,63 % P_2O_5 pri napätí 35 kV a 50 otáčkach za minútu najvyšší získaný podiel P_2O_5 predstavoval 93,88 %. Z nekalcinovanej vstupnej vzorky čierneho fosfátu s obsahom 36,65 % P_2O_5 bola najvyššia výťažnosť separácie pri napätí 30 kV a 30 otáčkach za minútu, keď sa podarilo odseparovať 91,94 % P_2O_5.

Na efektívne získavanie P_2O_5 z fosfátových rúd v závislosti od ich charakteristík možno použiť viaceré technologické postupy. Elektrostatická separácia bola overená ako vhodná ekologická a efektívna metóda získavania P_2O_5 z kalcinovaných, ale aj nekalcinovaných béžových a čiernych fosfátov. Kalcinácia pri teplote 1 050 °C okrem rozkladu organických zložiek umožnila navyše rozklad karbonátov na oxidy vápnika a horčíka, ako aj odstránenie väčšiny obsahu CO_2. Odstraňovanie organických látok je rozhodujúce aj vo fosfátovom priemysle, kde tento spôsob úpravy vstupnej suroviny umožňuje vyrábať vysokokvalitnú kyselinu fosforečnú ekonomickejšie.

Doručené / Received: 10. 7. 2024
Prijaté na publikovanie / Accepted: 17. 12. 2024

Mineralia Slovaca, Web ISSN 1338-3523, ISSN 0369-2086, https://doi.org/10.56623/ms.2024.56.2.6
56, 2 (2024), 195 – 214, © Authors 2024. CC BY 4.0

Methodology and results of geological survey of the environmental burden of the former Slovenský hodváb plants – Senica (Slovakia)

SLÁVKA GREXOVÁ[1], ZUZANA DANKOVÁ[1], MARTIN SUROVÝ[1], JURAJ KOTUČ[1], KAROLÍNA ADZIMOVÁ[1], ALEXANDRA BEKÉNYIOVÁ[1] and PETER ŠOTTNÍK[2]

[1]State Geological Institute of Dionýz Štúr, Regional centre Košice, Jesenského 8, SK-040 01 Košice, Slovak Republic; *slavka.grexova@geology.sk
[2]State Geological Institute of Dionýz Štúr, Department of Environmental Geochemistry, Mlynská dolina 1, SK-817 04 Bratislava, Slovak Republic

Abstract: In the years 2021–2023, the State Geological Institute of Dionýz Štúr, Slovakia, carried out a detailed geological survey of the environmental burden on the Senica site, identified as a probable environmental burden with a high priority within the project Geological survey of selected environmental burdens ŠGÚDŠ-3. The task was carried out in accordance with the strategic planning document for a systematic survey and removal of environmental burdens entitled *State Program for Remediation of Environmental Burdens of the Slovak Republic (2016–2021)* within the Operational Program of Environmental Quality. The goal of the survey was a detailed verification of all components of the environment at locations that, based on a preliminary risk assessment in the information system of environmental burdens, represented a potential risk for human health and the environment. The survey verified in detail an area of approximately 37 ha, on which 210 chemical indicators were analytically determined from a wide range of indicators according to the type of activity of the former Slovenský hodváb plants, which were evaluated in accordance with the current applicable legislation in the field of environmental burdens. The results of the survey did not confirm serious pollution of the underground water and rock environment, which would be in a causal or spatial context. An environmental and health risk was not detected by the risk analysis, it is not necessary to carry out remediation of the investigated area.

Key words: probable environmental burden, information system of environmental loads, geological survey of the environment, risk analysis

Graphical abstract

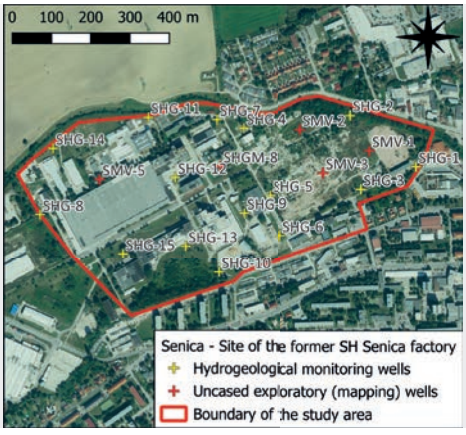

Highlights

- Detailed geological survey of the environment has not confirmed the expected pollution in the area of the former Slovenský hodváb plants in Senica, Slovakia.
- The environmental and health risks have not been confirmed by the elaborated risk analysis.
- Two-year groundwater quality monitoring is proposed before burden removing from the Register of Information system of environmental loads of the Slovak Republic.

1 Introduction

Environmental burdens are defined as polluted areas caused by human activity that pose a serious risk to human health or the rock environment, groundwater and soil. The problem of solving environmental burdens in Slovakia began in 2006 as part of the project Systematic identification of environmental burdens (Paluchová et al., 2008) with the aim to identify probable environmental burdens from the entire territory of the Slovak Republic. That resulted in the compilation of the Register of Environmental Burdens, in which registered burdens are sorted according to their relative risk to the life and health of residents as well as damage to ecosystems, and which is part of the Information System of Environmental Loads (IS EZ). The information system is continuously updated primarily on the basis of geological surveys and series of

remedial measures in accordance with the currently valid legislation: Act No. 569/2007 Coll., Act No. 409/2011 Coll. Act No. 364/2004 Coll., Act SNR No. 372/1990 Coll., Regulation of the Ministry of the Interior of the Slovak Republic dated January 28, 2015 No. 1/2015-7 to develop a risk analysis of the polluted area.

Currently, 1,782 loads are registered in Slovakia, divided into registers according to the status of their examination and the implementation of corrective measures with the aim of minimizing their negative impact on human health and the environment. This work presents the results of the geological task entitled *Geological survey of selected probable environmental loads 3 – which ŠGÚDŠ* solved within the Operational Program Environmental Quality – priority axis 1. The task was developed in accordance with the strategic planning document for the systematic survey and removal of environmental burdens entitled *State Program for Remediation of Environmental Burdens of the Slovak Republic (2016–2021)*, in which the relevant environmental burden of the Trnava Region is recorded in section 7.1.1. *The most risky locations in terms of the need to carry out a survey of probable environmental burdens and the need to develop a risk analysis*.

The environmental burden (EB) in the area of the former Slovenský hodváb (SH) plants is registered in the information system in category A as a probable environmental burden with a high priority denoted as SK/EZ/SE/2004 under the name SE/2004/Senica – the area of the former SH Senica. The area of the former plants is located in the built-up area of the inner city of Senica, in the industrial zone, in the area of the former manufacturing company Slovenský hodváb Senica. The territory is bordered on the eastern side by the Lidl store and the bus station, and on the northern side by the Teplica stream. The investigated area is roughly in a shape of rectangle of area approximately 37 ha (Fig. 1).

High priority of the environmental burden was assigned in the system of environmental loads primarily on the basis of a visual inspection of the site at the time of registration in 2014, which corresponded to the state of the finished industrial activity of the former plants (Fig. 2). The SH Senica plants were built in the 20st of the last century with the aim of producing synthetic fibers. The plants were liquidated in 2005. The activity connected with the creation of EB, has not been carried out since 1989. During their activity (production of synthetic fibers), an extensive fuel oil farm was built consisting of 7 fuel oil tanks, a boiler room, and a pumping station. The tanks have already been demolished. There was also a neutralization station, chemical warehouses (HCl, etc.). The activity that influenced the creation of EB is no longer carried out on the site, the operation is used for other purposes. In the western part of the area, there is currently a variety of industrial activity unrelated to the activity causing the load. The data on the holder / holders of the burden listed in the IS EZ system were out of date at the time of the survey, the former holder has changed since 2014 and, as a result of the sale, there is still a change of owners of various parcels of the environmental burden.

At the time of the geological survey in 2022–2023, the current visual condition did not correspond to the condition of the site at the time of its registration in 2014.

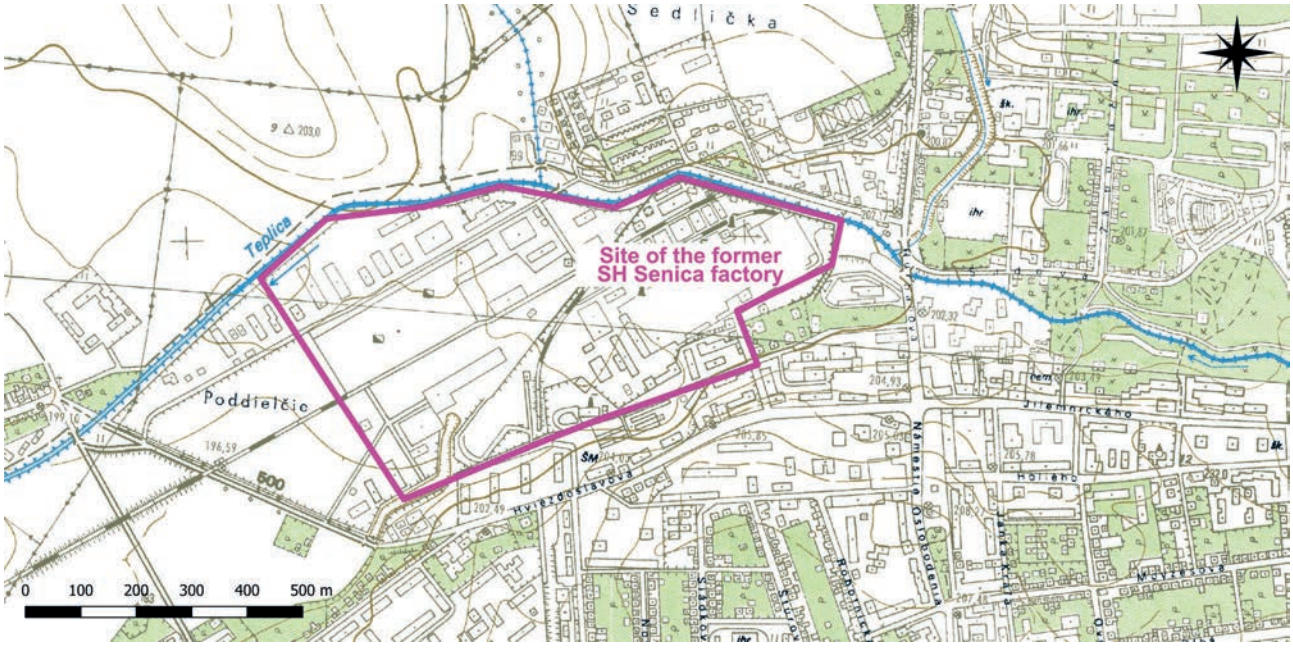

Fig. 1. Localization of the investigated site (IS EZ, 2014).

Fig. 2. A view of the site where tanks of the former fuel oil industry and chemicals were located (IS EZ, 2014).

In the eastern part of the territory, in the places of the most probable source of pollution, extensive construction and remediation activities were taking place, with land modification intended for further development activities of civil and housing construction. Decontamination and subsequent improvement of the land was carried out based on the recommendations of the environmental audit in the area of Slovenský hodváb PLUS, s.r.o. (Žitňan, 2011), consisting in the partial demolition and reconstruction of old decaying buildings, the removal of the existing fuel oil plant and demolition of the factory chimney (Fig. 3).

Directly in the area of the former Slovenský hodváb factories, groundwater quality monitoring was carried out in 2000 (Žitňan et al., 2000). The aim was to specify the direction of groundwater flow in the plants, to verify the quality of groundwater in the range of nonpolar solvents [NEL (IR)], SO_4 and Zn and measuring of physico-chemical parameters of existing wells in the SH area and three wells in the waste water treatment plant (WWTP) area. The results of the monitoring confirmed the south-west to west direction of groundwater flow in the SH area. From the analysed values, no exceeding values of STN 75 711 for Drinking water were proven in any sample, except for the conductivity in one water sample. Concentration of sulfate also did not exceed the respective limit values of STN valid at that time in any of the monitored objects, except for the values in the WWTP area, where they were on the border of the limit concentrations of the respective STN valid at that time. The contents of NEL (IR) in all monitored objects and in objects in the WWTP area did not exceed STN limit values. In 2011, an environmental audit was carried out in the plant area with the aim of an indicative verification of the pollution of the rock environment in the unsaturated zone and in the groundwater in existing objects and wells (reservoirs) in the eastern part of the area of the former SH plant (Žitňan, 2011). The scope of the monitored indicators was based on the nature of the activities and production processes (viscose production, fuel oil management) and on stored chemicals in the plant area, and thus formed an indicator of potential environmental contamination. A total of 16 soil samples with a sampling depth of up to 60 cm and 9 groundwater samples were taken. In addition, liquids were taken in various tanks and concrete tubs, the presence of which was confirmed at the time of the survey. The soil samples were analysed for the total NEL (IR) content and the content of selected indicators in the aqueous leachate. In the groundwater from existing wells, water samples were analysed in the range of $CHSK_{Cr}$, sulfates, sulfides, sodium and NEL (IR) indicators. The results were analysed according to the Instruction of the Ministry for the Administration and Privatization of the National Property of the Slovak Republic and the Ministry of the Environment of the Slovak Republic No. 1617/97-min. on the procedure for evaluating the company's obligations from the point of view of environmental protection in the privatization project submitted by the company as part of the privatization. Journal of the MŽP SR 1/98. Part VI. Indicators and standards for remediation of soil, soil and groundwater pollution. The results of the audit confirmed and located the contamination of the territory in the area of the track inside the area to a depth of 0.60 m. In the case of fuel oil farming, significantly high contents of petroleum substances NEL (IR) were confirmed, in some samples the values were high in the order of hundreds to thousands of $mg.kg^{-1}$. Most of the soil samples reached higher values than background values of category A (around 50 $mg.kg^{-1}$) and some of them already exceeded the limit value of category "B" and even the limit values for remediation category "C". Removal of contaminated soil by mechanical excavation was proposed. The result of the environmental audit was the finding that the groundwater is not critically contaminated and does not indicate the

Fig. 3. Views on the reclaimed eastern and western industrial part of the area after sanitation and reclamation as well as its surrounding (taken from Grexová et al., 2023).

need for remedial interventions. For a more detailed assessment of the extent of soil pollution in the basement of the halls and other buildings, it was recommended, after the renovation of the buildings and cleaning of the area, the implementation of a regular network of shallow boreholes up to approx. 1.0 m below the ground for soil sampling in the scope of the NEL (IR) and four complete analyses according to the instructions of the MSPNM SR and the Ministry of the Environment SR No. 1617/97-min. (Žitňan, 2011).

A complex geological survey ensuring detailed identification of surface and spatial pollution was not carried out in the area of the former plants.

2 Geological and hydrogeological characterization of the investigated site

According to the regional geological division of the Western Carpathians (Vass et al., 1988), the territory belongs to the area of intermountain basins and basins, the sub-region of the Vienna basin, the Senica part. The Vienna basin is of Baden origin, it is filled with Neogene (mainly marine) sediments several thousand meters thick. In the studied area, the entire layer sequence of the Neogene is developed, with the exception of the Aquitan with numerous hiatuses. The geological structure is complex, laterally and vertically variable. The basin itself is divided by a number of faults, which mostly

follow the Carpathian direction NE–SW. At the base, the Neogene is lithologically represented by a formation of sandstones, sands and sandy clays, in the upper positions (lower Pannonian) fine-sandy marly clays and fine-sandy clays predominantly greenish-gray with positions of marls were sedimented. The uppermost positions are built by pelitic sediments of the Helvetian. These are greenish-gray, mostly slightly gray to slightly sandy, loamy, semi-solid calcareous clays or loams in layered positions. The top positions of these rocks are intensively weathered to decomposed, of the nature of clays of low to high plasticity, firm consistency. In the Quaternary, tectonic differentiation according to faults and erosive-denudative modeling of the relief with accumulation of sediments continued in the territory. The Quaternary is built by Pleistocene fluvial sediments, which mainly build the terraces of Morava. Holocene alluvial sediments deposited in the floodplain of Teplice and its tributaries are lithologically represented by covering cohesive clays, sandy clays to clays, which form an overburden of clay-sandy to sandy gravels, sands with gravels, or clayey sands. Gravel can be characterized as monomictic, formed by well-worked sandstone clasts up to 5 cm in diameter, occasionally 7–10 cm. The cohesive soils of the alluvial floodplain facies are sometimes overlain by aeolian sediments. The geological structure of the studied area is influenced by the sediments of the Neogene fill and its Quaternary cover (Baňacký et al., 1973). The Quaternary is mainly represented by lithologically unorganized fluvial sediments of the Holocene – floodplain clays or sandy to gravelly clays of valley floodplains and mountain tributary floodplains (fhh). They are the youngest and most widespread fluvial sediments, emerging in the form of valley floodplains (floodplain terraces) of rivers and streams. Postglacial alluvial floodplain sediments form a substantial part of the fine-grained sedimentary surface cover of the sand-gravel assemblage of bottom accumulation of rivers, or just a separate filling of valleys in the cross profile of all streams. Alluvial sediments of larger rivers form the lithofacies of the most varied laterally and horizontally changing assemblage, manifested by the rapidly changing microrelief of the floodplains and the complicated structure and lithofacies composition of the sediments.

The upper parts of the floodplain of the Teplica stream consist of dusty sandy deposits 1.5–5.4 m thick. In some places, they contain thin layers and lenses of putrefaction (Baňacký et al., 1973). In the north and northwest, fluvial sediments of the older Pleistocene emerge – gravels and sandy gravels of higher middle terraces covered with loess, deluvial clays and washes. In the wider vicinity of the site, there are also eolian sediments of the younger Pleistocene (loess and fine sandy loess, calcareous and loess clays in general), proluvial sediments of the Holocene (mainly clays and sandy loams with rock fragments and muddy gravels in alluvial alluvial cones) and younger Pleistocene (clay and sandy gravels with rock fragments in low alluvial cones with a cover of loess and deluvial washes). The thickness of the Quaternary is variable, mostly from 2 m to 8 m (Žitňan, 2011).

Hydrogeological monitoring and temporarily equipped (mapping) boreholes (Grexová et al., 2023) verified quaternary (Holocene – anthropogenic sediments) to Neogene (Miocene – claystones, siltstones, sandstones) lithotypes in the investigated area. The Quaternary of the studied area is represented in the near-surface layer by fluvial sediments of the nature of clays and sandy gravels at a depth with an irregular thickness from 5.0 m to 9.0 m above sea level. (189.63–193.57 m above sea level). The Neogene bedrock is represented by Miocene clay-type sediments and clayey clays of a stiff to firm consistency. In the eastern part of the former SH plants, the thickness of Quaternary sediments ranges from 6.50 m to 9.0 m, in the western part of the former plants, the thickness of Quaternary sediments varied between 5.0 and 8.5 m. In summary, it can be concluded that the interface between the Quaternary and the Neogene varies at the level from 189.63 to 193.57 m above sea level, depending on the location of the wells near the main recipient of the Teplica River. Geological sections A–A', B–B', C–C' and D–D' in the area of the investigated area documenting the geological structure of the site of the former SH plants verified by survey in 2022–2023 are shown in Fig. 4. Based on the hydrogeological regionalization of Slovakia (Šuba et al., 1984), the territory belongs to the hydrogeological region N 002 Neogene Chvojnická pahorkatina. The region is bounded in the south by the Myjava plain, in the west by the Morava plain, in the northeast by the White Carpathians and in the east by the Myjava highlands. The region is built in the Neogene and Paleogene with a thin cover of Quaternary loess, loess clay, deluvium and, in the western part, also white sands. The investigated area itself is located in the extravillage of the cadastral territory of the city of Senica, in the right-hand valley floodplain of the Teplica stream.

The geological environment creates favorable conditions for the creation and accumulation of groundwater with the ceiling of the water collector at the level of 193.41–196.30 m above sea level. The depth of the groundwater level of a free nature is in the range of 1.80–5.50 m p.t. and the general flow direction is westward. The fairly strong permeability of fluvial gravels was documented by hydrodynamic tests with a filtration coefficient in the range of $6.65.10^{-4}$–$9.92.10^{-4}$ $m^2.s^{-1}$ (Grexová et al., 2023). The underground water of the investigated area has the character of a predominantly distinct basic type with a predominance of the calcium-hydrogen carbonate component. The chemical composition of groundwater of fluvial gravels in the substrate of

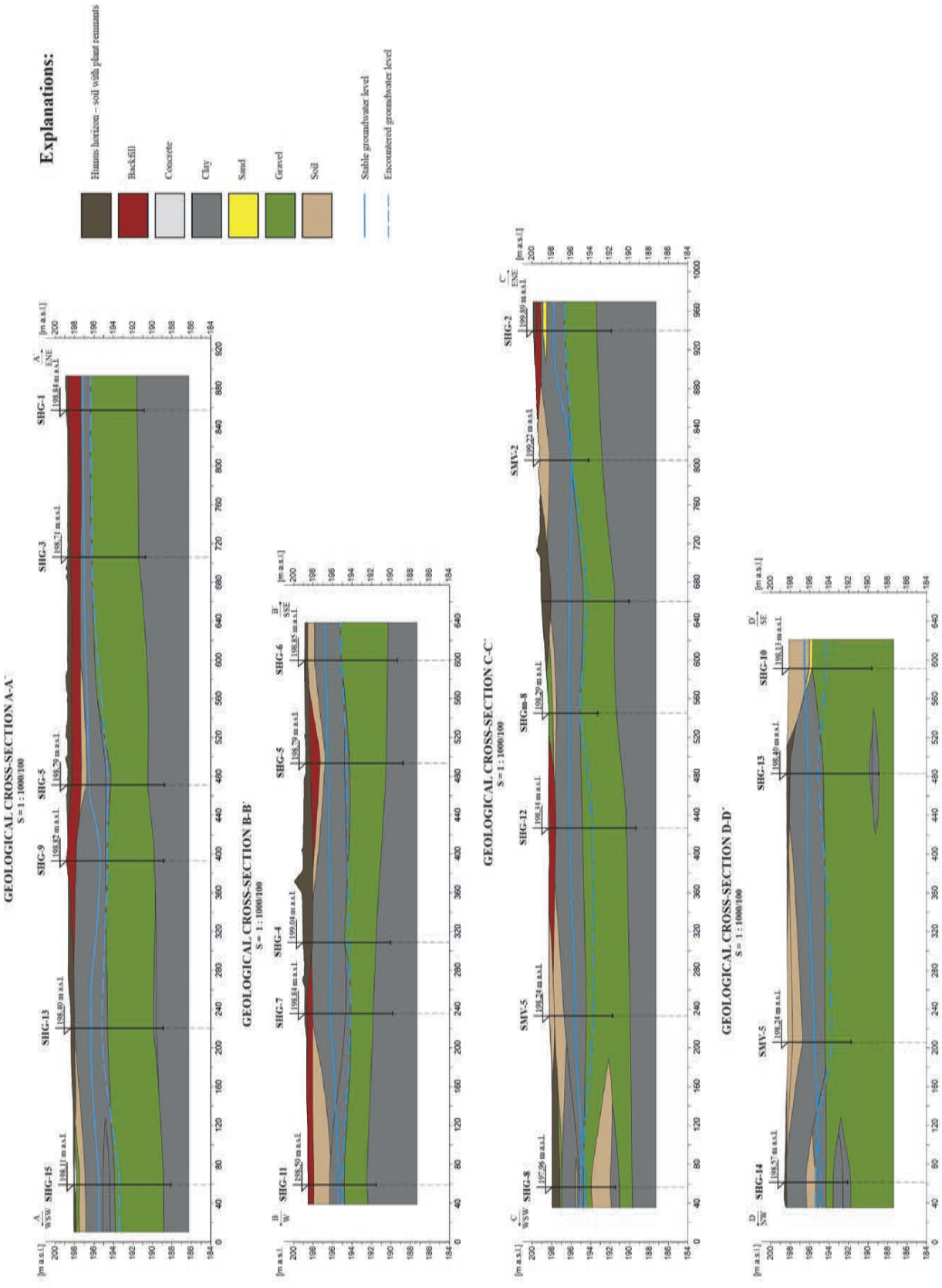

Fig. 4. A view of the reclaimed eastern and western industrial part of the area after sanitation and reclamation (taken from Grexová et al., 2023).

Holocene alluvial sediments is stable, predominantly bicarbonate component (HCO_3 > Ca + Mg), with the most common type of groundwater of carbonate class, calcium group, first to third class [CCaIa to CCaIIIa (Alekin)]. Overall picture the chemical composition of groundwater is documented by the graphic interpretation of the semi-logarithmic diagram according to Schoeller, which documents the stable chemical composition of groundwater in the investigated area of probable environmental stress, Fig. 5.

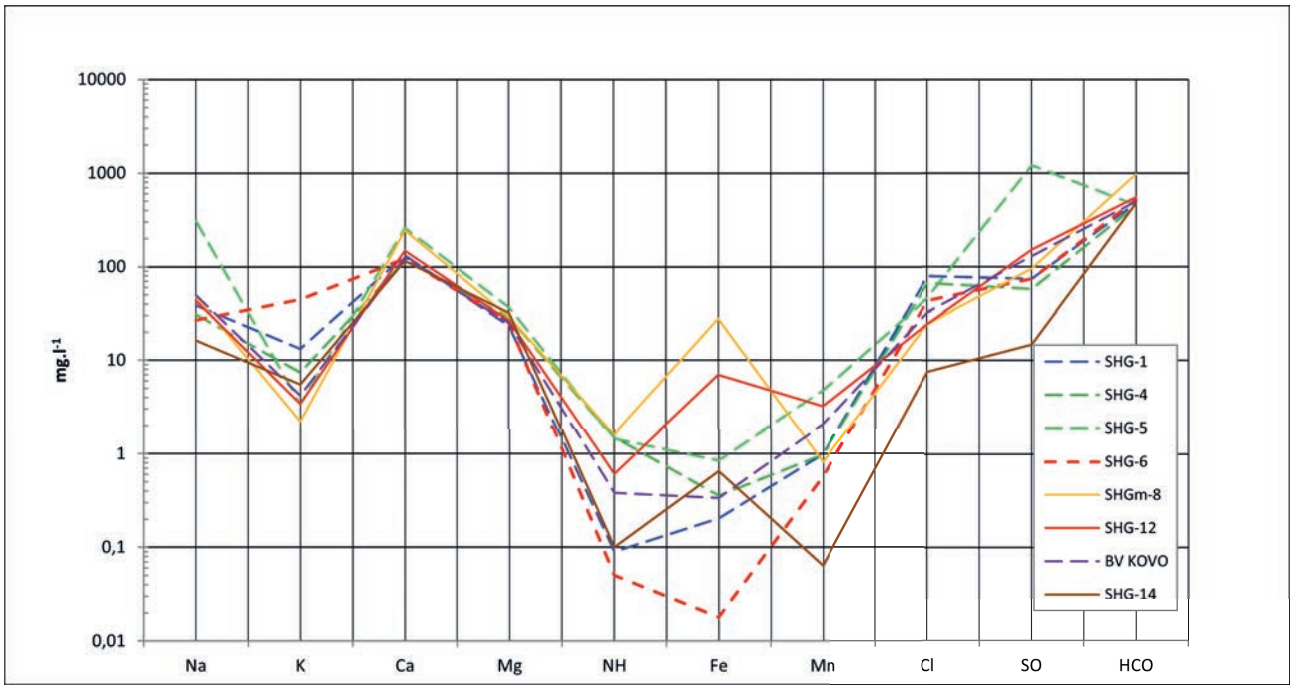

Fig. 5. Schoeller's graph of the ions concentration in groundwater in the area of the former SH plants (Grexová et al., 2023).

3 Methods

The methodology of the realized detailed geological survey based on the currently valid legislation of the Slovak Republic, namely the Methodological Guide for the Geological Survey of the Environment in a Polluted Area (SAŽP, 2020) and Directive of the Ministry of the Environment No. 1/2015-7 for the analysis of the risk of the polluted area.

A set of geological works was carried out on the site, aimed at a comprehensive survey and characterization of the pollution of all components of the environment, including the evaluation of the potential health and environmental risk resulting from any detected pollution. Realized works in the area of probable environmental burden included technical works (drilling works) for the purpose of specifying the geological structure of the site and the extent of contamination of the rock environment and underground and surface waters, measurements and sampling of the rock environment in the aeration zone and the saturation zone, sampling of underground, surface and wastewater from newly built and existing wells, atmospheric geochemical measurements, soil air sampling, chemical analyses of groundwater samples, chemical and granular analyses of rock samples. The methodology of the survey works is described in detail in the work of Grexová et al. (2023).

As a part of the technical works, 15 hydrogeological monitoring wells, 5 unequipped exploratory mapping wells and 15 manual diagnostic gasometric probes were drilled, Fig. 6. The depth of the built-in hydrogeological wells varied between 9 and 12 m, the depth of the mapping wells was 5 m. Manual probes were carried out to a maximum depth of 1 m. The basic parameters of the wells are listed in Tab. 1.

Atmogeochemical measurements

Atmogeochemical in-situ measurements of soil air were carried out using hammered tube probes with a total length of approx. 1 m in the locations of manual gasometric probes, hydrogeological and mapping wells, this means that the measurements correspond to the composition of soil air approx. 80 cm – 90 cm from the reclaimed surface of the investigated area with the aim of identifying volatile pollutants in the soil air, indicating contamination of the soil / rock environment with petroleum substances. The measurements were carried out using a portable field device

Tab. 1

Basic parameters of realized hydrogeological and mapping wells

Object	Depth [m]		Drilling			Equipment	
	Projected	Realized	Date of realization	Drilling diameter / ensuring [mm]	Range of depth [m]	Instalation diameter [mm]	Perforation [m]
Hydrogeological monitoring wells (129 m)							
SHG-1	10.0	8.0	15/5/2023	196/175	0/2/2–7/7–8	125	2.0–7.0
SHG-2	10.0	8.0	15/5/2023	196/175	0–3/3–5.5/5.5–8	125	3.0–6.5
SHG-3	10.0	8.0	15/5/2023	196/175	0–2.5/2.5–7/7–8	125	2.5–7.5
SHG-4	10.0	9.0	16/5/2023	196/175	0–4.5/4.5–7.5/7.5–9	125	4.5–8.5
SHG-5	10.0	10.0	15/5/2023	196/175	0–5.3/5.3–8.3/8.3–10	125	5.5–8.5
SHG-6	10.0	9.5	17/5/2023	196/175	0–3.5/3.5–8.5/8.5–9	125	3.5–8.5
SHG-7	10.0	9.0	16/5/2023	196/175	0–4/4–7/7–9	125	4.0–7.0
SHG-8	10.0	6.5	18/5/2023	196/175	0/3/3–5/5–6.5	125	3.0–4.5
SHG-9	10.0	10.0	17/5/2023	196/175	0–4/4.0–7.0/7–9	125	4.0–9.0
SHG-10	10.0	9.0	19/5/2023	196/175	0–4/4–8.5/8.5–9.5	125	4.0–8.5
SHG-11	10.0	7.0	18/5/2023	196/175	0–3/3–6/6–7	125	3.0–6.0
SHG-12	10.0	9.0	18/5/2023	196/175	0–3.5/3.5–8/8–9	125	3.0–8.0
SHG-13	10.0	9.5	17/5/2023	196/175	0–3/3–8.5/8.5–9.5	125	3.0–8.5
SHG-14	10.0	6.5	18/5/2023	196/175	0–3.5/3.5–5/5–6.5	125	3.5–5.0
SHG-15	10.0	10.0	17/5/2023	196/175	0/4.5/4.5–9/9–10	125	4.5–9.0
Exploration unequipped mapping wells (26.5 m)							
SMV-1	10.0	5.0	18/5/2023	156	0–3/3–5	110	3.0–5.0
SMV-2	10.0	5.0	18/5/2023	156	0–3/3–5	110	3.5–5.0
SMV-5	10.0	5.0	19/5/2023	156	0–3/3–5	110	4.5–6.5
SMV-3	10.0	5.0	19/5/2023	156	0–3/3–5	110	3.0–5.0
SHG_M-8	10.0	6.5	19/5/2023	156	0–3/3–5	110	3.0–5.0
Manual gasometric probes (13.45 m)							
SPS-1–SPS-15	1 m	0.0	XII/2022	–	0.5–1	0.50	–

ECOPROBE 5 from RS Dynamics, which enables, among other things, online measurements of methane, oxygen and carbon dioxide concentrations. The field instrument also determined the content of other relevant gases (O_2, CH_4, CO_2, PID) and total petroleum hydrocarbons (T.P) from the soil air. The measurement consisted in suctioning and subsequent analysis of soil air with a device from unequipped mapping wells, newly built hydrogeological wells and hand probes. The instrument used verified the overall spectrum of soil gas and vapor concentrations. A total of 35 atmogeochemical measurements were carried out.

Sampling works

Sampling works consisted of taking samples of soil, underground and surface water and river/bottom sediments,

taking soil air and taking waste water from the WWTP, Fig. 6. Groundwater and surface water samples were taken in two cycles, soil air and soil samples were taken once during drilling operations. The density, method and amount of samples taken was specified by the responsible researcher and was stated in the Sampling Plan of the rock environment, underground and surface water, developed according to Annex No. 17 of the Methodological Guide for the Geological Survey of the Environment in a Polluted Area, (SAŽP, 2020). A complex map of documentation points and environmental sampling is interpreted in Fig. 7.

Soil sampling was carried out with the aim to determine the area and spatial distribution of the rock environment pollution at different depth levels to map the centres of pollution and delineate the contamination clouds of the aeration zone and the saturation zone. Samples were taken using a shovel into PE bags or glass bottles in a total amount of 0.5–1 kg, depending on the purpose. During sampling, the pollution was evaluated sensory – smell and visual assessment of the signs of pollution. A total of 90 soil samples were taken, of which 83 soil samples were used to determine selected indicators, including control samples, 5 soil samples were used to determine the physico-mechanical properties of soils, 2 samples were used to determine leachability, including ecotoxicity on selected soil samples.

Soil air sampling was carried out using a soil probe at a depth of approximately 1.5 m located at the location of the drilling/probes. The wellhead was insulated. The pumping of soil air itself was performed by a peristaltic pump as a part of the ECOPROBE 5 device. The flow rate was set to 0.5 l/min for a pumping time of 5 min, which represents 2.5 l of extracted air. The soil air was adsorbed onto an SKC tube, which was sealed with plastic plugs immediately after sorption and placed in the cold. A total of 40 soil air samples were taken to determine selected indicators.

Sampling of groundwater and surface water and bottom sediments as part of the survey was carried out in accordance with the applicable STN EN ISO 5667 standards as well as the instructions of the accredited laboratory and technical possibilities in the field and was carried out in two rounds. A Gigant type pump was used for sampling. The following were determined directly in the field: temperature, pH, conductivity, ORP and O_2. A total of 53 groundwater samples and 9 surface water and sediment samples were taken for the analysis of selected indicators.

Part of the sampling work was also the determination of the organoleptic properties of the samples, i.e. temperature, colour, turbidity, transparency, or taste. These sensory evaluations were performed for each sample collected and documented in each sample collection protocol / record. A total of 153 organoleptic determinations were carried out. The comprehensive range of analyses is documented in Tab.2.

Fig. 6. Realization of geological works during the geological survey.

Tab. 2

Sampled objects and scope of analyses

Rock environment – soil	**Scope of analyses**
Wells: SHG-1, SHG-2, SHG-3, SHG-4, SHG-5, SHG-6, SHG-7, SHG-8, SHG-9, SHG-10, SHG-11, SHG-12, SHG,13, SHG-14, SHG-15, SMV-1, SMV-2, SMV-3, SMV-5, SHGm-8 Manual probes: SPS-1 to SPS-15	NEL-GC, ClU, BTEX, TOC, PAU, sulfur total, sulfur sulphide, trace elements (As, Cr, Cd, Cu, Pb, Zn, Hg, B), leachate, native sample + ecotoxicity in accordance with Decree No. 382/2018 Coll., physical and mechanical properties of soils
Rock environment – soil air	**Scope of analyses**
Sampling sites in the Teplica area: DS-1, DS-2, DS-3	NEL-GC, TOC, PAU, BTEX, CIU, trace metals: (As, Cr, Cd, Cu, Pb, Zn, Hg)
Underground water	**Scope of analyses**
Wells: SHG-1, SHG-2, SHG-3, SHG-4, SHG-5, SHG-6, SHG-7, SHG-8, SHG-9, SHG-10, SHG-11, SHG-12, SHG,13, SHG-14, SHG-15, SMV-1, SMV-2, SMV-3, SMV-5, SHGm-8, S-1, well BV-kovo	NEL-GC, PAU, BTEX, CIU, sulfur sulphide, B, TOC, As, Cr, Cd, Cu, Pb, Hg, Zn, basic physico-chemical analysis + Palmer–Gazda, microbiology (minimal),
Surface water	**Scope of analyses**
Sampling sites on the Teplica area: PV-1, PV-2, PV-3	Annex No. 1 GR No. 269/2010 part A, Annex No. 1 GR No. 269/2010, part B
Waste water	**Scope of analyses**
WWTP	Annex No. 6 GR No. 269/2010, tab. 6.8: water reaction-pH, insoluble substances (NL), CHSKCr, BSK_5

To evaluate the soil and groundwater pollution, chemical analyses were performed in the accredited Geoanalytical Laboratories of the ŠGÚDŠ in Spišská Nová Ves according to standard procedures. The samples were, depending on their nature, analysed by different analysers: atomic absorption spectrometry – mercury analyser, atomic emission spectrometry with inductively coupled plasma, coulometry, photometry, gas chromatography with electron capture detector, gas chromatography – mass spectrometric detector and – flame ionization detector, ion chromatography, mass spectrometry with inductively coupled plasma.

As a priority, samples of the rock environment of the aeration zone and saturation zone and groundwater were taken and evaluated with regard to the indication and intervention criteria specified in the directive of the Ministry of the Interior of the Slovak Republic no. 1/2015-7 to develop a risk analysis of the polluted area.

The indicator criterion (ID) is the limit value of the concentration of the pollutant determined in the rock environment and groundwater, exceeding which can endanger human health and the environment, which implies the need to start monitoring of the polluted area.

The intervention criterion (IT) is the critical value of the concentration of the pollutant determined in the rock environment and groundwater, the exceeding of which presupposes, already with the given method of land use, a high probability of endangering human health and the environment, which implies the necessity of developing a risk analysis of the polluted area. As it is planned in the future in the eastern part of the former SH Senica plants to change the use of the territory to a residential zone, and thus from an environmental point of view, a more sensitive territory, as a precaution, we proceeded to evaluate the intervention criteria (IT) in this part of the territory according to stricter criteria, and therefore ratings for residential zones.

Qualitative parameters of the groundwater taken from existing wells were compared in accordance with the requirements of decree No. 91/2023 of the Ministry of Health of the Slovak Republic, establishing indicators and limit values of drinking water quality and hot water quality, the procedure for monitoring drinking water, risk management of the drinking water supply system and risk management of domestic distribution systems.

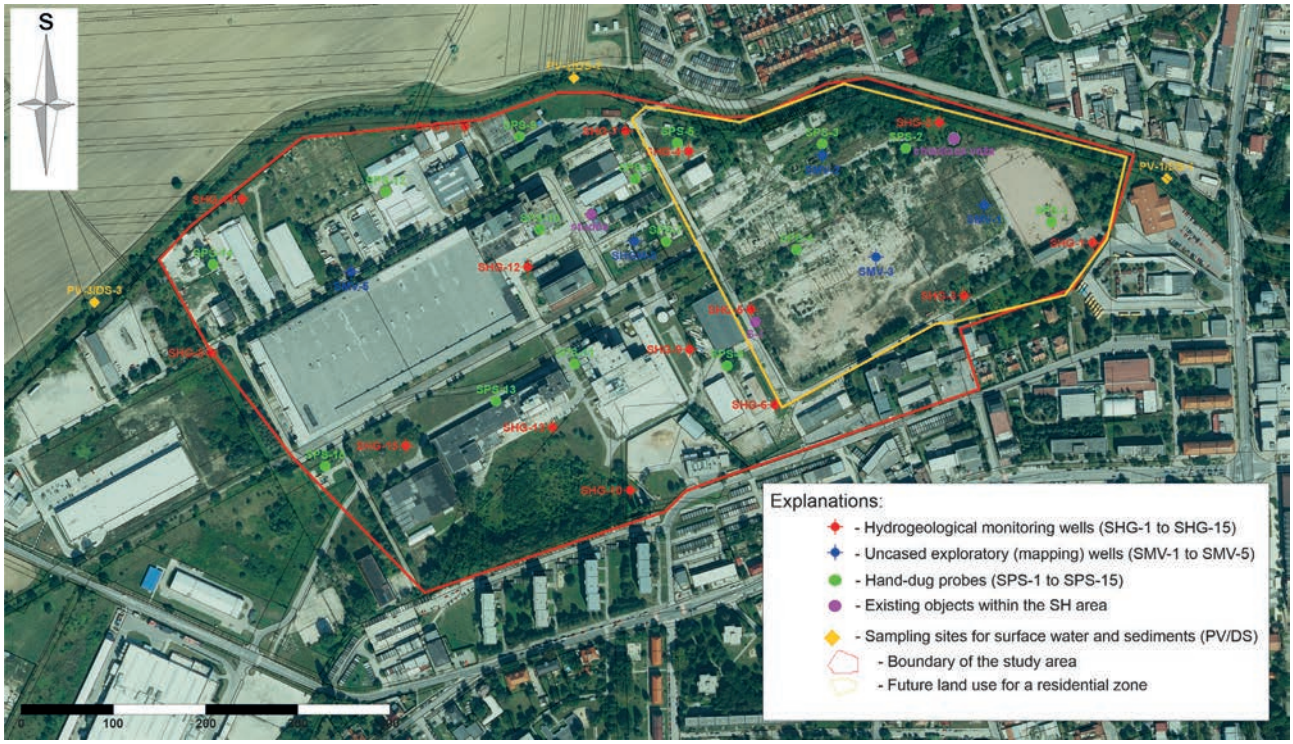

Fig. 7. Map of documentation points and sampling (taken from Grexová et al., 2023).

The evaluation of the soil air samples taken was carried out in accordance with the instruction of the Ministry for the Administration and Privatization of National Property of the Slovak Republic and the Ministry of the Environment of the Slovak Republic on dated December 15, 1997 No. 1617/97-min.

Qualitative parameters of sampled surface water and wastewater were compared in accordance with the requirements of SR Government Regulation No. 269/2010 Coll., which establishes requirements for achieving good water status.

The leachate and native sample, including ecotoxicity for soil classification in terms of waste management, were evaluated in accordance with the requirements of the Decree of the Ministry of the Interior of the Slovak Republic No. 382/2018 Coll. on waste dumping and storage of waste mercury.

In more detail, the methodology of the geological works carried out is given in the final report of Grexová et al. (2023).

4 Results

The aim of the detailed survey was to verify and identify the detected potential pollution of all components of the environment.

Pollution of the rock environment, of the soil and soil air

Before drilling, soil air samples were taken at the locations of manual probes and planned wells, in which, due to the nature of the site, the presence of petroleum hydrocarbons determined as benzene and toluene were detected. Higher concentrations of indicators exceeding

Tab. 3

Concentration of potential carcinogens in soil air samples (taken from Grexová et al., 2023)

Parameter	Unit	B	C	Planned residential zone				Reclaimed industrial zone			
				SPS-3	SPS-3_k	SPS-5	SPS-5_k	SPS-10	SPS-10_k	SPS-13	SPS-13_k
Benzene	mg/m^3	1	5	28	< 0.4	48	< 0.4	10	< 0.4	5	< 0.4
Toluene	mg/m^3	5	10	7	< 0 .4	19	< 0.4	< 1	< 0.4	5	< 0.4

B – to determine the origin of the pollution source
C – to start remediaton or other survey

concentrations B and C of MSPN instruction No. 1617/97-min., were confirmed only in manual probes of the SPS type. By repeated control sampling in which were not confirmed higher concentrations, we evaluated as pollution of a point nature, with the probability of affecting ongoing construction works and the possibility of free access for the public in the eastern part of the former plants, which is not related to the activity that conditions the inclusion of the investigated area into the system of environmental burdens (ISEZ), Tab. 3.

Results of soil air analyses from soil samples taken from the aeration zone and the saturation zone from wells (SHG, SMV) and probes (SPS) confirmed low concentrations in all analysed parameters not exceeding the indication and intervention criteria of the *Guidelines of the Ministry of the Environment SR No. 1/2015-7* to develop a risk analysis of the polluted area. Exceeding the indication and intervention criterion of the directive for residential zones was confirmed by higher concentrations of mercury (SPS-1: 3.76 mg.kg^{-1} of dry matter), copper (SPS-3: 593 mg.kg^{-1} of dry matter) and lead (SPS-3: 1 860 mg.kg^{-1} of dry matter). The detected higher concentrations were not confirmed by control samples (Cu – SPS_K-3: 32 mg.kg^{-1} of dry matter), (Pb – SPS_K-3: 24 mg.kg^{-1} of dry matter) located in the eastern part of the investigated site, Tab. 4.

From the hydrogeological monitoring wells of the SHG, elevated concentrations of trace metals exceeding the indication criterion of the directive were detected in the indicators of copper (548 mg.kg^{-1} of dry weight) and the intervention criterion for lead (593 mg.kg^{-1} of dry weight) only in the well SHG-10, located in the new of the industrial part of the area of the former Slovenský hodváb plants, whose current activity is not related to the activities of the factories causing environmental burden. Elevated concentrations of trace metals were also confirmed by control sampling, when according to more stringent criteria, and thus the assessment for residential zones, the concentrations of the monitored indicators slightly exceeded the intervention criterion, Tab. 4.

In this well, a high concentration of NEL-GC (nonpolar solvents analysed by gas chromatography) exceeding the indication criterion (774 mg.kg^{-1}of dry matter) was also detected, which was also confirmed by a control sample, which proved that the concentration was exceeded within the intervention criteria of the directive of the Ministry of the Interior of the Slovak Republic No. 1/2015-7 min. (774 and 3 179 mg.kg^{-1} of dry matter). Identification of

Tab. 4

Overview of indicators exceeding ID or IT criteria in accordance with the directive of the Ministry of the Environment of the Slovak Republic No. 1 / 2015-7 in a rock environment (taken from Grexová et al., 2023)

Indicator	Indication criteria	Intervetion criteria		Planned residential zone				Reclaimed industrial zone			
	(ID)	*Residential zones ITr*	**Industry ITi**	SPS-1	SPS-3	SPS_k-3	SMV-3	SPS-9	SPS_k-9	SHG-10	SHG_k-10
	[mg.kg^{-1} dry matter]			0–1,0 m u.t.			0,2–0,5 m u.t.	0–1,0 m u.t.		2 m u.t.	
I. METALS											
As	65	*70*	**140**	12	5	11	9	3	–	5	8
Cd	10	*20*	**30**	< 0.001	< 0.001	< 0.001	< 1	< 0.001	–	< 1	< 1
Cr_{total}	450	*500*	**1 000**	64	90	80	170	73	–	85	106
Cu	500	*600*	**1 500**	19	593	32	73	12	–	548	*713*
Hg	2.5	*10*	**20**	3.76	0.22	0.98	0.42	0.03	–	2.33	3.39
Pb	250	*300*	**800**	69	**1 860**	24	77	46	–	*593*	*460*
Zn	1 500	*2 500*	**5 000**	103	1 485	532	392	165	–	346	462
VIII. POLYCYCLIC AROMATIC HYDROCARBONS (HALOGENATED)											
NEL-GC (C_{10}–C_{40})	200	*250*	**500**	28	46	–	*346*	**1 001**	35	*774*	**3 179**

hydrocarbons in the rock environment in the investigated location, when the concentration of NEL-GC exceeded the IT criterion of the Ministry of the Interior of the Slovak Republic No. 1/2015-7 pointed out in the case of the hydrogeological monitoring borehole SHG-10 (1.5–2.0 m above sea level) and SHGK-10 (control sampling) and in the mapping borehole SMV-3 (0.2–0.5 m above sea level) for the dominant percentage representation of hydrocarbons of the C16–C24 series (heating oils; Fig. 8).

Local pollution by aliphatic petroleum hydrocarbons of the rock environment of the biological contact zone is illustrated in Fig. 9. The pollution is characterized by residual hydrocarbons that have the character of low-volatile hydrocarbons, with low solubility and a high degree of retardation (limitation of migration) in the rock matrix. The confirmation of the local presence of this hydrocarbon in part of the investigated area is, according to the oral information of the current owner, a consequence of the remediation of the hot water boiler for burning fuel oil in 2000, which in the past ensured the central heating of the city of Senica, and therefore with a high probability it is a residual pollution. In summary, it can be concluded that the slightly increased concentrations confirmed only in manual probes are with a high probability point pollution of a residual nature as a result of the implemented partial rehabilitation of objects in the planned residential

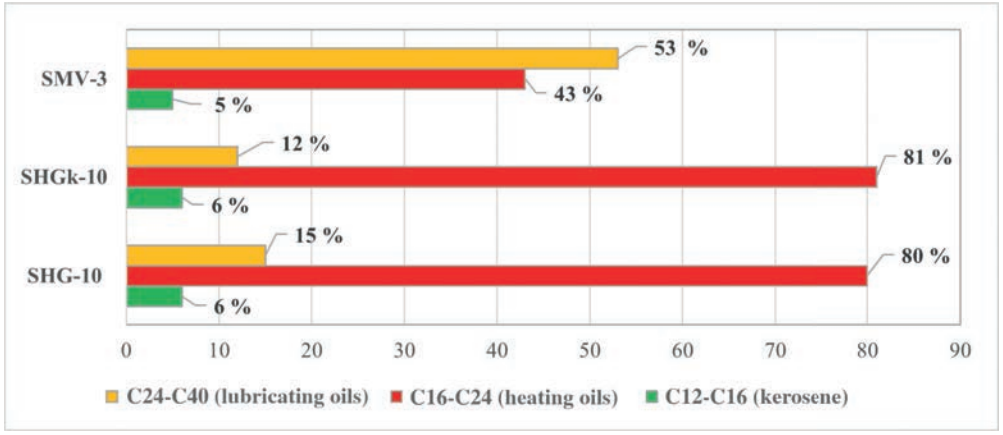

Fig. 8. Concentration of individual hydrocarbon fractions in the rock environment of the biological contact zone in the soil samples taken from the hydrogeological monitoring well and the unequipped mapping well with high C10–C40 (taken from Grexová et al., 2023).

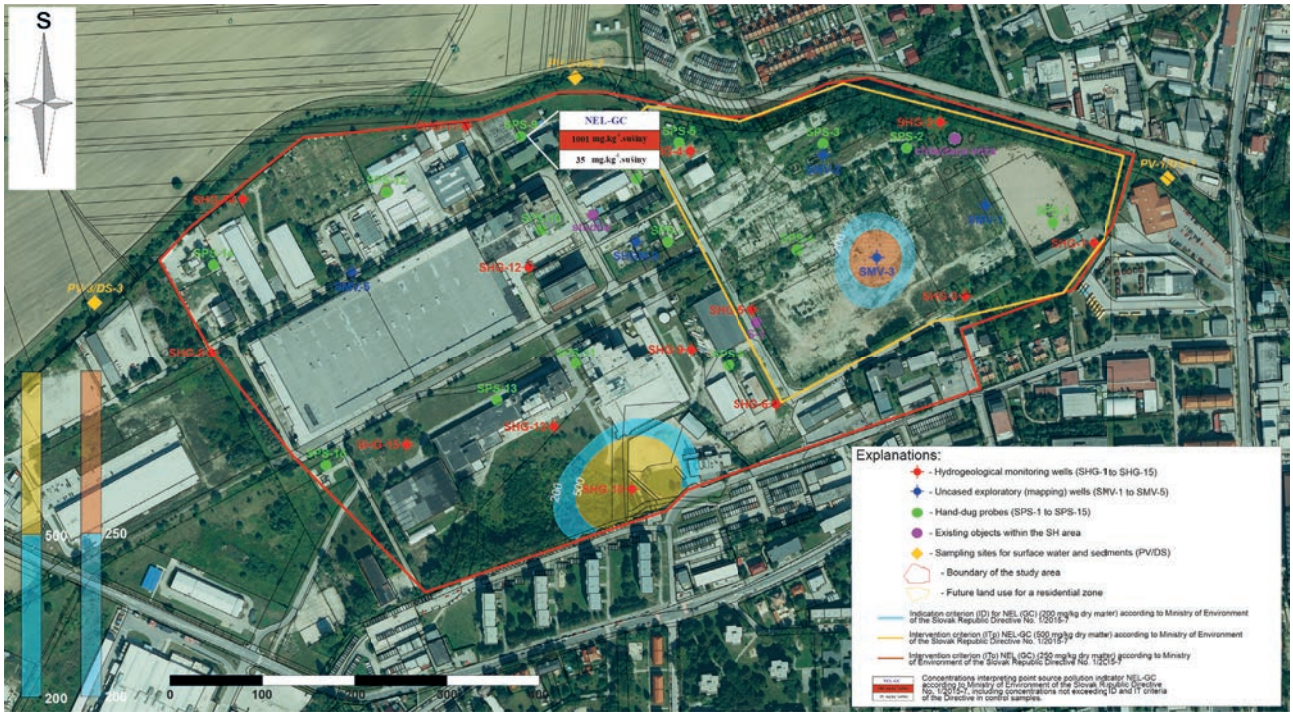

Fig. 9. Areal distribution of petroleum hydrocarbons in the studied site (taken from Grexová et al., 2023).

zone, which, according to the recommendations of the environmental audit (Žitňan, 2011), resulted in the removal of a potential source of contamination.

Groundwater pollution

Groundwater sampling carried out in two rounds with an interval of 30 days did not confirm water contamination, even in places where local residual pollution was confirmed. From all groundwater samples from hydrogeological – SHG wells, as well as unequipped SMV mapping wells and existing objects, the values of the monitored indicators were below the limit of detection, or at low values not exceeding the indication and intervention criterion of the Ministry of the Interior of the Slovak Republic No. 1/2015-7 to develop a risk analysis of the polluted area. An interesting fact was the slightly increased values of sulphide sulfur in the eastern part of the territory in only two of the five unequipped exploratory (mapping) wells located according to the historical map from 1958 in the places of the former old arm with maximum average concentrations not exceeding the indication criterion of the directive, Tab. 5. Sulphide sulfur occurs in waters as undissociated sulfane, simple HS^- and S^{2-} ions. Sulfane and its ionic forms are unstable in water. They can be chemically or biochemically oxidized to sulphates, it can be permanently present in water only in an anaerobic environment, therefore it is evidence for reduction processes in water. Since the exceeding of ID and IT limits was recorded only in samplings from unequipped mapping wells in the eastern part of the territory and in regime measurements in hydrogeological and mapping wells did not record negative values of oxidation-reduction potential (ORP) in this part of the investigated site, with a high probability this is the natural origin of occurrence in this environment, Tab. 6. Also, taking surface water samples from the stream of Teplica in two cycles in the direction of presumed pollution from the former plants did not confirm exceeding values of concentrations in any of the monitored indicators, as well as in groundwater samples.

Risk analysis of the investigated site

Risk analysis of the polluted area was also a part of the survey work. Its elaboration resulted from the legislative requirements of Directive No. 1/2015-7. Thus from the reason of the presence of pollutants exceeding the intervention and indication criteria in the rock environment of the biological contact zone in the aeration zone with the NEL indicator GC and trace metals Cu, Pb and Hg, an environmental and health risk assessment was required. An interpretation of the detected polluting substances in

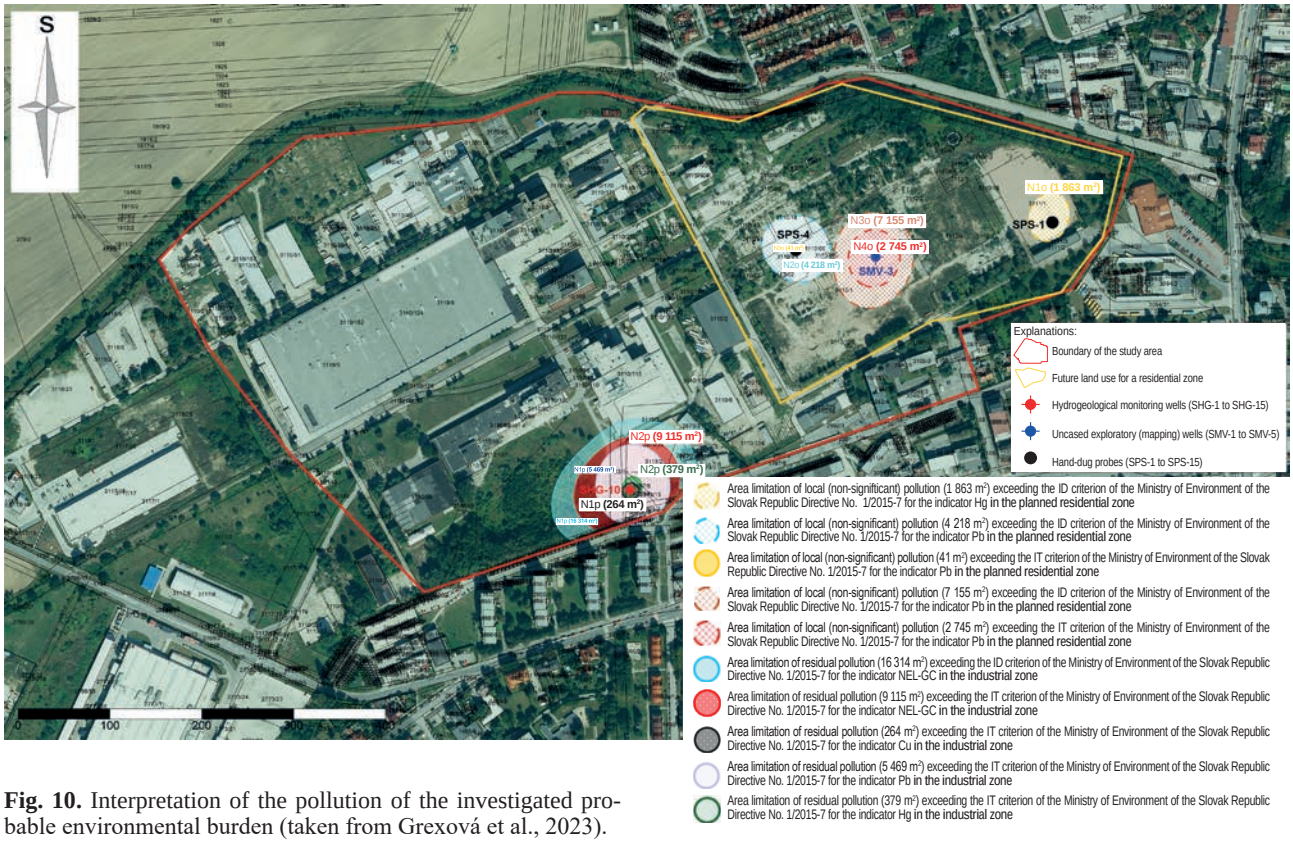

Fig. 10. Interpretation of the pollution of the investigated probable environmental burden (taken from Grexová et al., 2023).

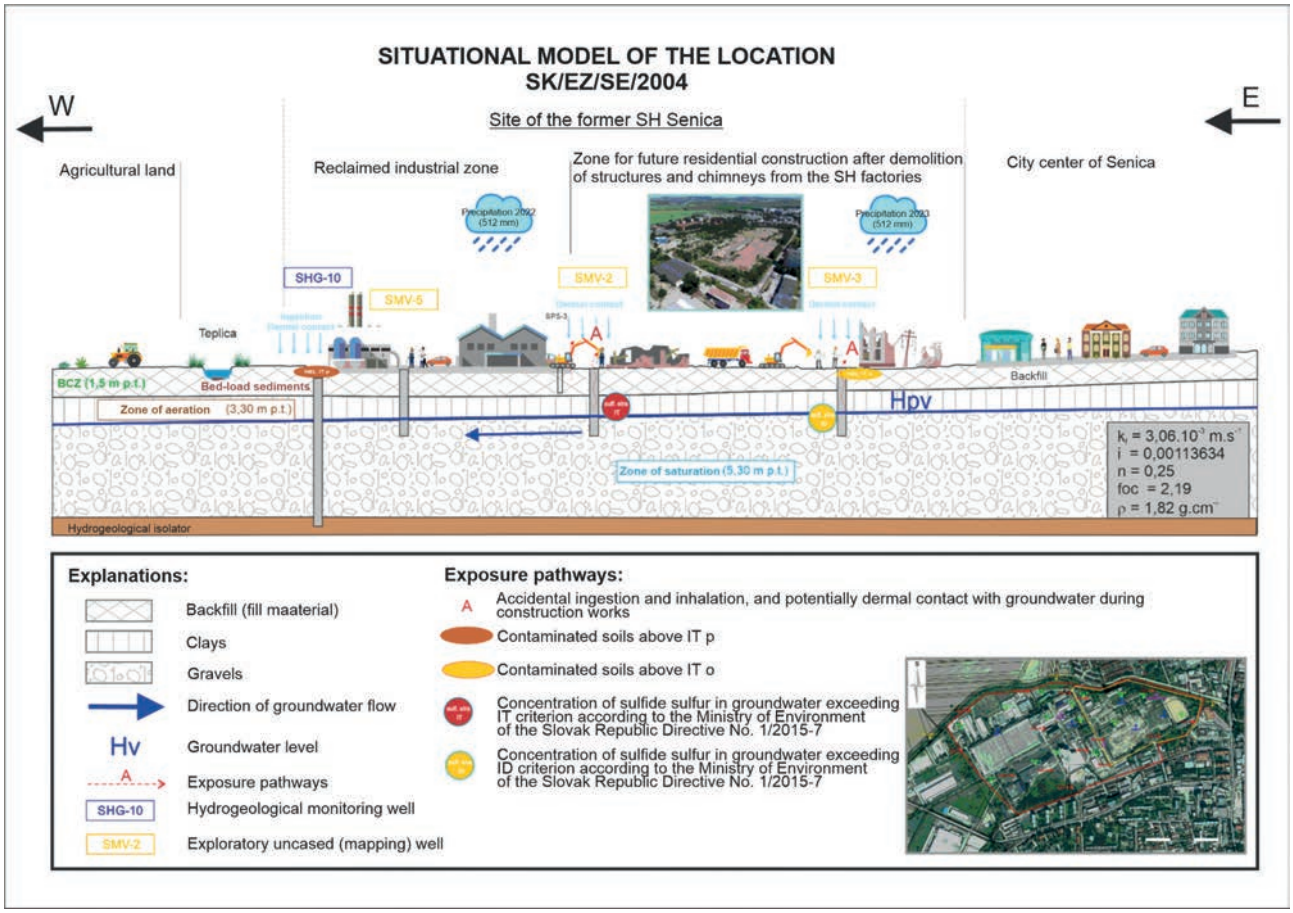

Fig. 11. Situation model of the site (taken from Grexová et al., 2023).

Tab. 5

Overview of indicators exceeding the ID or IT criteria in accordance with the directive of the Ministry of the Interior of the Slovak Republic No. 1/2015-7 in the groundwater of the investigated area (taken from Grexová et al., 2023)

Parameter	Directive No. 1/2015-7		SMV-1		SMV-3	
	ID [µg.l^{-1}]	IT [µg.l^{-1}]	1. sampling round	2. sampling round	1. sampling round	2. sampling round
IX. other						
Inorganic substances						
Sulfur sulphide (S sulp.)	*150*	300	330	370	< 10	*220*

the area of the former plants is shown in Fig. 10. Fig. 11 shows the situational model of the site, which is based on the results obtained from the geological survey according to Annex 4 to the directive of the Ministry of the Interior of the Slovak Republic No. 1/2015-7, which characterizes sources and centers of pollution, migration possibilities and possible transport routes of pollutants in the subject area. It also shows sources of environmental pollution as well as exposure scenarios in connection with the receptors present. The elaborated risk analysis did not identify an environmental or health risk, there was no need to propose costly remediation of the site.

Tab. 6

Results of field measurements of groundwater during the survey (source: Grexová et al., 2023)

Object	Date of sampling	Water temperature [° C]	Air temperature [° C]	pH	Electrolytic conductivity [mS.m^{-1}]	ORP [mV]	Dissolved O_2 [mg.l^{-1}]	At the temperature [° C]	Water saturation O_2 [%]	At the temperature [° C]
SHG-1	21.6.2023 10:42	13.5	23	7.02	109.0	198.9	1.720	13.5	16.80	13.5
SHG-2	21.6.2023 11:50	11.6	26	7.00	164.5	274.7	0.322	11.6	3.00	11.6
SHG-3	21.6.2023 9:54	12.6	22	7.00	121.6	249.2	0.268	12.6	2.60	12.6
SHG-4	27.6.2023 12:00	11.6	20	7,22	97.50	188.2	0.198	11.6	1.90	11.6
SHG-5	20.6.2023 15:52	12.7	30	7.20	279.0	57.6	1.300	12.7	12.50	12.7
SHG-6	21.6.2023 8:44	23.2	21	7.02	110.6	310.3	0.645	23.2	6.30	23.2
SHG-7	27.6.2023 12:30	12.3	20	7,29	85.9	59.8	0.470	12.3	4.40	12.3
SHG-8	21.6.2023 16:04	13.1	31	6.96	94.8	364.5	5.890	13.1	56.80	13.1
SHG-9	20.6.2023 12:08	13.6	28	6.85	166.3	104.1	0.267	13.6	2.60	13.6
SHG-10	20.6.2023 10:56	13.5	26	7.04	128.4	299.6	0.570	13.5	5.60	13.5
SHG-11	27.6.2023 11:25	11.8	20	7.07	180.1	178.5	0.240	11.8	2.40	11.8
SHG-12	20.6.2023 13:55	13.1	29	7.13	114.8	76.4	0.274	13.1	2.60	13.1
SHG-13	20.6.2023 11:40	13.4	27	7.05	115.7	184.0	0.525	13.4	5.20	13.4
SHG-14	21.6.2023 15:38	12.2	31	7.15	91.1	348.5	3.150	12.2	29.80	12.2
SHG-15	20.6.2023 12:35	13.4	28	7.13	114.5	165.8	0.516	13.4	4.90	13.4
SMV-1*	21.6.2023 11:16	13.1	24	7.02	137.2	8.4	0.552	13.1	5.30	13.1
SMV-2	21.6.2023 12:22	13.7	26	6.93	148,1	429.9	0.621	13.7	6.10	13.7
SMV-3*	21.6.2023 9:26	12.5	22	7.17	281.0	50.7	0.198	12.5	1.80	12.5
SMV-5	21.6.2023 15:00	12.3	28	6.99	129.3	143.1	0.273	12.3	2.60	12.3
SHGM-8	20.6.2023 15:18	12.8	30	6.85	159.7	0.9	0.195	12.8	1.80	12.8

* Objects with a higher concentration of sulphide sulfur content

5 Conclusion

In the years 2021 to 2023, ŠGÚDŠ carried out a detailed geological survey of the environment at a site of probable environmental burden with a high priority, where pollution of the rock environment and groundwater was assumed due to the industrial activity of the former Slovenský hodváb plants and the potential leakage of pollution from 7 fuel oil tanks and cooling towers. The quality of all the samples taken with the analytical evaluation of 210 indicators from an area of approximately 37 ha did not confirm the expected pollution resulting from the nature of the industrial activity of the environmental burden. From the obtained results in accordance with the currently valid legislative regulations, it can be concluded that no serious pollution of the underground water and rock environment was detected, either in the zone of aeration or in the zone of saturation with priority pollutants [NEL-GC, trace elements (As, Cr total, Cu , Hg, Pb, Zn), BTEX, CIU and PAU], which would be in a causal or spatial context.

Local pollution detected in the biological contact zone by the NEL-GC indicator, which was the only one of the wide range of indicators examined that exceeded the IT criterion of the Ministry of the Interior of the Slovak Republic No. 1/2015-7 is of a residual nature unrelated to the activities of the former SH plants. Pollution of groundwater with sulphide sulfur with increased concentrations exceeding the ID criterion of the Ministry of the Interior of the Slovak Republic No. 1/2015-7 in the planned residential zone, was sporadically and locally detected only in the eastern part of the investigated area, and only in exploratory unequipped mapping wells in the upper part of the incomplete watered collector. The presence of sulphide sulfur in the eastern part of the investigated area is of natural origin unrelated to reduction processes in water, which would be confirmed in this part of the environment.

Whereas the environmental and health risks have not been confirmed by the prepared risk analysis of the polluted area, it is not necessary to carry out remediation of the polluted area with the current use of the area. Due to the confirmed residual soil pollution in the western part of the newly built industrial part and the sporadic occurrence of sulphide sulfur in the groundwater, we recommend, as a precaution, two-year groundwater quality monitoring in this part of the site, after which, in the event of a favorable development of the groundwater quality, to remove the location from the Register of Information of the system of environmental loads of the Slovak Republic.

It can be concluded that the implementation of this survey is another positive step in the systematic solution of the problem of environmental burdens on the territory of the Slovak Republic, the results of which are the basis for the gradual improvement of the environment, including sustainability for future generations.

Acknowledgement

The contribution was made thanks to the financial support of the geological task *Geological survey of selected probable environmental burdens 3 – SGUDS* within the Operational Program Environmental Quality – priority axis 1: Sustainable use of natural resources through the development of environmental infrastructure, specific objective 1.4.2: Ensuring the remediation of environmental burdens in urban environment, as well as in abandoned industrial sites (including areas undergoing change), call code PKZP-PO1-SC142-2015-3, guideline No. 4, dated 18.10.2021.

References

Baňacký, V. & Sabol, A., 1973: Geological map of the Záhorská lowland. *Bratislava, GÚDŠ.*

Collective of authors, 2020: Methodological guide for environmental research in a polluted area., 1st ed. *Banská Bystrica, Slovak Environmental Agency, ISBN 978–80-8213--019-8, 170 p.*

Grexová, S., Danková, Z., Surový, M., Šottník, P., Kotuč, J., Adzimová, K., Zeman, I., Šefčík, P. & Lenhardtová, E., 2023: Geological survey of probable environmental burden "SE (2004) Senica – area of the former SH Senica" ISEZ SK/SE/2004. Final report. *Manuscript. Bratislava, archive ŠGÚDŠ.*

Paluchová, K., Auxt, A., Bruchánekova, A., Helma, J., Schwarz, J. & Pacola, E., 2008: Systematic identification of environmental burdens of the Slovak Republic, final report, SAŽP Banská Bystrica, MŽP SR Bratislava. *Manuscript. Bratislava, archive ŠGÚDŠ (arch. No. 89 101), 154 p.*

Šuba, J., 1984: Hydrogeological regionalization of Slovakia. *Bratislava, Slovak hydrometeorological institute, Hydrofond.*

Vass, D., Began, A., Gross, P., Kahan, Š., Köhler, E., Krystek, I., Lexa, J. & Nemčok, J., 1988: Regional geological division of the Western Carpathians and northern part of the Pannonian Basin on the territory of the Czechoslovakia 1 : 500 000. *Bratislava, GÚDŠ.*

Žitňan, M., 2000: Monitoring the quality of groundwater in the plant area and WWTP. *Manuscript. Bratislava, archive AQUA – GEO.*

Žitňan, M., 2011: Audit of environmental burdens in the premises of Slovenský hodváb PLUS, s.r.o. *Manuscript. Bratislava, archive AQUA – GEO.*

Laws and other legislative standards

Methodological instruction of the Ministry of the Environment of the Slovak Republic dated August 27, 1998 No. 549/98-2 for the assessment of risks from polluted sediments of streams and water reservoirs.

Regulation of the Government of the Slovak Republic No. 269/2010 Coll., which establishes the requirements for achieving good water status as amended. Instruction of the Ministry for the Administration and Privatization of National Property of the Slovak Republic and the Ministry of the Environment of the Slovak Republic dated December 15, 1997 No. 1617/97-min. on the procedure for evaluating the company's obligations from the point of view of environmental protection in the privatization project submitted by the company as part of the privatization.

Journal of the MŽP SR 1/98. Part VI. Indicators and standards for remediation of soil, soil and groundwater pollution, p. 47–51.

Použitá metodika a výsledky geologického prieskumu environmentálnej záťaže bývalých závodov Slovenský hodváb Senica

Environmentálne záťaže sú definované ako znečistené územia spôsobené činnosťou človeka, ktoré predstavujú závažné riziko pre ľudské zdravie alebo horninové prostredie, podzemnú vodu a pôdu. Problematika environmentálnych zaťaží na Slovensku sa začala riešiť v roku 2006 v rámci projektu *Systematická identifikácia environmentálnych záťaží* (Paluchová et al., 2008) s cieľom identifikácie pravdepodobných environmentálnych záťaží z celého územia Slovenskej republiky. Výsledkom bolo zostavenie *Registra environmentálnych záťaží*. Registrované záťaže sú v ňom zoradené podľa ich relatívnej rizikovosti ohrozenia života a zdravia obyvateľov, ako aj poškodenia ekosystémov. Register je súčasťou *Informačného systému environmentálnych záťaží* (IS EZ). Aktuálne je na Slovensku evidovaných 1 782 záťaží, rozdelených do registrov podľa stavu ich preskúmanosti a realizácie nápravných opatrení s cieľom minimalizácie ich negatívneho dosahu na zdravie človeka a životné prostredie.

Práce prezentované v tomto článku vychádzajú z výsledkov geologickej úlohy pod názvom *Geologický prieskum vybraných pravdepodobných environmentálnych záťaží 3 – ŠGÚDŠ*. Úloha sa riešila v rámci operačného programu *Kvalita životného prostredia – prioritná os 1*. Bola vypracovaná v súlade so strategickým plánovacím dokumentom v rámci systematického prieskumu a odstraňovania environmentálnych záťaží s názvom *Štátny program sanácie environmentálnych záťaží SR (2016 – 2021)*. Environmentálna záťaž v Trnavskom kraji, ktorá je predmetom nášho článku, je v ňom evidovaná v časti *7.1.1. Najrizikovejšie lokality z hľadiska potreby realizácie prieskumu pravdepodobných environmentálnych záťaží a potreby vypracovania rizikovej analýzy*. Environmentálna záťaž (ďalej EZ) v areáli bývalých závodov Slovenský hodváb je v informačnom systéme zaregistrovaná v kategórii A ako pravdepodobná environmentálna záťaž s vysokou prioritou s označením SK/EZ/SE/2004 pod názvom SE/2004/Senica – areál bývalého SH Senica.

Areál bývalých závodov je lokalizovaný v zastavanom území intravilánu mesta Senica, v priemyselnej zóne, v areáli bývalého výrobného podniku Slovenský hodváb Senica. Územie je z východnej strany ohraničené obchodnou prevádzkou Lidl a autobusovou stanicou, zo severnej strany tokom Teplica. Plocha skúmaného areálu predstavuje zhruba obdĺžnik s rozlohou približne 37 ha.

Vysoká priorita environmentálnej záťaže bola v systéme environmentálnych záťaží priradená predovšetkým na základe vizuálnej obhliadky lokality v čase registrácie v roku 2014, ktorá zodpovedala stavu ukončenej priemyselnej činnosti bývalých závodov. Závody SH Senica boli vybudované v 20. rokoch minulého storočia s cieľom výroby syntetických vlákien. Závody zanikli v roku 2005. Samotná činnosť podmieňujúca vznik EZ sa od roku 1989 už nevykonáva. V areáli podniku (výroba syntetických vlákien) bolo v čase aktívnej činnosti vybudované rozsiahle mazutové hospodárstvo (nádrže sú už zbúrané) pozostávajúce zo 7 nádrží na mazut, kotolne a stáčacieho miesta. Nachádzala sa tam aj neutralizačná stanica a sklady chemikálií (HCl a pod.). Činnosť podmieňujúca vznik EZ sa na lokalite už nevykonáva, prevádzka sa využíva na iné účely. V západnej časti areálu v súčasnosti prebieha rôznorodá priemyselná činnosť. Údaje o držiteľovi/držiteľoch záťaže uvedené v systéme ISEZ boli v čase realizovaného prieskumu neaktuálne. Od roku 2014 sa zmenil pôvodný držiteľ a v dôsledku odpredaja sa stále menia vlastníci na rôznych parcelách environmentálnej záťaže.

V čase prieskumu v rokoch 2022 – 2023 aktuálny vizuálny stav nezodpovedal stavu lokality v čase jej registrácie z roku 2014. Vo východnej časti územia v miestach najpravdepodobnejšieho zdroja znečistenia prebiehala rozsiahla stavebná a asanačná činnosť s úpravou pozemku určeného na ďalšie rozvojové aktivity občianskej a bytovej výstavby. Asanácia a následná úprava pozemku sa realizovala na základe odporúčaní environmentálneho auditu v objektoch areálu Slovenský hodváb PLUS, s. r. o. (Žitňan, 2011).

Metodika realizovaného podrobného prieskumu sa odvíja od aktuálne platnej legislatívy Slovenskej republiky, a to predovšetkým *Metodickej príručky geologického prieskumu životného prostredia v znečistenom území* (SAŽP, 2020) a smernice Ministerstva životného prostredia č. 1/2015-7 na analýzu rizika znečisteného územia.

Na lokalite sa uskutočnil súbor geologických prác zameraný na komplexný prieskum a charakterizáciu znečistenia všetkých zložiek životného prostredia vrátane zhodnotenia potenciálneho zdravotného a environmentálneho rizika vyplývajúceho z prípadného zisteného znečistenia. Realizované práce v oblasti výskytu pravdepodobnej environmentálnej záťaže zahŕňali technické práce (vrtné práce). Ich cieľom bolo spresnenie geologickej

stavby lokality a rozsahu znečistenia horninového prostredia a podzemnej aj povrchovej vody, meranie a odbery vzoriek horninového prostredia v pásme prevzdušnenia a pásme nasýtenia, odbery vzoriek podzemnej, povrchovej a odpadovej vody z novovybudovaných aj existujúcich vrtov, atmogeochemické merania, odbery pôdneho vzduchu, chemické analýzy odobratých vzoriek podzemnej vody a chemické a zrnitostné analýzy odobratých vzoriek horninového prostredia. Metodika prieskumných prác je detailne opísaná v práci Grexovej et al. (2023).

V rámci technických prác sa uskutočnilo 15 hydrogeologických monitorovacích vrtov, 5 nevystrojených prieskumných mapovacích vrtov a 15 ručných diagnostických plynometrických sond. Hĺbka zabudovaných hydrogeologických vrtov varírovala v rozsahu 9 až 12 m, hĺbka mapovacích vrtov bola 5 m. Ručné sondy sa robili do maximálnej hĺbky 1 m.

Pred realizáciou vrtných prác sa v miestach ručných sond a plánovaných vrtov odobrali vzorky pôdneho vzduchu. Vzhľadom na charakter lokality v nich bola zaznamenaná prítomnosť ropných uhľovodíkov stanovených ako benzén a toluén. Vyššie hodnoty koncentrácie ukazovateľov prekračujúce koncentráciu B a C pokynu *MSPN č. 1617/97-min*. boli potvrdené iba v ručne realizovaných sondách typu SPS. Hodnoty, ktoré neboli potvrdené opakovanými kontrolnými odbermi, sme vyhodnotili ako znečistenia bodového charakteru s pravdepodobnosťou ovplyvnenia prebiehajúcich prác stavebného charakteru a možnosťou voľného prístupu pre verejnosť vo východnej časti bývalých závodov, ktorá nemá súvis s činnosťou podmieňujúcou zaradenie skúmanej lokality do systému environmentálnych záťaží (ISEZ).

Na základe výsledkov analýz pôdneho vzduchu sa počas realizácie vrtných prác odobrali vzorky zemín z pásma prevzdušnenia a pásma nasýtenia z vrtov (SHG, SMV) a sond (SPS). Výsledky z nich potvrdili nízku koncentráciu vo všetkých analyzovaných ukazovateľoch neprekračujúcu indikačné a intervenčné kritériá stanovené smernicou MŽP SR č. 1/2015-7 na vypracovanie analýzy rizika znečisteného územia. Výnimkou bola len vyššia koncentrácia *ortuti* (SPS-1 – 3,76 mg . kg^{-1} . sušiny), *medi* (SPS-3 – 593 mg . kg^{-1} . sušiny) a *olova* (SPS-3 – 1 860 mg . kg^{-1} . sušiny) prekračujúca indikačné a intervenčné kritérium smernice pre obytné zóny. Z hydrogeologických monitorovacích vrtov SHG sa zistila zvýšená koncentrácia stopových kovov prekračujúca indikačné kritérium smernice v ukazovateli *meď* (548 mg . kg^{-1} . sušiny) a intervenčné kritérium v ukazovateli *olovo* (593 mg . kg^{-1} . sušiny) iba vo vrte SHG-10, situovanom v novej priemyselnej časti areálu bývalých závodov Slovenský hodváb. Jeho aktuálna činnosť ale nemá súvis s činnosťou závodov podmieňujúcou vznik environmentálnej záťaže. V tomto vrte sa zistila aj vysoká koncentrácia *NEL-GC* prekračujúca indikačné kritérium (774 mg . kg^{-1} . sušiny). To sa potvrdilo aj kontrolnou vzorkou, ktorá preukázala prekročenie koncentrácie v rámci intervenčného kritéria smernice MŽP SR č. 1/2015-7-min. (774 a 3 179 mg . kg^{-1} . sušiny). Identifikácia uhľovodíkov poukázala na dominantné percentuálne zastúpenie uhľovodíkov radu $C_{16} – C_{24}$ (vykurovacie oleje).

Lokálne znečistenie horninového prostredia biologickej kontaktnej zóny alifatickými ropnými uhľovodíkmi je charakterizované reziduálnymi uhľovodíkmi, ktoré majú charakter málo prchavých uhľovodíkov s nízkou rozpustnosťou a vysokým stupňom retardácie (obmedzenia migrácie) v horninovej matrici. S vysokou pravdepodobnosťou ide o bodové znečistenia reziduálneho charakteru v dôsledku realizovanej čiastočnej sanácie objektov v plánovanej obytnej zóne.

Odbery vzoriek podzemnej vody realizované v dvoch kolách s odstupom 30 dní nepotvrdili kontamináciu vody, a to ani v miestach, kde sa potvrdilo lokálne znečistenie reziduálneho charakteru.

Zaujímavou skutočnosťou boli mierne zvýšené hodnoty *sulfidickej síry* vo východnej časti územia iba v dvoch z piatich nevystrojených prieskumných (mapovacích) vrtov, podľa historickej mapy z roku 1958 lokalizovaných v miestach bývalého starého ramena. Maximálna priemerná koncentrácia neprekročila indikačné kritérium smernice. Keďže prekročenie limitov ID a IT bolo zaznamenané iba pri odberoch z nevystrojených mapovacích vrtov vo východnej časti územia a pri režimových meraniach v hydrogeologických a mapovacích vrtoch v tejto časti územia sa nezistili záporné hodnoty oxidačno-redukčného potenciálu, s vysokou pravdepodobnosťou ide o prirodzený pôvod výskytu v tomto prostredí.

Zvýšená koncentrácia v žiadnom zo sledovaných ukazovateľov, rovnako ako vo vzorkách podzemnej vody, sa nepotvrdila ani odbermi vzoriek z povrchového toku Teplica v dvoch cykloch v smere predpokladaného znečistenia z bývalých závodov.

Súčasťou prieskumných prác bola aj analýza rizika znečisteného územia, ktorej vypracovanie vyplynulo z legislatívnych požiadaviek smernice MŽP SR č.1/2015-7. Týkala sa prítomnosti znečisťujúcich látok prekračujúcich intervenčné a indikačné kritériá v horninovom prostredí biologickej kontaktnej zóny v pásme prevzdušnenia ukazovateľom NEL-GC a stopovými kovmi Cu, Pb a Hg, pri ktorých bolo potrebné hodnotenie environmentálneho a zdravotného rizika. Vypracovanou analýzou rizika znečisteného územia sa nepotvrdili environmentálne ani zdravotné riziká, preto pri súčasnom využití územia nie

je potrebné vykonať sanáciu znečisteného územia. Vzhľadom na potvrdené reziduálne znečistenie zemín v západnej, novovybudovanej časti priemyselnej časti a sporadický výskyt sulfidickej síry v podzemnej vode bolo z princípu opatrnosti navrhnuté v tejto časti územia dvojročné monitorovanie kvality podzemnej vody. Po ňom v prípade priaznivého vývoja kvality podzemnej vody bude lokalita vyradená z registra *Informačného systému environmentálnych záťaží Slovenskej republiky.*

Realizácia tohto prieskumu je ďalším pozitívnym krokom v rámci systematického riešenia problematiky environmentálnych záťaží na území Slovenskej republiky. Jeho výsledky sú podkladom na postupné zlepšovanie životného prostredia vrátane udržateľnosti pre ďalšie generácie.

Doručené / Received: 25. 10. 2024
Prijaté na publikovanie / Accepted: 17. 12. 2024

Inštrukcie autorom

Etika publikovania, záväzná pri publikovaní v časopise Mineralia Slovaca: *www.geology.sk/mineralia položka* ***Publikačná etika***

1. Geovedný časopis Mineralia Slovaca publikuje scientometricky hodnotné recenzované pôvodné vedecké články s vysokým citačným potenciálom. V úvode príspevku musí autor jasne deklarovať, čím konkrétnym je jeho príspevok prínosný pre rozvoj geovied. Rešeršné štúdie sa publikujú len ojedinele.

2. Články na publikovanie (manuskripty) sa do redakcie zasielajú poštou (dva vytlačené exemplára a CD so všetkými súbormi v editovateľnej podobe) alebo e-mailom (editovateľné súbory a kompletná verzia vo formáte PDF).

3. Súčasne s článkom je potrebné redakcii poslať autorské vyhlásenie o originalite textu a obrázkov. Kópie obrázkov z iných publikácií musia byť legalizované získaním práva na publikovanie. Vyhlásenie musí obsahovať meno autora (autorov), akademický titul a trvalé bydlisko.

4. Rozsah manuskriptu na publikovanie je najviac 25 rukopisných strán (MS Word, Times New Roman, veľkosť písmen 12 bodov, riadkovanie 1,5) vrátane literatúry, obrázkov a vysvetliviek. V prípade veľkého odborného prínosu sú v ojedinelých prípadoch povolené aj dlhšie články.

5. Články sú publikované v angličtine so slovenským resumé v závere článku (za zoznamom citovanej literatúry).

Text

1. Abstrakt stručne sumarizuje článok. Môže mať najviac 200 slov a nemá obsahovať citácie. Počet kľúčových slov je maximálne 6. Text má mať úvod, charakteristiku (stav) skúmaného problému, použitú metodiku, nové zistenia, ich interpretáciu, diskusiu, záver a zoznam literatúry. Východiskové údaje musia byť zreteľne odlíšené od interpretácií. V texte musia byť odvolávky na všetky použité obrázky a tabuľky.

2. Hierarchiu nadpisov v texte je potrebné vyznačiť ceruzkou na ľavom okraji strany manuskriptu: 1 – najvyššia, 2 – nižšia, 3 – najnižšia.

3. V texte sa uprednostňuje citácia v zátvorke, napr. (Dubčák, 1987; Hrubý et al., 1988), pred formou ... podľa Dubčáka (1987).

4. Pozícia obrázkov a tabuliek v texte sa označí. Nie je vhodné, aby text v editore MS Word obsahoval vložené obrázky, ale náhľadová verzia v pdf ich má obsahovať.

5. Grécke písmená treba identifikovať na ľavom okraji slovom (napr. sigma). Potrebné je odlišovať pomlčku od spojovníka. Symboly, matematické značky, názvy skamenelín a pod., ktoré sa majú vysádzať kurzívou, autor v rukopise podčiarkne vlnovkou.

Obrázky a tabuľky

1. Ilustrácie a tabuľky vysokej kvality bývajú publikované buď **na šírku stĺpca (81 mm), alebo strany (170 mm).** Optimálna veľkosť písma a čísiel v publikovaných obrázkoch je 2 mm. Všetky texty v obrázkoch a tabuľkách, rovnako ako popisy k nim musia byť v angličtine. **Maximálny rozmer ilustrácie a tabuľky vytlačený v časopise je 170 x 230 mm.** Väčšie (skladané) ilustrácie sú publikované len v ojedinelých prípadoch.

2. Pri počítačovej tvorbe obrázkov odporúčame používať programy s vektorovým zobrazením (Corel Draw, Adobe Illustrator a pod.). Čiary tzv. vlasovej hrúbky, softvérová alebo rastrová výplň plôch (napr. v Corel Draw) nie sú prípustné. Výplne v obrázkoch musia pozostávať zo samostatne vysádzaných objektov.

3. Ilustrácie vrátane fotografií musia obsahovať **grafickú mierku** v centimetrovej či metrovej škále, prípadne sa rozmer zobrazených objektov vyjadrí v popise obrázka. Mapy a profily musia mať aj **azimutálnu orientáciu** a jednotné vysvetlivky, ktoré sa uvedú pri prvom obrázku. Zoskupené obrázky, napr. fotografie a diagramy, sa uvádzajú ako jeden obrázok s jednotlivými časťami označenými písmenami (a, b, c atď.).

4. Pri zasielaní fotografií vo forme počítačových súborov (formáty JPG alebo TIF) sa požaduje rozlíšenie minimálne 600 DPI. Publikovanie farebných ilustrácií môže byť spoplatnené.

Literatúra

1. Minimálne 50 % citácií musí reprezentovať publikácie od roku 2000. V zozname literatúry sa v abecednom poradí uvádza len literatúra citovaná v danom článku.

2. Spôsob uvádzania literatúry v zozname literatúry

Knižná publikácia: Gazda, L. & Čech, M., 1988: Paleozoikum medzevského príkrovu. *Bratislava, Alfa, 155 s.*

Článok v časopise: Vrba, P., 1989: Strižné zóny v metapelitoch. *Miner. Slov., 21, 135 – 142.*

Zborník: Návesný, D., 1987: Vysokodraselné ryolity. *In: Romanov, V. (ed.): Stratiformné ložiská gemerika. Špec. publ. Košice, Slov. geol. spol., 203 – 215.*

Manuskript: Radvanský, F., Slivka, B., Viktor, J. & Srnka, T., 1985: Žilné ložiská jedľoveckého príkrovu gemerika. Záverečná správa z úlohy SGR--geofyzika. *Manuskript. Spišská Nová Ves, archív Št. Geol. Úst. D. Štúra, 28 s.*

3. Pri článku viac ako dvoch autorov sa v texte cituje iba prvý autor s dodatkom et al., ale v zozname literatúry sa uvádzajú všetci.

Instructions to authors

Publication ethics, being obligatory for publishing in the journal Mineralia Slovaca: *www.geology.sk/mineralia item* ***Publication ethics***

1. Geoscientific journal Mineralia Slovaca publishes scientometrically valuable original peer-reviewed scientific articles with a high citation potential. In the introduction of each article the author(s) must clearly declare, which innovative data the paper brings for the development of geosciences. The retrieval studies are published only exceptionally.

2. The articles for publishing (manuscripts) must be sent to Editorial Office by post (two printed copies and CD with editable files), or by e-mail (editable files plus complete preview version in PDF format).

3. Simultaneously with the article the Editorial Office must receive the author´s proclamation that no part of the manuscript was already published and figures and tables are original as well. Copied illustrations from other publications must contain a copyright.

4. The extent of the manuscript for publishing is limited to 25 manuscript pages (MS Word, 12 points Times New Roman, line spacing 1.5) including figures, tables, explanations and references. In the case of contribution with a high scientific value, the longer manuscripts for publishing are exceptionally permitted.

5. Articles are published in English, with Slovak summary at their end. In a case of foreign authors not able to submit the article summary in Slovak, the Editorial Office translates their English summary to Slovak version.

Text

1. Abstract briefly summarizing the article is limited to 200 words, no references are allowed. The maximum number of key words is 6. Text of the article has to contain the introduction, characterization (state) of investigated problem, applied methodology, presented new data, discussion, conclusion and references. The obtained data must be distinctly separated from interpretations. All applied figures and tables must be referred in the text.

2. The hierarchy of headings in the manuscript must be clearly indicated.

3. The references in the text prefer parentheses, e.g. (Dubčák, 1987; Hrubý et al., 1988). The form "according to Dubčák (1987)" should be used only exceptionally.

4. Position of figures and tables must be indicated in the manuscript. Editable text of manuscript sent to editorial office must be without figures and tables, though the preview PDF has to contain them in a correct position.

5. Greek letter in the text must be identified at the left margin of the text (e.g. sigma). The text should strictly distinguish the dash from hyphen. Symbols, mathematic signs, names of fossils, etc., which should be printed in italics, must be underlined in the manuscript.

Figures and tables

1. The high quality figures and tables can be published either in **maximum width of column (81 mm) or page (170 mm).** The optimum size of letters and numbers in the camera-ready figure is 2 mm. All texts in figures and tables, as well as descriptions and notes to figures and tables must be in English. **Maximum dimension of figures and tables in the journal is 170 x 230 mm. Larger (fanfolded)** illustrations are published only exceptionally.

2. For figures drawing the editorial office recommends the vector graphics editors (Corel Draw, Adobe Illustrator, etc.). The very thin lines (hair lines), the pre-defined software or raster fillings of polygons (e.g. in Corel Draw) are not allowed. The filling must consist from separately set objects.

3. Each illustration including photographs must contain graphic (metric) scale, eventually the dimensions of visualized objects have to be stated in the describing text to figure. Maps and profiles must contain also the azimuth orientation, their detail explanations are stated at the first figure. Grouped figures, e.g. photographs and diagrams, are compiled as one figure with separate parts designated by letters (a, b, c, etc.).

4. The photographs sent as JPG of TIF files are required for having minimum 600 DPI resolution. Publishing of colour illustrations can be charged by a fee.

References

1. Minimum 50 % of referred works must represent contemporary publications after 2000. The references in alphanumeric order encompass only literature cited in the article.

2. Examples of referring:

Book: Gazda, L. & Čech, M., 1988: Paleozoic of the Medzev nappe. *Bratislava, Alfa, 155 p.*

Article in journal: Vrba, P., 1989: Shear zones in the metapelite complexes. *Miner. Slov., 21, 135–142.*

Anniversary volume: Návesný, D., 1987: High-potassium rhyolites. *In: Romanov, V. (ed.): Stratiform deposits of Gemericum. Spec. publ. Košice, Slov. geol. soc., 203–215.*

Manuscript: Radvanský, F., Slivka, B., Viktor, J. & Srnka, T., 1985: Vein deposits of the Jedľovec nappe of Gemericum. Final report from the project SGR-geophysics. *Manuscript. Spišská Nová Ves, Archive Št. Geol. Úst. D. Štúra, 28 p.*

3. The article with more than two authors is referred by the name of the first author with the amendment et al., but the list of references contains names of all authors.

Ďalšie informácie / Further information: mineralia.slovaca@geology.sk; zoltan.nemeth@geology.sk

OBSAH – CONTENT

PÔVODNÉ ČLÁNKY – ORIGINAL PAPERS

Indexed / Abstracted / Accessed by SCOPUS, WEB OF SCIENCE and EBSCO
Indexované / abstraktované / sprístupňované databázami SCOPUS, WEB OF SCIENCE a EBSCO

www.geology.sk/mineralia